The Role of Eclogites in the Growth of Archean Cratons: A Case Study from West Africa

A thesis presented

by

Matthias Götz Barth

to

The Department of Earth and Planetary Sciences

in partial fulfillment of the requirements
for the degree of

Doctor of Philosophy

in the subject of

Geology

Harvard University
Cambridge, Massachusetts

March 2001

The Role of Eclogites in the Growth of Archean Cratons: A Case Study from West Africa

Matthias Götz Barth

Thesis Advisor: Roberta L. Rudnick

Abstract

This study investigates crustal growth and tectonic processes that occurred during the Archean, with West Africa as an example. Specifically, it tests the hypothesis that some xenolithic eclogites have a complementary evolution to the Archean tonalite-trondhjemite-granodiorite (TTG) suites, which are important constituents of Archean cratons; that is, to see if the eclogites and TTGs can be matched both geochemically and in time of their formation.

I determined oxygen isotope, mineral trace element, measured and reconstructed whole rock compositions for low MgO (6-13 wt% MgO in the whole rock) and high MgO (16-20 wt% MgO) eclogite xenoliths from the Koidu Kimberlite Complex, Sierra Leone. While the $\delta^{18}O$ values of garnets in high MgO eclogites lie within the range for mantle peridotites, low MgO garnets have more variable $\delta^{18}O$ values (4.7 to 6.8‰) and extend beyond the mantle range. All low MgO eclogites show reconstructed trace element patterns that are depleted in Ba, Th, U, and light REE. These observations, coupled with low SiO_2 contents, and Nb-rich but LREE-depleted reconstructed whole rock compositions, suggest the low MgO eclogites are remnants of altered oceanic crust that was partially melted during subduction. The high MgO eclogites have whole rock

major element compositions suggestive of a cumulate origin, generated either as high-pressure garnet-pyroxene cumulates or as crustal (low-pressure) plagioclase-pyroxene-olivine cumulates.

Additionally, Re-Os whole rock isotopic data for these eclogites yield an Archean age (3.3±0.6 Ga). This age overlaps the age range for crust formation and metamorphism on the Man Shield. In situ U-Pb ages of zircons from crustal rocks from the Man Shield have been measured by laser ablation ICP-MS. A tonalitic gneiss has discordant zircons with rare old cores (~3.6 Ga) and an upper Concordia intercept at 2889 ± 12 Ma. Zircons from a mafic lower crustal granulite xenolith from Koidu are concordant at 2686 ± 32 Ma. These results, together with previously published ages for the Man Shield, indicate an Early Archean crust formation event followed by major crustal growth at 2.9-3.0 Ga and a last major metamorphic event at 2.7 Ga. These data show that the eclogites and the continental crust of the West African Craton overlap in time of formation, linking the two groups of rocks in time and space. They also imply that Archean crustal growth was accomplished, in part, by direct addition of evolved magmas from the mantle.

Table of Contents

Acknowledgements

This part of my thesis is the most difficult to write. Few people will read my thesis but most of these people will read the acknowledgements first. I really would prefer to avoid the old-fashioned style where the graduate student begins his acknowledgements with expressing his eternal gratitude to his mother and his thesis advisor for making this work possible. Some authors start with thanking their mentor who introduced them to minerals, rocks, and natural sciences. But I stumbled across geology by sheer chance. I could begin by showing appreciation to Matthias Barth for doing a lot of the dirty work but this would be utterly inappropriate. Most of the time when I stepped by his office he was sleeping on his couch, surfing the web, or doing other things entirely unrelated to this thesis. Sometimes he really tried the patience of his advisor. To my rescue comes one of the greatest inventions of mankind – the chronological statement. Here we go:

I would like to thank my M.S. thesis advisor Steve Foley for encouraging me to start this journey.

Roberta Rudnick provided invaluable advice and good humor throughout my studies. I shall never forget that she recommended *The Hitchhiker's Guide to the Galaxy* as preparation for my oral exams. Adam Dziewonski, Paul Hoffman, Stein Jacobsen, and Bill McDonough are thanked for their support and being on various committees. Rick Carlson, Steve Haggerty, Ingo Horn, David Lange, Hugh Rollinson, Mike Spicuzza, and John Valley provided samples and helped me with my analytical work in several excellent laboratories. This work benefited from discussions with many people,

particularly Debbie Hassler, Cin-Ty Lee, and Thomas Zack. Numerous undergraduate assistants did a large part of the dirty work such as crushing rocks and preparing mineral separates. The National Science Foundation provided financial support.

My family and my friends kept my head in the air and my feet close to the ground. Thanks to all of you! Despair, Inc.™ made me smile in the darkest hours of graduate school (just before everything turned pitch black). The GeoClub refrigerator provided essential life support.

Last but not least Gareth Davies, Martyn Drury, and Paul Mason motivated me to finish my thesis and this journey faster than I ever imagined.

To the memory of my sister

Cornelia Monika Barth

Chapter 1

Introduction

1.1. Objective

This study investigates crustal growth and tectonic processes in the Archean in order to enhance our understanding of Earth's processes at a very significant time of Earth's evolution. Specifically, it tests the hypothesis that some xenolithic eclogites, carried to the surface in kimberlite pipes, have a complementary evolution to Archean tonalite-trondhjemite-granodiorite (TTG) suites, which are important constituents of Archean cratons. This hypothesis has been proposed on the basis of circumstantial evidence of general complementary geochemical characteristics in the two groups of rocks. No attempt has been made up to now to test the hypothesis by examining in detail rocks from the same geographic area to see if the eclogites and TTGs can be matched both geochemically and in time of their formation.

The results of the test have implications for the nature of Archean tectonic processes and crustal evolution, and the origin of TTGs and eclogite xenoliths. If some eclogite xenoliths can be shown to be remnants of altered oceanic crust and to be residues of partial melting, complementary to spatially associated TTGs, it implies that subduction was operative in the Archean and that Archean crustal growth was accomplished, in part, by direct addition of evolved magmas from the mantle. Alternatively, if it can be established that the TTGs are partial melts of the mafic lower part of thickened continental crust, it can be inferred that TTGs are collision-related. In that case

delamination of lower continental crust is likely to be an important process for the removal of the mafic to ultramafic residue of the granitoids and, thus, for the generation of xenolithic eclogites. A third potential link between TTGs and eclogites may be caused by possible Archean tectonics that differ from present-day plate tectonics (preplate tectonics, see below). The data collected provides a strong base for determining how the two groups of rocks evolved and what major processes were operative in the crust and mantle during the Archean.

The Man Shield in West Africa contains both mantle-derived eclogite xenoliths and Archean TTGs. This study is a specific test of geological-geochemical evolution in a spatially restricted crust-mantle domain. Representative sample suites and suitable specimens for analysis have been selected based on extensive petrographic and basic geochemical work that has already been done on both of these sets of rocks.

1.2. TTGs, Eclogites, and a Possible Crust-Mantle Connection

Granitoids of the TTG suite and grey gneisses, their high-grade metamorphic equivalent, are the dominant constituent of the Earth's early continental crust[1]. These Na-rich rocks consist of plagioclase, quartz, and biotite with minor K-feldspar and hornblende. Their distinct trace element compositions reveal depletions in Nb, Ta, Ti, and P relative to other incompatible elements such as La. The rare earth element (REE)

[1] K-rich granites are widespread and voluminous constituents of Archean cratons, second only to TTGs (Condie, 1993). These plutons were formed by partial melting of igneous (i.e., TTGs) and sedimentary rocks in the middle and lower crust, in most cases with little involvement from mantle-derived magmas (Sylvester, 1994). Thus, granites contribute to the evolution of Archean crust but not to its growth.

patterns are strongly fractionated ($(La/Yb)_N = 38$), with low heavy REE contents and, on average, no significant Eu anomaly (Condie, 1993; Martin, 1994). Taken together, these trace element characteristics indicate that TTGs formed in equilibrium with garnet and probably rutile or ilmenite. The presence of garnet requires a depth of melting >40 km, but the precise depth and the tectonic setting remain uncertain. Melting may have occurred in the deeper, mafic portion of a thickened continental crust (Atherton and Petford, 1993) or within oceanic crust that was subducted into the upper mantle (Martin, 1986). Possible residues are garnet-bearing amphibolite or eclogite.

Since the volume of mafic residue produced during the production of the TTG exceeds by far the volume of mafic lower crust currently present in Archean cratons (Ireland et al., 1994; Rudnick and Fountain, 1995), a lower crustal source requires a mechanism for the disposal of the larger part of the residue, i.e., large-scale delamination of the lower crust. In the alternative scenario of TTG genesis by partial melting of subducted oceanic crust, the residue (the oceanic crust of the slab) is transported into the mantle. In either case one would expect to find remnants of the residue in the lower crust or lithospheric mantle, as it is unlikely that the disposal process was 100% efficient[2].

The generation of TTG magmas within the garnet stability field requires temperatures higher than 900 °C (Wyllie et al., 1997, and references therein). These temperatures may have been reached more easily in the Archean than at present due to believed higher mantle temperatures and heat flow. It is unchallenged that the radiogenic heat production was higher in the Archean than at present, but the relation between

[2] Cook et al. (1998) have produced seismic images that may be the first evidence for tectonic imbrication of oceanic lithosphere in the subcontinental mantle of northwestern Canada.

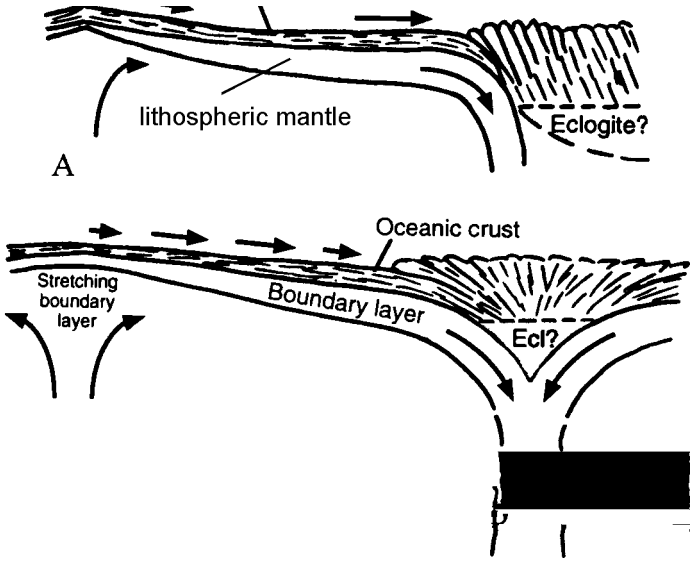

Figure 1.1. A: Sketch of conjectured regime preceding plate tectonics proper, in which mantle part of oceanic lithosphere is thick enough to behave rigidly, but whole mantle-plus-crust package is buoyant; lithospheric mantle part is negatively buoyant and subducts by shearing off from crustal part, which accumulates at surface. Detachment of crust would be aided by higher temperatures that would exist at base of crustal part. This regime resembles one proposed by Park (1981). Crustal pile might differentiate internally and come to resemble an island arc, especially if its deeper parts transformed to dense eclogite that would sink. **B:** Sketch of conjectured preplate regime in which thin, soft, thermal boundary layer forms under thick basaltic crust and "drips" back into deep mantle. Crust would accumulate over downwellings and might also come to resemble island arcs and to have eclogite sinkers, as suggested for regime A. This kind of regime has also been proposed by Campbell and Griffiths (1992), who quantified some aspects of it and noted some possible implications for chemical evolution of mantle. After Davies (1992).

mantle temperature and time remains poorly constrained due to uncertainties in the K/U ratio of the Earth's mantle, the style of mantle convection, and many other parameters. It has been proposed that steeper geothermal gradients in the Archean caused partial melting of subducted oceanic crust (Martin, 1986). Smaller lithospheric plates and/or higher spreading rates in the Archean (e.g., Abbott and Hoffman, 1984) result in the subduction of younger slabs and, therefore, higher temperatures at the slab/mantle wedge interface (e.g., Peacock, 1996). Higher mantle temperatures result in higher melt production at mid-ocean ridges, thicker oceanic crust, more depleted lithospheric mantle and, therefore, more buoyant slabs. More buoyant slabs may have caused flat subduction (Abbott et al., 1994), resulting in higher temperatures at a given depth, or – if the slab was positively buoyant – a different tectonic style (preplate tectonics; Davies, 1992). In this scenario (Fig. 1.1) oceanic crust might have accumulated over downwellings and, after cooling, "dripped" back into the mantle.

Eclogite xenoliths, rocks of broadly basaltic composition that have a predominant assemblage of garnet and omphacite, are minor but ubiquitous constituents in mantle xenolith suites brought up by kimberlites in Archean (and Proterozoic) cratons. Phase petrology suggests high equilibration pressures and temperatures diagnostic of the upper mantle. The different hypotheses proposed for the origin of eclogite xenoliths can be divided into two groups:

1. The "mantle" hypothesis: eclogites are produced by direct high-pressure crystallization from peridotite-generated magmas that ascend through the lithosphere, by exsolution of garnet from clinopyroxene, or by decomposition of majorite.

2. The "crustal" hypothesis: eclogites are remnants of subducted (Archean?) oceanic crust or are produced by metamorphism of basaltic lower continental crust.

Evidence for the mantle hypothesis includes mineralogical layering, cumulate textures, and mantle-like oxygen isotope signatures (Smyth et al, 1989; Snyder et al., 1997). In addition, high Cr_2O_3 contents of some eclogite xenoliths are taken as support for the mantle hypothesis (Taylor and Neal, 1989).

The most compelling evidence for the crustal origin of eclogite xenoliths are stable isotope compositions that deviate from established peridotitic values, i.e., $\delta^{18}O$ values that lie beyond 5.5 ± 0.4‰ (Mattey et al., 1994), but are similar to the range of oxygen isotopes observed in ophiolites (Muehlenbachs, 1986). This fractionation of stable isotopes requires low-temperature processes at or close to the surface of the Earth (Clayton et al., 1975). In addition, high Al contents of kyanite-bearing xenolithic eclogites have been cited as an argument for low-pressure crystallization of plagioclase-rich protoliths (crustal pressures rather than upper mantle; Jacob et al., 1998; Jacob and Foley, 1999). Eclogite xenoliths may represent fragments of lower continental crust (Pearson et al., 1991; El Fadili and Demaiffe, 1999) or fragments of subducted oceanic crust, which may or may not have been through a melting episode associated with subduction (Helmstaedt and Doig, 1975; MacGregor and Manton, 1986; Taylor and Neal, 1989; Ireland et al., 1994; Jacob et al., 1994).

Eclogite xenoliths are common in kimberlite xenolith suites and have major element and, in some cases, trace element compositions similar to those expected for TTG residues (Rudnick, 1995; Rollinson, 1997).

1.3. Sierra Leone — Previous Work

The region selected to carry out this study is the Man Shield in West Africa (Fig. 1.2). The Man Shield lies near the former center of a Precambrian craton that was rifted apart by the opening of the Atlantic Ocean to form the West African Craton and the Guyana Shield in South America. It is situated in the southern West African Craton and has been divided into three age provinces (MacFarlane et al., 1981): Leonean (~3.0 Ga), Liberian (~2.7 Ga), and Eburnian (~2.0 Ga). However, due to the limited radiometric dating (Rb-Sr and Pb-Pb whole rock) there is a debate as to whether the Leonean and Liberian are two separate events or a single, long-lived event (Williams, 1978). A younger Pan-African age province defines a tectonic event at ~550 Ma in the coastal belt of Sierra Leone and Liberia (Fig. 1.2).

The Archean basement (Leonean and Liberian provinces) of Sierra Leone is typical of granite-greenstone terrains found in ancient continental nuclei. The older TTG gneisses (~3 Ga, Beckinsale et al., 1980) form between 60-70% of the outcrop area and are the major rock type of the Man Shield. Younger granites (2.7-2.8 Ga) intrude the margins of the greenstone belts or occur as thick sheets cross-cutting the greenstones at high structural levels. Detailed mapping by Rollinson (Rollinson, 1978) has identified a range of compositions in the TTG gneisses from diorite to granodiorite. The Koidu kimberlite complex occurs in the interior of this basement. Country rocks to the kimberlites include amphibolite-facies migmatites, TTG gneisses, ironstones, and ultramafic suites. To the northeast of the kimberlites lies a band of amphibolite-facies TTG gneisses striking NW- SE. Unpublished petrographic and geochemical data show

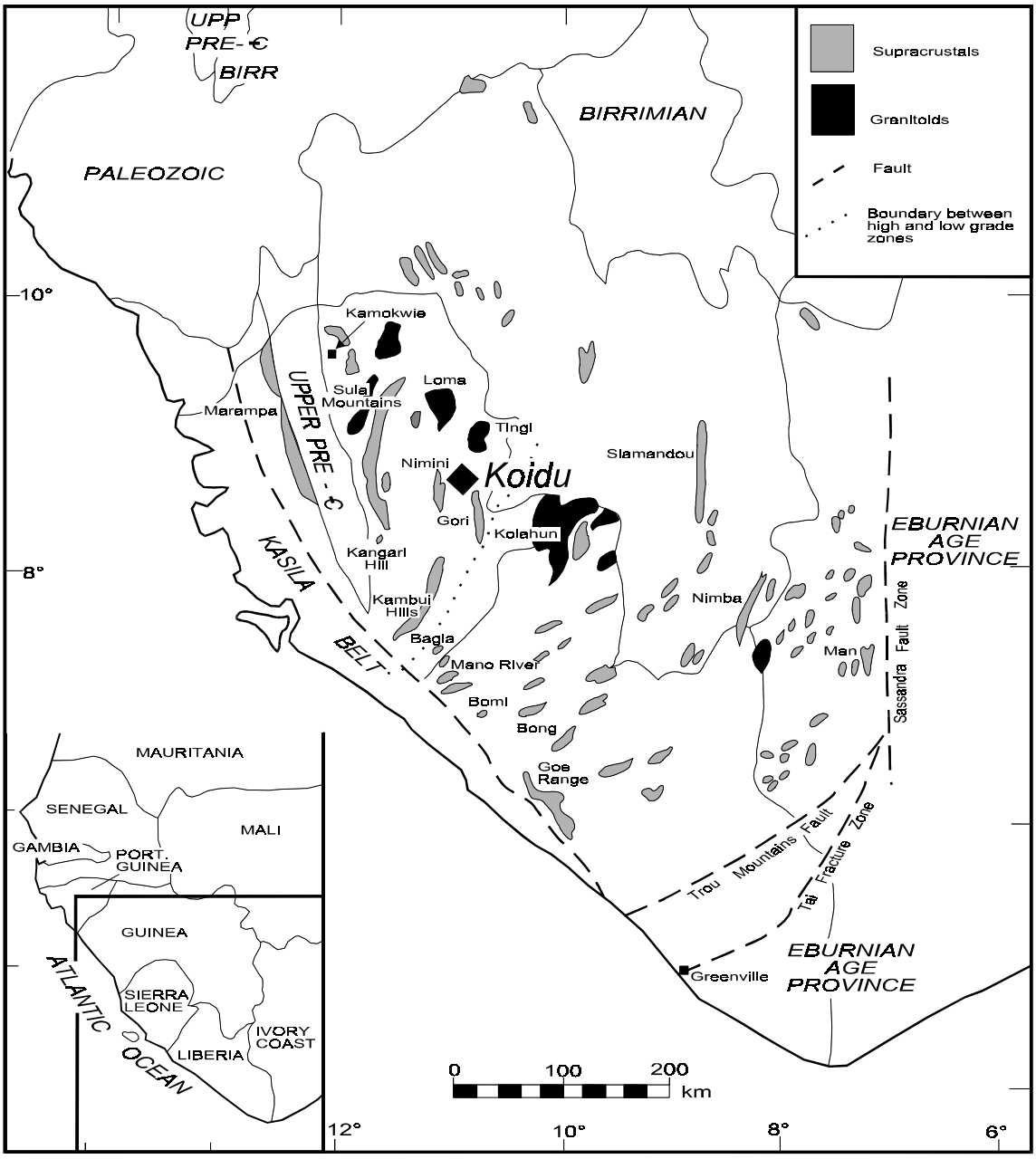

Figure 1.2. Generalized geological map of West Africa (from Rollinson, 1978)

them to be typical of TTGs found elsewhere (Rollinson, 1997).

A suite of eclogite xenoliths from the Mesozoic Koidu kimberlite complex was collected and characterized by Prof. Steve Haggerty and co-workers (Tompkins and Haggerty, 1984; Hills and Haggerty, 1989; Fung and Haggerty, 1995). Dr. Hugh Rollinson has collected an extensive suite of TTGs (Rollinson, 1978). Hills and Haggerty (1989) and Fung and Haggerty (1995) describe the petrography and report mineral chemical data for 87 eclogite xenoliths from the Koidu pipes. In addition, whole rock XRF data for major and trace elements are published for 25 of these samples. The Koidu eclogites fall into two groups, based on their major element chemistry: 1) a high-MgO group (>16 wt% MgO) that is essentially bi-mineralic, with only minor rutile, ilmenite, and/or sulphide occurring in addition to garnet and omphacite, and 2) a low-MgO group (6-13 wt% MgO), which commonly contains accessory phases such as kyanite, graphite, quartz (after coesite), diamond, amphibole, and/or corundum plus rutile, ilmenite, and/or sulphides in addition to garnet and omphacite. The difference in bulk composition between these two groups is apparent from their garnet compositions alone (Fig. 1.3). Generally, both high- and low-MgO eclogites fall into group II eclogites of McCandless and Gurney (1989), i.e., low-Na garnets and low-K omphacite, except for the diamond-bearing eclogites and a single graphite-bearing eclogite that fall into group I. High MgO garnets fall exclusively within the field of group A eclogites as defined by Coleman et al. (1965) and Taylor and Neal (1989); the low MgO garnets occupy the group B and C eclogite regions.

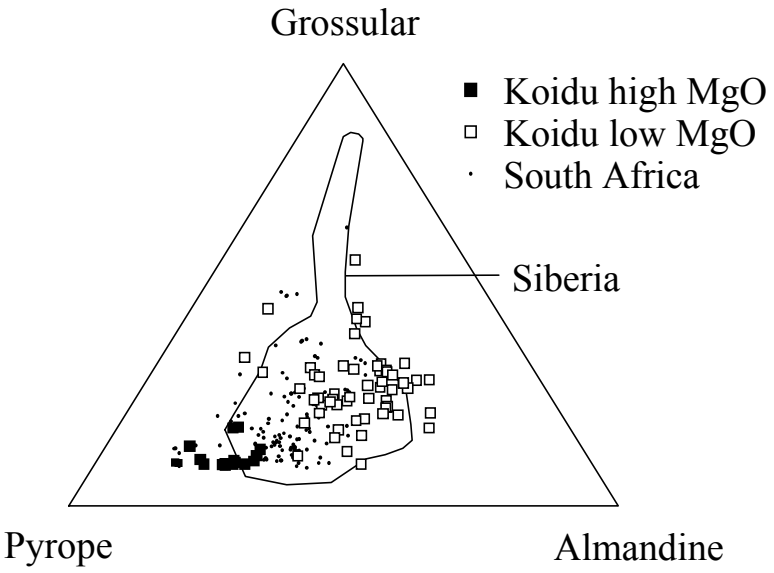

Figure 1.3. Garnet compositions from Koidu eclogites compared with those from other areas. The field encompasses data from Siberia. Diamondiferous eclogites are restricted to the low-MgO group.

Recently, it has been demonstrated that the Koidu low-MgO eclogites have complementary major element compositions to granitoids from the West African Craton, suggesting that both were derived from a common basaltic parent rock (Rollinson, 1997). These studies provide an excellent starting point for the present investigation.

The next three chapters describe the chemical and isotopic studies undertaken on the eclogites (and to a limited extent on the TTGs). The final chapter provides a synthesis of the findings in the context of global eclogite and TTG studies. The appendix presents evidence for a mass imbalance in the Bulk Silicate Earth (BSE) for Nb and Ta (Appendix

A) and discusses the importance of rutile-bearing refractory eclogite as a required reservoir to solve the Nb and Ta mass imbalance in the BSE (Appendix B).

1.4. References

Abbott D. H. and Hoffman S. E. (1984) Archaean plate tectonics revisited. 1. Heat flow, spreading rate, and the age of the subducting oceanic lithosphere and their effects on the origin and evolution of continents. *Tectonics* **3**, 429-448.

Abbott D., Drury R., and Smith W. H. F. (1994) Flat to steep transition in subduction style. *Geology* **22**, 937-940.

Atherton M. P. and Petford N. (1993) Generation of sodium-rich magmas from newly underplated basaltic crust. *Nature* **362**, 144-146.

Beckinsale R. D., Gale N. H., Pankhurst R. J., Macfarlane A., Crow M. J., Arthurs J. W., and Wilkinson A. F. (1980) Discordant Rb-Sr and Pb-Pb whole rock isochron ages for the Archaean basement of Sierra Leone. *Precambrian Res.* **13**, 63-76.

Campbell I. H. and Griffiths R. W. (1992) The changing nature of mantle hotspots through time: Implications for the chemical evolution of the mantle. *J. Geol.* **92**, 497-523.

Clayton R. N., Goldsmith J. R., Karel K., Mayeda T. K., and Newton R. C. (1975) Limits on the effect of pressure on isotopic fractionation. *Geochim. Cosmochim. Acta* **39**, 1197-1201.

Coleman R. G., Lee D. E., Beatty L. B., and Brannock W. W. (1965) Eclogites and eclogites: Their differences and similarities. *Geol. Soc. Am. Bull.* **76**, 483-508.

Condie K. C. (1993) Chemical composition and evolution of the upper continental crust: Contrasting results from surface samples and shales. *Chem. Geol.* **104**, 1-37.

Cook F. A., van der Velden A. J., Hall K. W., and Roberts B. J. (1998) Tectonic delamination and subcrustal imbrication of the Precambrian lithosphere in northwestern Canada mapped by LITHOPROBE. *Geology* **26**, 839-842.

Davies G. F. (1992) On the emergence of plate tectonics. *Geology* **20**, 936-966.

El Fadili S. and Demaiffe D. (1999) Petrology of eclogite and granulite nodules from the Mbuji Mayi kimberlites (Kasai, Congo): Significance of kyanite-omphacite intergrowths. In *Proceedings of the 7th International Kimberlite Conference*, Vol.

1 (ed. J. J. Gurney, J. L. Gurney, M. D. Pascoe, and S. H. Richardson), pp. 205-213. Red Roof Design cc.

Fung A. T. and Haggerty S. E. (1995) Petrography and mineral compositions of eclogites from the Koidu Kimberlite Complex, Sierra Leone. *J. Geophys. Res.* **100**, 20,451-20,473.

Helmstaedt H. and Doig R. (1975) Eclogite nodules from kimberlite pipes of the Colorado Plateau - samples of subducted Franciscan-type oceanic lithosphere. *Phys. Chem. Earth* **9**, 95-111.

Hills D. V. and Haggerty S. E. (1989) Petrochemistry of eclogites from the Koidu Kimberlite Complex, Sierra Leone. *Contrib. Mineral. Petrol.* **103**, 397-422.

Ireland T. R., Rudnick R. L., and Spetsius Z. (1994) Trace elements in diamond inclusions from eclogites reveal link to Archean granites. *Earth Planet. Sci. Lett.* **128**, 199-213.

Jacob D., Jagoutz E., Lowry D., Mattey D., and Kudrjavtseva G. (1994) Diamondiferous eclogites from Siberia: Remnants of Archean oceanic crust. *Geochim. Cosmochim. Acta* **58**, 5195-5207.

Jacob D., Jagoutz E., Lowry D., and Zinngrebe E. (1998) Comment on 'The origins of Yakutian eclogite xenoliths' by G. A. Snyder, L. A. Taylor, G. Crozaz, A. N. Halliday, B. L. Beard, V. N. Sobolev and N. V. Sobolev. *J. Petrol.* **39**, 1527-1533.

Jacob D. E. and Foley S. F. (1999) Evidence for Archean ocean crust with low high field strength element signature from diamondiferous eclogite xenoliths. *Lithos* **48**, 317-336.

Macfarlane A., Crow M. J., Arthurs J. W., Wilkinson A. F., and Aucott J. W. (1981) The geology and mineral resources of northern Sierra Leone. *Overseas Mem. Inst. Geol. Sci.* **7**, 103 p.

MacGregor I. D. and Manton W. I. (1986) Roberts Victor eclogites: ancient oceanic crust. *J. Geophys. Res.* **91**, 14,063-14,079.

Martin H. (1986) Effect of steeper Archean geothermal gradient on geochemistry of subduction-zone magmas. *Geology* **14**, 753-756.

Martin H. (1994) The Archean grey gneisses and the genesis of continental crust. In *Archean Crustal Evolution* (ed. K. C. Condie), pp. 205-259. Elsevier.

Mattey D., Lowry D., and Macpherson C. (1994) Oxygen isotope composition of mantle peridotite. *Earth Planet. Sci. Lett.* **128**, 231-241.

McCandless T. E. and Gurney J. J. (1989) Sodium in garnet and potassium in clinopyroxene: criteria for classifying mantle eclogites. In *Kimberlites and related rocks*, Vol. 2 (ed. J. Ross), pp. 827-832. Blackwell Scientific.

Muehlenbachs K. (1986) Alteration of the oceanic crust and the ^{18}O history of seawater. In *Stable isotopes in high temperature geological processes* (ed. J. W. Valley, H. P. J. Taylor, and J. R. O'Neil), pp. 425-444. Mineralogical Society of America.

Park R. G. (1981) Origin of horizontal structure in high-grade Archaean terrains. In *Archean Geology*, Vol. 7 (ed. J. E. Glover and D. I. Groves), pp. 481-490.

Peacock S. M. (1996) Thermal and petrologic structure of subduction zones. In *Subduction top to bottom* (ed. G. E. Bebout, D. W. Scholl, S. H. Kirby, and J. P. Platt), pp. 119-133. AGU.

Pearson N. J., O'Reilly S. Y., and Griffin W. L. (1991) The granulite to eclogite transition beneath the eastern margin of the Australian craton. *Eur. J. Mineral.* **3**, 293-322.

Rollinson H. R. (1978) Zonation of supracrustal relics in the Archaean of Sierra Leone, Liberia, Guinea and Ivory Coast. *Nature* **272**, 440-442.

Rollinson H. (1997) Eclogite xenoliths in west African kimberlites as residues from Archaean granitoid crust formation. *Nature* **389**, 173-176.

Rudnick R. L. (1995) Eclogite xenoliths: samples of Archean ocean floor. *Sixth Internat. Kimerlite Conf.*, 473-475.

Rudnick R. L. and Fountain D. M. (1995) Nature and composition of the continental crust: A lower crustal perspective. *Rev. Geophys.* **33**, 267-309.

Smyth J. R., Caporuscio F. A., and McCormick T. C. (1989) Mantle eclogites: evidence of igneous fractionation in the mantle. *Earth Planet. Sci. Lett.* **93**, 133-141.

Snyder G. A., Taylor L. A., Crozaz G., Halliday A. N., Beard B. L., Sobolev V. N., and Sobolev N. V. (1997) The origins of Yakutian eclogite xenoliths. *J. Petrol.* **38**, 85-113.

Sylvester P. J. (1994) Archean granite plutons. In *Archean crustal evolution* (ed. K. C. Condie), pp. 261-314. Elsevier.

Taylor L. A. and Neal C. R. (1989) Eclogites with oceanic crustal and mantle signatures from the Bellsbank kimberlite, South Africa, Part I: Mineralogy, petrography, and whole rock chemistry. *J. Geol.* **97**, 551-567.

Tompkins L. A. and Haggerty S. E. (1984) The Koidu Kimberlite Complex, Sierra Leone: Geological setting, petrology and mineral chemistry. In *Kimberlites; I, Kimberlites and related rocks*, Vol. 11A (ed. J. Kornprobst), pp. 83-105. Elsevier.

Williams H. R. (1978) The Archaean geology of Sierra Leone. *Precambrian Res.* **6**, 251-268.

Wyllie P. J., Wolf M. B., and van der Laan S. R. (1997) Conditions for formation of tonalites and trondhjemites: magmatic sources and products. In *Greenstone Belts* (ed. M. J. de Wit and L. D. Ashwal), pp. 256-266. Oxford University Press.

Chapter 2

Geochemistry of Xenolithic Eclogites from West Africa, Part I: A Link between low MgO Eclogites and Archean Crust Formation

Matthias G. Barth[1*], Roberta L. Rudnick[1†], Ingo Horn[1◊], William F. McDonough[1†], Michael J. Spicuzza[2], John W. Valley[2], and Stephen E. Haggerty[3]

[1] Department of Earth and Planetary Sciences, Harvard University, 20 Oxford Street, Cambridge, MA 02138, USA
[2] Department of Geology and Geophysics, University of Wisconsin, 1215 W. Dayton Street, Madison, WI 53706, USA
[3] Department of Geosciences, University of Massachusetts, Morrill Science Center, Amherst, MA 01003, USA

present address:

* Faculty of Earth Sciences, Utrecht University, Budapestlaan 4, 3584 CD Utrecht, The Netherlands
† Department of Geology, University of Maryland, College Park, MD 20742, USA
◊ Laboratory for Inorganic Chemistry, ETH Zürich, Universitätsstrasse 6, CH-8092 Zürich, Switzerland

Geochimica et Cosmochimica Acta (2001) **65**, 1499-1527

2.1. Abstract

Oxygen isotope, mineral trace element, and measured and reconstructed whole rock compositions are reported for low MgO (6-13 wt% MgO in the whole rock) eclogite xenoliths from the Koidu Kimberlite Complex, Sierra Leone. The $\delta^{18}O$ values of garnet (4.7 to 6.8‰), determined by laser fluorination on clean mineral separates, extend beyond the range for mantle peridotites. All low MgO eclogites have reconstructed trace element patterns that are depleted in Ba, Th, U, and light REE, with jadeite-rich samples having more variable trace element patterns than jadeite-poor samples. These observations, coupled with low SiO_2 contents, and Nb-rich but LREE-depleted reconstructed whole rock compositions, suggest the low MgO eclogites are remnants of altered oceanic crust that was partially melted during subduction. Partial melting of a mafic protolith at high pressure (leaving a garnet-bearing residue) is the preferred model to explain the origin of Archean Tonalite-Trondhjemite-Granodiorite (TTG) suites, which make up large portions of the crust in Archean cratons. We therefore suggest that the Koidu low MgO eclogites may be residues from Archean continental crust formation.

2.2. Introduction

Eclogite xenoliths are minor but ubiquitous constituents of mantle xenolith suites brought up by kimberlites in Archean (and Proterozoic) cratons. High equilibration temperatures and the presence of diamond in some eclogite xenoliths suggest derivation from the upper mantle. However, the origin of their protoliths and the subsequent metamorphic evolution of these bi-mineralic rocks are less certain. The different hypotheses proposed for the origin of eclogite xenoliths can be divided into two groups. According to the "mantle" hypothesis, eclogites are produced by high-pressure crystallization from peridotite-generated magmas that ascend through the lithosphere (Smyth et al., 1989; Caporuscio and Smyth, 1990). The "crustal" hypothesis argues that eclogites are remnants of subducted (Archean?) oceanic crust, which may or may not have been through a melting episode associated with subduction (Helmstaedt and Doig, 1975; MacGregor and Manton, 1986; Taylor and Neal, 1989; Ireland et al., 1994; Jacob et al., 1994). A variant of the crustal hypothesis, that has not been widely explored, is that eclogites may be products of metamorphism of mafic lower continental crust, i.e., products of isobaric cooling at high pressure of gabbroic to anorthositic protoliths (Pearson et al., 1991; El Fadili and Demaiffe, 1999).

Evidence cited in support of the mantle hypothesis includes mineralogical layering, cumulate textures, exsolution of garnet from pyroxene, mantle-like oxygen isotope signatures (Smyth et al., 1989; Snyder et al., 1997), and high Cr_2O_3 contents in some xenolithic eclogites (Taylor and Neal, 1989).

The most compelling evidence for the crustal origin of eclogite xenoliths are oxygen isotope compositions that deviate from established peridotitc values, i.e., whole rock $\delta^{18}O$ values that lie beyond $5.5 \pm 0.4‰$ (Mattey et al., 1994a), but within the range of oxygen isotopes observed in the basaltic sections of ophiolites (see Muehlenbachs, 1986). The fractionation of oxygen isotopes requires low-temperature processes at or close to the surface of the Earth (Clayton et al., 1975). Therefore, samples from the upper mantle with $\delta^{18}O$ outside the mantle range are interpreted either as parts of subducted slabs or as having been contaminated with melts or fluids from subducted slabs. Similar arguments can be made based on carbon isotopes (see Schulze et al., 1997). Moreover, high Al contents of some xenolithic eclogites (manifested by the occurrence of accessory phases such as kyanite and corundum) have been cited as evidence for low-pressure crystallization of plagioclase-rich protoliths (crustal pressures rather than upper mantle; Jacob et al., 1998; Jacob and Foley, 1999).

In addition to stable isotopes, trace element geochemistry is a powerful tool with which to investigate the concealed evolutionary record of eclogites and to constrain possible precursors. However, a significant problem in any geochemical study of eclogite xenoliths is to determine the pristine, pre-entrainment composition of these rocks. All eclogite xenoliths exhibit variable degrees of alteration produced by partial melting, metasomatism and/or by interaction with their kimberlitic hosts (Ireland et al., 1994; McCormick et al., 1994; Harte and Kirkley, 1997; Snyder et al., 1997). In general, omphacite is affected more severely than garnet (Taylor and Neal, 1989; Fung and Haggerty, 1995), with kyanite-bearing eclogites showing the highest degrees of alteration (Harte and Kirkley, 1997; Snyder et al., 1997). In order to see through these effects of

alteration, the original whole rock composition must be calculated from the unaltered parts of primary mantle phases. Recent work has utilized in situ trace element measurements for this purpose (e.g., Jerde et al., 1993; Ireland et al., 1994; Harte and Kirkley, 1997; Jacob and Foley, 1999).

Xenolithic eclogites from the Koidu kimberlite complex in Sierra Leone, West Africa, fall into two groups, based on their major element and mineral chemistry (Fig. 2.1; Hills and Haggerty, 1989; Fung and Haggerty, 1995): a high MgO group (>16 wt% MgO) and a low MgO group (6-13 wt% MgO). It has recently been suggested that the Koidu low MgO eclogites have complementary major element compositions to granitoids from the West African Craton, indicating that both were derived from a common basaltic parent rock with a composition similar to greenstone belt basalts in Sierra Leone (Rollinson, 1997). In order to investigate this possibility and to constrain the origin(s) and evolution of the Koidu eclogites we have undertaken an oxygen isotope and trace element study of these rocks. This paper reports the oxygen isotopic compositions and the trace element compositions of low MgO eclogites previously studied by Hills and Haggerty (1989) and Fung and Haggerty (1995). Chemical and isotopic characterization and the genesis of the high MgO eclogites will be presented in a second paper.

2.3. Geological Background and Sample Description

The Mesozoic Koidu kimberlite complex is located on the Man Shield in West Africa, which lies near the former center of a Precambrian craton that was rifted apart by the opening of the Atlantic Ocean in the Mesozoic to form the West African Craton and

the Guyana Shield in South America. The Man Shield is situated in the southern West African Craton and has been divided into three age provinces (Macfarlane et al., 1981): Leonean (~3.0 Ga), Liberian (~2.7 Ga), and Eburnian (~2.0 Ga). However, due to the limited radiometric dating (Rb-Sr and Pb-Pb whole rock) there is a debate as to whether the Leonean and the Liberian are two separate events or a single, long-lived event (Williams, 1978). A younger Pan-African age province defines a tectonic event at ~550 Ma in the coastal belt of Sierra Leone and Liberia.

The Archean basement (Leonean and Liberian provinces) of Sierra Leone is typical of granite-greenstone terrains found in ancient continental nuclei. The older tonalite-trondhjemite-granodiorite (TTG) gneisses (~2.9 Ga; Beckinsale et al., 1980; Barth et al., 1999) form between 60-70% of the outcrop area and are the major rock type of the Man Shield. Younger granites (2.7-2.8 Ga) intrude the margins of the greenstone belts or occur as thick sheets cross-cutting the greenstone belts at high structural levels. The composition of the TTG gneisses range from diorite to granodiorite (Rollinson, 1978). The Koidu kimberlite complex occurs in the interior of this basement. Country rocks to the kimberlites include amphibolite-facies migmatites, TTG gneisses, ironstones, and ultramafic suites.

Hills and Haggerty (1989) and Fung and Haggerty (1995) describe the petrography and report mineral chemical data for 87 eclogite xenoliths and whole rock XRF major and trace element data for 25 of these samples from the Koidu pipes. The high MgO group (>16 wt% MgO) is essentially bi-mineralic, with only minor ilmenite, and/or sulfide occurring in addition to garnet and omphacite. The low MgO group (6-13 wt% MgO) commonly contains accessory phases such as kyanite, graphite, quartz (after

coesite), diamond, amphibole, and/or corundum plus rutile, ilmenite, and/or sulfides in addition to garnet and omphacite. Generally, both high and low MgO eclogites fall into group II eclogites of McCandless and Gurney (1989), i.e., low Na garnets and low K omphacite, except for the diamond-bearing eclogites and a single graphite-bearing eclogite that fall into group I.

The Koidu eclogites range from nearly pristine rocks with alteration restricted to grain boundaries (e.g., KEC 81-5) to samples with highly altered, opaque clinopyroxene with small relict areas of pristine omphacite in the centers of crystals (e.g., KEC 91-1; see Fig. 1 of Hills and Haggerty, 1989). Numerous secondary minerals occur in veins within the more altered eclogites. These minerals include phlogopite, amphibole, plagioclase, ilmenite, rutile, sulfide, spinel, and carbonates. Thus, rutile occurs both as primary and secondary phase. Secondary (metasomatic) rutile is distinguished by much higher and heterogeneous Nb and Ta contents and occasionally by a skeletal texture. Of the samples analyzed by laser ablation ICP-MS, only samples KEC 81-10A, KEC 81-18, and KEC 81-21 contain metasomatic rutile. Based on textures, trace element homogeneity, and evidence for equilibrium between rutile and primary silicates, all rutiles reported in Table 2.5 and in Rudnick et al. (2000) are considered primary.

The Koidu eclogites show a large range of textures, estimated equilibration temperatures, and pressures, extending from 760 °C at 2.8 GPa to 1188 °C at 5 GPa (using the Ellis and Green (1979) geothermometer and the Kalahari geotherm of Rudnick and Nyblade (1999)). The P-T ranges of the high and low MgO eclogites differ significantly (Hills and Haggerty, 1989; Fung and Haggerty, 1995); many high MgO

eclogites record conditions between 1080-1130 °C and 4.0-4.5 GPa, whereas the low MgO eclogites cluster between 880-930 °C and 3.3-3.6 GPa.

2.4. Analytical Methods

Mineral separates for laser fluorination oxygen isotope ratio analysis were prepared by standard procedures including initial crushing in alumina ceramics followed by magnetic separation. Purity of samples was ensured by hand picking, with sample weights for each analysis ranging between 1 and 3 mg. Oxygen isotope ratios were measured at the University of Wisconsin, Madison, using a laser-assisted fluorination technique described by Valley et al. (1995). This method provides high oxygen yields for refractory minerals like garnet. In most cases repeat analyses fall within 0.1 ‰ of each other, demonstrating the good reproducibility of the technique and the purity of the mineral separates. Measured values were corrected (≤0.1‰) based on three to four analyses of garnet standard UWG-2 at the start of each day (Table 2.2; Valley et al., 1995). Corrected values are reported relative to V-SMOW (Coplen, 1996).

Whole rock trace element compositions were determined by inductively coupled plasma-mass spectrometry (ICP-MS). Samples were dissolved in a mixture of ultrapure, concentrated HF–HNO_3 and then spiked with a mixed multi-element/enriched isotope internal standard solution prior to analysis, following the technique of Eggins et al. (1997). Complete dissolution of the samples was ensured by the use of conventional oven bombs. Analyses were performed on a Fisons (VG Elemental) PQ II+ in pulse counting mode (three points per peak). Sensitivity of the instrument was on average ~50 MHz

(million counts per second per ppm) for ^{115}In. Standard data and typical precision are reported in Barth et al. (2000).

Trace element compositions of garnets, omphacites, rutiles, and ilmenites were determined by laser ablation (LA-) ICP-MS, utilizing both a home-built excimer system (Horn et al., 2000), and later, the Merchantek DUV system, which was developed from our proto-type design. Ablation is achieved by a 193 nm Ar-F excimer laser system using a pulse repetition rate of 10 Hz and pulse energy of ≤0.5 mJ (Horn et al., 2000). Analyses were performed in pulse counting mode (one point per peak); dwell time and quadrupole settling time were set to 10 ms and 5 ms, respectively. Data reduction follows the procedure outlined in Longerich et al. (1996). The amount of material ablated in laser sampling is different for each spot analysis. Consequently, the detection limits are different for each spot and are calculated for each individual acquisition. Typical pit diameters and ablation time for silicates were ~150 μm and 60 s, respectively, resulting in detection limits of 20 ppb for Ta, Th and U, 50 ppb for the REE (rare earth elements), 0.5 ppm for Rb and Sr and 1 ppm for Sc. ^{44}Ca and ^{49}Ti were used as internal standards for silicate and oxide analyses, respectively. For our analyses we calibrated against the silicate glass reference materials NIST 610 and NIST 612, and the USGS glass standards BCR-2g and BIR-1g were measured to monitor accuracy (Table 2.1).

Table 2.1. USGS reference glass standards BCR-2g and BIR-1g analyzed by LA-ICP-MS during the course of this study. All concentrations are given in ppm (µg/g) except TiO_2 and MnO in wt%. n. d. = not determined. b. d. = below detection limit.

	isotope analyzed	NIST 610 reference value	NIST 612 reference value	BCR-2g reference value	BCR-2g ppm	RSD %	n	BIR-1g reference value	BIR-1g ppm	RSD %	n
Sc	45	441.1	41.05	32.6	35.1	7.9	68	44.0	46.1	8.9	28
TiO_2 (wt%)	49	0.07	0.01	2.24	2.54	10.3	68	1.06	1.10	13.4	28
V	51	441.7	37.56	407	423	6.9	62	339	332	4.8	28
Cr	52	405.2	34.9	16	17	19.7	54	382	403	5.7	26
MnO (wt%)	55	0.06	0.01	0.18	0.20	9.1	44	0.16	0.19	7.3	28
Ni	60	443.9	38.8	13	13	18.8	24	175	188	12.7	28
Zn	66	456.3	37.92	130	163	12.2	14	71	98	9.4	16
Ga	69	438.1	35.88	22	22	6.8	10	16	16	4.2	4
Rb	85	431.1	31.06	47.5	48.6	10.2	64	0.20	0.22	28.3	4
Sr	88	497.4	75.33	337	318	5.2	66	104	102	5.0	28
Y	89	449.9	36.57	32.5	31.5	7.9	66	13.3	13	7.2	28
Zr	90	439.9	35.18	176	165	7.9	66	11.9	12	6.9	28
Nb	93	419.4	38.9	13.1	11.7	8.1	66	0.47	0.49	18.8	20
Mo	95	376.8	38.30	287	263	12.0	14	0.5	b. d.		
Sn	118	396.3	37.67	2.7	4.3	20.5	10	0.54	2.87	23.4	3
Sb	121	368.5	38.44	0.62	b. d.			0.58	0.63	24.5	6
Cs	133	360.9	41.8	1.19	1.16	13.8	51	0.008	b. d.		
Ba	138	424.1	38.94	684	647	7.5	52	6.2	6.5	6.8	12
La	139	457.4	35.68	25.3	23.9	5.1	52	0.59	0.61	8.7	12
Ce	140	447.8	37.91	53.6	49.3	7.7	66	1.87	1.80	9.5	28
Pr	141	429.8	37.45	6.83	6.40	6.5	18		n. d.		
Nd	146	430.8	34.6	28.6	26.8	5.6	52	2.3	2.2	6.2	10
Sm	147	450.5	36.8	6.67	6.29	8.4	65	1.01	1.05	12.2	23
Eu	151	461.1	34.4	2.00	1.80	8.1	52	0.48	0.52	12.9	12
Gd	157	419.9	36.95	6.80	6.15	9.2	46	1.64	1.80	9.3	12
Tb	159	442.8	36.93	1.04	0.95	7.5	18		n. d.		
Dy	162	426.5	35.97	6.38	6.13	8.7	65	2.33	2.29	10.3	26
Ho	165	449.4	37.27	1.29	1.19	8.3	24		n. d.		
Er	166	426	37.91	3.66	3.48	9.9	52	1.48	1.65	10.7	12
Tm	169	420.1	37.33	0.54	0.49	10.3	18		n. d.		
Yb	174	461.5	38.14	3.34	3.17	10.3	65	1.48	1.51	9.9	24
Lu	175	434.7	37.2	0.51	0.48	12.8	52	0.23	0.23	14.1	14
Hf	178	417.7	38.14	4.8	4.8	11.1	64	0.46	0.55	13.9	21
Ta	181	376.6	39.33	0.78	0.72	13.7	66	0.031	0.031	24.1	8
W	182	445.3	39.55	0.44	0.70	30.4	12	0.2	b. d.		
Pb	208	413.3	38.96	10.3	11.0	9.4	41	2.85	3.54	12.4	16
Th	232	450.6	36.66	5.98	5.55	9.8	65	0.025	0.033	26.6	15
U	238	457.1	36.66	1.7	1.6	11.5	65	0.022	0.029	26.1	12

Notes to Table 2.1:
Reference values from Simon E. Jackson's Lamtrace© with updates from Pearce et al. (1997) for NIST 610 and NIST 612 and from Reid et al. (1999) for Zr and Hf in BCR-2g.

2.5. Results

2.5.1. Oxygen Isotopes

Garnet oxygen isotopic data were obtained for 31 low MgO eclogites (Table 2.2, Fig. 2.1). Garnet is usually the freshest phase in eclogite xenoliths, is more resistant to isotopic resetting than clinopyroxene (Deines and Haggerty, 2000), and shows a larger range in composition (e.g., FeO content) than clinopyroxene (cpx). Garnet analyses are representative of the whole rock oxygen isotopic composition because the theoretical and observed high-temperature isotope fractionation between garnet and cpx is small (<0.4‰; Rosenbaum and Mattey, 1995; Kohn and Valley, 1998; Snyder et al., 1998), with garnet generally being lighter than cpx.

Values of $\delta^{18}O$ in the Koidu eclogites range between 4.68 and 6.78‰ for garnet (n = 31, Fig. 2.1), between 5.12 and 5.73‰ for cpx (n = 3), and between 5.48 and 5.70‰ for kyanite (n = 3). Thus, neither very heavy nor very light values, as reported from South African eclogites (between 2.2 and 8.0‰, determined by conventional fluorination; MacGregor and Manton, 1986) are observed.

Eighteen of the low MgO garnets lie within the mantle range (based on garnets from peridotites; $\delta^{18}O = 5.4 \pm 0.4$‰; Mattey et al., 1994b) but 13 samples exceed the mantle range, being both isotopically lighter and heavier (Fig. 2.1). Values of $\delta^{18}O$ do not show a correlation with other elements (e.g., FeO, CaO) of garnet or whole rock, as reported for some Siberian eclogite xenoliths (Jacob et al., 1994; Jacob and Foley, 1999).

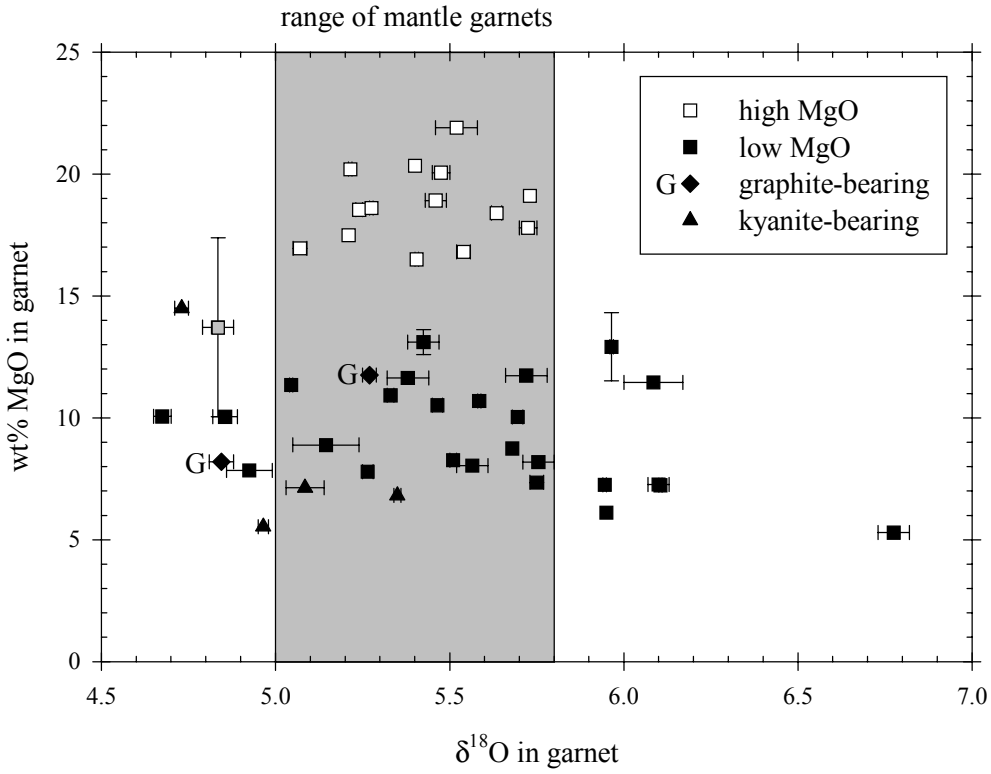

Figure 2.1. MgO in garnet vs. $\delta^{18}O$ in garnet for Koidu eclogites. Open squares represent high MgO eclogites; solid symbols show low MgO eclogites. The gray square denotes the transitional eclogite KEC 86-19. Solid squares are bi-mineralic eclogites, solid diamonds are graphite-bearing eclogites (G), and solid triangles are kyanite-bearing eclogites. Horizontal error bars show average reproducibility (½ of the difference between 2 separate measurements); vertical error bars indicate mineral zoning. The gray field depicts the range of mantle garnets that is shifted towards lighter isotopic composition by 0.1‰ relative to the whole rock mantle range due to the fractionation between garnet and whole rock.

Table 2.2. Oxygen isotopic composition of Koidu eclogite mineral separates determined by laser fluorination (all samples have KEC prefix). All values are averages of two measurements except for KEC 81-18, which is a single measurement. 1 σ is the average reproducibility, i.e., ½ of the difference between two separate measurements. Samples are corrected to garnet standard UWG-2 = 5.8‰ (Valley et al., 1995).

sample	$\delta^{18}O_{SMOW}$	1 σ	jadeite in cpx [mol%]	Sample	$\delta^{18}O_{SMOW}$	1 σ	jadeite in cpx [mol%]
low MgO garnets – bi-mineralic eclogites				*low MgO garnets – graphite-bearing eclogites*			
80-A2	5.75	0.02	27%	86-12	4.85	0.04	39%
81-3	5.27	0.01	36%	86-70	5.27	0.02	27%
81-4	5.05	0.01	23%				
81-5	5.57	0.04	6%	*low MgO garnets – kyanite-bearing eclogites*			
81-7	5.59	0.00	33%				
81-8	5.15	0.10	43%	86-1	4.73	0.02	27%
81-10A	5.72	0.06	45%	86-3	4.97	0.02	49%
81-18	5.95	-	29%	86-4	5.09	0.05	48%
81-21	6.09	0.08	34%	86-74B	5.35	0.01	45%
86-6	5.95	0.01	27%				
86-13	5.51	0.01	32%	*kyanite*			
86-14	5.68	0.00	25%				
86-34	5.38	0.06	45%	86-3	5.56	0.02	
86-36	5.97	0.01	38%	86-4	5.48	0.02	
86-56	5.33	0.01	24%	86-74B	5.70	0.11	
86-71A	4.86	0.03					
91-2	5.70	0.02	31%	*clinopyroxene*			
91-4	4.68	0.02	27%				
91-7	5.43	0.04		86-90	5.12	0.04	
core			47%	81-5	5.44	0.01	
rim			74%	91-2	5.73	0.08	
91-11	4.93	0.06	32%				
91-13	5.47	0.02	30%	*garnet standard UWG-2*			
91-20	5.76	0.05	22%				
91-22	6.11	0.00	26%	*1/22/98*	5.90	0.06	(n = 3)
91-23	6.10	0.03	27%	*6/2/99*	5.79	0.10	(n = 3)
91-58	6.78	0.05	37%	*6/3/99*	5.79	0.05	(n = 3)

Three cpx and three kyanite separates were analyzed to determine the degree of oxygen isotopic equilibrium within the xenoliths. The observed isotope fractionation for the three kyanite-garnet pairs ranges between 0.35 and 0.59‰; fractionation for the three cpx-garnet pairs vary from -0.16 to 0.04‰. Values of $\Delta^{18}O_{ky\text{-}gt}$ are well within the range

of isotope fractionations measured by laser fluorination in eclogite xenoliths from other locations (e.g., Mattey et al., 1994b), suggesting that the kyanite-garnet pairs are at (or at least close to) high-temperature isotopic equilibrium. Values of $\Delta^{18}O_{cpx\text{-}gt}$ are lower than the predicted values (0.1-0.4‰, Rosenbaum and Mattey, 1995) but it remains unresolved if this difference indicates isotopic disequilibrium or is due to differences in crystal chemistry or analytical uncertainty. Deines and Haggerty (2000) suggested that metasomatic events just prior (on the order of millions of years) to the kimberlite eruption can lower the $\delta^{18}O$ of pyroxene without significantly affecting the isotope record of garnet. Moreover, garnet is easier to analyze by laser fluorination than cpx (Valley et al., 1995) and values of $\alpha(CO_2\text{-}H_2O)$ used by different laboratories vary by up to 0.4‰ (Valley et al., 1995), requiring corrections in order to compare data sets from different laboratories.

2.5.2. Trace Element Mineral Chemistry

The trace element compositions of minerals from 21 Koidu low MgO eclogites (including garnet, cpx plus rutile or ilmenite), determined by laser ablation ICP-MS, are presented in Tables 2.3, 2.4, and 2.5. Additional rutile analyses have been published in Rudnick et al. (2000). Trace element analyses of the high MgO eclogites will be presented in a companion paper. None of the samples analyzed for trace elements contain apatite or rutile exsolution lamellae (cf. Fung and Haggerty, 1995). All samples show variable degrees of modal metasomatism. Therefore, care was taken to perform analyses on crack-free, unaltered areas of the minerals. The combination of the high-quality optical imaging system of the Harvard laser ablation setup and the time-resolved analysis

of the ablation signals ensures that altered and/or metasomatized parts of the silicate minerals were recognized and excluded from the average trace element analyses. Rutile typically shows oriented exsolution lamellae of ilmenite ± spinel at 90° angles, which were probably formed by unmixing related to cooling and/or changes in pressure. (See Haggerty (1983), and references therein, for a discussion of the origins of ilmenite lamellae in rutile.) Some rutiles show thin (several μm) ilmenite rims. Laser ablation analyses include exsolution lamellae but exclude ilmenite rims. Due to the limited grain size and the nearly opaque nature of rutile in the thick sections (~100 μm) analyzed, altered parts of the rutile grains could not always be avoided during analysis. However, these were easily distinguished by their high abundances of incompatible trace elements (e.g., Sr, Ba) and were excluded from the averages.

Garnets are light rare earth element (LREE)-depleted with chondrite-normalized La contents (La_N) from 0.01 to 0.25 (Fig. 2.2; in some samples La is below the detection limit). Most garnets have relatively flat heavy rare earth element (HREE) patterns, with $(Dy/Yb)_N$ from 0.58 to 2.2. In addition, all garnets have high HREE contents (Yb_N from 6.7 to 32), with the kyanite-bearing samples having the lowest and the graphite-bearing samples having the highest HREE contents. All garnets analyzed from kyanite-bearing samples have positive Eu anomalies (Eu/Eu* = 1.18 to 1.44) and those in graphite-bearing samples have negative Eu anomalies (Eu/Eu* = 0.82 to 0.90). All garnets show variable degrees of Zr, Hf, and Ti depletion (Fig. 2.3) except for two samples without primary rutile (KEC 81-10A and KEC 81-21). Garnets from samples with jadeite-poor (<30%) cpx have the strongest negative Zr, Hf, and Ti anomalies, while some of the

Figure 2.2. Chondrite-normalized garnet REE data for Koidu low MgO eclogite xenoliths. A: jadeite-poor eclogites (<30 mol% jadeite in cpx). B: jadeite-rich eclogites (>30 mol% jadeite in cpx). C: graphite-bearing eclogites. D: kyanite-bearing eclogites. Element abundances are normalized to the chondrite values of Boynton (1984).

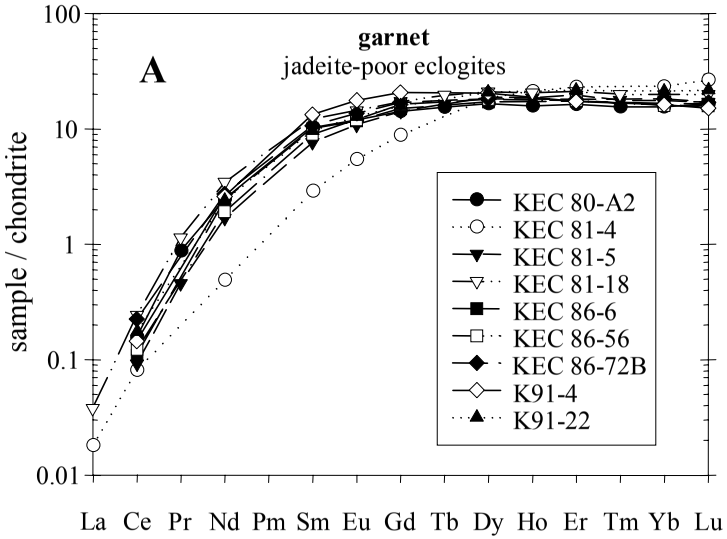
A
garnet
jadeite-poor eclogites
sample / chondrite
100
10
1
0.1
0.01
La Ce Pr Nd Pm Sm Eu Gd Tb Dy Ho Er Tm Yb Lu
KEC 80-A2
KEC 81-4
KEC 81-5
KEC 81-18
KEC 86-6
KEC 86-56
KEC 86-72B
K91-4
K91-22

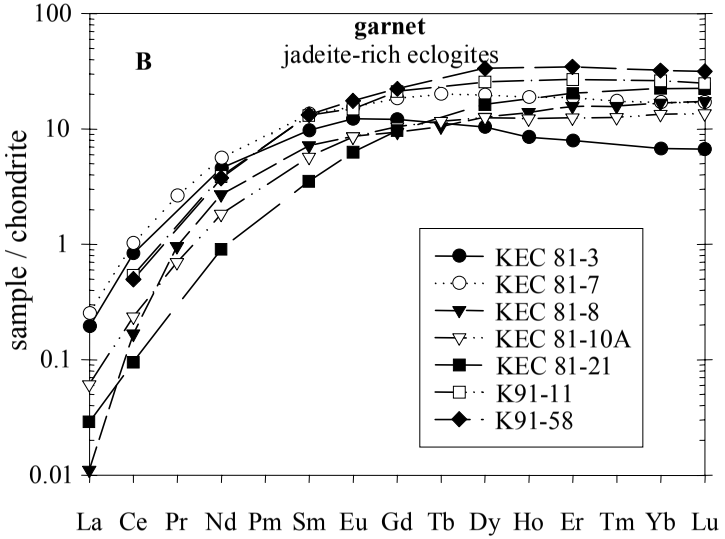
B
garnet
jadeite-rich eclogites
sample / chondrite
100
10
1
0.1
0.01
La Ce Pr Nd Pm Sm Eu Gd Tb Dy Ho Er Tm Yb Lu
KEC 81-3
KEC 81-7
KEC 81-8
KEC 81-10A
KEC 81-21
K91-11
K91-58

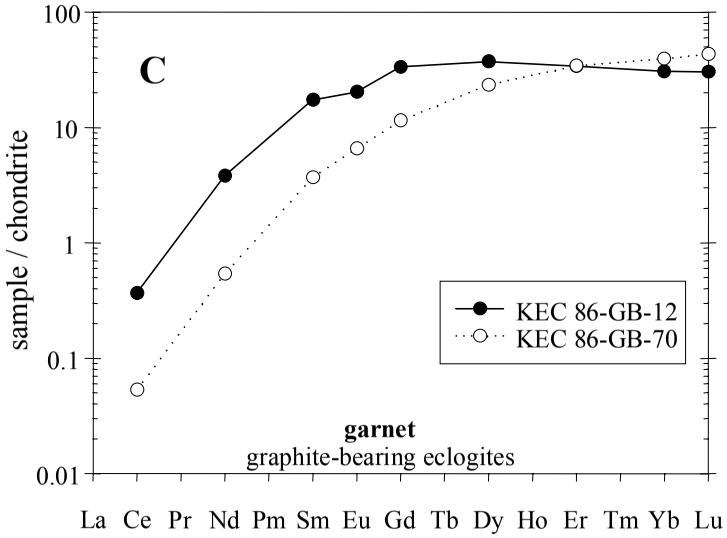
C
sample / chondrite
100
10
1
0.1
0.01
La Ce Pr Nd Pm Sm Eu Gd Tb Dy Ho Er Tm Yb Lu
KEC 86-GB-12
KEC 86-GB-70
garnet
graphite-bearing eclogites

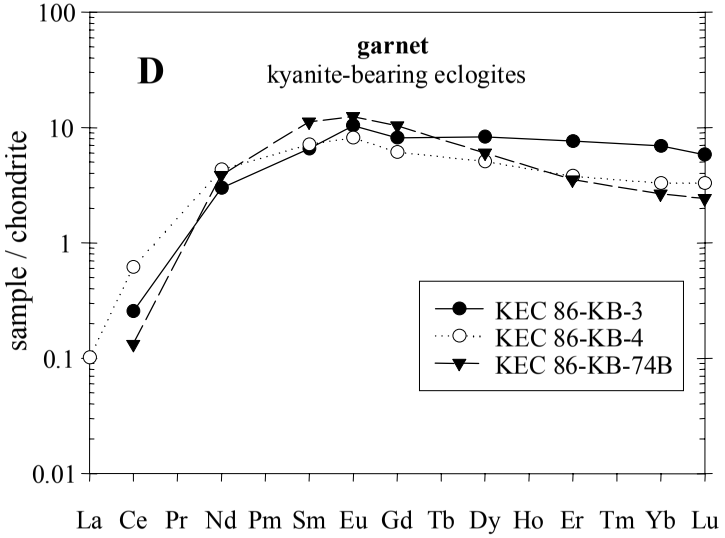
D
garnet
kyanite-bearing eclogites
sample / chondrite
100
10
1
0.1
0.01
La Ce Pr Nd Pm Sm Eu Gd Tb Dy Ho Er Tm Yb Lu
KEC 86-KB-3
KEC 86-KB-4
KEC 86-KB-74B

Figure 2.3. Mantle-normalized garnet trace element diagrams for Koidu low MgO eclogite xenoliths. A: jadeite-poor eclogites (<30 mol% jadeite in cpx). B: jadeite-rich eclogites (>30 mol% jadeite in cpx). C: graphite-bearing eclogites. D: kyanite-bearing eclogites. Element abundances are normalized to the primitive mantle values of McDonough and Sun (1995).

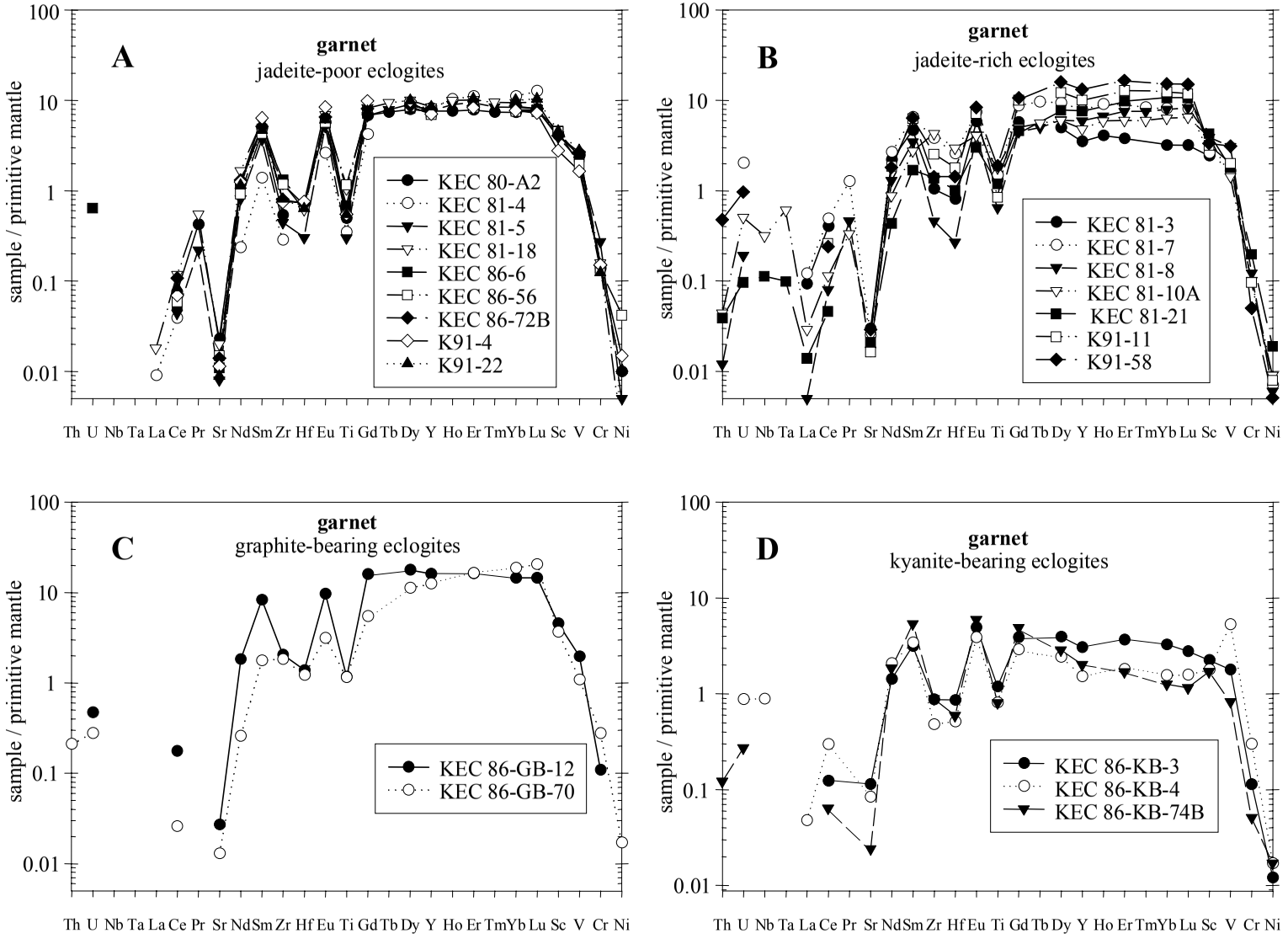
A
garnet
jadeite-poor eclogites
sample / primitive mantle
100
10
1
0.1
0.01
KEC 80-A2
KEC 81-4
KEC 81-5
KEC 81-18
KEC 86-6
KEC 86-56
KEC 86-72B
K91-4
K91-22
Th U Nb Ta La Ce Pr Sr Nd Sm Zr Hf Eu Ti Gd Tb Dy Y Ho Er Tm Yb Lu Sc V Cr Ni
B
garnet
jadeite-rich eclogites
KEC 81-3
KEC 81-7
KEC 81-8
KEC 81-10A
KEC 81-21
K91-11
K91-58
C
garnet
graphite-bearing eclogites
KEC 86-GB-12
KEC 86-GB-70
D
garnet
kyanite-bearing eclogites
KEC 86-KB-3
KEC 86-KB-4
KEC 86-KB-74B

Table 2.3. Trace element compositions of garnets determined by LA-ICP-MS. Concentrations are given in ppm (µg/g). low jadeite = <30 mol% jadeite in cpx. high jadeite = >30 mol% jadeite in cpx. n. d. = not determined. Cs, Ba, and Pb were measured but below the detection limit in all samples analyzed. Typical detection limits are 0.2 ppm for Cs, 0.05 ppm for Ba, and 0.2 ppm for Pb (see Longerich et al. (1996) for definition of LA-ICP-MS detection limits).

sample	**KEC 80-A2**		**KEC 81-4**		**KEC 81-5**		**KEC 81-18**		**KEC 86-6**		**KEC 86-56**	
	low jadeite		low jadeite		low jadeite		low jadeite		low jadeite		low jadeite	
spots	n = 10	1 σ	n = 7	1 σ	n = 7	1 σ	n = 7	1 σ	n = 7	1 σ	n = 7	1 σ
Sc	66.5	2.5	50.2	1.9	63.5	2.2	66.9	2.6	73.8	2.2	73.1	2.8
V	203	5	n.d.		179	9	207	31	195	15	161	12
Cr	361	9	n.d.		715	52	414	42	369	9	347	10
Ni	19.8	1.7	n.d.		10.6	1.4	4.7	0.2	< 30		83.1	6.0
Ga	n.d.		n.d.		n.d.		n.d.		13.3	0.8	13.0	0.6
Rb	< 0.3		< 0.3		< 0.2		< 0.3		< 0.5		< 1	
Sr	0.45	0.22	< 0.2		0.16	0.03	0.39	0.03	0.21	0.01	0.30	0.02
Y	32.8	1.6	35.1	2.4	32.7	1.0	36.4	1.0	31.8	0.3	30.0	1.2
Zr	5.66	0.42	3.01	0.61	4.65	0.24	12.8	0.1	13.8	0.5	12.4	0.4
Nb	< 0.2		< 0.2		< 0.1		< 0.03		< 0.5		< 0.6	
La	< 0.05		0.006	-	< 0.03		0.012	0.001	< 0.05		< 0.06	
Ce	0.13	0.01	0.065	0.024	0.074	0.011	0.20	0.04	0.088	0.012	0.10	0.01
Pr	0.11	0.01	n.d.		0.056	0.006	0.14	0.01	n.d.		n.d.	
Nd	1.48	0.12	0.29	0.07	1.01	0.03	2.07	0.13	1.46	0.06	1.15	0.06
Sm	2.00	0.16	0.56	0.02	1.49	0.07	2.38	0.16	1.97	0.10	1.76	0.16
Eu	0.88	0.08	0.40	0.05	0.80	0.02	1.06	0.05	0.86	0.02	0.89	0.05
Gd	3.70	0.28	2.30	0.11	3.67	0.08	4.48	0.13	3.89	0.11	4.24	0.28
Tb	0.73	0.03	n.d.		0.78	0.03	0.93	0.03	n.d.		n.d.	
Dy	5.35	0.22	6.00	0.45	6.09	0.25	6.76	0.18	5.52	0.11	5.81	0.36
Ho	1.13	0.06	1.53	0.17	1.34	0.06	1.48	0.06	n.d.		n.d.	
Er	3.43	0.09	4.87	0.64	4.13	0.13	4.42	0.10	3.67	0.07	3.70	0.25
Tm	0.51	0.02	n.d.		0.57	0.03	0.65	0.02	n.d.		n.d.	
Yb	3.26	0.21	4.92	0.59	3.69	0.08	4.14	0.15	3.46	0.07	3.35	0.25
Lu	0.53	0.04	0.85	0.07	0.55	0.02	0.64	0.03	0.53	0.01	0.51	0.04
Hf	0.14	0.04	< 0.15		0.085	0.013	0.17	0.02	0.19	0.02	0.20	0.02
Ta	< 0.04		< 0.08		< 0.02		< 0.01		< 0.02		< 0.02	
Th	< 0.04		< 0.03		< 0.02		< 0.01		< 0.01		< 0.01	
U	< 0.03		< 0.03		< 0.02		< 0.02		< 0.01		< 0.01	

Table 2.3 continued.

sample	KEC 86-72B low jadeite		K91-4 low jadeite		K91-22 low jadeite		KEC 81-3 high jadeite		KEC 81-7 high jadeite		KEC 81-8 high jadeite	
spots	n = 7	1 σ	n = 7	1 σ	n = 7	1 σ	n = 7	1 σ	n = 7	1 σ	n = 7	1 σ
Sc	65.7	2.7	45.0	1.0	74.1	1.6	39.6	0.8	42.2	2.3	63.0	2.1
V	218	34	135	2	228	10	n.d.		136	3	252	13
Cr	395	23	395	7	325	8	n.d.		< 18		319	15
Ni	< 50		29.3	3.3	20.3	1.4	n.d.		14.6	3.8	11.2	1.7
Ga	n.d.		13.7	0.9	16.3	0.4	n.d.		n.d.		n.d.	
Rb	< 1		< 0.25		< 0.62		< 0.1				< 0.2	
Sr	0.28	0.07	0.23	0.03	0.18	0.003	0.60	0.10	0.49	0.02	0.34	0.04
Y	34.0	1.3	30.4	1.4	36.6	2.4	15.0	0.6	33.6	0.8	25.4	1.2
Zr	8.34	0.66	7.85	0.67	8.48	1.18	10.9	0.6	40.0	1.3	4.83	0.17
Nb	< 0.4		< 0.09		< 0.26		< 0.1		< 0.1		< 0.03	
La	< 0.2		< 0.04		< 0.06		0.06	0.01	0.078	0.014	0.003	-
Ce	0.18	0.02	0.12	0.06	0.14	0.04	0.67	0.04	0.83	0.11	0.13	0.01
Pr	n.d.		n.d.		n.d.		n.d.		0.32	0.02	0.12	0.01
Nd	1.64	0.19	1.56	0.07	1.44	0.12	2.74	0.13	3.36	0.16	1.62	0.08
Sm	2.08	0.10	2.60	0.38	1.89	0.24	1.89	0.13	2.64	0.22	1.40	0.11
Eu	1.00	0.09	1.30	0.12	0.94	0.06	0.90	0.04	1.14	0.06	0.63	0.04
Gd	4.40	0.24	5.36	0.47	4.10	0.34	3.13	0.19	4.77	0.20	2.43	0.11
Tb	n.d.		n.d.		n.d.		n.d.		0.95	0.07	0.50	0.02
Dy	5.88	0.43	6.59	0.33	6.73	0.67	3.34	0.12	6.34	0.27	4.07	0.20
Ho	n.d.		n.d.		n.d.		0.61	0.02	1.36	0.09	0.99	0.06
Er	3.79	0.13	3.63	0.23	4.56	0.36	1.67	0.15	3.94	0.22	3.29	0.22
Tm	n.d.		n.d.		n.d.		n.d.		0.56	0.01	0.51	0.03
Yb	3.80	0.22	3.40	0.20	4.44	0.25	1.41	0.08	3.55	0.10	3.50	0.26
Lu	0.55	0.05	0.49	0.03	0.70	0.05	0.21	0.02	0.55	0.02	0.56	0.03
Hf	0.20	0.11	0.21	0.06	0.18	0.01	0.23	0.02	0.73	0.05	0.076	0.008
Ta	< 0.07		< 0.03		< 0.05		< 0.03		< 0.02		< 0.01	
Th	< 0.05		< 0.03		< 0.05		< 0.04		< 0.02		0.001	0.001
U	< 0.05		< 0.02		< 0.02		< 0.03		0.041	0.014	0.004	0.001

Table 2.3 continued.

sample	KEC 81-10A high jadeite		KEC 81-21 high jadeite		K91-11 high jadeite		K91-58 high jadeite		KEC 86-KB-3 kyanite-bearing		KEC 86-KB-4 kyanite-bearing	
spots	n = 7	1 σ	n = 7	1 σ	n = 9	1 σ	n = 7	1 σ	n = 5	1 σ	n = 8	1 σ
Sc	62.9	3.3	69.7	1.1	51.7	1.6	54.2	1.1	36.4	1.9	28.9	1.5
V	117	14	148	12	165	10	255	10	147	6	433.1	31.3
Cr	266	34	519	44	254	28	131	5	297	26	783.7	43.8
Ni	18.2	2.3	36.6	2.1	15.7	1.9	9.9	0.6	23.3	3.2	33.2	4.8
Ga	n.d.		n.d.		14.40	0.65	18.40	0.60	n.d.		n.d.	
Rb	< 0.3		0.66	0.07	< 1.05		< 0.8		< 0.6		< 0.5	
Sr	0.50	0.03	0.41	0.03	0.33	0.03	0.58	0.07	2.28	0.14	1.66	0.07
Y	20.7	2.8	32.8	2.5	43.4	2.4	56.7	1.0	13.2	0.5	6.53	0.42
Zr	44.9	6.3	14.6	2.6	26.7	2.2	15.0	0.8	9.12	0.30	5.05	0.37
Nb	0.21	0.03	0.07	0.02	< 0.23		< 0.24		< 0.2		< 0.2	
La	0.019	0.002	0.009	0.001	< 0.08		< 0.08		< 0.1		0.029	0.003
Ce	0.19	0.02	0.08	0.02	0.44	0.06	0.40	0.09	0.21	0.07	0.50	0.08
Pr	0.085	0.012	n.d.		n.d.		n.d.		n.d.		n.d.	
Nd	1.10	0.11	0.54	0.08	2.34	0.08	2.25	0.13	1.78	0.20	2.58	0.27
Sm	1.11	0.12	0.69	0.12	2.55	0.18	2.59	0.16	1.28	0.17	1.39	0.28
Eu	0.63	0.07	0.46	0.08	1.10	0.09	1.29	0.05	0.76	0.06	0.60	0.11
Gd	2.71	0.35	2.51	0.25	5.47	0.34	5.77	0.28	2.11	0.15	1.58	0.15
Tb	0.55	0.05	n.d.		n.d.		n.d.		n.d.		n.d.	
Dy	4.03	0.49	5.26	0.28	8.23	0.77	10.78	0.49	2.66	0.23	1.63	0.25
Ho	0.88	0.10	n.d.		n.d.		n.d.		n.d.		n.d.	
Er	2.63	0.27	4.29	0.26	5.65	0.53	7.25	0.27	1.60	0.20	0.79	0.10
Tm	0.41	0.03	n.d.		n.d.		n.d.		n.d.		n.d.	
Yb	2.80	0.16	4.71	0.26	5.48	0.52	6.70	0.15	1.44	0.11	0.69	0.14
Lu	0.44	0.03	0.72	0.05	0.80	0.09	1.01	0.06	0.19	0.02	0.11	0.04
Hf	0.83	0.15	0.29	0.06	0.51	0.12	0.40	0.07	0.24	-	0.15	0.06
Ta	0.022	0.007	0.004	0.002	< 0.06		< 0.06		< 0.06		< 0.02	
Th	0.004	0.001	0.003	0.002	< 0.04		0.04	0.03	< 0.05		< 0.03	
U	0.010	0.001	0.003	0.001	< 0.04		0.02	0.01	< 0.08		0.018	0.005

Table 2.3 continued.

sample	**KEC 86-KB-74B** kyanite-bearing		**KEC 86-GB-12** graphite-bearing		**KEC 86-GB-70** graphite-bearing	
spots	n = 7	1 σ	n = 7	1 σ	n = 7	1 σ
Sc	27.6	1.6	73.7	2.4	59.4	2.0
V	67.4	8.4	162	6	89.3	5.9
Cr	134	6	285	13	723	57
Ni	32.7	5.7	< 25		33.0	-
Ga	9.91	0.33	10.7	0.5	10.3	0.8
Rb	< 0.9		< 0.7		< 1	
Sr	0.48	0.15	0.54	0.05	0.25	-
Y	8.67	0.74	68.9	1.6	53.6	0.6
Zr	9.32	4.42	21.5	3.0	19.2	1.7
Nb	< 0.4		< 0.6		< 0.9	
La	< 0.05		< 0.06		< 0.08	
Ce	0.11	0.02	0.29	0.03	0.043	0.006
Pr	n.d.		n.d.		n.d.	
Nd	2.31	0.14	2.29	0.18	0.32	0.05
Sm	2.18	0.17	3.37	0.11	0.72	0.10
Eu	0.91	0.02	1.49	0.05	0.48	0.03
Gd	2.67	0.12	8.65	0.38	2.96	0.10
Tb	n.d.		n.d.		n.d.	
Dy	1.93	0.13	11.95	0.36	7.56	0.10
Ho	n.d.		n.d.		n.d.	
Er	0.74	0.08	7.15	0.18	7.18	0.15
Tm	n.d.		n.d.		n.d.	
Yb	0.55	0.04	6.39	0.13	8.24	0.26
Lu	0.08	0.01	0.98	0.02	1.38	0.04
Hf	0.17	0.06	0.39	0.06	0.35	0.06
Ta	< 0.02		< 0.03		< 0.03	
Th	< 0.01		< 0.01		< 0.02	
U	0.006	0.001	0.010	0.006	< 0.01	

garnets of the jadeite-rich eclogites have only slightly negative Zr and Hf anomalies. In the majority of garnets, Nb and Ta are below the detection limit (0.03 to 0.3 ppm and 0.01 to 0.08 ppm for Nb and Ta, respectively, depending on spot size). Nb and Ta depletions in garnet correlate with the presence of rutile. Samples KEC 81-10A and KEC 81-21 (without primary rutile) contain the highest concentrations of Nb and Ta. The concentration of alkali and alkaline earth elements in garnets are generally very low (e.g., 0.2 to 0.6 ppm Sr) or below the detection limits (e.g., Rb, Cs, Ba), but Sr ranges between 1.6 to 2.3 ppm in kyanite-bearing samples. Th and U concentrations are very low (3 to 41 ppb) or below the detection limits.

Clinopyroxenes have convex-upward REE patterns and are LREE-enriched relative to the HREE (Fig. 2.4). La_N contents range from 0.8 to 14 and Yb_N ranges from 0.15 to 1.1. Most clinopyroxenes show pronounced Nb and Ta depletions and variable degrees of Zr and Ti depletion (except that in samples KEC 81-10A and KEC 81-21, which lack primary rutile; Fig. 2.5). The concentrations of Rb, Cs, and Ba are generally below the detection limit. Cpx in only one of the kyanite-bearing eclogites (KEC 86-KB-3) was measured because cpx in the other kyanite-bearing samples was pervasively altered to white, fine-grained aggregates.

Rutiles in the low MgO eclogites have highly variable concentrations of Nb and Ta, with Nb/Ta ranging from subchondritic to superchondritic (Table 2.5 and Rudnick et al., 2000). The rutiles have high and relatively homogeneous W, Mo, Zr, Hf, Sn, and V contents and REE and Sb contents below the detection limit. Secondary (metasomatic) rutile in KEC 81-10A and KEC 81-21 is distinguished by much higher and heterogeneous Nb and Ta contents (16,000 ppm Nb and 900-1,700 ppm Ta) and occasionally by a

Figure 2.4. Chondrite-normalized clinopyroxene REE data for Koidu low MgO eclogite xenoliths. Top: jadeite-poor eclogites (<30 mol% jadeite in cpx). Middle: jadeite-rich eclogites (>30 mol% jadeite in cpx). Bottom: kyanite- and graphite-bearing eclogites. Normalized as in Figure 2.2.

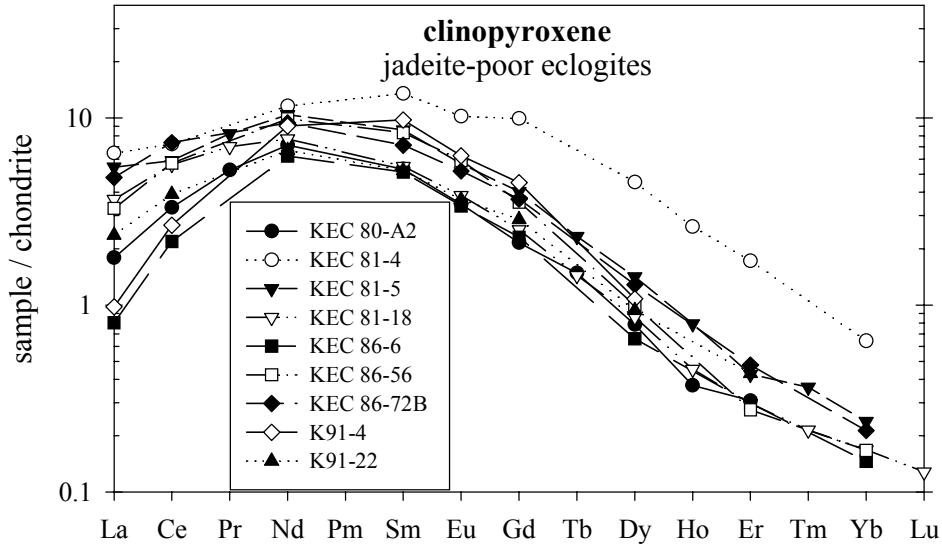
clinopyroxene
jadeite-poor eclogites
sample / chondrite
10
1
0.1
KEC 80-A2
KEC 81-4
KEC 81-5
KEC 81-18
KEC 86-6
KEC 86-56
KEC 86-72B
K91-4
K91-22
La Ce Pr Nd Pm Sm Eu Gd Tb Dy Ho Er Tm Yb Lu

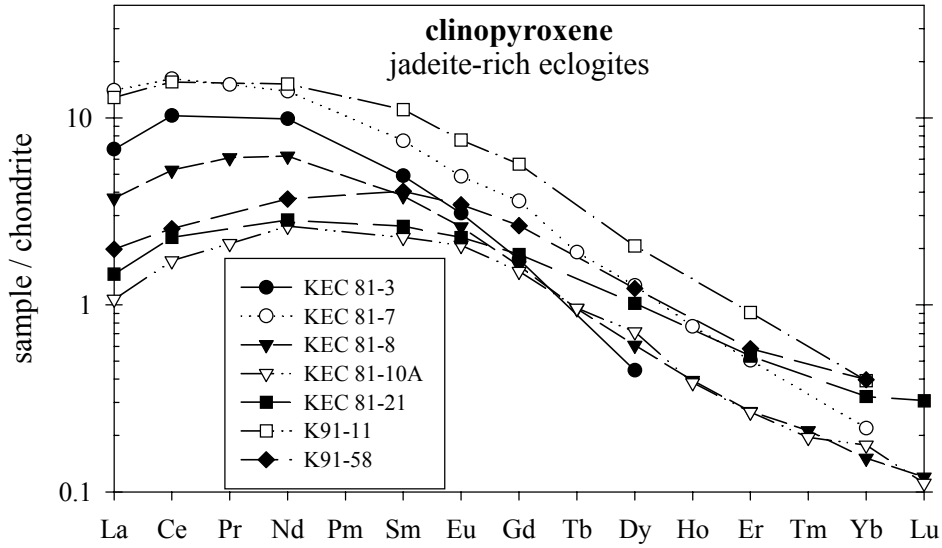
clinopyroxene
jadeite-rich eclogites
sample / chondrite
10
1
0.1
KEC 81-3
KEC 81-7
KEC 81-8
KEC 81-10A
KEC 81-21
K91-11
K91-58
La Ce Pr Nd Pm Sm Eu Gd Tb Dy Ho Er Tm Yb Lu

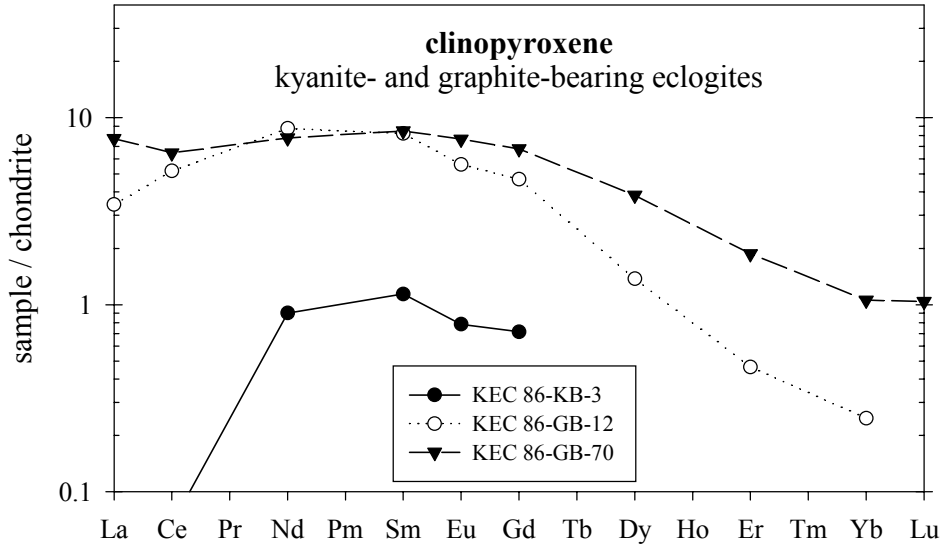
clinopyroxene
kyanite- and graphite-bearing eclogites
sample / chondrite
10
1
0.1
KEC 86-KB-3
KEC 86-GB-12
KEC 86-GB-70
La Ce Pr Nd Pm Sm Eu Gd Tb Dy Ho Er Tm Yb Lu

Figure 2.5. Mantle-normalized clinopyroxene trace element diagrams for Koidu low MgO eclogite xenoliths. Top: jadeite-poor eclogites (<30 mol% jadeite in cpx). Middle: jadeite-rich eclogites (>30 mol% jadeite in cpx). Bottom: kyanite- and graphite-bearing eclogites. Normalized as in Figure 2.3.

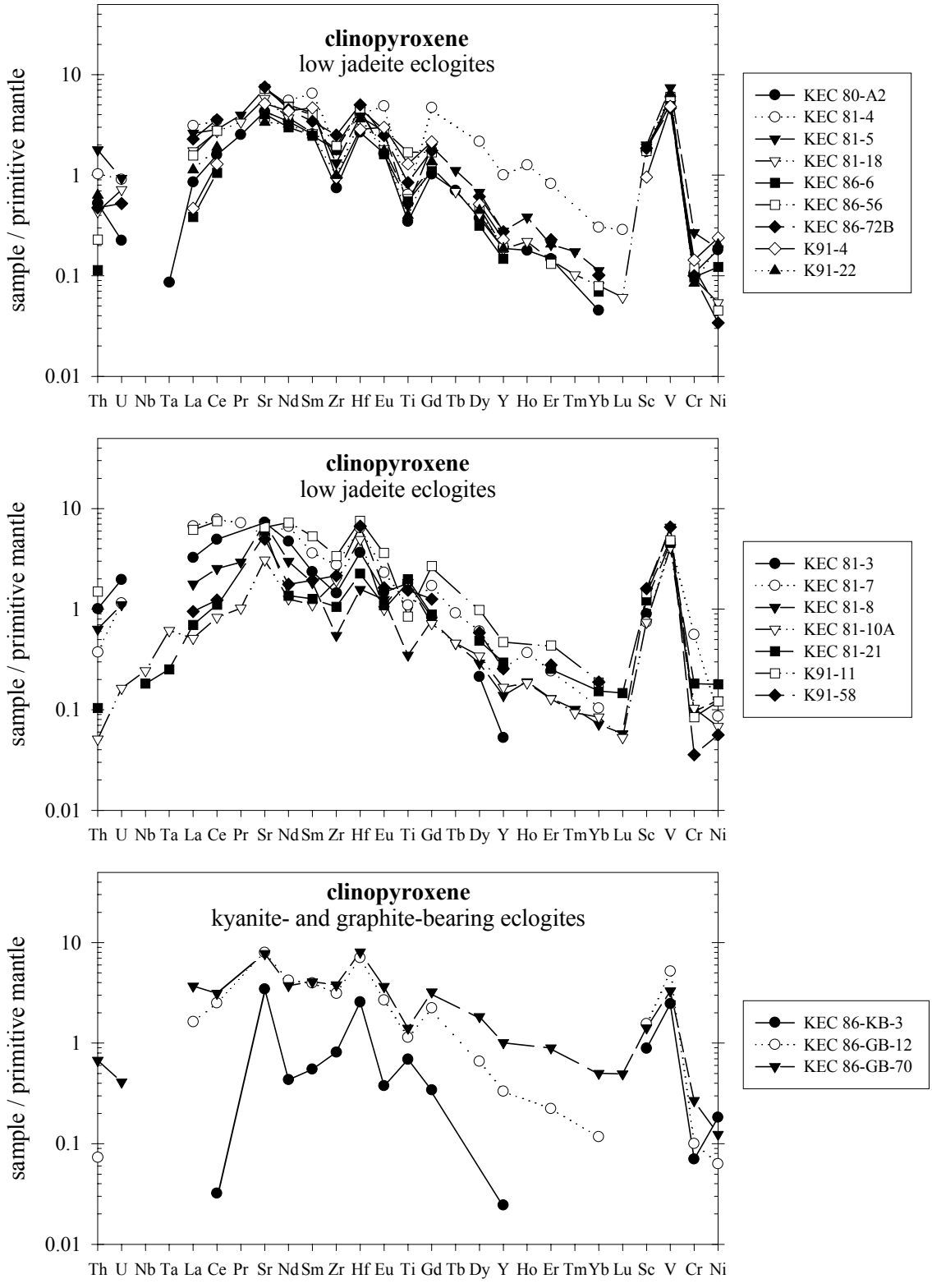
clinopyroxene
low jadeite eclogites
sample / primitive mantle
10
1
0.1
0.01
Th U Nb Ta La Ce Pr Sr Nd Sm Zr Hf Eu Ti Gd Tb Dy Y Ho Er Tm Yb Lu Sc V Cr Ni
KEC 80-A2
KEC 81-4
KEC 81-5
KEC 81-18
KEC 86-6
KEC 86-56
KEC 86-72B
K91-4
K91-22
clinopyroxene
low jadeite eclogites
sample / primitive mantle
10
1
0.1
0.01
Th U Nb Ta La Ce Pr Sr Nd Sm Zr Hf Eu Ti Gd Tb Dy Y Ho Er Tm Yb Lu Sc V Cr Ni
KEC 81-3
KEC 81-7
KEC 81-8
KEC 81-10A
KEC 81-21
K91-11
K91-58
clinopyroxene
kyanite- and graphite-bearing eclogites
sample / primitive mantle
10
1
0.1
0.01
Th U Nb Ta La Ce Pr Sr Nd Sm Zr Hf Eu Ti Gd Tb Dy Y Ho Er Tm Yb Lu Sc V Cr Ni
KEC 86-KB-3
KEC 86-GB-12
KEC 86-GB-70

Table 2.4. Trace element composition of clinopyroxene determined by LA-ICP-MS. Concentrations are given in ppm (μg/g). low jadeite = <30 mol% jadeite in cpx. high jadeite = >30 mol% jadeite in cpx. n. d. = not determined. Cs was measured but below the detection limit in all samples analyzed.

sample	**KEC 80-A2** low jadeite		**KEC 81-4** low jadeite		**KEC 81-5** low jadeite		**KEC 81-18** low jadeite		**KEC 86-6** low jadeite		**KEC 86-56** low jadeite	
spots	n = 10	1 σ	n = 7	1 σ	n = 7	1 σ	n = 7	1 σ	n = 7	1 σ	n = 7	1 σ
Sc	28.0	2.0	32.9	0.8	32.4	1.3	30.7	0.4	30.1	2.0	28.2	1.3
V	492	13	n.d.		607	6	423	16	417	5	494	11
Cr	279	20	n.d.		706	21	248	17	253	5	313	7
Ni	355	35	n.d.		362	40	107	8	239	7	87.7	20.2
Ga	n.d.		n.d.		n.d.		n.d.		16.6	0.7	18.6	0.5
Rb	< 0.4		< 0.07		< 0.3		< 0.08		< 0.5		< 0.7	
Sr	85.7	4.6	70.7	4.3	147	6	116	3	80.6	1.5	144	2
Y	0.81	0.08	4.33	0.13	1.19	0.07	0.79	0.02	0.64	0.06	0.82	0.04
Zr	7.84	0.62	19.7	2.0	13.9	0.4	19.1	1.2	18.8	2.4	20.6	0.6
Nb	< 0.1		< 0.05		< 0.08		< 0.02		< 0.5		< 0.5	
Ba	< 0.06		0.20	0.03	0.082	0.014	0.081	0.025	0.035	0.012	0.053	0.012
La	0.56	0.05	2.01	0.17	1.69	0.27	1.13	0.10	0.25	0.02	1.02	0.04
Ce	2.68	0.23	5.85	0.29	4.77	0.58	4.55	0.51	1.76	0.13	4.62	0.08
Pr	0.64	0.04	n.d.		1.00	0.08	0.86	0.07	n.d.		n.d.	
Nd	4.29	0.41	6.94	0.23	6.24	0.43	4.63	0.36	3.75	0.16	5.94	0.20
Sm	1.04	0.07	2.64	0.07	1.68	0.09	1.07	0.09	1.00	0.10	1.63	0.06
Eu	0.25	0.02	0.75	0.03	0.42	0.03	0.28	0.03	0.25	0.03	0.43	0.02
Gd	0.56	0.03	2.57	0.11	1.04	0.11	0.65	0.07	0.60	0.06	0.92	0.04
Tb	0.070	0.006	n.d.		0.11	0.01	0.068	0.007	n.d.		n.d.	
Dy	0.25	0.03	1.46	0.06	0.46	0.03	0.28	0.01	0.21	0.01	0.32	0.02
Ho	0.027	0.003	0.19	0.01	0.057	0.010	0.03	0.00	n.d.		n.d.	
Er	0.065	0.004	0.36	0.03	0.089	0.012	0.062	0.009	0.063	0.010	0.058	0.004
Tm	< 0.02		n.d.		0.012	-	0.007	0.002	n.d.		n.d.	
Yb	0.02	-	0.13	0.01	0.050	0.002	0.035	0.004	0.031	0.004	0.035	0.002
Lu	< 0.02		0.020	0.001	< 0.02		0.004	0.000	< 0.02		< 0.01	
Hf	0.75	0.15	1.15	0.08	1.09	0.08	1.24	0.06	1.28	0.07	1.30	0.04
Ta	0.003	-	< 0.02		< 0.02		< 0.01		< 0.02		< 0.02	
Pb	n.d.		n.d.		n.d.		n.d.		0.10	0.01	0.17	0.02
Th	0.042	0.015	0.082	0.008	0.14	0.02	0.035	0.005	0.009	0.002	0.018	0.005
U	0.005	0.001	0.018	0.002	0.019	0.002	0.015	0.004	< 0.01		< 0.01	

Table 2.4 continued.

sample	KEC 86-72B low jadeite		K91-4 low jadeite		K91-22 low jadeite		KEC 81-3 high jadeite		KEC 81-7 high jadeite		KEC 81-8 high jadeite	
spots	n = 7	1 σ	n = 7	1 σ	n = 7	1 σ	n = 7	1 σ	n = 7	1 σ	n = 7	1 σ
Sc	30.0	0.6	15.5	0.1	30.3	0.5	14.6	1.1	12.0	0.7	23.6	1.1
V	381	29	396	6	531	7.38	n.d.		368	4	534	29
Cr	262	47	375	7	221	8.81	n.d.		1470	596	251	17
Ni	66.4	5.9	468	17	399	11	n.d.		168	5	246	25
Ga	n.d.		21.7	0.6	19.2	0.4	n.d.		n.d.		n.d.	
Rb	< 0.4		< 0.67		0.60	0.07	< 0.1		< 0.4		< 0.1	
Sr	150	10	102	4	66.8	6.8	145	5	108	2	143	13
Y	1.18	0.04	0.98	0.10	0.80	0.06	0.23	0.04	1.12	0.03	0.60	0.02
Zr	26.3	0.8	9.94	0.66	10.5	3.2	15.2	1.0	28.9	0.8	5.74	0.19
Nb	< 0.2		< 0.4		< 0.16		< 0.1		< 0.1		< 0.03	
Ba	0.066	0.004	0.10		0.05	0.00	0.15	0.06	0.38	0.03	0.048	0.017
La	1.49	0.06	0.30	0.02	0.73	0.06	2.11	0.09	4.35	0.20	1.15	0.17
Ce	5.96	0.18	2.16	0.11	3.17	0.20	8.29	0.33	13.07	0.31	4.24	0.52
Pr	n.d.		n.d.		n.d.		n.d.		1.84	0.06	0.75	0.07
Nd	5.64	0.20	5.43	0.33	4.02	0.19	5.92	0.33	8.30	0.21	3.74	0.29
Sm	1.39	0.10	1.90	0.23	1.02	0.06	0.96	0.17	1.55	0.10	0.74	0.06
Eu	0.38	0.02	0.46	0.04	0.27	0.02	0.23	0.03	0.36	0.02	0.19	0.01
Gd	0.95	0.06	1.17	0.11	0.74	0.10	0.45	0.05	0.93	0.09	0.42	0.03
Tb	n.d.		n.d.		n.d.		n.d.		0.094	0.008	0.045	0.004
Dy	0.41	0.02	0.35	0.04	0.30	0.06	0.14	0.02	0.39	0.04	0.20	0.01
Ho	n.d.		n.d.		n.d.		< 0.03		0.055	0.005	0.028	0.004
Er	0.10	0.01	< 0.2		0.09	0.01	< 0.09		0.10	0.01	0.057	0.006
Tm	n.d.		n.d.		n.d.		n.d.		< 0.02		0.007	0.001
Yb	0.037	0.006	< 0.15		< 0.08		< 0.09		0.046	0.009	0.032	0.002
Lu	< 0.03		< 0.06		< 0.03		< 0.03		< 0.02		0.004	0.001
Hf	1.42	0.17	0.81	0.11	1.03	0.17	0.98	0.06	1.82	0.10	0.44	0.05
Ta	< 0.03		< 0.07		< 0.03		< 0.03		< 0.02		< 0.01	
Pb	0.25	0.03	0.26	0.04	0.22	0.02	n.d.		n.d.		n.d.	
Th	0.037	0.010	< 0.06		0.050	0.009	0.078	0.014	0.032	0.004	0.050	0.009
U	0.011	0.003	< 0.04		< 0.02		0.036	0.003	0.023	0.002	0.022	0.004

Table 2.4 continued.

sample	KEC 81-10A high jadeite		KEC 81-21 high jadeite		K91-11 high jadeite		K91-58 high jadeite		KEC 86-KB-3 kyanite-bearing		KEC 86-GB-12 graphite-bearing	
spots	n = 7	1 σ	n = 7	1 σ	n = 7	1 σ	n = 6	1 σ	n = 6	1 σ	n = 7	1 σ
Sc	12.0	0.5	19.7	0.3	23.4	0.4	26.0	0.8	14.4	0.5	25.2	1.5
V	335	18	373	19	397	2	538	13	202	6	424	4
Cr	270	24	479	11	222	21	94	7	184	13	264	4
Ni	132	24	350	7	237	5	110	4	360	7	123	7
Ga	n.d.		n.d.		17.8	0.4	26.5	0.6	n.d.		17.5	0.5
Rb	< 0.1		0.36	0.08	1.08	0.07	0.90	0.09	< 0.6		< 0.6	
Sr	61	2	119	9	130	3	99	6	68.5	48.5	158	3
Y	0.72	0.07	1.27	0.07	2.02	0.06	1.10	0.10	0.10	0.03	1.43	0.09
Zr	20.1	2.6	11.1	3.05	35.5	0.7	22.6	2.5	8.52	1.47	32.9	2.5
Nb	0.16	0.02	0.12	0.03	< 0.11		< 0.16		< 0.2		< 0.5	
Ba	0.041	0.008	0.061	0.013	2.08	0.23	0.066	0.015	< 0.1		0.63	0.04
La	0.33	0.04	0.45	0.02	3.98	0.14	0.61	0.06	< 0.1		1.06	0.06
Ce	1.39	0.11	1.85	0.11	12.5	0.3	2.07	0.23	0.051	0.023	4.18	0.19
Pr	0.26	0.02	n.d.		n.d.		n.d.		n.d.		n.d.	
Nd	1.58	0.10	1.70	0.13	9.08	0.41	2.21	0.08	0.54	0.17	5.24	0.31
Sm	0.45	0.04	0.51	0.05	2.16	0.17	0.79	0.08	0.22	0.02	1.60	0.09
Eu	0.15	0.01	0.17	0.02	0.56	0.05	0.25	0.02	0.06	0.01	0.41	0.03
Gd	0.39	0.06	0.48	0.05	1.46	0.13	0.69	0.13	0.19	0.01	1.21	0.05
Tb	0.045	0.005	n.d.		n.d.		n.d.		n.d.		n.d.	
Dy	0.23	0.05	0.33	0.05	0.66	0.07	0.39	0.04	< 0.3		0.44	0.05
Ho	0.028	0.005	n.d.		n.d.		n.d.		n.d.		n.d.	
Er	0.056	0.006	0.11	0.02	0.19	0.02	0.12	0.03	< 0.2		0.097	0.011
Tm	0.006	0.001	n.d.		n.d.		n.d.		n.d.		n.d.	
Yb	0.037	0.013	0.067	0.014	0.082	0.002	0.083	0.011	< 0.16		0.052	0.011
Lu	0.004	0.001	0.010	0.004	< 0.02		< 0.03		< 0.05		< 0.02	
Hf	1.40	0.25	0.64	0.11	2.14	0.14	1.89	0.12	0.73	0.12	1.99	0.16
Ta	0.023	0.008	0.009	0.003	< 0.03		< 0.05		< 0.06		< 0.02	
Pb	n.d.		0.24	0.03	1.24	0.12	0.37	0.06	n.d.		0.47	0.03
Th	0.004	0.001	0.008	0.002	0.12	0.02	< 0.03		< 0.07		< 0.01	
U	0.003	0.001	< 0.01		< 0.03		< 0.01		< 0.04		< 0.01	

Table 2.4 continued.

sample	**KEC 86-GB-70** graphite-bearing	
spots	n = 7	1 σ
Sc	23.0	1.4
V	271	3
Cr	703	14
Ni	243	12
Ga	14.1	0.5
Rb	< 0.8	
Sr	154	3
Y	4.36	0.13
Zr	39.9	1.2
Nb	< 0.7	
Ba	1.51	0.12
La	2.39	0.10
Ce	5.24	0.24
Pr	n.d.	
Nd	4.68	0.27
Sm	1.65	0.10
Eu	0.56	0.03
Gd	1.76	0.07
Tb	n.d.	
Dy	1.24	0.06
Ho	n.d.	
Er	0.393	0.033
Tm	n.d.	
Yb	0.221	0.023
Lu	0.033	0.005
Hf	2.28	0.11
Ta	< 0.02	
Pb	0.76	0.03
Th	0.054	0.008
U	0.008	0.001

skeletal texture. Secondary rutile with much higher Nb contents than primary rutile has also been reported for eclogite xenoliths from the Kasai-Congo craton Ilmenite in sample K91-58, the sole ilmenite-bearing low MgO eclogite analyzed, has trace element contents similar to rutile but lower Zr and Hf and higher Ni concentrations.

Trace element contents of kyanite are below detection limits, except for V, Cr, and Ga. However, due to the lack of an appropriate internal standard (counting rates for both Al and ^{29}Si were above the pulse-counting threshold), absolute concentrations could not be calculated.

Table 2.5. Trace element composition of rutile determined by LA-ICP-MS. Concentrations are given in ppm (μg/g). low jadeite = <30 mol% jadeite in cpx. high jadeite = >30 mol% jadeite in cpx. n. d. = not determined. Rb, Sr, Y, and REE were measured but below the detection limit in all samples analyzed. Additional data given in Rudnick et al. (2000).

sample	**K91-4** low jadeite		**K91-22** low jadeite		**K91-11** high jadeite		**K91-58** high jadeite	
mineral	rutile	1 σ	rutile	1 σ	rutile	1 σ	ilmenite	1 σ
spots	n = 7		n = 7		n = 7		n = 10	
Sc	3.12		5.43	0.80	< 4.5		6.62	0.26
V	1995	92	2400	42	1283	41	1535	89
Cr	1272	108	716	43	509	28	178	41
MnO wt%	0.020	0.011	0.020	0.010	0.008	0.007	0.32	0.05
FeO wt%	2.43	0.38	2.89	0.57	3.63	0.80	31.5	2.8
Ni	< 50		26.1		39.4	9.0	105	14
Zn	27.2	10.5	20.7	2.6	44.3	17.4	414	102
Zr	636	70	548	24	1653	111	233	24
Nb	69.9	1.2	83.0	5.2	1060	9	1785	93
Mo	< 8		6.13	1.03	8.16	1.75	< 4	
Sn	49.5	7.9	31.1	1.9	37.4	3.3	5.01	0.48
Sb	< 1.6		< 0.9		< 1		< 0.7	
Hf	18.8	3.2	25.3	3.6	39.6	4.9	4.73	1.34
Ta	8.58	0.29	2.55	1.42	8.18	0.31	79.4	16.8
W	3.24	0.76	8.38	3.88	14.86	0.80	0.83	0.47
Pb	< 0.5		< 0.3		< 0.3		0.28	0.03
Th	< 0.2		< 0.1		< 0.1		< 0.1	
U	0.66	0.03	3.15	0.59	3.36	0.17	< 0.1	

2.5.3. Clinopyroxene/Garnet Trace Element Partitioning

Both the absolute trace element concentrations and the cpx/garnet partition coefficients ($D^{cpx/gt}$) of the samples analyzed in our study show a wide range of values. $D^{cpx/gt}$ for the Koidu eclogite suite varies by two orders of magnitude for highly incompatible elements such as LREE and Sr but the variation is less with decreasing incompatibility. Such systematics are typical for high-temperature equilibrium trace element partitioning in eclogite xenolith suites (Harte and Kirkley, 1997) and indicate that the Koidu eclogites were at or close to trace element equilibrium at the time of their entrainment into the kimberlite. The changes in $D^{cpx/gt}$ for trace elements are correlated with Ca/(Ca + Mg) or Ca/(R^{2+}), where R^{2+} refers to all divalent cations, in garnet and cpx, such that $D^{cpx/gt}$ decrease as the Ca/(R^{2+}) increase (Harte and Kirkley, 1997). In particular, $D^{cpx/gt}$ for trace elements show good correlations with the molar Ca partition coefficient (D_{Ca*}), which reflects a major compositional variable of the cpx and garnets (Fig. 2.6; Harte and Kirkley, 1997). D_{Ca*} *vs.* $D^{cpx/gt}$ for compatible elements, e.g. Y (with respect to garnet and cpx), show good agreement with the trends established by Harte and Kirkley (1997) for the Roberts Victor eclogites (dashed lines in Fig. 2.6). The Koidu eclogites, however, have higher $D^{cpx/gt}$ for incompatible trace elements (e.g., Sr, Nd), especially in Ca-rich samples. This discrepancy can be explained, at least in part, by the temperature difference between the Roberts Victor eclogite suite and the Koidu suite. Based on the lattice-strain model (Blundy and Wood, 1994; Wood and Blundy, 1997), one would expect greater fractionation of incompatible elements at lower equilibration temperatures. The lower average equilibration temperature of the Koidu low MgO eclogites (880-930°C, Fung and Haggerty, 1995) compared with the samples of the

Roberts Victor suite (~1100°C at 5 GPa, Harte and Kirkley, 1997) may result in the observed higher $D^{cpx/gt}$.

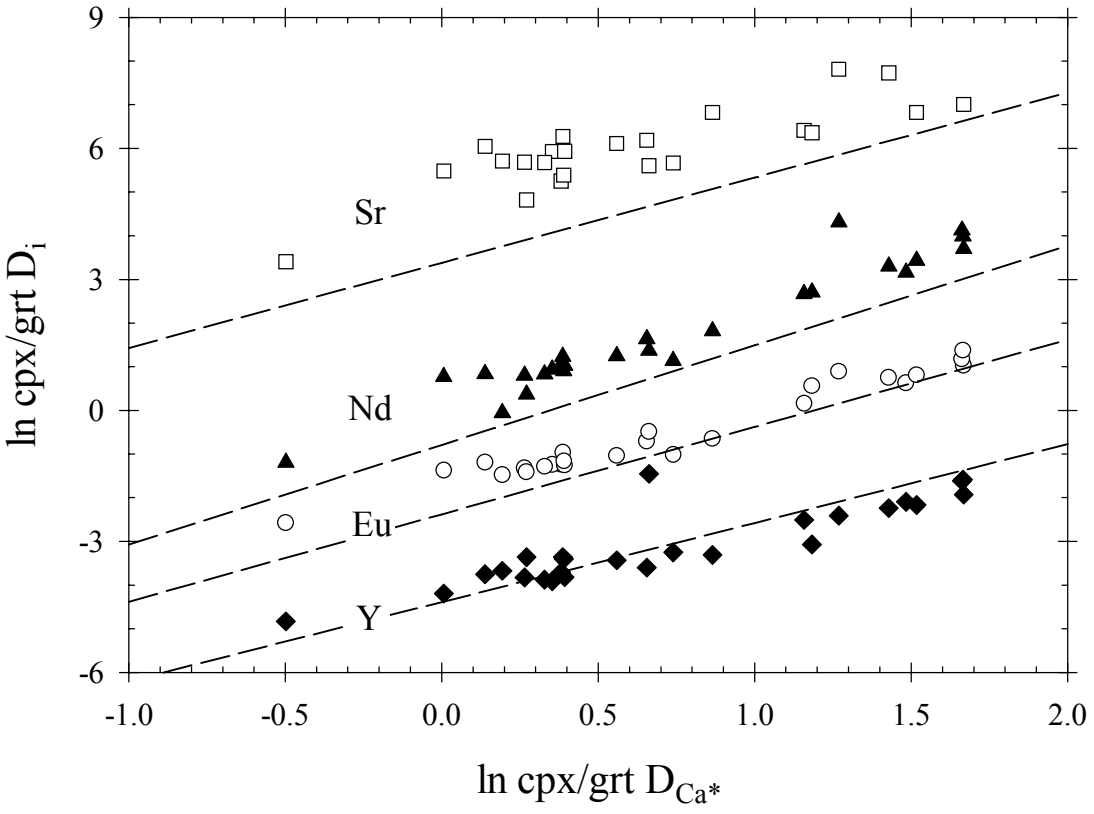

Figure 6. Natural logarithms of clinopyroxene/garnet partition coefficients, ln D_i (ppm in cpx/ppm in gt), for Sr, Nd, Eu, and Y plotted against natural logarithms of molar partition coefficients for the major cation Ca, ln D_{Ca*}. Data from the present paper and Barth et al., in prep. Dashed lines are the regression lines of Harte and Kirkley (1997) of an eclogite suite from Roberts Victor, South Africa.

2.5.4. Whole Rock Chemistry

Trace element compositions of 16 Koidu low MgO eclogite whole rock powders were determined by solution ICP-MS (Table 2.6, Fig. 2.7). All samples show variable enrichments in incompatible trace elements and flat HREE patterns (except KEC 86-74B, which is HREE depleted). Many samples have pronounced positive Nb anomalies and low Ti concentrations relative to REE. Some samples show negative Zr and Hf anomalies (e.g., KEC 81-5).

The whole rock analyses of these kimberlite-borne eclogite xenoliths are invariably enriched in incompatible trace elements relative to the compositions determined from the primary minerals alone (Fig. 2.8). Highly incompatible elements are affected more than moderately incompatible and compatible elements; for example, La shows high and variable enrichments in the analyzed whole rock while Yb is little affected by alteration. Except for rutile, accessory phases (e.g., apatite, zircon) can be ruled out as important hosts of trace elements because these phases are not observed in the samples.

In addition to the incompatible trace elements, some major elements appear to have been added to the xenoliths, as the measured whole rock compositions have higher concentrations than any of the extant primary phases. This is clearly the case for MgO, where some eclogite xenoliths have higher MgO contents in the whole rock than either garnet or cpx (see Fig. 12 in Fung and Haggerty, 1995). Thus, inexact modal estimates or small analytical uncertainties alone cannot explain the deviations between measured and reconstructed whole rock composition. Geological processes that may have contributed to these discrepancies include (1) metasomatism of eclogite in the mantle by passing silicate

Figure 2.7. Mantle-normalized whole rock trace element diagrams for Koidu low MgO eclogite xenoliths. Samples are sorted by number. Normalized as in Figure 2.3.

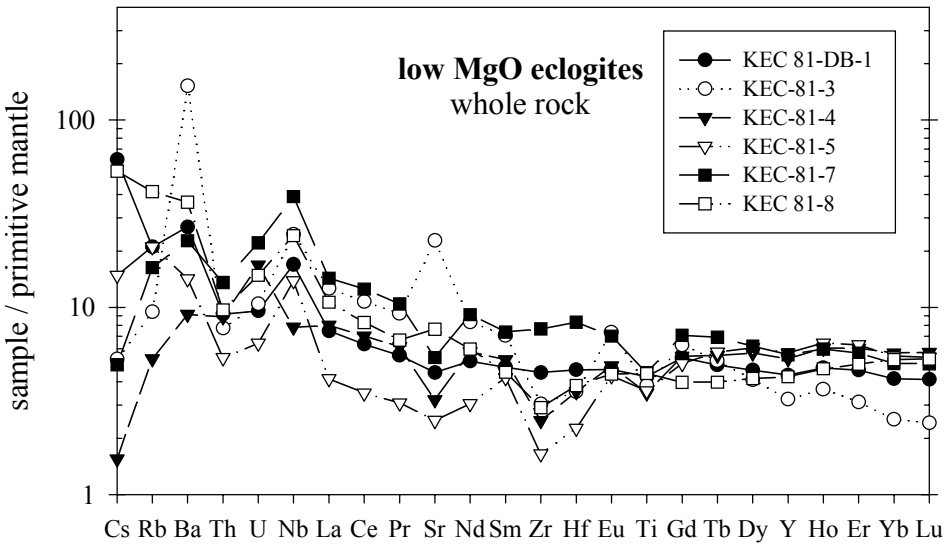
low MgO eclogites
whole rock
KEC 81-DB-1
KEC-81-3
KEC-81-4
KEC-81-5
KEC-81-7
KEC 81-8
sample / primitive mantle
100
10
1
Cs Rb Ba Th U Nb La Ce Pr Sr Nd Sm Zr Hf Eu Ti Gd Tb Dy Y Ho Er Yb Lu

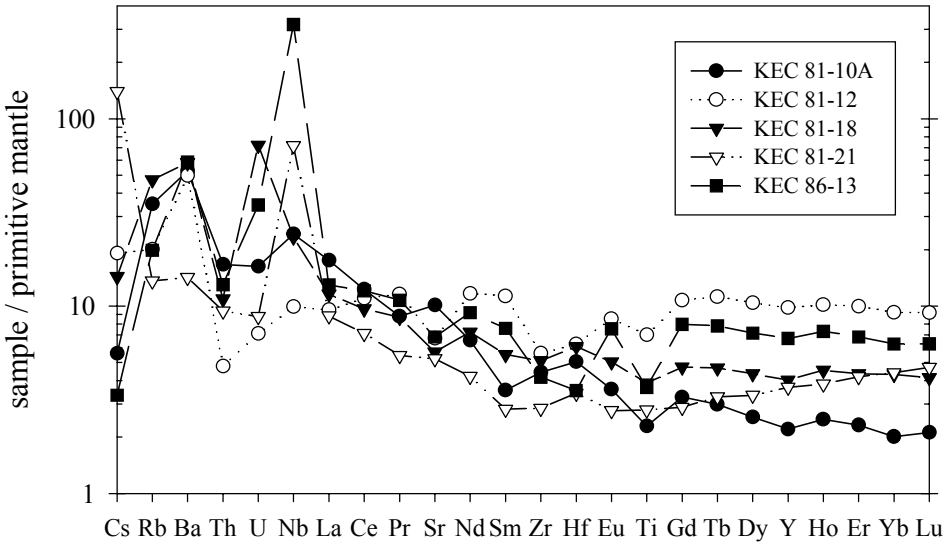
KEC 81-10A
KEC 81-12
KEC 81-18
KEC 81-21
KEC 86-13
sample / primitive mantle
100
10
1
Cs Rb Ba Th U Nb La Ce Pr Sr Nd Sm Zr Hf Eu Ti Gd Tb Dy Y Ho Er Yb Lu

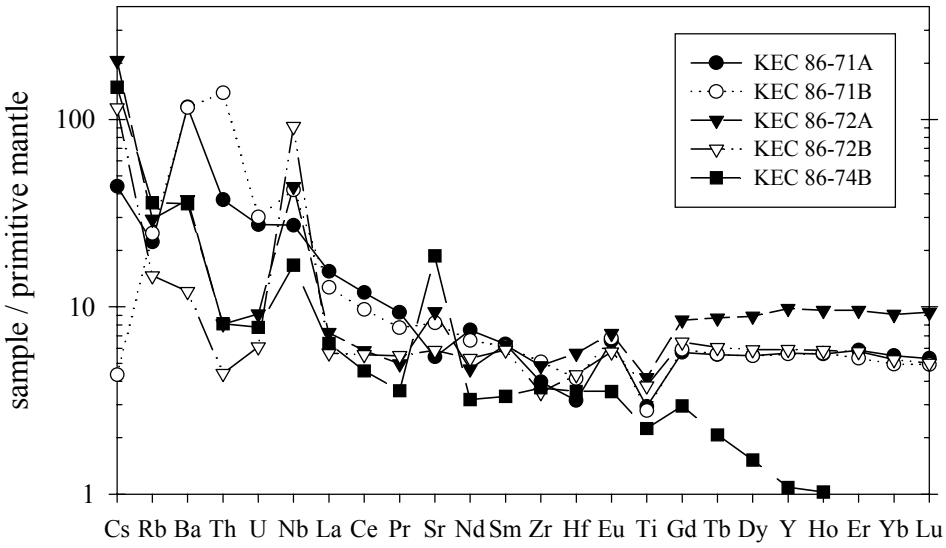
KEC 86-71A
KEC 86-71B
KEC 86-72A
KEC 86-72B
KEC 86-74B
sample / primitive mantle
100
10
1
Cs Rb Ba Th U Nb La Ce Pr Sr Nd Sm Zr Hf Eu Ti Gd Tb Dy Y Ho Er Yb Lu

Table 2.6. Whole rock compositions of the Koidu low MgO eclogites measured by solution ICP-MS. Concentrations are given in ppm (μg/g).

	KEC-81-3	KEC-81-4	KEC-81-5	KEC-81-7	KEC 81-8	KEC 81-10A	KEC 81-12	KEC 81-18
Ga	15.3	11.6	12.0	12.0	13.3	10.6	14.4	10.7
Rb	5.66	3.18	12.6	9.77	24.9	21.0	12.0	28.3
Sr	451	63.8	49.6	107	152	201	134	113
Y	13.9	22.8	24.5	24.0	18.3	9.47	42.1	17.3
Zr	32.0	26.1	17.3	80.4	30.6	46.5	58.6	53.6
Nb	16.1	5.16	9.10	25.6	15.9	16.0	6.53	15.4
Cs	0.11	0.03	0.31	0.10	1.12	0.12	0.40	0.30
Ba	1001	60.4	93.7	149	240	347	328	384
La	8.17	5.19	2.70	9.28	6.91	11.4	6.17	7.49
Ce	18.0	11.7	5.84	21.0	13.9	20.5	18.4	16.2
Pr	2.35	1.56	0.78	2.65	1.70	2.24	2.94	2.21
Nd	10.4	7.23	3.82	11.4	7.47	8.20	14.6	9.07
Sm	2.87	2.13	1.71	2.99	1.83	1.45	4.59	2.24
Eu	1.13	0.75	0.66	1.08	0.68	0.55	1.31	0.77
Gd	3.41	2.98	2.72	3.86	2.17	1.78	5.84	2.57
Tb	0.51	0.55	0.57	0.68	0.39	0.30	1.11	0.46
Dy	2.76	3.83	4.10	4.18	2.81	1.72	7.01	2.93
Ho	0.54	0.90	0.96	0.89	0.70	0.37	1.52	0.68
Er	1.36	2.65	2.76	2.49	2.18	1.01	4.37	1.90
Yb	1.11	2.51	2.42	2.21	2.32	0.88	4.08	1.90
Lu	0.16	0.39	0.36	0.34	0.36	0.14	0.62	0.28
Hf	1.00	1.00	0.64	2.36	1.08	1.43	1.77	1.72
Th	0.61	0.71	0.43	1.08	0.77	1.32	0.38	0.87
U	0.21	0.34	0.13	0.45	0.30	0.33	0.14	1.46

Table 2.6 continued.

	KEC 81-21	KEC 81-DB-1	KEC 86-13	KEC 86-71A	KEC 86-71B	KEC 86-72A	KEC 86-72B	KEC 86-74B
Ga	11.5	12.4	11.3	11.7	11.7	13.5	13.2	16.3
Rb	8.17	12.6	11.9	13.3	14.8	17.6	8.78	21.6
Sr	104	89.3	136	108	163	187	116	372
Y	15.8	18.7	28.9	24.3	24.0	42.0	25.4	4.67
Zr	29.9	47.1	43.7	41.7	53.3	50.8	36.6	38.7
Nb	47.2	11.1	209	17.9	27.6	28.8	60.2	11.0
Cs	2.93	1.29	0.07	0.92	0.09	4.34	2.42	3.12
Ba	93.8	177	387	769	762	246	79.6	234
La	5.73	4.85	8.41	10.0	8.21	4.71	3.67	4.12
Ce	11.9	10.7	20.2	19.9	16.2	9.77	9.28	7.62
Pr	1.38	1.41	2.73	2.37	1.96	1.26	1.39	0.91
Nd	5.26	6.45	11.5	9.39	8.27	5.82	6.62	4.00
Sm	1.14	1.94	3.08	2.57	2.49	2.54	2.38	1.35
Eu	0.42	0.72	1.16	1.01	1.04	1.11	0.88	0.54
Gd	1.57	2.93	4.35	3.10	3.22	4.61	3.52	1.61
Tb	0.32	0.49	0.77	0.55	0.55	0.86	0.60	0.20
Dy	2.25	3.12	4.83	3.70	3.68	6.00	3.98	1.03
Ho	0.57	0.71	1.09	0.83	0.84	1.43	0.87	0.15
Er	1.84	2.03	2.99	2.57	2.32	4.19	2.52	0.36
Yb	1.94	1.83	2.77	2.41	2.18	4.01	2.30	0.27
Lu	0.32	0.28	0.42	0.36	0.33	0.63	0.34	0.03
Hf	0.97	1.31	1.00	0.89	1.17	1.60	1.23	1.00
Th	0.75	0.73	1.03	2.96	11.0	0.64	0.35	0.65
U	0.18	0.19	0.70	0.56	0.61	0.19	0.12	0.16

or carbonate magmas, (2) alteration and development of secondary phases associated with the host kimberlite (either prior to or during entrainment), and (3) weathering and interaction with groundwater that reacts with and percolates through the kimberlite and entrained xenoliths.

The high concentrations of incompatible trace elements and MgO in the kimberlite would result in a significant increase of these elements in xenoliths that were infiltrated by kimberlitic melts without significantly affecting other major elements or HREE. Infiltration and alteration by the host kimberlite is manifested by the presence of secondary phlogopite and amphibole in veins and along grain boundaries, which may be up to 20 modal % in some samples (Hills and Haggerty, 1989). Correlations between primary and secondary phase compositions indicate that the eclogitic minerals have been directly involved in the generation of the secondary phases (McCormick et al., 1994). That is, the secondary phases are probably products of kimberlitic melts reacting with primary garnet and clinopyroxene. The secondary phases are generally a lower pressure assemblage than the primary phases, suggesting that these phases crystallized en route to the surface, in the kimberlite pipe (McCormick et al., 1994).

To evaluate this process quantitatively, we have performed mixing calculations between the host kimberlite (Taylor et al., 1994) and the reconstructed eclogites. For many samples, the differences between measured and reconstructed whole rock composition can be explained by addition of variable amounts of kimberlite. For example, the addition of ~5 wt% kimberlite to the reconstructed whole rock composition of KEC 81-7 yields a reasonable approximation to the measured trace element composition (Fig. 2.8). However, higher amounts of kimberlite addition (~10%) are required to replicate the

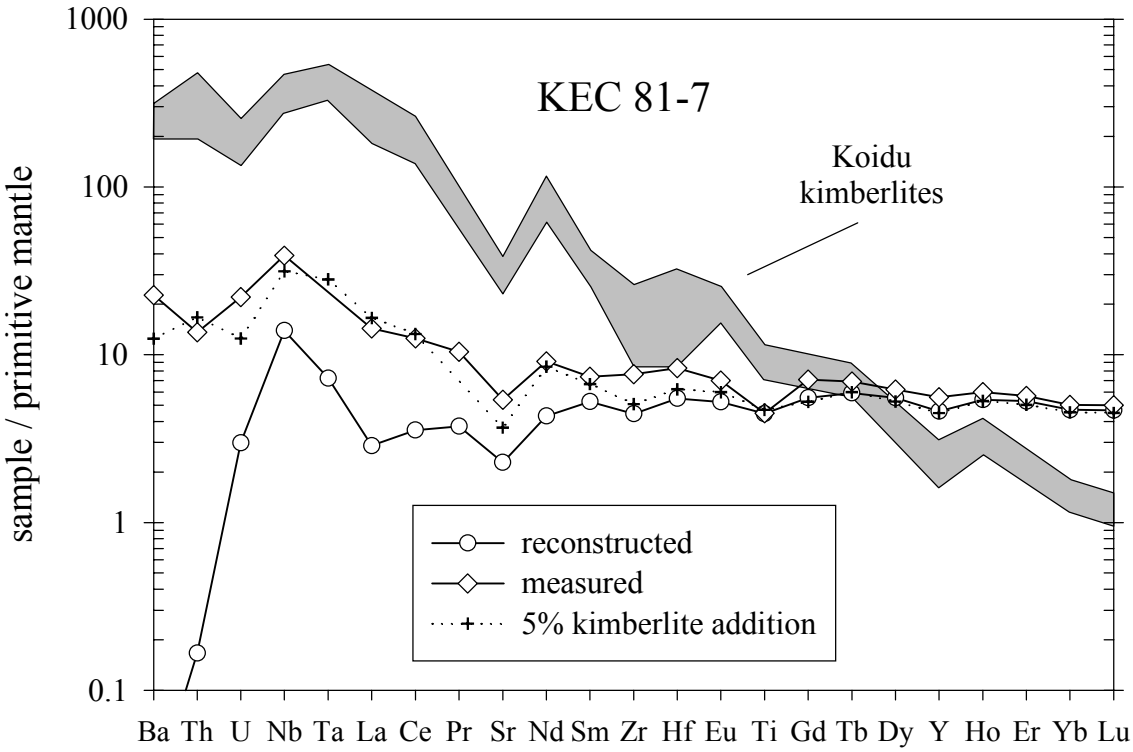

Figure 2.8. Mantle-normalized trace element diagram illustrating kimberlite contamination. Gray field shows the range of kimberlite compositions at Koidu, Sierra Leone (Taylor et al., 1994). Open circles denote the reconstructed whole rock composition of sample KEC 81-7; open diamonds denote the measured whole rock composition. Crosses show calculated mixture of the reconstructed eclogite with 5% average Koidu kimberlite added. Normalized as in Figure 2.3.

measured MgO content. Large variations in the relative fractionation of Nb and U, very high Nb contents in some samples (e.g., KEC 81-3 and KEC 86-13), and the occurrence of secondary rutile require at least one additional metasomatic process in these samples.

Because several processes may be overprinted in these rocks, it is particularly difficult to constrain the nature of metasomatic processes other than kimberlite infiltration.

2.5.5. Whole Rock Reconstruction

In order to evaluate the chemical composition of the eclogites prior to their entrainment in the kimberlite, whole rock trace element patterns have been reconstructed based on the trace element contents measured in primary garnet, cpx, and oxides using previously published modal abundances (Table 2.7; Hills and Haggerty, 1989; Fung and Haggerty, 1995) and Ti mass balance (see below).

The overall REE patterns of eclogite xenoliths are fairly insensitive to uncertainties in the proportions of garnet and cpx (Jerde et al., 1993). All eclogites have relatively flat HREE (Fig. 2.9). The jadeite-poor eclogites have very homogeneous LREE-depleted patterns, whereas the jadeite-rich eclogites have more variable LREE-depleted patterns. Samples KEC 81-3, KEC 81-10A, and KEC 86-KB-3 have positive Eu anomalies and samples KEC 86-GB-12 and K91-11 have small negative Eu anomalies. Note that REE could only be reconstructed for one kyanite-bearing sample due to the low concentrations in the clinopyroxenes. However, small positive Eu anomalies in garnets from the three kyanite-eclogites (Fig. 2.2d) suggests that positive Eu anomalies are ubiquitous features of these rocks.

Some trace elements, such as the HFSE (high field-strength elements – Ti, Zr, Hf, Nb and Ta), may be largely contained in accessory phases such as rutile. This presents a problem for whole rock reconstructions as it is generally difficult to determine precise

Figure 2.9. Chondrite-normalized reconstructed whole rock REE data for Koidu low MgO eclogite xenoliths. Top: jadeite-poor eclogites (<30 mol% jadeite in cpx). Middle: jadeite-rich eclogites (>30 mol% jadeite in cpx). Bottom: kyanite- and graphite-bearing eclogites. Normalized as in Fig. 2.2.

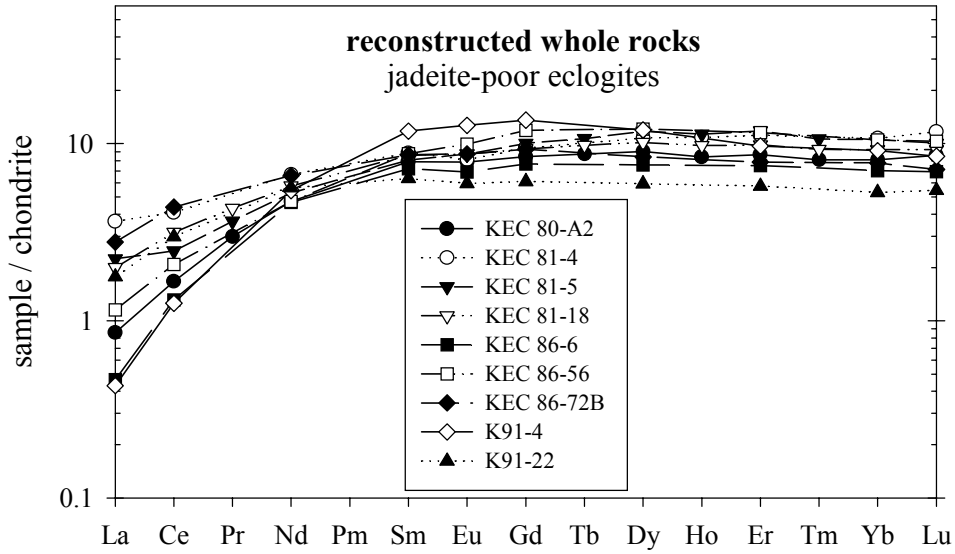
reconstructed whole rocks
jadeite-poor eclogites
sample / chondrite
10
1
0.1
KEC 80-A2
KEC 81-4
KEC 81-5
KEC 81-18
KEC 86-6
KEC 86-56
KEC 86-72B
K91-4
K91-22
La Ce Pr Nd Pm Sm Eu Gd Tb Dy Ho Er Tm Yb Lu

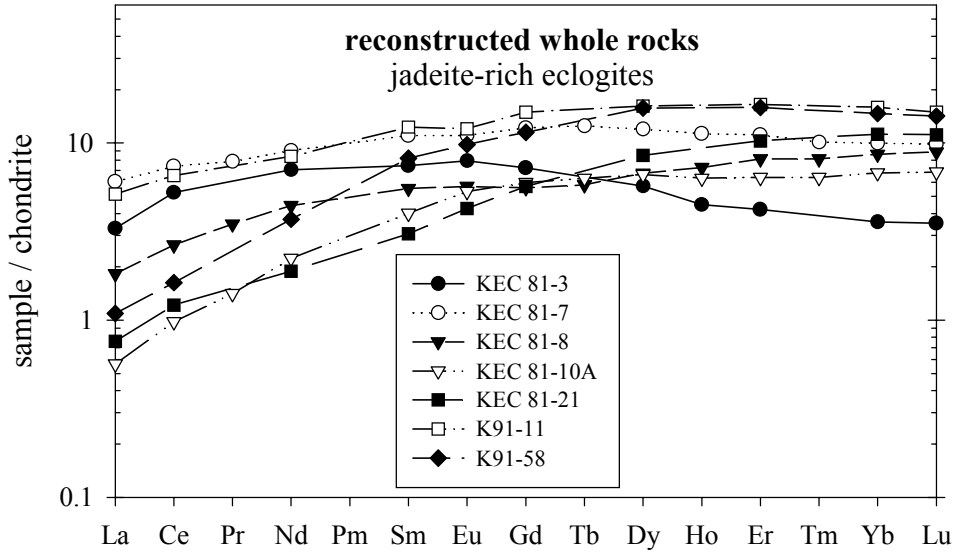
reconstructed whole rocks
jadeite-rich eclogites
sample / chondrite
10
1
0.1
KEC 81-3
KEC 81-7
KEC 81-8
KEC 81-10A
KEC 81-21
K91-11
K91-58
La Ce Pr Nd Pm Sm Eu Gd Tb Dy Ho Er Tm Yb Lu

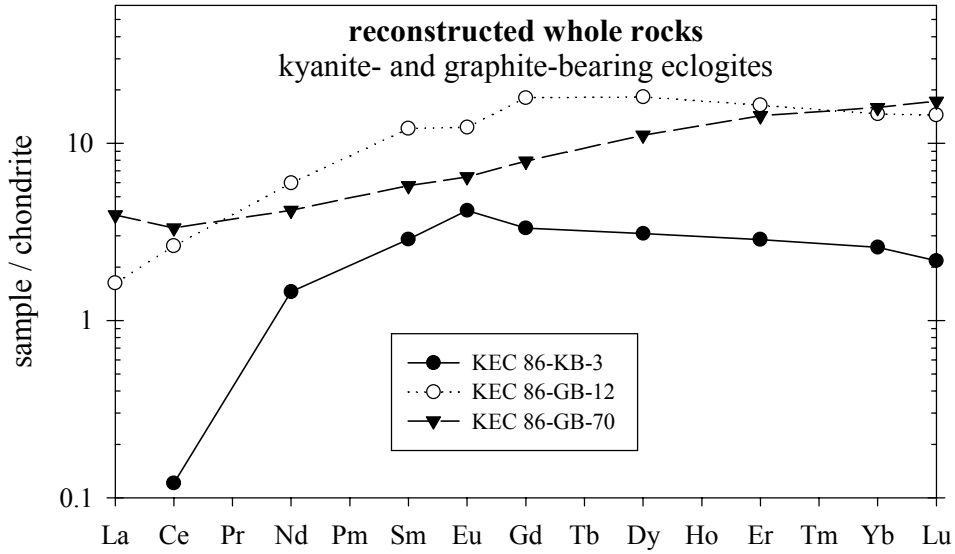
reconstructed whole rocks
kyanite- and graphite-bearing eclogites
sample / chondrite
10
1
0.1
KEC 86-KB-3
KEC 86-GB-12
KEC 86-GB-70
La Ce Pr Nd Pm Sm Eu Gd Tb Dy Ho Er Tm Yb Lu

Table 2.7. Reconstructed whole rock compositions of the Koidu low MgO eclogites and the median low MgO eclogite. Concentrations are given in ppm (µg/g). low jadeite = <30 mol% jadeite in cpx. high jadeite = >30 mol% jadeite in cpx. wr = modal amount of rutile calculated by mass balance using whole rock Ti contents. c = modal amount of rutile calculated assuming no Ti anomaly. See text for details. n. d. = not determined. b. d. = below detection limit. Mineral modes are published in Hills and Haggerty (1989) and Fung and Haggerty (1995). Reconstructed major element compositions are given in Fung and Haggerty or are calculated from the data in Hills and Haggerty.

	median low MgO eclogite	KEC 80-A2 low jadeite 0.68% rutile	KEC 81-4 low jadeite 0.62% rutile	KEC 81-5 low jadeite 0.66% rutile	KEC 81-18 low jadeite 0.65% rutile	KEC 86-6 low jadeite 0.6% rutile	KEC 86-56 low jadeite 0.7% rutile	KEC 86-72B low jadeite 0.63% rutile
		c	wr	wr	wr	c	c	wr
Sc	42	48	40	50	47	48	57	45
Ti	4541	4541	4223	4293	4663	4028	6286	4526
V	297	352	n. d.	364	332	336	297	322
Cr	319	319	n. d.	715	326	305	339	320
Ni	125	179	n. d.	154	59	138	84	38
Sr	52	41	39	60	62	47	50	87
Y	17	17	18	20	17	14	20	15
Zr	21.7	9.8	19	14	24	24	27	27
Nb	0.75	12	0.09	0.16	0.64	0.20	0.87	27
La	0.55	0.26	1.1	0.69	0.61	0.14	0.35	0.86
Ce	2.1	1.3	3.3	2.0	2.5	1.1	1.7	3.5
Pr	0.43	0.36	n. d.	0.44	0.52	n. d.	n. d.	n. d.
Nd	3.1	2.8	4.0	3.1	3.4	2.8	2.8	3.9
Sm	1.6	1.5	1.7	1.6	1.7	1.4	1.7	1.7
Eu	0.59	0.57	0.59	0.64	0.64	0.50	0.72	0.64
Gd	2.4	2.2	2.4	2.6	2.4	2.0	3.0	2.4
Tb		0.41	n. d.	0.50	0.46	n. d.	n. d.	n. d.
Dy	3.2	2.9	3.4	3.8	3.2	2.4	3.8	2.7
Ho		0.60	0.77	0.81	0.69	n. d.	n. d.	n. d.
Er	2.1	1.8	2.3	2.5	2.1	1.6	2.4	1.6
Yb	1.9	1.7	2.2	2.2	1.9	1.5	2.2	1.6
Lu	0.30	0.27	0.38	0.32	0.30	0.22	0.33	0.23
Hf	0.94	0.54	0.88	0.72	1.00	1.11	0.94	1.1
Ta	0.036	0.26	0.003	0.015	0.028	0.026	0.060	0.26
Pb	0.15	n. d.	n. d.	n. d.	n. d.	0.06	0.06	0.14
Th	0.019	0.020	0.046	0.058	0.019	0.005	0.006	0.022
U	0.019	0.036	0.041	0.024	0.044	0.007	0.019	0.051

Table 2.7 continued.

	K91-4 low jadeite 1.07% rutile	K91-22 low jadeite 0.5% rutile	KEC 81-3 high jadeite 0.42% rutile	KEC 81-7 high jadeite 0.65% rutile	KEC 81-8 high jadeite 0.82% rutile	KEC 81-10A high jadeite no rutile	KEC 81-21 high jadeite no rutile	K91-11 high jadeite 1.1% rutile
	c	c	wr	wr	wr	wr	wr	c
Sc	32	41	28	29	43	37	44	40
Ti	7266	3430	4608	5367	5367	2188	1928	7405
V	268	465	n. d.	239	399	226	263	269
Cr	396	249	n. d.	622	287	268	499	244
Ni	220	303	n. d.	79	125	75	197	103
Sr	45	50	68	45	70	31	61	52
Y	17	10	8.1	20	13	11	17	27
Zr	15.5	12.7	16	47	9.5	32.5	12.8	48.1
Nb	0.75	0.41	5.3	9.2	1.7	0.18	0.10	12
La	0.13	0.55	1.0	1.9	0.56	0.18	0.24	1.58
Ce	1.0	2.4	4.2	5.9	2.1	0.8	1.0	5.2
Pr	n. d.	n. d.	n. d.	0.95	0.42	0.17	n. d.	n. d.
Nd	3.2	3.4	4.2	5.4	2.6	1.3	1.1	5.0
Sm	2.3	1.2	1.5	2.1	1.1	0.8	0.6	2.4
Eu	0.92	0.44	0.58	0.81	0.41	0.39	0.31	0.87
Gd	3.5	1.6	1.9	3.1	1.4	1.5	1.5	3.8
Tb	n. d.	n. d.	n. d.	0.59	0.27	0.30	n. d.	n. d.
Dy	3.8	1.9	1.8	3.8	2.2	2.1	2.7	5.1
Ho	n. d.	n. d.	0.32	0.80	0.52	0.45	n. d.	n. d.
Er	2.0	1.2	0.88	2.3	1.7	1.3	2.2	3.4
Yb	1.9	1.1	0.75	2.1	1.8	1.4	2.3	3.3
Lu	0.27	0.17	0.11	0.32	0.28	0.22	0.36	0.47
Hf	0.67	0.94	0.68	1.6	0.50	1.11	0.47	1.58
Ta	0.092	0.013	0.066	0.27	0.013	0.023	0.007	0.090
Pb	0.11	0.17	n. d.	n. d.	n. d.	n. d.	0.12	0.65
Th	b. d.	0.038	0.037	0.013	0.025	0.004	0.006	0.047
U	0.007	0.016	0.055	0.061	0.080	0.007	0.001	0.037

Table 2.7 continued.

	K91-58 high jadeite 1.2% ilmenite	KEC 86-KB-3 kyanite-bearing 0.25% rutile	KEC 86-GB-12 graphite-bearing 1.2% rutile	KEC 86-GB-70 graphite-bearing 0.45% rutile
	c	c	c	c
Sc	38	19	46	35
Ti	5620	2212	8168	3987
V	424	142	286	175
Cr	112	228	263	643
Ni	66	144	58	136
Sr	54	26	75	78
Y	26	5.0	33	23
Zr	21.7	8.1	52	34
Nb	21	0.059	0.37	1.1
La	0.33	b. d.	0.50	1.2
Ce	1.3	0.10	2.1	2.7
Pr	n. d.	n. d.	n. d.	n. d.
Nd	2.2	0.87	3.5	2.5
Sm	1.6	0.56	2.3	1.1
Eu	0.71	0.31	0.89	0.47
Gd	2.9	0.79	4.6	2.0
Tb	n. d.	n. d.	n. d.	n. d.
Dy	5.0	1.0	5.8	3.6
Ho	n. d.	n. d.	n. d.	n. d.
Er	3.3	0.60	3.4	3.0
Yb	3.0	0.54	3.0	3.3
Lu	0.45	0.070	0.46	0.55
Hf	1.27	0.43	1.8	1.5
Ta	0.95	0.013	0.036	0.078
Pb	0.26	n. d.	0.22	0.40
Th	0.017	0.002	0.003	0.034
U	0.009	0.011	0.004	0.017

modal proportions of accessory phases by point counting coarse-grained rocks like eclogites. For this reason, we have calculated the modal abundance of rutile from Ti mass balance between the measured whole rock and mineral compositions (Rudnick et al., 2000). Proportions and Ti concentrations of garnet and cpx (Hills and Haggerty, 1989; Fung and Haggerty, 1995) were used to calculate the Ti content of the silicate fraction. This is invariably less than the measured whole rock. The missing Ti is assigned to rutile and the modal proportion is thus calculated. This method yields the maximum amount of rutile or ilmenite in the sample, since it does not account for any Ti in secondary phases such as metasomatic rutile, amphibole (0.5-2.5 wt% TiO_2), or phlogopite (1.6-4 wt% TiO_2). However, only one sample analyzed (KEC 81-18) contains two generations of rutile (KEC 81-10A and KEC 81-21 contain metasomatic rutile but no primary rutile). Therefore any overestimation is small and within the errors of the estimated absolute uncertainty (±0.05%; Rudnick et al., 2000). The reconstructed Nb concentration never exceeds the measured Nb concentration, suggesting that overestimation of the amount of rutile is not a problem. For samples lacking bulk rock TiO_2 concentrations, modal rutile was calculated by assuming that the bulk rock has no Ti anomaly on a multi-element mantle-normalized diagram (Fig. 2.10).

The reconstructed whole rocks show a wide range of Nb/La and Nb/Ta ratios, ranging from negative to strongly positive Nb and Ta anomalies (Fig. 2.10; Rudnick et al., 2000). The jadeite-rich eclogites have high Sr/Nd (except KEC 81-7), whereas the jadeite-poor eclogites have approximately chondritic Sr/Nd ratios. Many eclogites have low abundances of Zr (and in some samples also low Hf) relative to Sm. This Zr depletion is not due to overlooked accessory phases such as zircon in the whole rock

Figure 2.10. Mantle-normalized reconstructed whole rock trace element diagrams for Koidu low MgO eclogite xenoliths. Top: jadeite-poor eclogites (<30 mol% jadeite in cpx). Middle: jadeite-rich MgO eclogites (>30 mol% jadeite in cpx). Bottom: kyanite- and graphite-bearing eclogites. Normalized as in Figure 2.3.

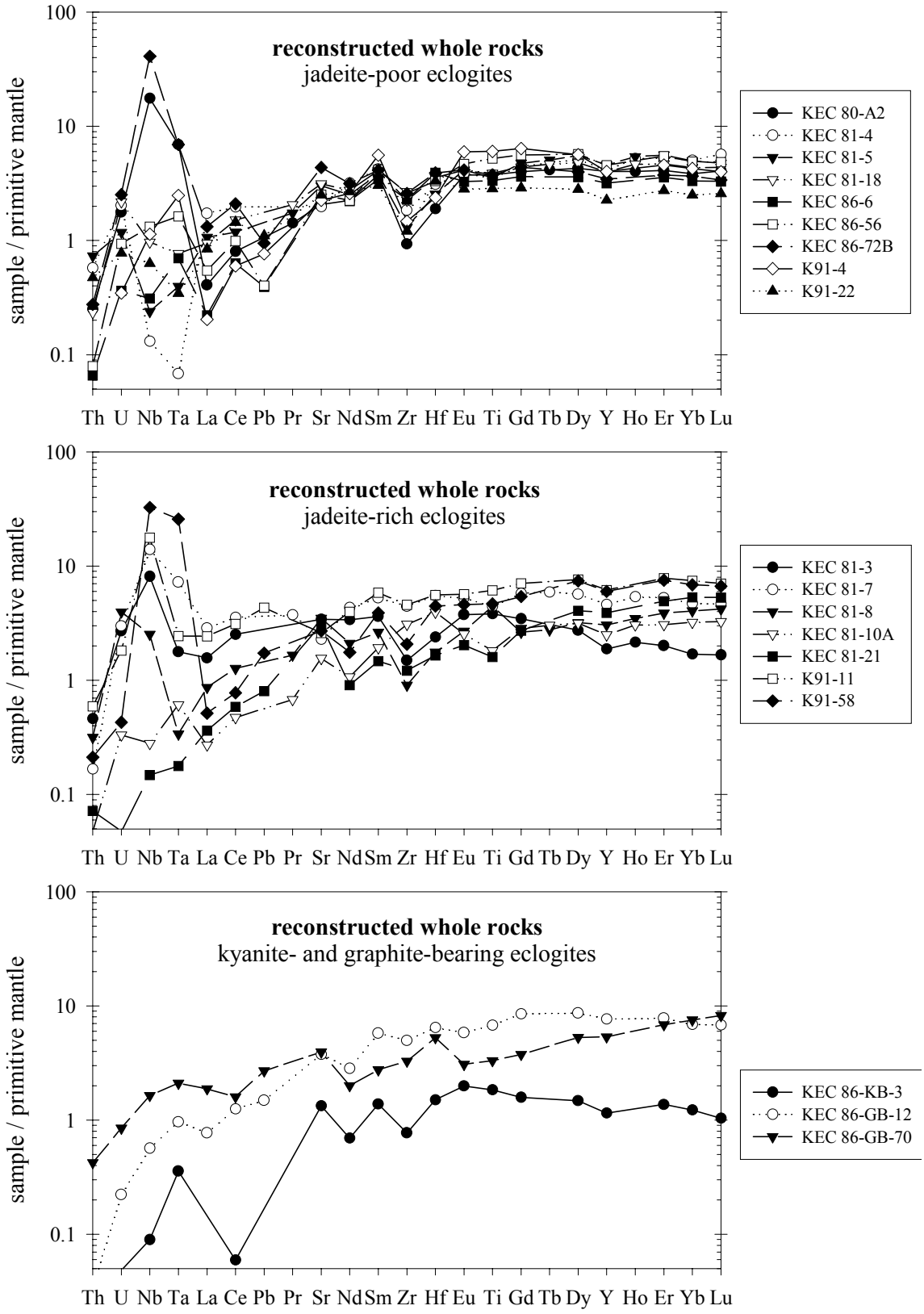
reconstructed whole rocks
jadeite-poor eclogites
sample / primitive mantle
100
10
1
0.1
Th U Nb Ta La Ce Pb Pr Sr Nd Sm Zr Hf Eu Ti Gd Tb Dy Y Ho Er Yb Lu
KEC 80-A2
KEC 81-4
KEC 81-5
KEC 81-18
KEC 86-6
KEC 86-56
KEC 86-72B
K91-4
K91-22
reconstructed whole rocks
jadeite-rich eclogites
sample / primitive mantle
100
10
1
0.1
Th U Nb Ta La Ce Pb Pr Sr Nd Sm Zr Hf Eu Ti Gd Tb Dy Y Ho Er Yb Lu
KEC 81-3
KEC 81-7
KEC 81-8
KEC 81-10A
KEC 81-21
K91-11
K91-58
reconstructed whole rocks
kyanite- and graphite-bearing eclogites
sample / primitive mantle
100
10
1
0.1
Th U Nb Ta La Ce Pb Pr Sr Nd Sm Zr Hf Eu Ti Gd Tb Dy Y Ho Er Yb Lu
KEC 86-KB-3
KEC 86-GB-12
KEC 86-GB-70

reconstruction because the measured whole rocks also show Zr depletions. All eclogites have low Th concentrations, low Th/U ratios, and relatively uniform Sr contents. The jadeite-rich eclogites have more heterogeneous trace element patterns than the jadeite-poor eclogites.

Ancient metasomatic enrichment, prior to the kimberlite-related alteration, is a mantle process that can significantly change the chemical composition of mantle-derived samples. Metasomatism by passing melts is expected to increase Mg# (molar Mg/(Mg+Fe)), Ba, Nb, Zr, and LREE contents of the original eclogite (Dawson, 1984; Harte, 1987; Zindler and Jagoutz, 1988; Ireland et al., 1994). Evidence of metasomatic enrichment of a LREE depleted rock are sigmoidal and 'double hump' cpx and/or whole rock REE patterns (Johnson et al., 1990; Ireland et al., 1994). Such REE patterns are predicted for early stages of metasomatism by melt percolation models (Navon and Stolper, 1987). The final results of porous flow are smooth, LREE-enriched patterns (Navon and Stolper, 1987; Takazawa et al., 1992). These re-enriched REE patterns cannot easily be distinguished from undepleted, enriched rocks once the re-enriched rock reaches trace element equilibrium at upper mantle conditions. The Koidu low MgO eclogites analyzed have smooth, LREE-depleted cpx and reconstructed whole rock REE patterns and are depleted to very depleted in other highly incompatible trace elements such Ba and Th. Furthermore, the Koidu eclogites have Mg# (45-71) that are significantly lower than Ireland et al.'s (1994) metasomatized eclogites (Mg# = 74) or primitive, peridotite-derived melts (Mg# 74-80). Thus, we conclude that garnet and cpx in the low MgO eclogites do not show evidence for equilibration or exchange with ancient metasomatic agents.

2.6. Origins of the Koidu low MgO Eclogites

The mafic compositions and lithospheric equilibration conditions of the Koidu low MgO eclogites could be the result of (1) mantle melting and crystallization of these magmas and their cumulates at high pressures ("mantle" hypothesis), (2) metamorphism and foundering of underplated basaltic magmas at the base of the continental crust, and (3) metamorphism ± partial melting of subducted oceanic crust. A number of observations lead us to favor the last hypothesis.

2.6.1. Primary Mantle Melts and Cumulates

In the "mantle" hypothesis, peridotite melting must have occurred at pressures exceeding 3 GPa, since pressure estimates of the low MgO eclogites cluster between 3.3 and 3.6 GPa (see above). However, the major element compositions of the Koidu low MgO eclogites differ significantly from primary, high-pressure mantle melts (Table 3.8, Fig. 2.11). Mantle melting at high pressures generates picritic melts with higher MgO and lower Al_2O_3 and Na_2O contents than found in the Koidu low MgO eclogites. This is due to decreased stability of olivine and increased stability of garnet and jadeite with increasing pressure (Falloon and Green, 1988; Kinzler and Grove, 1992; Kushiro, 1996; Walter, 1998). The low Mg#'s (45-71, only the diamond-bearing sample KEC 80-DB-3 (not analyzed here) has Mg# = 79) of the Koidu eclogites are considered primary, since both mantle metasomatism and partial melting will increase the Mg#. The protoliths of the low MgO eclogites were thus most likely evolved basaltic melts, because their Mg#'s are generally too low to be primary mantle melts (Mg# 70-80). Similarly, their Ni

Figure 2.11. Plots of SiO_2 and CaO vs. MgO whole rock content. Solid squares: reconstructed Koidu low MgO eclogites (Hills and Haggerty, 1989; Fung and Haggerty, 1995). Open circles: Sula Mountain greenstone belt basalts (Rollinson, 1997). Small diamonds: Residues from eclogite melting experiments (Carroll and Wyllie, 1990; Rapp and Watson, 1995; Sen and Dunn, 1994; Winther and Newton, 1991; Wolf and Wyllie, 1994) assuming equal proportions of residual garnet and cpx. Melts in equilibrium with eclogite have silicic to intermediate compositions (high Al_2O_3, trondhjemitic-tonalitic, granodioritic, quartz dioritic). Dotted triangles and reverse triangles: Experimental pyrolite melts at 1 and 3 GPa, respectively (Baker and Stolper, 1994; Walter, 1998). Gray field shows Archean basalts and komatiites compiled from the literature. White field depicts unaltered mid-ocean ridge basalt (MORB) from the RidgePet Database.

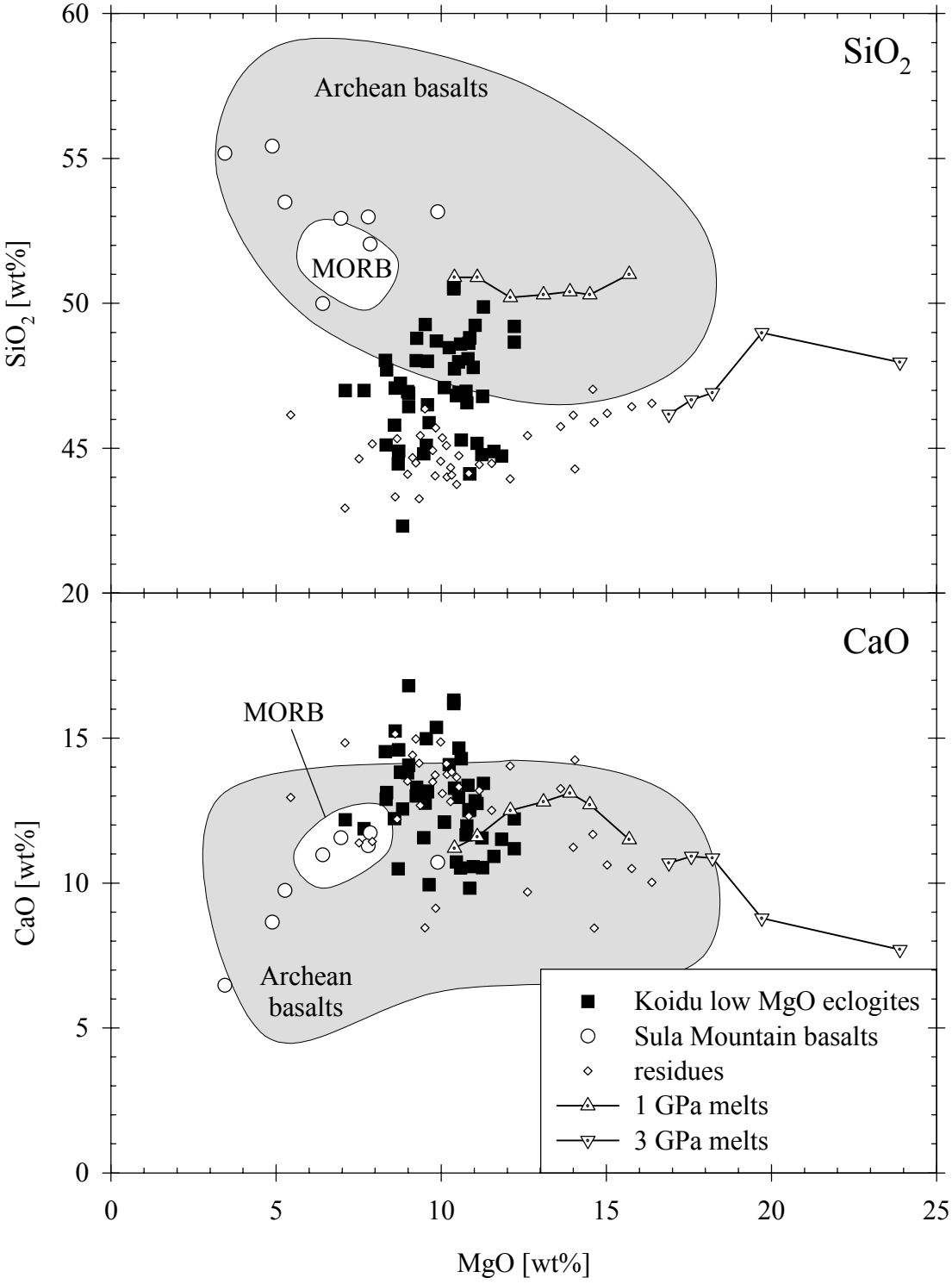
SiO2
Archean basalts
MORB
SiO2 [wt%]
CaO
MORB
Archean
basalts
CaO [wt%]
Koidu low MgO eclogites
Sula Mountain basalts
residues
1 GPa melts
3 GPa melts
MgO [wt%]
0
5
10
15
20
25
20
45
50
55
60

Table 2.8. Whole rock chemistry of the Koidu low MgO eclogites. All samples have the KEC suffix. m = measured by XRf. c = reconstructed using mineral chemistry and modal abundances. Data from Hills and Haggerty (1989) and Fung and Haggerty (1995).

Sample	81-DB-1	81-3	81-4	81-5	81-7	81-8	81-10A	81-12	81-18	81-21	86-13	86-71A	86-71B	86-72A	86-72B	86-KB-74A
	m	m	m	m	m	m	m	m	m	m	m	m	m	m	m	m
SiO_2	46.25	45.38	48.53	43.66	45.49	47.47	50.13	46.70	48.90	48.75	48.07	46.33	46.10	42.80	46.41	46.03
TiO_2	0.86	0.77	0.70	0.73	0.90	0.89	0.46	1.41	0.78	0.56	0.74	0.59	0.56	0.84	0.76	0.45
Al_2O_3	14.57	16.95	12.63	17.15	15.51	15.61	13.78	14.88	12.36	13.80	14.16	18.37	17.80	17.25	14.34	26.71
FeO_t	12.83	10.48	13.07	16.22	11.74	10.61	8.34	15.67	11.44	10.99	13.78	11.27	11.04	17.60	13.83	6.28
MnO	0.24	0.16	0.23	0.31	0.21	0.19	0.17	0.31	0.21	0.20	0.26	0.22	0.23	0.38	0.26	0.09
MgO	10.94	9.24	12.56	10.35	12.96	10.08	11.44	7.62	12.01	12.16	10.14	10.08	9.75	7.90	9.50	6.19
CaO	12.96	15.16	10.40	10.73	11.51	12.30	12.06	11.07	11.62	11.13	10.68	11.15	12.57	11.78	12.79	11.72
Na_2O	1.12	1.80	1.59	0.87	1.42	2.17	3.24	1.85	1.48	2.57	2.02	1.21	1.32	1.14	2.11	2.40
K_2O	0.40	0.19	0.23	0.37	0.38	0.84	0.73	0.73	1.04	0.29	0.59	0.58	0.86	0.45	0.23	0.47
P_2O_5	0.04	0.10	0.04	0.03	0.08	0.04	0.06	0.16	0.04	0.05	0.07	0.08	0.05	0.04	0.04	0.03
Total	100.21	100.23	99.98	100.42	100.20	100.20	100.41	100.40	99.88	100.50	100.51	99.88	100.28	100.18	100.27	100.37
Mg #	60.3	61.1	63.1	53.2	66.3	62.9	71.0	46.4	65.2	66.4	56.7	61.5	61.2	44.5	55.0	63.7

Sample	K86-14	K86-34	K86-56	K91-2	K91-4	K91-11	K91-13	K91-17	K91-20	K91-22	K91-23	K91-25	K91-27	K91-29	K91-33	K91-36
	c	c	c	c	c	c	c	c	c	c	c	c	c	c	c	c
SiO_2	46.92	46.82	44.78	47.98	45.17	44.46	49.87	45.88	48.47	50.57	50.50	46.95	49.20	45.11	42.31	46.50
TiO_2	0.10	0.17	0.10	0.27	0.17	0.17	0.09	0.27	0.15	0.09	0.07	0.16	0.13	0.18	0.10	0.11
Al_2O_3	13.85	17.98	16.88	13.58	15.82	16.79	12.38	16.08	11.93	10.44	10.53	14.95	14.56	15.17	18.03	11.98
FeO_t	12.09	10.79	14.12	11.00	13.00	17.00	9.92	15.24	12.61	9.60	9.60	12.17	8.99	15.67	16.45	16.62
MnO	0.24	0.16	0.33	0.22	0.23	0.31	0.20	0.35	0.20	0.16	0.14	0.25	0.20	0.33	0.32	0.29
MgO	10.54	10.46	11.23	10.53	11.09	8.70	11.28	9.63	10.24	10.38	10.38	8.98	12.21	8.33	8.83	9.58
CaO	14.65	10.72	11.55	12.95	12.74	10.49	13.44	9.94	14.08	16.31	16.19	13.80	12.21	12.89	12.55	13.17
Na_2O	1.83	3.04	1.40	2.96	1.58	1.85	3.05	2.54	2.53	2.77	2.78	2.76	2.73	2.02	1.01	1.82
K_2O	0.01	0.01		0.02	0.01	0.02	0.01	0.02	0.01	0.01	0.01	0.01	0.03	0.02		0.02
P_2O_5	0.12	0.12	0.12	0.09	0.06	0.13	0.02	0.07	0.07	0.06	0.04	0.05	0.05	0.10	0.12	0.11
Total	100.35	100.27	100.51	99.60	99.87	99.92	100.26	100.02	100.29	100.39	100.24	100.08	100.31	99.82	99.72	100.20
Mg #	60.9	63.3	58.6	63.1	60.3	47.7	67.0	53.0	59.1	65.8	65.8	56.8	70.8	48.7	48.9	50.7

Table 2.8 (continued).

Sample	K91-38	K91-42	K91-43	K91-49	K91-52	K91-58	K91-60	K91-61	K91-62
	c	c	c	c	c	c	c	c	c
SiO_2	47.70	44.89	48.62	48.81	44.81	46.99	46.99	44.73	47.24
TiO_2	0.11	0.14	0.16	0.25	0.25	0.35	0.10	0.16	0.11
Al_2O_3	15.55	18.29	13.99	13.60	15.80	14.92	16.16	19.26	14.37
FeO_t	11.78	12.30	11.42	10.67	16.62	15.31	13.76	10.88	13.65
MnO	0.22	0.25	0.18	0.17	0.33	0.30	0.25	0.23	0.25
MgO	8.35	11.60	10.84	10.87	9.47	7.10	7.66	11.83	8.77
CaO	13.12	10.92	12.50	12.53	11.56	12.18	11.87	11.51	13.82
Na_2O	3.38	1.59	2.60	3.13	1.63	3.31	3.33	1.64	2.15
K_2O	0.01		0.01	0.01	0.01	0.01		0.01	0.02
P_2O_5	0.17	0.14	0.03	0.02	0.04	0.06	0.03	0.10	0.03
Total	100.39	100.12	100.35	100.06	100.52	100.53	100.15	100.35	100.41
Mg #	55.8	62.7	62.9	64.5	50.4	45.3	49.8	66.0	53.4

contents are generally lower than observed in primary mantle melts (38-303 ppm vs. ≥320 ppm, Frey et al., 1978). Note that MORBs (mid-ocean ridge basalts) and probably most Archean basalts are not simple low-pressure partial melts, but involve a component of higher pressure partial melting, and have evolved by significant olivine fractionation from more primitive liquids (e.g., Baker and Stolper, 1994). Cumulates from mantle melts will have even higher Mg#'s and Ni contents than melts. For example, Taylor and Neal's (1989) Group A eclogites, which they interpreted as high pressure cumulates of a mantle melt along with trapped liquid, have Mg#'s between 82 and 87 and Ni contents between 493 and 659 ppm.

The occurrence of kyanite and corundum in some low MgO eclogites also argues against an origin for the eclogites as crystallized primary melts or their cumulates (Jacob et al., 1998). During the early stages of melt formation and migration in the upper mantle, melts most likely migrate by porous flow and interact extensively with the wall rocks. That is, the melts are in equilibrium with peridotitic mantle. Kyanite-bearing eclogites, however, are not in equilibrium with peridotitic mantle at high pressures and would react with olivine to form aluminous pyroxene and garnet (Milholland and Presnall, 1998). Thus, if kyanite-bearing eclogites represent cumulates of fractionated high-pressure mantle melts, these melts must have been isolated from peridotite. If melts migrate in channels or fractures (conduits and dikes), it is possible that early cumulates precipitated on cool peridotite wallrocks serve to isolate magma from wallrocks, resulting in dikes that are often mineralogically zoned (cf. pyroxenite dikes in ophiolites). In contrast to many pyroxenite xenolith suites (e.g., Irving, 1980; Wilshire et al., 1980), there is no evidence that the Koidu eclogites formed in this manner. Mineralogically zoned eclogites

and composite xenoliths (eclogite cross-cutting peridotite) have not been found in the Koidu xenolith suite (Tompkins and Haggerty, 1984). On the other hand, kyanite is a common accessory phase in massif eclogites (apparent former ocean floor) in some Phanerozoic fold belts (e.g., Mottana et al., 1990). Moreover, the presence of positive Eu anomalies in kyanite-bearing eclogites (this study and Taylor and Neal, 1989) and negative Eu anomalies in graphite-bearing eclogites point to accumulation and fractionation of plagioclase, respectively, and, therefore, to a shallow, crustal origin.

2.6.2. Underplated Basalts

Some eclogite xenoliths may represent basaltic magmas that underplated the lower continental crust and cooled into the eclogite facies at Moho depths (Pearson et al., 1991; El Fadili and Demaiffe, 1999). Although estimated equilibration pressures of the Koidu low MgO eclogites in excess of 2.8 GPa and the occurrence of diamond in some samples imply that these eclogites are derived from the lithospheric mantle (>100 km depth), it is conceivable that the eclogites represent former crustal material that has delaminated from the lower continental crust. A number of geochemical observations, however, are inconsistent with this interpretation. Neither crystal fractionation nor assimilation of continental crust is likely to account for the low $\delta^{18}O$ values observed in some of the low MgO eclogites. Contamination of basaltic magmas with continental crust increases $\delta^{18}O$ and could thus possibly explain eclogites with high $\delta^{18}O$, but these eclogites do not show any other indicators of crustal contamination such as negative Eu and Nb anomalies or high SiO_2 and incompatible trace element contents. We conclude

that the Koidu eclogites are unlikely to represent foundered or delaminated lower continental crust.

2.6.3. Subducted Oceanic Crust

Stable isotopes (oxygen, carbon, and sulfur) are perhaps the most reliable tracers of rocks affected by low-temperature processes that originated at near-surface conditions such as hydrothermal alteration. The large range of $\delta^{18}O$ values observed in many xenolithic eclogites can be explained by hydrothermal alteration of an oceanic crustal protolith (MacGregor and Manton, 1986; Neal et al., 1990; Jacob et al., 1994; Beard et al., 1996), similar to the $\delta^{18}O$ variations observed in ophiolite sequences (Gregory and Taylor, 1981; Muehlenbachs, 1986). The changing fractionation between seawater and basalt with increasing temperature (i.e., depth) causes heavy isotopic values ($\delta^{18}O >$ 5.5‰) at low temperatures and shallow levels of the oceanic crust and light isotopic values ($\delta^{18}O < 5.5$‰) at greater depth where temperatures are higher. Recent studies have documented the preservation of these pre-subduction/collision oxygen isotope signatures of altered basalts and gabbros in massif eclogites and eclogite-facies rocks (e.g., Getty and Selverstone, 1994; Putlitz et al., 2000).

The Koidu low MgO eclogites have more variable oxygen isotopic compositions than mantle-derived peridotite xenoliths (Fig. 2.1). That is, $\delta^{18}O$ in garnet in the Koidu low MgO eclogites ranges from 4.68 to 6.78‰, averaging 5.48 ± 0.96‰ (2 σ, n = 31), while garnet in peridotites derived from the lithospheric mantle averages 5.37 ± 0.36‰ (n = 44; Mattey et al., 1994b). The variable $\delta^{18}O$ of the Koidu low MgO eclogites suggests a

low-pressure protolith such as altered oceanic crust, although the absolute range in values is not as large as those observed in ophiolite sections.

Values of $\delta^{18}O$ of the low MgO eclogites do not correlate with major or trace elements, reflecting the heterogeneous nature of hydrothermal alteration and/or of the protoliths of the eclogites. Garnets in the kyanite-bearing eclogites have low to normal $\delta^{18}O$ (4.73-5.35‰), suggestive of high-T alteration in the deeper, gabbroic parts of oceanic crust, which is consistent with their origin as plagioclase-rich cumulates. In addition, the correlation between jadite content (hence bulk rock Na) and variability of highly incompatible trace elements suggests that the more jadeite-rich samples experienced more intensive hydrothermal alteration, although jadite does not correlation with $\delta^{18}O$ (Table 2.2).

The silica content of the low MgO eclogites is low compared with Archean basalts and present-day MORB (Fig. 2.11). The low silica content could be due to loss of a silicic melt (or fluid) during subduction, loss of SiO_2 during seafloor alteration, or a combination of these processes. Both low-T and high-T seafloor alteration result in stronger depletions of Ca than of SiO_2 in altered basalts (Ridley et al., 1994; Staudigel et al., 1996; Hart et al., 1999). The Koidu low MgO eclogites, however, do not show depletions in CaO relative to Archean basalts and present-day MORB (Fig. 2.11). We therefore favor partial melting and extraction of a silicic melt as an explanation for the low silica content of these eclogites. The similarity of the compositions of the Koidu eclogites and of residues derived from eclogite melting experiments (Winther and Newton, 1991; Sen and Dunn, 1994; Wolf and Wyllie, 1994; Rapp and Watson, 1995) and their distinct compositions when compared to Archean basalts and MORB (Fig.2.11)

supports this conclusion. Taken together, major element and oxygen isotope systematics suggest that the Koidu low MgO eclogites are derived from altered Archean oceanic crust that underwent an episode of partial melting or dehydration during subduction.

2.7. Trace Element Characteristics of the Protoliths of the low MgO Eclogites

Elements that are not greatly affected by hydrothermal alteration and subduction zone metamorphism (conservative elements) can be utilized to determine the geochemical character of the protoliths of the eclogites. Elements commonly considered to be immobile during hydrothermal alteration, or at least only weakly mobile, include the trivalent HREEs, Y, TiO_2, and Al_2O_3, all of which have concentrations in hydrothermal fluids orders of magnitude lower than in oceanic crust (Ridley et al., 1994, and references therein). The HFSE are conserved during low-T alteration of the oceanic crust and change in abundance only by simple dilution/accumulation due to the mobility of other elements; Nb/Ta and Zr/Hf remain nearly constant (Staudigel et al., 1996). In contrast, the HFSE may dissolve under the low pH conditions of high-T hydrothermal solutions and may be enriched in altered samples where secondary (hydrothermal) rutile has precipitated (Ridley et al., 1994).

During shallow subduction probably only H_2O, K, and Rb are significantly removed from the altered crust. Deeper subduction is likely to be more efficient in removing elements from the oceanic crust, but the relatively small amount of water available makes it difficult to change the composition of the downgoing slab significantly by this process (Staudigel et al., 1995, and references therein). Moreover, the HFSE and

HREE will be largely retained by the residue if it contains rutile and garnet, respectively (Brenan et al., 1995; Stalder et al., 1998).

If the subducting oceanic crust is relatively warm, it may undergo partial melting. The most likely melting regions are associated with dehydration boundaries of the dominant hydrous phases in the subducted slab (Peacock, 1996). That is, dehydration melting is probably caused by amphibole breakdown and the formation of eclogite (Martin, 1986). During amphibole breakdown Nb, Ta, and HREE are compatible in a rutile-bearing eclogitic residue, but Zr and Hf may be depleted (Rapp et al., 1999; Foley et al., 2000). Partial melting may change Nb/Ta, Zr/Hf, and Nb/La ratios but will not greatly affect the overall abundances of HREE. Partition coefficients for Nb and Ta between rutile-bearing eclogite and melt are close to unity (Rapp et al., 1999; Foley et al., 2000). Therefore, the Nb/Ta ratio may be fractionated if D_{Nb} and D_{Ta} are not equal, but the overall abundances of Nb and Ta in the residue will change only slightly. For example, 25% depletion of Ta is sufficient to change Nb/Ta from the chondritic value of 17.4 to the observed median value of the eclogites of 22.4 (see below).

Considering the above observations, the Nb, Ta, and HREE contents of the reconstructed rutile-bearing eclogites are likely to reflect the approximate content (probably within a factor of 2-3 for Nb and Ta) of these elements in the crustal precursor. If eclogites exhibit no Nb anomaly or have a positive anomaly, then the Nb concentration can be used to distinguish between incompatible element enriched and depleted precursor rocks. As few or no Archean magmas with positive Nb anomalies are known (Arndt et al., 1997), one can assume that trace elements with similar incompatibility (e.g., Th and La) had similar or higher normalized concentrations in the precursor.

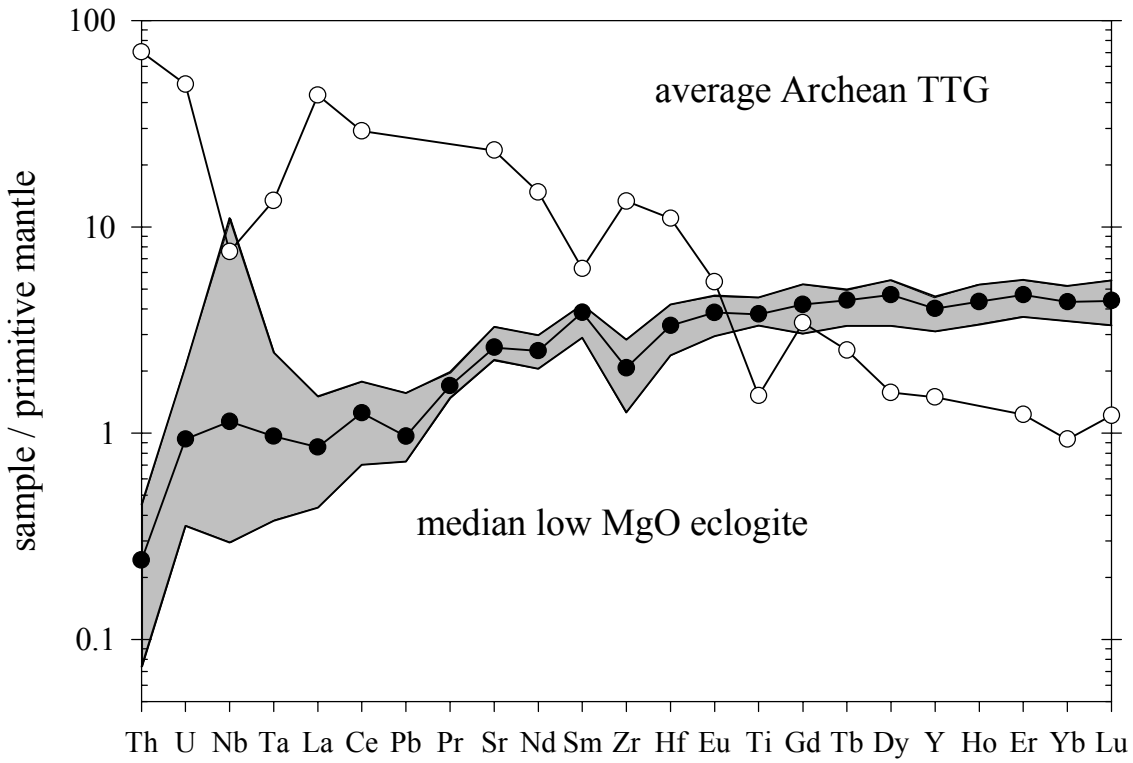

Figure 2.12. Mantle-normalized trace element diagram for the median reconstructed whole rock low MgO eclogite (solid circles). Gray field shows the range of compositions between the first and third quartile. Open circles denote average Archean tonalite-trondhjemite-granodiorite suites (TTG; Martin, 1994). Note the high Nb/La, Nb/Ta, and Sm/Zr ratios of the median eclogite and the complementary low Nb/La, Nb/Ta, and Sm/Zr ratios of the average Archean TTG. Normalized as in Figure 2.3.

To determine a representative trace element composition of the low MgO eclogites, we adopted the median value. This approach is justified because the low MgO eclogites represent a single population (cf. Fig. 1 in Rudnick et al., 2000). That is, the compatible trace elements (with respect to a rutile-bearing eclogite) such as the HREE

show a normal distribution, while Nb, Ta, and incompatible trace elements (e.g., La) approximate a log-normal distribution. In both cases, the median coincides with the center of the distribution. The median of the reconstructed low MgO eclogites shows LREE depletion, a flat HREE pattern, high Sr/Nd, and a positive Nb anomaly (Table 2.7, Fig. 2.12). These features necessitate that the protoliths experienced an episode of partial melting or dehydration of rutile-bearing garnet amphibolite or eclogite during subduction. Based on major element chemistry, Rollinson (1997) proposed that the low MgO eclogites are residues left after 20% partial melting of a protolith similar to the Archean tholeiitic basalts from the Sula Mountains greenstone belt in Sierra Leone (Fig. 2.11). These late Archean basalts show REE patterns that are slightly LREE depleted to slightly LREE enriched (Rollinson, 1999). Partial melting or dehydration of the subducted basalt causes loss of LREE while a large portion of Nb and most of the HREE stay in the residue, due to the high partition coefficients of rutile and garnet, respectively (Fig. 2.13). Conservative trace element compositions also suggest that the low MgO eclogites probably underwent an episode of partial melting rather than dehydration during subduction, as far as a distinction between both can be made (cf. Bureau and Keppler, 1999). The reconstructed eclogites have low Zr/Sm ratios and low Zr concentrations. During partial melting, $D_{Zr,Hf}^{rutile/melt}$ are one to two orders of magnitude lower than $D_{Nb,Ta}^{rutile/melt}$ (Rapp et al., 1999; Foley et al., 2000). In contrast, $D_{Zr,Hf}^{rutile/fluid}$ and $D_{Nb,Ta}^{rutile/fluid}$ are the same order of magnitude (Brenan et al., 1994; Stalder et al., 1998), suggesting that dehydration would not lead to Zr depletion. Another feature that suggests the eclogites are residues is the low concentration of Th (and to a lesser extent of U) observed in the median eclogite (Table 2.7). These elements are highly incompatible in clinopyroxene, garnet (Green,

Figure 2.13. Plot of the reconstructed whole rock Nb (top) and La (bottom) content vs. $(La/Yb)_N$ for the Koidu low MgO eclogites. Gray circles show the median low MgO eclogite composition (Table 2.7). Solid diamonds are jadeite-poor eclogites (<30 mol% jadeite in cpx), solid squares are jadeite rich eclogites (>30 mol% jadeite in cpx). Large gray squares depict the median composition of the Sula mountain greenstone belt basalts (Rollinson, 1997); open triangles depict individual basalt analyses. The lines illustrate possible partial melting trends where the eclogites get strongly depleted in La but only slightly depleted in Nb, the Nb and Yb contents remain approximately constant due to the high partition coefficients of rutile and garnet, respectively. Solid and dotted lines show batch and fractional melting, respectively. Numbers denote the degree of partial melting, assuming 0.5% rutile and a garnet/cpx ratio of 40:60 in the residue. Partition coefficients are taken from Barth et al. (1997), Foley et al. (2000), and Klein et al. (2000).

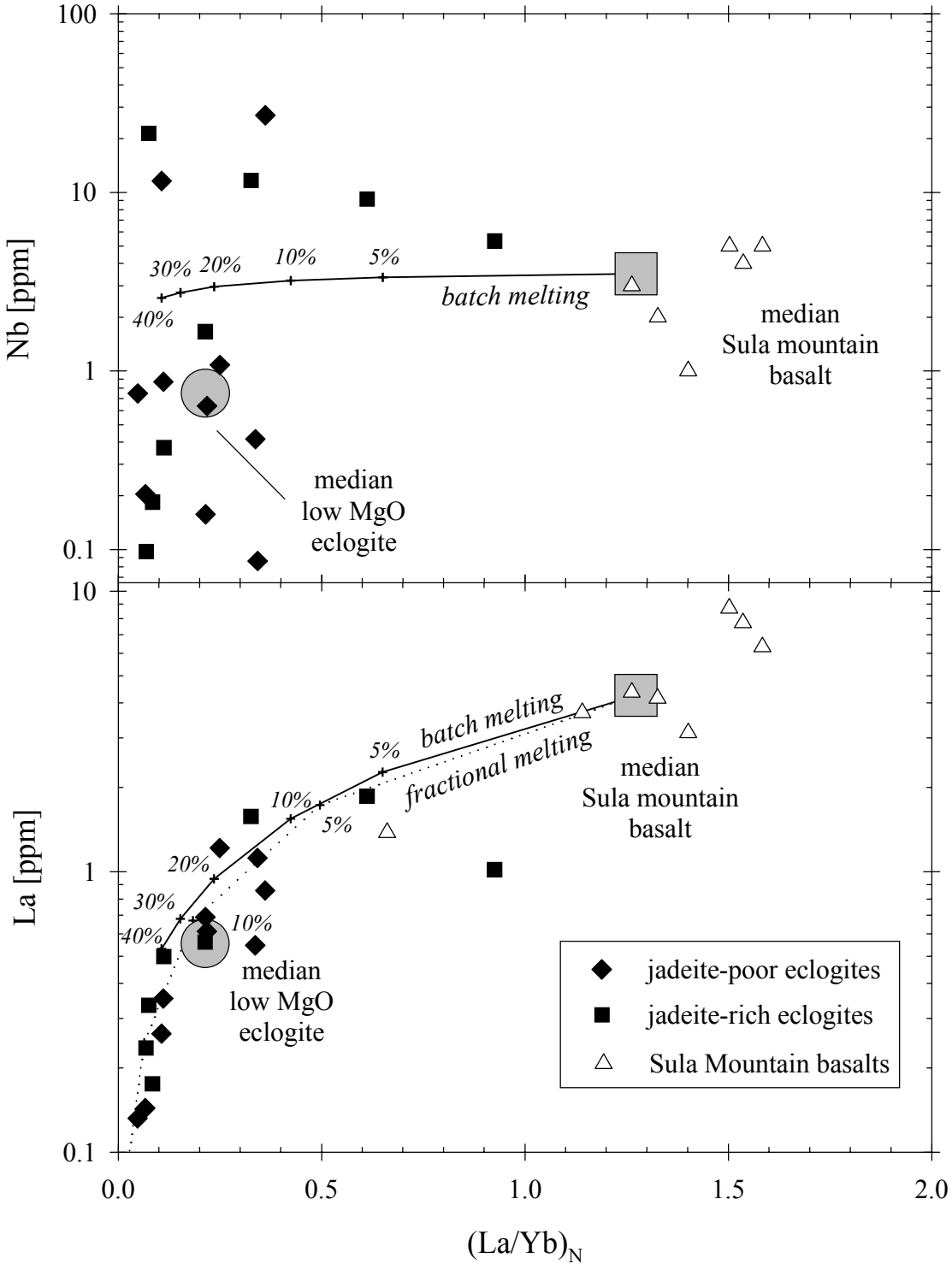
100
10
1
0.1
Nb [ppm]
30%
20%
10%
5%
40%
batch melting
median
Sula mountain
basalt
median
low MgO
eclogite
10
1
0.1
La [ppm]
5%
batch melting
fractional melting
10%
5%
20%
30%
40%
10%
median
Sula mountain
basalt
median
low MgO
eclogite
jadeite-poor eclogites
jadeite-rich eclogites
Sula Mountain basalts
0.0
0.5
1.0
1.5
2.0
(La/Yb)N

1994, and references therein), and (presumably) rutile (except U^{6+}) during partial melting. In contrast, Th is considered to be immobile during dehydration of eclogite (Becker et al., 2000) and is thus not expected to be depleted by dehydration alone. Our median eclogite has an order of magnitude lower Th concentration than the model eclogite Becker et al. (2000):19 ppb vs. 168 ppb, cf. 187 ppb in MORB, Hofmann, 1988, which they interpret to represent dehydrated (subducted), altered MORB.

While the uncertainties of pressure and temperature of partial melting, melting reactions, and the exact composition of the protoliths preclude quantitative modeling, the following observations can be made from simple partial melting calculations (Fig. 2.13).

(1) The depleted trace element patterns of the Koidu eclogites can be reproduced by 15-40% batch melting (or lower degrees of continuous melting) of a basaltic protolith with a flat or slightly LREE enriched trace element pattern. Such patterns are typical of greenstone belt basalts (e.g., Archean Sula Mountains basalts; Rollinson, 1999) or oceanic plateau basalts. This degree of melting coincides with that required to form TTG as determined from eclogite melting experiments.

(2) The calculated residues have much lower Sr concentrations than the Koidu eclogites, suggesting that either residual plagioclase was present during partial melting (Martin, 1999) or that the precursor was enriched in Sr (perhaps due to alteration processes) compared to typical Archean tholeiitic basalts.

(3) Simple partial melting models fail to account for the large range of Nb and Ta contents of the xenolith population (0.06 to 43 ppm Nb, 0.003 to 2.2 ppm Ta). Because Nb and Ta are slightly incompatible to slightly compatible in the bulk eclogite (depending on the modal amount of rutile and the partition coefficients appropriate for

the pressure and temperature of partial melting), their concentrations in the residue remain comparatively constant during partial melting. Note that the Nb and Ta concentrations are not correlated with the calculated amount of rutile (see above), suggesting that the range of Nb concentrations cannot be caused by variable amounts of residual rutile alone. Thus, the wide range in concentrations may reflect basaltic protoliths with variable degrees of incompatible element enrichment. Alternatively, the variable Nb and Ta concentrations may be caused by redistribution of HFSE during high-T seafloor alteration (Ridley et al., 1994), the dependence of D_{Nb} and D_{Ta} on melt composition, as observed in haplogranitic systems (Horng and Hess, 2000) or additional, yet unresolved, processes.

2.8. Implications for Archean Crust Generation

The low MgO eclogites from Koidu, Sierra Leone, have variable oxygen isotopic compositions that exceed the mantle range and reconstructed trace element patterns that are depleted in Ba, Th, U, and light REE but have a positive Nb anomaly. The Koidu low MgO eclogites may represent fragments of processed oceanic crust that are residues from Archean continental crust formation. The subducted oceanic crust was partially melted in order to produce tonalite-trondhjemite-granodiorite suites (TTG), and thus created these residual eclogites, which were subsequently emplaced into the subjacent lithospheric environment.

The complementary silicic melt to the median low MgO eclogite is enriched in incompatible trace elements and has Nb and HREE depletions, as observed in TTG suites, which make up large portions of the crust in Archean cratons. TTGs also show

high Zr/Sm and Th/U (Condie, 1993; Martin, 1994), complementary to the eclogites (Fig. 2.12). Therefore, the low MgO eclogites have the trace element characteristics expected for residues from TTG generation. This notion is supported by the restitic major element composition of these xenoliths (Fig. 2.11; Rollinson, 1997). Thus, the Koidu low MgO eclogites may represent parts of the missing mafic reservoir needed to explain the silicic composition of the crust in Archean cratons. The volume of mafic residue produced during the production of TTGs exceeds by far the volume of mafic lower crust and eclogite in the lithospheric mantle currently present in Archean cratons (Ireland et al., 1994). During partial melting of subducted oceanic crust, portions of the residue (the oceanic crust of the slab) are likely to be transported deeper into the mantle, possibly all the way to the core-mantle boundary. The silicic melts rise (driven by the density contrast between melt and solids) and variably interact with the peridotitic mantle wedge on their way to the surface (Rudnick et al., 1994; Kelemen et al., 1998, Rapp et al., 1999), forming the Archean TTG suties (Martin, 1986). It is also likely that portions of the slab may be left behind in the lithosphere and later sampled by passing kimberlites (e.g., Valley et al., 1998).

Although the Koidu low MgO eclogites probably represent ancient altered oceanic crust that has been recycled in the mantle and partially melted at high pressures, this does not mean that the tectonic environment was exactly analogous to modern subduction zones; (i.e., similar to slab melting and generation of adakites in the Aleutians, southern Andes, and Kamtchatka; Drummond et al., 1996; Kepezhinskas et al., 1997; Yogodzinski and Kelemen, 1998). An alternative scenario to slab melting is tectonic emplacement of oceanic crust in the lowermost continental crust and partial

melting in the garnet stability field. Such overthickening of continental crust may be caused by terrain collision (e.g., de Wit, 1998) or could be associated with oceanic plateaux (Stein and Goldstein, 1996). Higher mantle temperatures in the Archean may have resulted in more buoyant slabs due to higher melt production at mid-ocean ridges, thicker oceanic crust, and more depleted lithospheric mantle. If slabs were positively buoyant and difficult to subduct, a different tectonic style would have been necessary to remove heat from the Archean mantle (e.g., Davies, 1992). Rather than being subducted, oceanic crust might have accumulated over downwellings and, after cooling, "dripped" back into the mantle (Park, 1981; Campbell and Griffiths, 1992). Irrespective of the exact tectonic setting, the Koidu low MgO eclogites demonstrate recycling of oceanic crust and formation of Archean continental crust at convergent plate boundaries.

2.9. Acknowledgements

We thank Kate Tomford, April Larson, Bridget Sinnott, and Taylor Perron for help with sample preparation and mineral separation. Discussions with Debbie Hassler, Cin-Ty Lee, and Thomas Zack and reviews by Harry Becker and Dorrit Jacob helped to improve the manuscript. This study has been supported by NSF grants EAR 980467 to R.L.R.; EAR 9711008 to R.L.R. and W.F.M.; EAR 96-28260 and DOE 93ER14389 to J.W.V.; and EAR 98-05091 to S.E.H.

2.10. References

Arndt N. T., Albarède F., and Nisbet E. G. (1997) Mafic and ultramafic magmatism. In *Greenstone Belts* (ed. M. J. de Wit and L. D. Ashwal), pp. 233-254. Oxford University Press.

Baker M. B. and Stolper E. M. (1994) Determining the composition of high-pressure mantle melts using diamond aggregates. *Geochim. Cosmochim. Acta* **58**, 2811-2827.

Barth M. G., Foley S. F., and Horn I. (1997) Experimental trace-element partitioning in tonalitic systems. *Seventh Annual V. M. Goldschmidt Conference*, 18.

Barth M. G., Rudnick R. L., Carlson R. W., Horn I., and McDonough W. F. (1999) Geochronological Re-Os and U-Pb constraints on the eclogite-tonalite connection in the Archean Man Shield, West Africa. *EOS Trans. AGU* **80**, F1193.

Barth M. G., McDonough W. F., and Rudnick R. L. (2000) Tracking the budget of Nb and Ta in the continental crust. *Chem. Geol.* **165**, 197-213.

Beard B. L., Fraracci K. N., Taylor L. A., Snyder G. A., Clayton R. A., Mayeda T. K., and Sobolev N. V. (1996) Petrography and geochemistry of eclogites from the Mir kimberlite, Yakutia, Russia. *Contrib. Mineral. Petrol.* **125**, 293-310.

Becker H., Jochum K. P., and Carlson R. W. (2000) Trace element fractionation during dehydration of eclogites from high-pressure terranes and the implications for element fluxes in subduction zones. *Chem. Geol.* **163**, 65-99.

Beckinsale R. D., Gale N. H., Pankhurst R. J., Macfarlane A., Crow M. J., Arthurs J. W., and Wilkinson A. F. (1980) Discordant Rb-Sr and Pb-Pb whole rock isochron ages for the Archaean basement of Sierra Leone. *Precambrian Res.* **13**, 63-76.

Blundy J. and Wood B. (1994) Prediction of crystal-melt partition coefficients from elastic moduli. *Nature* **372**, 452-454.

Boynton W. V. (1984) Cosmochemistry of the REE: Meteorite studies. In *REE geochemistry* (ed. P. Henderson). Elsevier.

Brenan J. M., Shaw H. F., Phinney D. L., and Ryerson F. J. (1994) Rutile-aqueous fluid partitioning of Nb, Ta, Hf, Zr, U and Th; implications for high field strength element depletions in island-arc basalts. *Earth Planet. Sci. Lett.* **128**, 327-339.

Brenan J. M., Shaw H. F., Ryerson F. J., and Phinney D. L. (1995) Mineral-aqueous fluid partitioning of trace elements at 900 °C and 2.0 GPa; constraints on the trace element chemistry of mantle and deep crustal fluids. *Geochim. Cosmochim. Acta* **59**, 3331-3350.

Bureau H. and Keppler H. (1999) Complete miscibility between silicate melts and hydrous fluids in the upper mantle: experimental evidence and geochemical implications. *Earth Planet. Sci. Lett.* **165**, 187-196.

Campbell I. H. and Griffiths R. W. (1992) The changing nature of mantle hotspots through time: Implications for the chemical evolution of the mantle. *J. Geol.* **92**, 497-523.

Caporuscio F. A. and Smyth J. R. (1990) Trace element crystal chemistry of mantle eclogites. *Contrib. Mineral. Petrol.* **105**, 550-561.

Carroll M. R. and Wyllie P. J. (1990) The system tonalite-H_2O at 15 kbar and the genesis of calc-alkaline magmas. *Am. Mineral.* **75**, 345-357.

Clayton R. N., Goldsmith J. R., Karel K., Mayeda T. K., and Newton R. C. (1975) Limits on the effect of pressure on isotopic fractionation. *Geochim. Cosmochim. Acta* **39**, 1197-1201.

Condie K. C. (1993) Chemical composition and evolution of the upper continental crust: Contrasting results from surface samples and shales. *Chem. Geol.* **104**, 1-37.

Coplen T. B. (1996) New guidelines for reporting stable hydrogen, carbon, and oxygen isotope-ratio data. *Geochim. Cosmochim. Acta* **60**, 3359-3360.

Davies G. F. (1992) On the emergence of plate tectonics. *Geology* **20**, 936-966.

Dawson J. B. (1984) Contrasting types of upper-mantle metasomatism. In *Kimberlites II: The mantle and crust-mantle relationships* (ed. J. Kornprobst), pp. 289-294. Elsevier.

de Wit M. J. (1998) On Archean granites, greenstones, cratons and tectonics: does the evidence demand a verdict? *Precambrian Res.* **91**, 181-226.

Deines P. and Haggerty S. E. (2000) Small-scale oxygen isotope variations and petrochemistry of ultradeep (>300 km) and transition zone xenoliths. *Geochim. Cosmochim. Acta* **64**, 117-131.

Drummond M. S., Defant M. J., and Kepezhinskas P. K. (1996) Petrogenesis of slab-derived trondhjemite-tonalite-dacite/adakite magmas. *Trans. Royal Soc. Edinburgh, Earth Sci.* **87**, 205-215.

Eggins S. M., Woodhead J. D., Kinsley L. P. J., Mortimer G. E., Sylvester P., McCulloch M. T., Hergt J. M., and Handler M. R. (1997) A simple method for the precise determination of > 40 trace elements in geological samples by ICPMS using enriched isotope internal standardisation. *Chem. Geol.* **134**, 311-326.

El Fadili S. and Demaiffe D. (1999) Petrology of eclogite and granulite nodules from the Mbuji Mayi kimberlites (Kasai, Congo): Significance of kyanite-omphacite

intergrowths. In *Proceedings of the 7th International Kimberlite Conference*, Vol. 1 (ed. J. J. Gurney, J. L. Gurney, M. D. Pascoe, and S. H. Richardson), pp. 205-213. Red Roof Design.

Ellis D. J. and Green D. H. (1979) An experimental study of the effect of Ca upon garnet-clinopyroxene Fe-Mg exchange equilibria. *Contrib. Mineral. Petrol.* **71**, 13-22.

Falloon T. J. and Green D. H. (1988) Anhydrous partial melting of peridotite from 8 to 35 kbar and the petrogenesis of MORB. In *Oceanic and continental lithosphere: Similarities and differences* (ed. M. A. Menzies and K. G. Cox), pp. 379-414. Clarendon Press.

Foley S. F., Barth M. G., and Jenner G. A. (2000) Rutile/melt partition coefficients for trace elements and an assessment of the influence of rutile on the trace element characteristics of subduction zone magmas. *Geochim. Cosmochim. Acta* **64**, 933-938.

Frey F. A., Green D. H., and Roy S. D. (1978) Integrated models of basalt petrogenesis: A study of quartz tholeiites to olivine melilitites from south eastern Australia utilizing geochemical and experimental petrological data. *J. Petrol.* **19**, 463-513.

Fung A. T. and Haggerty S. E. (1995) Petrography and mineral compositions of eclogites from the Koidu Kimberlite Complex, Sierra Leone. *J. Geophys. Res.* **100**, 20,451-20,473.

Getty S. R. and Selverstone J. (1994) Stable isotopic and trace element evidence for restricted fluid migration in 2 GPa eclogites. *J. metamorphic Geol.* **12**, 747-760.

Green T. H. (1994) Experimental studies of trace-element partitioning applicable to igneous petrogenesis — Sedona 16 years later. *Chem. Geol.* **117**, 1-36.

Gregory R. T. and Taylor H. P. (1981) An oxygen isotope profile in a section of Cretaceous oceanic crust, Samail ophiolite, Oman: Evidence for $\delta^{18}O$ buffering of the oceans by deep (>5 km) seawater-hydrothermal circulation at mid-ocean ridges. *J. Geophys. Res.* **86**, 2737-2755.

Haggerty S. E. (1983) The mineral chemistry of new titanates from the Jagersfontein kimberlite, South Africa: Implications for metasomatism in the upper mantle. *Geochim. Cosmochim. Acta* **47**, 1833-1854.

Hart S. R., Blusztajn J., Dick H. J. B., Meyer P. S., and Muehlenbachs K. (1999) The fingerprint of seawater circulation in a 500-meter section of ocean crust gabbros. *Geochim. Cosmochim. Acta* **63**, 4059-4080.

Harte B. (1987) Metasomatic events recorded in mantle xenoliths: an overview. In *Mantle Xenoliths* (ed. P. H. Nixon), pp. 625-640. John Wiley & Sons.

Harte B. and Kirkley M. B. (1997) Partitioning of trace elements between clinopyroxene and garnet: data from mantle eclogites. *Chem. Geol.* **136**, 1-24.

Helmstaedt H. and Doig R. (1975) Eclogite nodules from kimberlite pipes of the Colorado Plateau - samples of subducted Franciscan-type oceanic lithosphere. *Phys. Chem. Earth* **9**, 95-111.

Hills D. V. and Haggerty S. E. (1989) Petrochemistry of eclogites from the Koidu Kimberlite Complex, Sierra Leone. *Contrib. Mineral. Petrol.* **103**, 397-422.

Hofmann A. W. (1988) Chemical differentiation of the Earth: the relationship between mantle, continental crust, and oceanic crust. *Earth Planet. Sci. Lett.* **90**, 297-314.

Horn I., Rudnick R. L., and McDonough W. F. (2000) Precise elemental and isotopic ratio determination by combined solution nebulization and laser ablation ICP-MS: application to U/Pb geochronology. *Chem. Geol.* **164**, 281-301.

Horng W.-S. and Hess P. C. (2000) Partition coefficients of Nb and Ta between rutile and anhydrous haplogranite melts. *Contrib. Mineral. Petrol.* **138**, 176-185.

Ireland T. R., Rudnick R. L., and Spetsius Z. (1994) Trace elements in diamond inclusions from eclogites reveal link to Archean granites. *Earth Planet. Sci. Lett.* **128**, 199-213.

Irving A. J. (1980) Petrology and geochemistry of composite ultramafic xenoliths in alkalic basalts and implications for magmatic processes within the mantle. *Am. J. Sci.* **280A**, 389-426.

Jacob D., Jagoutz E., Lowry D., Mattey D., and Kudrjavtseva G. (1994) Diamondiferous eclogites from Siberia: Remnants of Archean oceanic crust. *Geochim. Cosmochim. Acta* **58**, 5195-5207.

Jacob D., Jagoutz E., Lowry D., and Zinngrebe E. (1998) Comment on 'The origins of Yakutian eclogite xenoliths' by G. A. Snyder, L. A. Taylor, G. Crozaz, A. N. Halliday, B. L. Beard, V. N. Sobolev and N. V. Sobolev. *J. Petrol.* **39**, 1527-1533.

Jacob D. E. and Foley S. F. (1999) Evidence for Archean ocean crust with low high field strength element signature from diamondiferous eclogite xenoliths. *Lithos* **48**, 317-336.

Jerde E. A., Taylor L. A., Crozaz G., Sobolev N. V., and Sobolev V. N. (1993) Diamondiferous eclogites from Yakutia, Siberia: evidence for a diversity of protoliths. *Contrib. Mineral. Petrol.* **114**, 189-202.

Johnson K. T., Dick H. J. B., and Shimizu N. (1990) Melting in the oceanic upper mantle: an ion microprobe study of diopsides in abyssal peridotites. *J. Geophys. Res.* **95**, 2661-2678.

Kelemen P. B., Hart S. R., and Bernstein S. (1998) Silica enrichment in the continental upper mantle via melt/rock reaction. *Earth Planet. Sci. Lett.* **164**, 387-406.

Kepezhinskas P., McDermott F., Defant M. J., Hochstaedter A., Drummond M. S., Hawkesworth C. J., Koloskov A., Maury R. C., and Bellon H. (1997) Trace element and Sr-Nd-Pb isotopic constraints on a three-component model of Kamchatka Arc petrogenesis. *Geochim. Cosmochim. Acta* **61**, 577-600.

Kinzler R. J. and Grove T. L. (1992) Primary magmas of mid-ocean ridge basalts 1. Experiments and methods. *J. Geophys. Res.* **97**, 6885-6906.

Klein M., Stosch H.-G., Seck H. A., and Shimizu N. (2000) Experimental partitioning of high field strength and rare earth elements between clinopyroxene and garnet in andesitic to tonalitic systems. *Geochim. Cosmochim. Acta* **64**, 99-115.

Kohn M. J. and Valley J. W. (1998) Effects of cation substitutions in garnet and pyroxene on equilibrium oxygen isotope fractionations. *J. metamorphic Geol.* **16**, 625-639.

Kushiro I. (1996) Partial melting of a fertile mantle peridotite at high pressures: an experimental study using aggregates of diamond. In *Earth processes: reading the isotopic code*, Vol. 95 (ed. A. Basu and S. Hart), pp. 109-122. American Geophysical Union.

Longerich H. P., Jackson S. E., and Günther D. (1996) Laser ablation inductively coupled plasma mass spectrometric transient signal data acquisition and analyte concentration calculation. *J. Anal. At. Spectrom.* **11**, 899-904.

Macfarlane A., Crow M. J., Arthurs J. W., Wilkinson A. F., and Aucott J. W. (1981) The geology and mineral resources of northern Sierra Leone. *Overseas Mem. Inst. Geol. Sci.* **7**, 103 p.

MacGregor I. D. and Manton W. I. (1986) Roberts Victor eclogites: ancient oceanic crust. *J. Geophys. Res.* **91**, 14,063-14,079.

Martin H. (1986) Effect of steeper Archean geothermal gradient on geochemistry of subduction-zone magmas. *Geology* **14**, 753-756.

Martin H. (1994) The Archean grey gneisses and the genesis of continental crust. In *Archean Crustal Evolution* (ed. K. C. Condie), pp. 205-259. Elsevier.

Martin H. (1999) Adakitic magmas: modern analogues of Archaean granitoids. *Lithos* **46**, 411-429.

Mattey D., Lowry D., and Macpherson C. (1994a) Oxygen isotope composition of mantle peridotite. *Earth Planet. Sci. Lett.* **128**, 231-241.

Mattey D. P., Lowry D., Macpherson C. G., and Chazot G. (1994b) Oxygen isotope composition of mantle minerals by laser fluorination analysis: homogeneity in peridotites, heterogeneity in eclogites. *Mineral. Mag.* **58A**, 573-574.

McCandless T. E. and Gurney J. J. (1989) Sodium in garnet and potassium in clinopyroxene: criteria for classifying mantle eclogites. In *Kimberlites and related rocks*, Vol. 2 (ed. J. Ross), pp. 827-832. Blackwell Scientific.

McCormick T. C., Smyth J. R., and Caporuscio F. A. (1994) Chemical systematics of secondary phases in mantle eclogites. In *Kimberlites, Related Rocks and Mantle Xenoliths*, Vol. 1 (ed. H. O. A. Meyer and O. H. Leonardos), pp. 405-419. CPRM.

McDonough W. F. and Sun S.-S. (1995) Composition of the Earth. *Chem. Geol.* **120**, 223-253.

Milholland C. S. and Presnall D. C. (1998) Liquidus phase relations in the CaO-MgO-Al_2O_3-SiO_2 system at 3.0 GPa: the aluminous pyroxene thermal divide and high-pressure fractionation of picritic and komatiitic magmas. *J. Petrol.* **39**, 3-27.

Mottana A., Carswell D. A., Chopin C., and Oberhänsli R. (1990) Eclogite facies mineral parageneses. In *Eclogite Facies Rocks* (ed. D. A. Carswell), pp. 16-52. Blackie.

Muehlenbachs K. (1986) Alteration of the oceanic crust and the ^{18}O history of seawater. In *Stable isotopes in high temperature geological processes* (ed. J. W. Valley, H. P. J. Taylor, and J. R. O'Neil), pp. 425-444. Mineralogical Society of America.

Navon O. and Stolper E. (1987) Geochemical consequences of melt percolation: The upper mantle as a chromatographic column. *J. Geol.* **95**, 285-308.

Neal C. R., Taylor L. A., Davidson J. P., Holden P., Halliday A. N., Nixon P. H., Paces J. B., Clayton R. N., and Mayeda T. K. (1990) Eclogites with oceanic crustal and mantle signatures from the Bellsbank kimberlite, South Africa, part 2: Sr, Nd, and O isotope geochemistry. *Earth Planet. Sci. Lett.* **99**, 362-379.

Park R. G. (1981) Origin of horizontal structure in high-grade Archaean terrains. In *Archean Geology*, Vol. 7 (ed. J. E. Glover and D. I. Groves), pp. 481-490.

Peacock S. M. (1996) Thermal and petrologic structure of subduction zones. In *Subduction top to bottom* (ed. G. E. Bebout, D. W. Scholl, S. H. Kirby, and J. P. Platt), pp. 119-133. AGU.

Pearce N. J. G., Perkins W. T., Westgate J. A., Gorton M. P., Jackson S. E., Neal C. R., and Chenery S. P. (1997) A compilation of new and published major and trace element data for NIST SRM 610 and NIST SRM 612 glass reference materials. *Geostand. Newslett.* **21**, 115-144.

Pearson N. J., O'Reilly S. Y., and Griffin W. L. (1991) The granulite to eclogite transition beneath the eastern margin of the Australian craton. *Eur. J. Mineral.* **3**, 293-322.

Putlitz B., Matthews A., and Valley J. W. (2000) Oxygen and hydrogen isotope study of high-pressure metagabbros and metabasalts (Cyclades, Greece): implications for the subduction of oceanic crust. *Contrib. Mineral. Petrol.* **138**, 114-126.

Rapp R. P., Shimizu N., Norman M. D., and Applegate G. S. (1999) Reaction between slab-derived melts and peridotite in the mantle wedge: experimental constraints at 3.8 GPa. *Chem. Geol.* **160**, 335-356.

Rapp R. P. and Watson E. B. (1995) Dehydration melting of metabasalts at 8-32 kbar: Implications for continental growth and crust-mantle recycling. *J. Petrol.* **36**, 891-931.

Reid J. E., Horn I., Longerich H. P., Forsythe L., and Jenner G. A. (1999) Determination of Zr and Hf in a flux-free fusion of whole rock samples using laser ablation inductively coupled plasma-mass spectrometry (LA-ICP-MS) with isotope dilution calibration. *Geostand. Newslett.* **23**, 149-155.

Ridley W. I., Perfit M. R., Jonasson I. R., and Smith M. F. (1994) Hydrothermal alteration in oceanic ridge volcanics: A detailed study at the Galapagos Fossil Hydrothermal Field. *Geochim. Cosmochim. Acta* **58**, 2477-2494.

Rollinson H. R. (1978) Zonation of supracrustal relics in the Archaean of Sierra Leone, Liberia, Guinea and Ivory Coast. *Nature* **272**, 440-442.

Rollinson H. (1997) Eclogite xenoliths in west African kimberlites as residues from Archaean granitoid crust formation. *Nature* **389**, 173-176.

Rollinson H. (1999) Petrology and geochemistry of metamorphosed komatiites and basalts from the Sula Mountains greenstone belt, Sierra Leone. *Contrib. Mineral. Petrol.* **134**, 86-101.

Rosenbaum J. M. and Mattey D. (1995) Equilibrium garnet-calcite oxygen isotope fractionation. *Geochim. Cosmochim. Acta* **59**, 2839-2842.

Rudnick R. L., Barth M., Horn I., and McDonough W. F. (2000) Rutile-bearing refractory eclogites: the missing link between continents and depleted mantle. *Science* **287**, 278-281.

Rudnick R. L., McDonough W. F., and Orpin A. (1994) Northern Tanzanian peridotite xenoliths: A comparison with Kaapvaal peridotites and inferences on metasomatic interactions. In *Kimberlites, related rocks and mantle xenoliths* (ed. H. O. A. Meyer and O. H. Leonardos), pp. 336-353. CPRM.

Rudnick R. L. and Nyblade A. A. (1999) The thickness and heat production of Archean lithosphere: constraints from xenolith thermobarometry and surface heat flow. In *Mantle petrology: field observations and high pressure experimentation: a tribute to Francis R. (Joe) Boyd* (ed. Y. Fei, C. M. Bertka, and B. O. Mysen), pp. 3-12. The Geochemical Society.

Schulze D. J., Valley J. W., Viljoen K. S., Stiefenhofer J., and Spicuzza M. (1997) Carbon isotope composition of graphite in mantle eclogites. *J. Geol.* **105**, 379-386.

Sen C. and Dunn T. (1994) Dehydration melting of a basaltic composition amphibolite at 1.5 and 2.0 GPa: implications for the origin of adakites. *Contrib. Mineral. Petrol.* **117**, 394-409.

Smyth J. R., Caporuscio F. A., and McCormick T. C. (1989) Mantle eclogites: evidence of igneous fractionation in the mantle. *Earth Planet. Sci. Lett.* **93**, 133-141.

Snyder G. A., Taylor L. A., Beard B. L., Crozaz G., Halliday A. N., Sobolev V. N., and Sobolev N. V. (1998) Reply to a comment by D. Jacob *et al.* on 'The origins of Yakutian eclogite xenoliths'. *J. Petrol.* **39**, 1535-1543.

Snyder G. A., Taylor L. A., Crozaz G., Halliday A. N., Beard B. L., Sobolev V. N., and Sobolev N. V. (1997) The origins of Yakutian eclogite xenoliths. *J. Petrol.* **38**, 85-113.

Stalder R., Foley S. F., Brey G. P., and Horn I. (1998) Mineral-aqueous fluid partitioning of trace elements at 900-1200 °C and 3.0-5.7 GPa: New experimental data for garnet, clinopyroxene, and rutile, and implications for mantle metasomatism. *Geochim. Cosmochim. Acta* **62**, 1781-1801.

Staudigel H., Davies G. R., Hart S. R., Marchant K. M., and Smith B. M. (1995) Large scale isotopic Sr, Nd and O isotopic anatomy of altered oceanic crust: DSDP/ODP sites 417/418. *Earth Planet. Sci. Lett.* **130**, 169-185.

Staudigel H., Plank T., White B., and Schmincke H.-U. (1996) Geochemical fluxes during seafloor alteration of the basaltic upper oceanic crust: DSDP Sites 417 and 418. In *Subduction top to bottom* (ed. G. E. Bebout, D. W. Scholl, S. H. Kirby, and J. P. Platt), pp. 19-38. AGU.

Stein M. and Goldstein S. L. (1996) From plume head to continental lithosphere in the Arabian-Nubian shield. *Nature* **382**, 773-778.

Takazawa E., Frey F. A., Shimizu N., Obata M., and Bodinier J. L. (1992) Geochemical evidence for melt migration and reaction in the upper mantle. *Nature* **359**, 55-58.

Taylor L. A. and Neal C. R. (1989) Eclogites with oceanic crustal and mantle signatures from the Bellsbank kimberlite, South Africa, Part I: Mineralogy, petrography, and whole rock chemistry. *J. Geol.* **97**, 551-567.

Taylor W. R., Tompkins L. A., and Haggerty S. E. (1994) Comparative geochemistry of West African kimberlites: Evidence for a micaceous kimberlite endmember of sublithospheric origin. *Geochim. Cosmochim. Acta* **58**, 4017-4037.

Tompkins L. A. and Haggerty S. E. (1984) The Koidu Kimberlite Complex, Sierra Leone: Geological setting, petrology and mineral chemistry. In *Kimberlites; I, Kimberlites and related rocks*, Vol. 11A (ed. J. Kornprobst), pp. 83-105. Elsevier.

Valley J. W., Kinny P. D., Schulze D. J., and Spicuzza M. J. (1998) Zircon megacrysts from kimberlite; oxygen isotope variability among mantle melts. *Contrib. Mineral. Petrol.* **133**, 1-11.

Valley J. W., Kitchen N., Kohn M. J., Niendorf C. R., and Spicuzza M. J. (1995) UWG-2, a garnet standard for oxygen isotope ratios: Strategies for high precision and accuracy with laser heating. *Geochim. Cosmochim. Acta* **59**, 5223-5231.

Walter M. J. (1998) Melting of garnet peridotite and the origin of komatiite and depleted lithosphere. *J. Petrol.* **39**, 29-60.

Williams H. R. (1978) The Archaean geology of Sierra Leone. *Precambrian Res.* **6**, 251-268.

Wilshire H. G., Pike J. E. N., Meyer C. E., and Schwarzman E. C. (1980) Amphibole-rich veins in lherzolite xenoliths, Dish Hill and Deadman Lake, California. *Am. J. Sci.* **280A**, 576-593.

Winther K. T. and Newton R. C. (1991) Experimental melting of hydrous low-K tholeiite: evidence on the origin of Archean cratons. *Bull. Geol. Soc. Denmark* **39**, 213-228.

Wolf M. B. and Wyllie P. J. (1994) Dehydration-melting of amphibolite at 10 kbar: the effects of temperature and time. *Contrib. Mineral. Petrol.* **115**, 369-383.

Wood B. J. and Blundy J. D. (1997) A predictive model for rare earth element partitioning between clinopyroxene and anhydrous silicate melt. *Contrib. Mineral. Petrol.* **129**, 166-181.

Yogodzinski G. M. and Kelemen P. B. (1998) Slab melting in the Aleutians: implications of an ion probe study of clinopyroxene in primitive adakite and basalt. *Earth Planet. Sci. Lett.* **158**, 53-65.

Zindler A. and Jagoutz E. (1988) Mantle cryptology. *Geochim. Cosmochim. Acta* **52**, 319-333.

Chapter 3

Geochemistry of Xenolithic Eclogites from West Africa, Part II: Origins of the High MgO Eclogites

Matthias G. Barth[1], Roberta L. Rudnick[1*], Ingo Horn[1◊], William F. McDonough[1*], Michael J. Spicuzza[2], John W. Valley[2], and Stephen E. Haggerty[3]

[1] Department of Earth and Planetary Sciences, Harvard University, 20 Oxford Street, Cambridge, MA 02138, USA
[2] Department of Geology and Geophysics, University of Wisconsin, 1215 W. Dayton Street, Madison, WI 53706, USA
[3] Department of Geosciences, University of Massachusetts, Morrill Science Center, Amherst, MA 01003, USA

present address:

* Department of Geology, University of Maryland, College Park, MD 20742, USA
◊ Laboratory for Inorganic Chemistry, ETH Zürich, Universitätsstrasse 6, CH-8092 Zürich, Switzerland

to be submitted to *Geochimica et Cosmochimica Acta*

02/07/2001

3.1. Abstract

Oxygen isotope, mineral trace element, and measured and reconstructed whole rock compositions are reported for the high MgO eclogite xenolith suite (16-20 wt% MgO in the whole rock) from the Koidu Kimberlite complex, Sierra Leone. The high MgO eclogites have slightly depleted to enriched rare earth element (REE) patterns, which may reflect variable degrees of metasomatic light REE addition. High MgO and Al_2O_3 contents of the eclogites are suggestive of a cumulate origin, either as high-pressure garnet-pyroxene cumulates or low-pressure (<1 GPa) plagioclase-pyroxene-olivine cumulates. In either case, crystal fractionation trends suggest that these eclogites formed at lower pressures than their current estimated equilibrium pressures. Relatively flat heavy to middle REE patterns, Sr anomalies, and low to moderate transition element contents are consistent with a low-pressure origin of the high MgO eclogites as metamorphosed olivine gabbros and troctolites. In this case, the high MgO eclogites could represent either the basal section of subducted oceanic crust or foundered mafic lower continental crust.

3.2. Introduction

Eclogite xenoliths are minor but ubiquitous constituents in mantle xenolith suites brought up by kimberlites in Precambrian cratons. High equilibration temperatures and the presence of diamond in some eclogite xenoliths suggest derivation from the upper mantle. However, the origin of their protoliths and the subsequent metamorphic evolution of these bi-mineralic rocks are less certain. The different hypotheses proposed for the origin of eclogite xenoliths can be divided into two groups. According to the "mantle" hypothesis, eclogites are produced by high-pressure crystallization from peridotite-generated magmas that ascend through the lithosphere (Smyth et al., 1989; Caporuscio and Smyth, 1990). The "crustal" hypothesis argues that eclogites are remnants of subducted (Archean?) oceanic crust, which may or may not have been through a melting episode associated with subduction (Helmstaedt and Doig, 1975; MacGregor and Manton, 1986; Taylor and Neal, 1989; Ireland et al., 1994; Jacob et al., 1994; Barth et al., 2001). A variant of the crustal hypothesis, that has not been widely explored, is that eclogites may be products of metamorphism of mafic lower continental crust, i.e., products of isobaric cooling at high pressure of gabbroic to anorthositic protoliths (Griffin et al., 1990; El Fadili and Demaiffe, 1999).

Xenolithic eclogites from the Koidu kimberlite complex in Sierra Leone, West Africa fall into two groups, based on distinct major element and mineral chemistry (Fig. 3.1; Hills and Haggerty, 1989; Fung and Haggerty, 1995): a high MgO group (>16 wt% MgO) and a low MgO group (6-13 wt% MgO). This paper is the second that examines oxygen isotope and trace element characteristics of these eclogites. The first paper reports

the oxygen isotopic compositions and the trace element compositions of the low MgO eclogites (Barth et al., 2001). In the present paper, we present the oxygen isotopic compositions, the trace element characteristics and genesis of the high MgO eclogites previously studied by Hills and Haggerty (1989) and Fung and Haggerty (1995).

3.3. Geological Background and Analytical Methods

Hills and Haggerty (1989) and Fung and Haggerty (1995) describe the petrography and report mineral chemical data for 87 eclogite xenoliths and whole rock XRF major and trace element data for 25 of these samples from the Koidu pipes. The high MgO group (>16 wt% MgO) is essentially bi-mineralic, with only minor ilmenite, and/or sulfide occurring in addition to garnet and omphacite. The low MgO group (6-13 wt% MgO) commonly contains accessory phases such as kyanite, graphite, quartz (after coesite), diamond, amphibole, and/or corundum plus rutile, ilmenite, and/or sulfides in addition to garnet and omphacite. Generally, both high and low MgO eclogites fall into the classification of group II eclogites of McCandless and Gurney (1989), i.e., low Na garnets and low K omphacite, except for the diamond-bearing eclogites and a single graphite-bearing eclogite that fall into group I.

The Koidu eclogites show a large range of textures, estimated equilibration temperatures, and pressures, extending from 760 °C at 2.8 GPa to 1188 °C at 5 GPa (using the Ellis and Green (1979) geothermometer and the Kalahari geotherm of Rudnick and Nyblade (1999)). The P-T ranges of the high and low MgO eclogites differ significantly (Hills and Haggerty, 1989; Fung and Haggerty, 1995); many high MgO

eclogites record conditions between 1080-1130 °C and 4.0-4.5 GPa, whereas the low MgO eclogites cluster between 880-930 °C and 3.3-3.6 GPa.

Mineral separates for laser fluorination oxygen isotope ratio analysis were prepared by standard procedures including initial crushing in alumina ceramics followed by magnetic separation. Purity of samples was ensured by hand picking, with sample weights for each analysis ranging between 1 and 3 mg. Oxygen isotope ratios were measured at the University of Wisconsin, Madison, using a laser-assisted fluorination technique described by Valley et al. (1995). This method provides high oxygen yields for refractory minerals like garnet. In most cases repeat analyses fall within 0.1 ‰ of each other, demonstrating the good reproducibility of the technique and the purity of the mineral separates. Measured values were corrected (≤0.1‰) based on three to four analyses of garnet standard UWG-2 at the start of each day (Valley et al., 1995). Corrected values are reported relative to V-SMOW (Coplen, 1996).

Whole rock trace element compositions were determined by inductively coupled plasma-mass spectrometry (ICP-MS). Analyses were performed on a Fisons (VG Elemental) PQ II+ in pulse counting mode (three points per peak). Trace element compositions of garnets, omphacites, and ilmenites were determined by laser ablation ICP-MS. Ablation is achieved by a 193 nm Ar-F excimer laser system using a pulse repetition rate of 10 Hz and pulse energy of 0.5 mJ (Horn et al., 2000). Analyses were performed in pulse counting mode (one point per peak). Analytical details and standard values are given in Barth et al. (2001).

3.4. Results

3.4.1. Oxygen Isotopes

Garnet oxygen isotopic data were obtained for 15 high MgO eclogites (Fig. 3.1, Table 1.1). Garnet is usually the freshest phase in eclogite xenoliths, is more resistant to isotopic resetting than clinopyroxene (Deines and Haggerty, 2000), and shows a larger range in composition (e.g., FeO content) than clinopyroxene (cpx). Garnet analyses are representative of the whole rock oxygen isotopic composition because the theoretical and observed high-temperature isotope fractionation between garnet and cpx is small (<0.4‰; Rosenbaum and Mattey, 1995; Kohn and Valley, 1998; Snyder et al., 1998), with garnet generally being lighter than cpx.

Unlike the low MgO eclogite group, the high MgO garnets have a restricted range of $\delta^{18}O$ values (5.07 to 5.73‰), falling entirely within the mantle range ($\delta^{18}O$ = 5.5±0.4‰ based on xenolithic peridotites; Mattey et al., 1994; Fig. 3.1). Sample KEC 86-19 is the only high MgO eclogite with $\delta^{18}O$ falling outside the mantle range. It is a unique sample in that it exhibits strongly zoned garnets (iron-rich cores and magnesium-rich rims), two generations of coexisting clinopyroxene, and it is lacking ilmenite, which is present in most other high MgO eclogites (Hills and Haggerty, 1989). KEC 86-19 has been classified as a high MgO eclogite based on the bulk rock MgO content (16.3 wt%) but cpx and the iron-rich garnet cores fall in the fields defined by low MgO eclogites. KEC 86-19, therefore, is transitional between the high and low MgO eclogites.

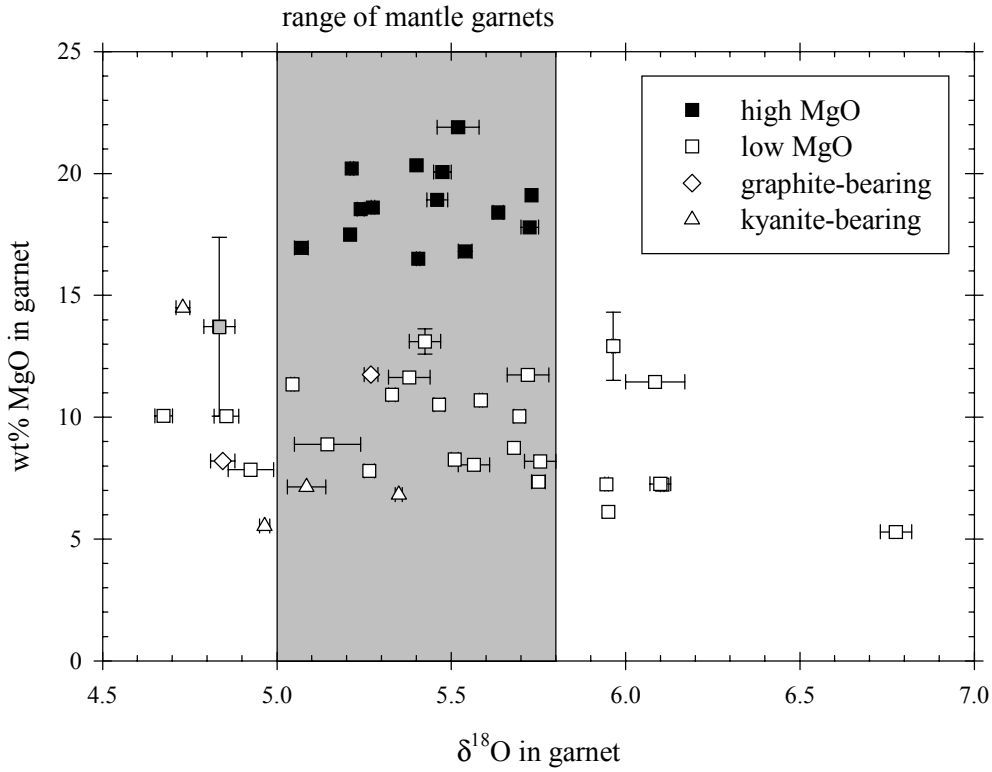

Figure 3.1. MgO in garnet vs. $\delta^{18}O$ in garnet for Koidu eclogites. Solid squares represent high MgO eclogites; open symbols show low MgO eclogites (Barth et al., 2001). The gray square denotes the transitional eclogite KEC 86-19. Open squares are bi-mineralic eclogites, open diamonds are graphite-bearing eclogites, and open triangles are kyanite-bearing eclogites. Horizontal error bars show average reproducibility (each wing is ½ of the difference between 2 separate measurements); vertical error bars indicate mineral zoning. The gray field depicts the range of mantle garnets that is shifted towards lighter isotopic composition by 0.1‰ relative to the whole rock mantle range due to the fractionation between garnet and whole rock.

The low MgO eclogites have more variable oxygen isotope ratios than mantle-derived peridotite xenoliths, suggesting a low-pressure protolith such as altered oceanic crust (see Barth et al., 2001, for details).

Table 3.1. Oxygen isotopic composition of Koidu high MgO eclogite garnet separates determined by laser fluorination. All values of $\delta^{18}O$ are averages of two measurements except for KEC 86-107, which is a single measurement. 1 σ is the average reproducibility, i.e., ½ of the difference between two separate measurements. Samples are corrected to garnet standard UWG-2 = 5.8‰ (Valley et al., 1995).

sample	$\delta^{18}O_{SMOW}$	1 σ	jadeite in cpx [mol%]
KEC 80-B1	5.73	0.03	12%
KEC 81-2	5.54	0.02	13%
KEC 81-11	5.52	0.06	16%
KEC 86-2	5.64	0.02	11%
KEC 86-8	5.48	0.03	11%
KEC 86-15	5.21	0.00	21%
KEC 86-60	5.24	0.01	13%
KEC 86-73A	5.73	0.00	17%
KEC 86-90	5.28	0.00	11%
KEC 86-107	5.40	-	18%
K91-6	5.07	0.02	22%
K91-10	5.22	0.01	13%
K91-16	5.41	0.00	12%
K91-46	5.46	0.03	12%
transitional eclogite – garnet			
KEC 86-19	4.84	0.04	
core			19%
rim			46%

3.4.2. Trace Element Mineral Chemistry

The trace element compositions of minerals from 7 Koidu high MgO eclogites (garnet, cpx, and ilmenite), determined by laser ablation ICP-MS, are presented in Tables 3.2 – 3.4. All samples show variable degrees of modal and rare cryptic metasomatism (see below). Therefore, care was taken to perform analyses on crack-free, unaltered areas of the minerals. The combination of the high-quality optical imaging system of the Harvard laser ablation system and the time-resolved analysis of the ablation signals ensures that altered and/or metasomatized parts of the silicate minerals were recognized and excluded from the trace element analyses. Due to the limited grain size and the opaque nature of ilmenite in the thick sections (~100 μm) analyzed, altered parts of the ilmenite grains could not always be avoided during analysis. However, these were easily distinguished by their high abundances of incompatible trace elements (e.g., Sr, Ba) and were excluded from the averages.

Garnets (Table 3.2) are light rare earth element (LREE)-depleted with chondrite-normalized La contents (La_N) from 0.05 to 0.10 or below the detection limit (Fig. 3.2). All garnets, excluding the transitional sample KEC 86-19, have relatively flat heavy rare earth element (HREE) patterns with $(Dy/Yb)_N$ from 0.64 to 0.97, and have high HREE contents (Yb_N from 10 to 18). Sample KEC 86-19 shows a positive slope in the HREE (Yb_N = 85). Garnet in only one sample (KEC 86-58) has a negative Eu anomaly (Eu/Eu* = 0.75). All garnets show variable degrees of high field strength element (HFSE) depletions (Fig. 3.3), with Nb and Ta below the detection limit (0.3 to 0.03 ppm and 0.08 to 0.01 ppm for Nb and Ta, respectively, depending on the spot size) for most samples

(except KEC 80-B1, KEC 86-19, and KEC 86-107). The garnets show pronounced negative Ti anomalies but only slight depletions in Zr and Hf relative to Sm. The concentration of alkali and alkaline earth elements in garnet are generally very low (e.g., Sr ≤0.4 ppm) or are below the detection limit (e.g., Rb, Cs, Ba).

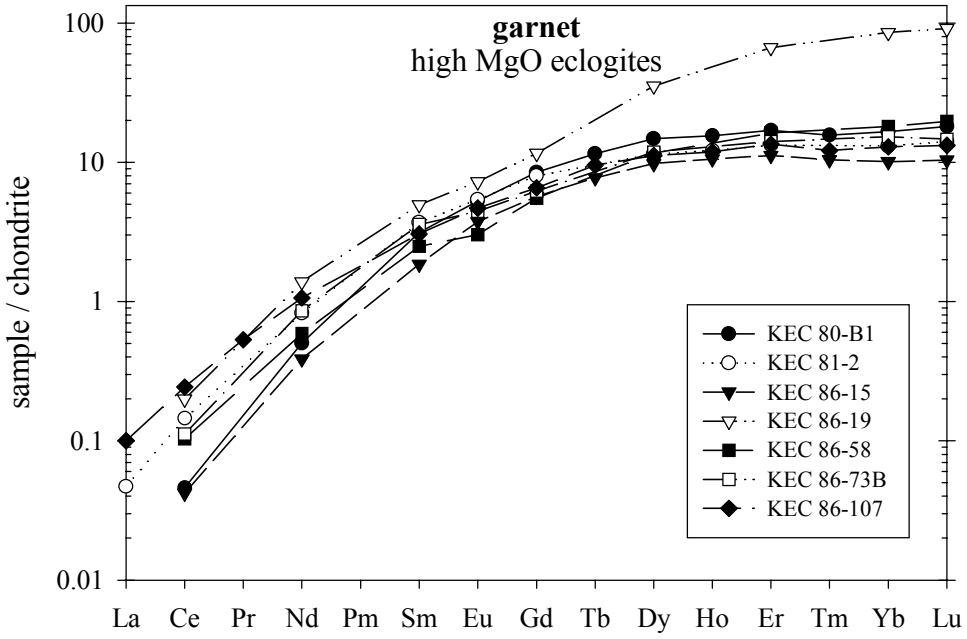

Figure 3.2. Chondrite-normalized garnet REE data for Koidu high MgO eclogite xenoliths. Element abundances are normalized to the chondrite values of Boynton (1984).

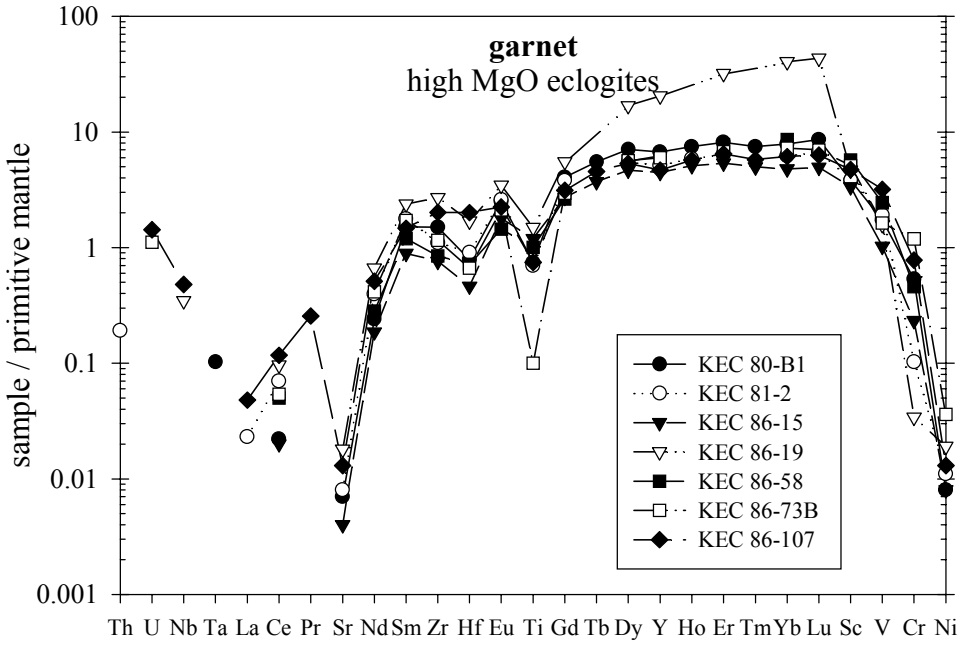

Figure 3.3. Mantle-normalized garnet trace element diagram for Koidu high MgO eclogite xenoliths. Element abundances are normalized to the primitive mantle values of McDonough and Sun (1995).

Table 3.2. Trace element composition of garnet determined by LA-ICP-MS. Concentrations are given in ppm (μg/g). n. d. = not determined. Cs, Ba, and Pb were measured but below the detection limit in all samples analyzed.

sample	**KEC 80-B1**		**KEC 81-2**		**KEC 86-15**		**KEC 86-19**		**KEC 86-58**		**KEC 86-73B**		**KEC 86-107**	
spots	n = 9	1 σ	n = 9	1 σ	n = 7	1 σ	n = 7	1 σ	n = 7	1 σ	n = 6	1 σ	n = 4	1 σ
Sc	62.2	1.6	62.1	5.0	54.2	4.5	75.7	6.8	92.9	5.5	82.7	7.4	76.5	2.9
V	143	11	156	18	83.9	15.2	129	7	200	21	134	26	262	18
Cr	1398	138	268	2	612	191	90.1	42.4	1206	48	3122	372	2041	161
Ni	15.5	3.3	22.3	0.2	15.3	1.7	36.9	2.9	< 50		71.4	-	24.9	3.2
Ga	n.d.		n.d.		n.d.		n.d.		10.5	0.9	n.d.		n.d.	
Rb	< 0.2		< 0.2		< 0.3		< 0.3		< 1.4		< 0.9		< 0.2	
Sr	< 0.2		0.16	-	0.07	-	0.36	0.14	< 0.3		< 0.3		0.26	0.06
Y	28.7	1.6	22.0	0.8	19.1	1.2	87.9	29.5	26.7	1.5	25.7	1.1	20.1	1.6
Zr	15.7	1.2	11.5	0.7	7.99	0.65	28.4	8.9	8.87	1.48	12.1	1.1	21.2	0.8
Nb	< 0.1		< 0.4		< 0.1		0.23	0.03	< 1.1		< 0.5		0.31	0.14
La	< 0.03		0.015	0.002	< 0.03		< 0.03		< 0.1		< 0.2		0.031	0.012
Ce	0.037	0.006	0.12	0.02	0.034	0.014	0.16	0.04	0.08	0.02	0.090	0.002	0.20	0.05
Pr	< 0.05		n.d.		< 0.02		n.d.		n.d.		n.d.		0.06	0.02
Nd	0.30	0.05	0.50	0.03	0.23	0.03	0.83	0.13	0.35	0.03	0.52	0.09	0.64	0.10
Sm	0.61	0.09	0.72	0.20	0.36	0.03	0.97	0.10	0.49	0.07	0.70	0.11	0.60	0.06
Eu	0.39	0.04	0.40	0.06	0.28	0.01	0.53	0.03	0.22	0.02	0.33	0.04	0.34	0.04
Gd	2.20	0.25	2.07	0.17	1.47	0.18	3.00	0.35	1.43	0.13	1.60	0.23	1.70	0.07
Tb	0.55	0.04	n.d.		0.37	0.02	n.d.		n.d.		n.d.		0.45	0.04
Dy	4.75	0.23	3.69	0.14	3.14	0.18	11.33	3.67	3.75	0.31	3.81	0.22	3.60	0.30
Ho	1.11	0.07	0.87	0.04	0.76	0.06	n.d.		n.d.		n.d.		0.85	0.04
Er	3.56	0.23	2.78	0.16	2.35	0.23	13.97	3.62	3.40	0.31	2.96	0.16	2.83	0.24
Tm	0.51	0.04	n.d.		0.34	0.03	n.d.		n.d.		n.d.		0.39	0.02
Yb	3.47	0.32	2.73	0.18	2.11	0.19	17.85	2.87	3.78	0.34	3.19	0.17	2.70	0.14
Lu	0.58	0.07	0.45	0.04	0.33	0.03	2.93	0.38	0.63	0.07	0.47	0.01	0.43	0.04
Hf	0.22	0.03	0.26	0.02	0.13	0.02	0.48	0.16	0.20	0.04	0.19	0.01	0.57	0.03
Ta	0.004	-	< 0.04		< 0.02		< 0.02		< 0.03		< 0.07		< 0.02	
Th	< 0.01		0.015	-	< 0.02		< 0.01		< 0.02		< 0.04		< 0.02	
U	< 0.01		< 0.03		< 0.01		< 0.01		< 0.02		0.023	0.005	0.029	0.007

Cpx (Table 3.3) have convex-upward REE patterns and are LREE-enriched relative to the HREE (Fig. 3.4). La_N contents range from 6.1 to 54 and Yb_N ranges from 0.32 to 1.2. Cpx in only one sample (KEC 86-58) has a negative Eu anomaly (Eu/Eu* = 0.86). The cpx of the high MgO eclogites show greater degrees of LREE enrichment compared to cpx of the low MgO eclogites (Barth et al., 2001). All cpx show pronounced HFSE anomalies (Fig. 3.5). The concentrations of Rb and Cs are generally below the detection limit, whereas very small concentrations of Ba (0.1 to 0.6 ppm) have been measured.

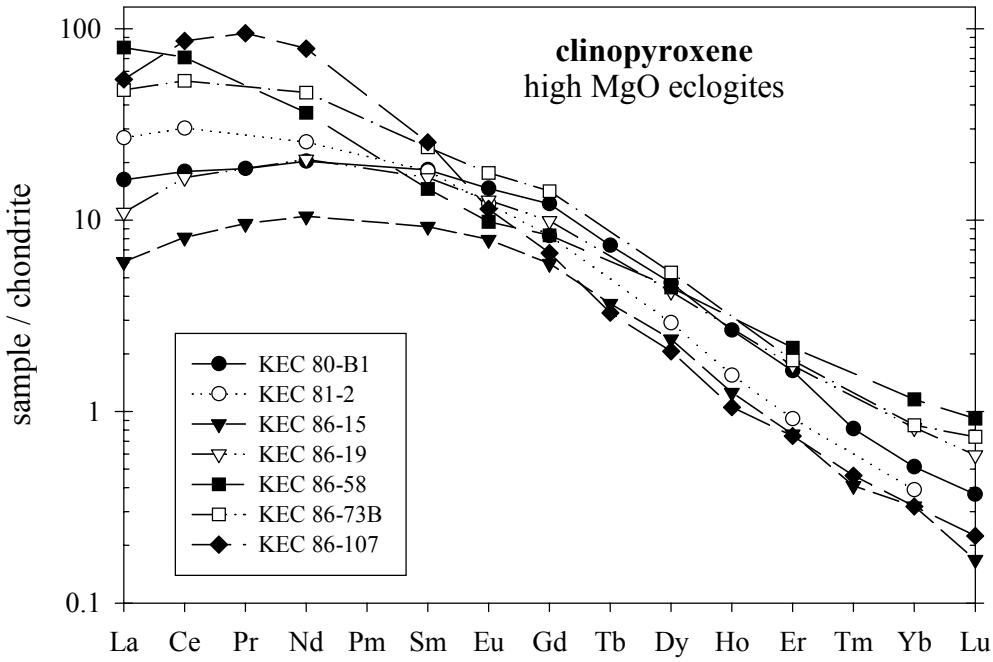

Figure 3.4. Chondrite-normalized clinopyroxene REE data for Koidu high MgO eclogite xenoliths. Normalized as in Figure 3.2.

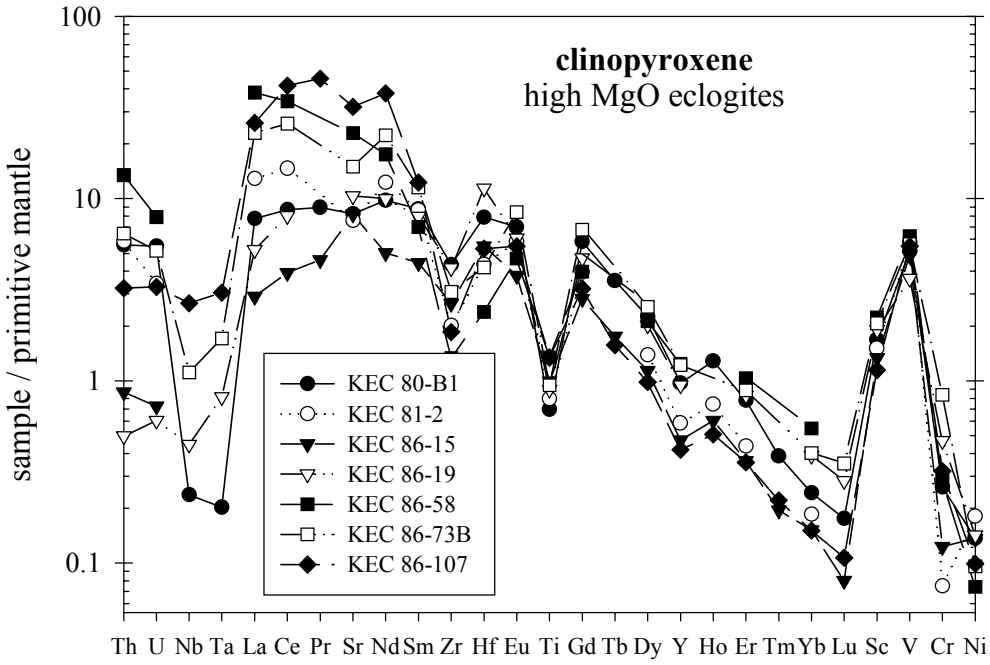

Figure 3.5. Mantle-normalized clinopyroxene trace element diagram for Koidu high MgO eclogite xenoliths. Normalized as in Figure 3.3.

Ilmenites (Table 3.4) have highly variable concentrations of Nb and Ta, with Nb/Ta ranging from subchondritic to superchondritic. The ilmenites have relatively homogeneous concentrations of W, Zr, Hf, V, and Ni. Ilmenites in the high MgO eclogites have similar trace element patterns to rutiles in the low MgO eclogites but higher Ni and lower Zr and Hf concentrations.

Table 3.3. Trace element composition of clinopyroxene determined by LA-ICP-MS. Concentrations are given in ppm (μg/g). n. d. = not determined. Cs was measured but below the detection limit in all samples analyzed.

sample	**KEC 80-B1**		**KEC 81-2**		**KEC 86-15**		**KEC 86-19**		**KEC 86-58**		**KEC 86-73B**		**KEC 86-107**	
spots	n = 10	1 σ	n = 9	1 σ	n = 7	1 σ	n = 7	1 σ	n = 7	1 σ	n = 2	1 σ	n = 7	1 σ
Sc	27.3	1.3	24.4	1.0	21.6	0.3	30.8	0.4	36.1	3.0	33.5	2.6	18.5	0.5
V	421	16	472	6	399	20	299	30	510	12	461	9	449	34
Cr	685	61	196	4	323	23	1232	430	740	42	2201	123	838	160
Ni	268	25	354	4	267	16	278	32	146	7	188	9	195	18
Ga	n.d.		n.d.		n.d.		n.d.		8.53	0.68	n.d.		n.d.	
Rb	< 0.1		< 0.4		< 0.1		< 0.2		< 0.8		< 0.3		< 0.08	
Sr	164	9	151	13	163	3	206	5	456	106	298	2	634	106
Y	4.18	0.12	2.51	0.20	2.03	0.09	4.07	0.09	5.32	0.64	5.25	0.12	1.80	0.08
Zr	45.5	1.5	21.2	1.9	27.9	0.5	43.8	2.6	14.0	1.3	32.3	1.1	19.5	1.4
Nb	0.16	0.04	< 0.3		< 0.04		0.29	0.04	< 0.6		0.73	0.03	1.75	0.13
Ba	0.13	0.03	0.40	0.05	0.12	0.02	0.21	0.01	0.54	0.19	0.32	0.02	0.58	0.12
La	5.04	0.32	8.35	1.18	1.88	0.11	3.40	0.10	24.75	7.76	14.87	0.69	16.89	1.52
Ce	14.6	0.7	24.5	3.0	6.57	0.29	13.5	0.4	57.3	13.5	43.2	2.0	69.91	6.89
Pr	2.27	0.06	n.d.		1.17	0.05	n.d.		n.d.		n.d.		11.57	1.51
Nd	12.2	0.4	15.4	1.1	6.29	0.21	12.5	0.2	21.8	2.9	27.8	1.8	47.34	5.73
Sm	3.57	0.22	3.52	0.28	1.80	0.04	3.25	0.10	2.84	0.23	4.68	0.31	4.98	0.79
Eu	1.08	0.05	0.90	0.09	0.58	0.04	0.93	0.03	0.72	0.02	1.30	0.00	0.84	0.10
Gd	3.16	0.14	2.15	0.18	1.53	0.09	2.57	0.09	2.16	0.07	3.67	0.18	1.74	0.06
Tb	0.35	0.01	n.d.		0.17	0.01	n.d.		n.d.		n.d.		0.16	0.01
Dy	1.52	0.10	0.94	0.12	0.77	0.03	1.36	0.06	1.43	0.10	1.72	0.10	0.66	0.05
Ho	0.19	0.01	0.11	0.02	0.09	0.01	n.d.		n.d.		n.d.		0.076	0.005
Er	0.34	0.03	0.19	0.02	0.16	0.02	0.36	0.02	0.45	0.08	0.39	0.02	0.16	0.01
Tm	0.026	0.004	n.d.		0.013	0.002	n.d.		n.d.		n.d.		0.015	0.002
Yb	0.11	0.01	0.082	0.012	0.067	0.005	0.17	0.02	0.24	0.04	0.18	0.04	0.067	0.010
Lu	0.012	0.003	0.003	-	0.005	-	0.019	0.002	0.030	0.008	0.024	0.001	0.007	0.002
Hf	2.24	0.11	1.23	0.16	1.55	0.06	3.22	0.17	0.68	0.05	1.19	0.06	1.50	0.13
Ta	0.007	0.002	< 0.02		0.006	0.003	0.030	0.008	< 0.02		0.063	0.006	0.11	0.04
Pb	n.d.		n.d.		n.d.		0.28	0.02	3.79	0.63	1.68	0.00	n.d.	
Th	0.44	0.06	0.46	0.08	0.069	0.018	0.039	0.005	1.07	0.25	0.51	0.04	0.26	0.05
U	0.11	0.02	0.069	0.013	0.015	0.003	0.012	0.002	0.16	0.03	0.11	0.01	0.067	0.011

Table 3.4. Trace element composition of ilmenite determined by LA-ICP-MS. Concentrations are given in ppm (µg/g). n. d. = not determined. Ba, Rb, Sr, Y, and REE were measured but below the detection limit in all samples analyzed.

sample	**KEC 80-B1**		**KEC 81-2**		**KEC 86-15**		**KEC 86-58**		**KEC 86-73B**		**KEC 86-107**	
spots	n = 4	1 σ	n = 8	1 σ	n = 9	1 σ	n = 1	1 σ	n = 4	1 σ	n = 4	1 σ
Sc	7.5	0.9	7.2	1.4	4.8		13	-	10	1.7	17	5.1
V	1242	46	1378	44	1020	223	726	-	1008	23	2231	405
Cr	1191	28	654	74	637	131	797	-	3310	105	10554	3273
MnO wt%	0.25	0.04	0.20	0.03	0.22	0.06	0.46	-	0.31	0.01	0.42	0.04
Ni	1177	137	1977	118	1321	129	1550	-	945	81	1136	131
Zn	n.d.		n.d.		n.d.		76	-	114	4	221	48
Zr	111	4	95	3.5	41	15	34	-	134	9	846	209
Nb	64	0.4	1961	49	118	16	368	-	5740	42	4927	434
Mo	n.d.		n.d.		n.d.		< 4.5		< 1.5		2.0	0.43
Sn	n.d.		n.d.		n.d.		1.98	-	4.13	-	13.3	4.3
Sb	n.d.		n.d.		n.d.		< 0.4		< 1		< 2	
Hf	2.39	0.26	2.17	0.12	1.07	0.08	0.74	-	1.73	0.40	24.1	7.0
Ta	3.27	0.05	78.4	5.8	5.10	0.84	5.47	-	380	15	465	27
W	n.d.		n.d.		n.d.		1.48	-	0.80	0.14	0.48	0.27
Pb	n.d.		n.d.		< 0.2		0.33	-	< 0.9		< 2	
Th	0.021	0.024	0.005	0.004	< 0.02		0.22	-	< 0.1		0.027	0.024
U	0.17	0.07	0.15	0.15	0.05	0.05	0.32	-	0.079	0.034	0.25	0.22

3.4.3. Whole Rock Chemistry

Trace element compositions of 9 Koidu high MgO eclogite whole rock powders were determined by solution ICP-MS (Table 3.5, Fig. 3.6) in order to assess the amount of trace element enrichment produced by secondary phases. All samples show variable enrichments in incompatible trace elements and relatively flat HREE patterns (except KEC 86-19, which is HREE enriched). Most samples have pronounced positive Nb anomalies and low Ti concentrations relative to REE. Some samples show negative Zr and Hf anomalies (e.g., KEC 86-58).

The whole rock analyses of these kimberlite-borne eclogite xenoliths are enriched in incompatible trace elements relative to the compositions determined from the primary minerals alone (Fig. 3.7). Highly incompatible elements are affected more than moderately incompatible and compatible elements; for example, La shows high and variable enrichments in the analyzed whole rock while Yb is little affected by alteration. Except for ilmenite, accessory phases (e.g., apatite, zircon) can be ruled out as important hosts of trace elements because these phases are not observed in the samples.

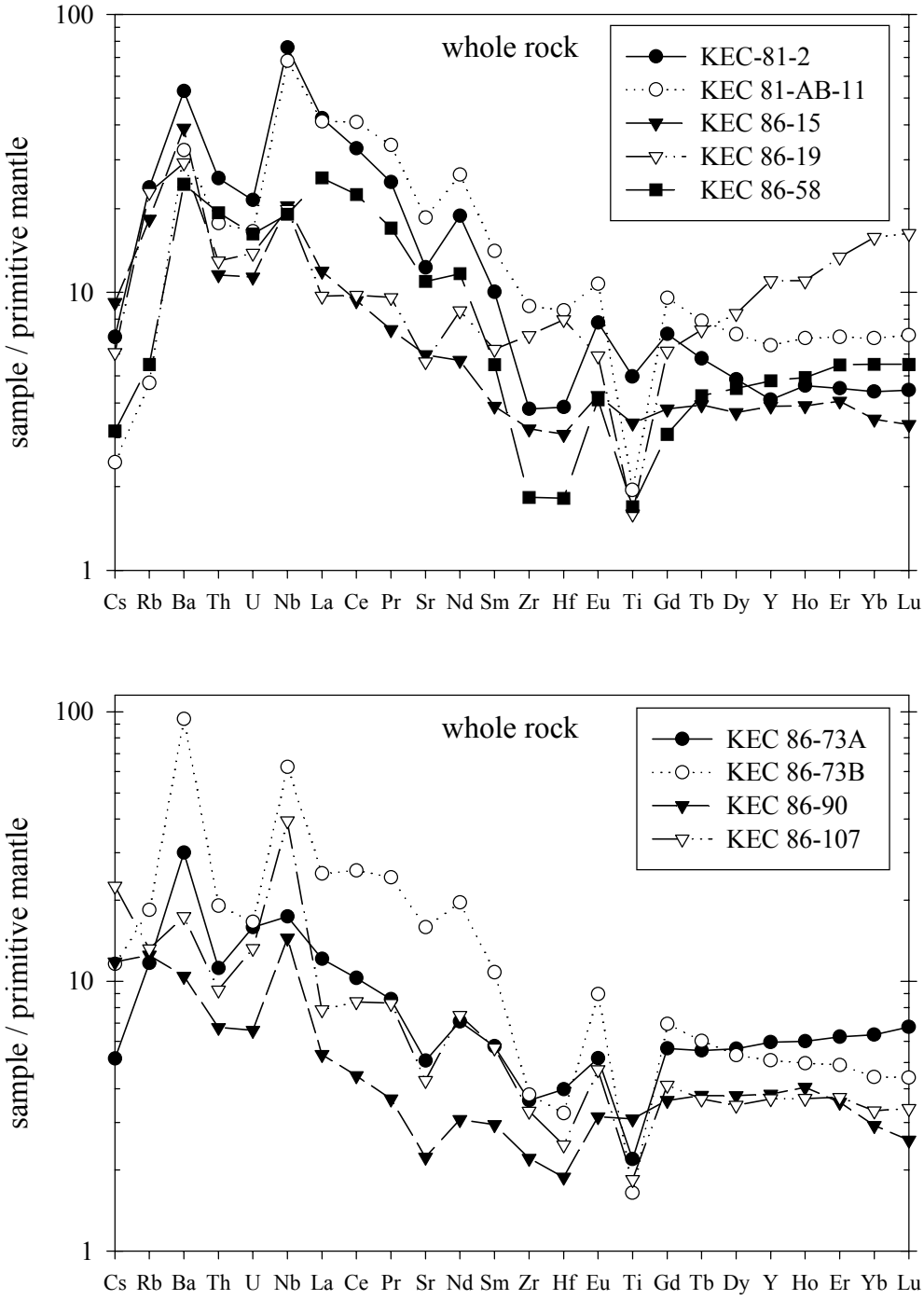

Figure 3.6. Mantle-normalized measured whole rock trace element diagrams for Koidu high MgO eclogite xenoliths. Samples are sorted by number. Normalized as in Figure 3.3.

Table 3.5. Whole rock compositions of the Koidu high MgO eclogites measured by solution ICP-MS. Concentrations are given in ppm (µg/g).

	KEC-81-2	KEC 81-AB-11	KEC 86-15	KEC 86-19	KEC 86-58	KEC 86-73A	KEC 86-73B	KEC 86-90	KEC 86-107
Ga	10.5	9.08	10.6	10.7	8.76	10.1	7.95	10.8	8.55
Rb	14.3	2.83	11.0	13.7	3.30	7.01	11.0	7.49	7.91
Sr	244	369	119	112	218	101	316	44.3	85.2
Y	17.7	27.7	16.7	47.3	20.7	25.6	21.9	16.4	15.8
Zr	39.9	93.6	33.8	73.4	19.2	38.0	39.9	23.1	34.6
Nb	50.0	44.7	13.5	13.1	12.6	11.4	41.1	9.52	25.9
Cs	0.14	0.05	0.19	0.13	0.07	0.11	0.24	0.25	0.47
Ba	349	214	257	193	162	198	622	68.9	115
La	27.4	26.7	7.71	6.28	16.7	7.85	16.3	3.47	5.08
Ce	55.2	68.6	15.6	16.3	37.6	17.2	43.2	7.47	14.1
Pr	6.33	8.60	1.86	2.43	4.33	2.18	6.17	0.93	2.10
Nd	23.6	33.2	7.10	10.7	14.6	8.86	24.5	3.84	9.34
Sm	4.07	5.72	1.58	2.53	2.23	2.33	4.38	1.19	2.30
Eu	1.20	1.65	0.65	0.91	0.63	0.80	1.38	0.48	0.72
Gd	3.85	5.19	2.07	3.34	1.68	3.06	3.77	1.97	2.24
Tb	0.57	0.78	0.39	0.73	0.42	0.55	0.60	0.37	0.36
Dy	3.28	4.75	2.48	5.65	3.04	3.79	3.59	2.54	2.34
Ho	0.69	1.02	0.58	1.64	0.74	0.89	0.74	0.60	0.55
Er	1.98	3.02	1.78	5.86	2.40	2.72	2.14	1.56	1.63
Yb	1.94	3.01	1.54	6.95	2.43	2.80	1.95	1.29	1.46
Lu	0.30	0.47	0.23	1.10	0.37	0.46	0.30	0.17	0.23
Hf	1.09	2.44	0.87	2.26	0.51	1.13	0.92	0.53	0.70
Th	2.04	1.41	0.92	1.03	1.53	0.89	1.51	0.54	0.74
U	0.44	0.34	0.23	0.28	0.33	0.32	0.34	0.13	0.27

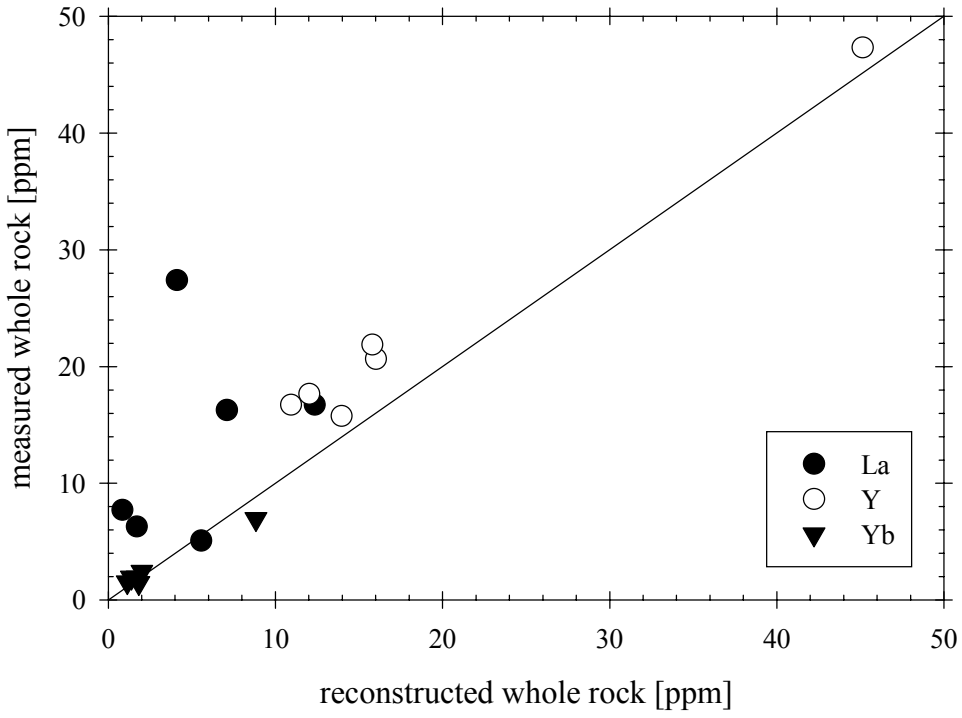

Figure 3.7. Plot of the reconstructed whole rock compositions vs. the measured whole rock compositions of the Koidu high MgO eclogites.

3.4.4. Whole Rock Reconstruction

In order to evaluate the chemical composition of the eclogites prior to their entrainment in and interaction with the kimberlite, primary whole rock compositions have been reconstructed based on the trace element contents measured in primary garnet, cpx, and ilmenite using previously published modal abundances of garnet and cpx (Table 3.6; Hills and Haggerty, 1989; Fung and Haggerty; 1995).

Some trace elements, such as the HFSE, may be largely contained in accessory phases such as ilmenite. This presents a problem for whole rock reconstructions as it is

generally difficult to determine precise modal proportions of accessory phases by point-counting such coarse-grained rocks. For this reason, we have calculated the modal abundance of ilmenite from Ti mass balance between the measured whole rock and mineral compositions (see Rudnick et al., 2000 and Barth et al., 2001 for details). For samples lacking bulk rock TiO_2 concentrations, modal ilmenite was calculated assuming that the bulk rock has no Ti-anomaly on a multi-element mantle-normalized diagram (Fig. 3.9).

The high MgO eclogites have slightly LREE-depleted to LREE-enriched patterns with flat HREE, except KEC 86-19, which shows HREE-enrichment (Fig. 3.8). The reconstructed whole rocks show a wide range of Nb/La and Nb/Ta ratios, ranging from subchondritic to superchondritic (Fig. 3.9). The high MgO eclogites have low Zr concentrations relative to Sm. This Zr depletion is not due to overlooked accessory phases such as zircon in the whole rock reconstructions because the measured whole rocks also show Zr depletions. Note that the sample with the lowest HREE contents (KEC 86-15) has a positive Sr anomaly while samples with higher HREE contents (e.g., KEC 86-107) have negative Sr anomalies. The eclogites have low to moderate U and Th contents with variable Th/U ratios.

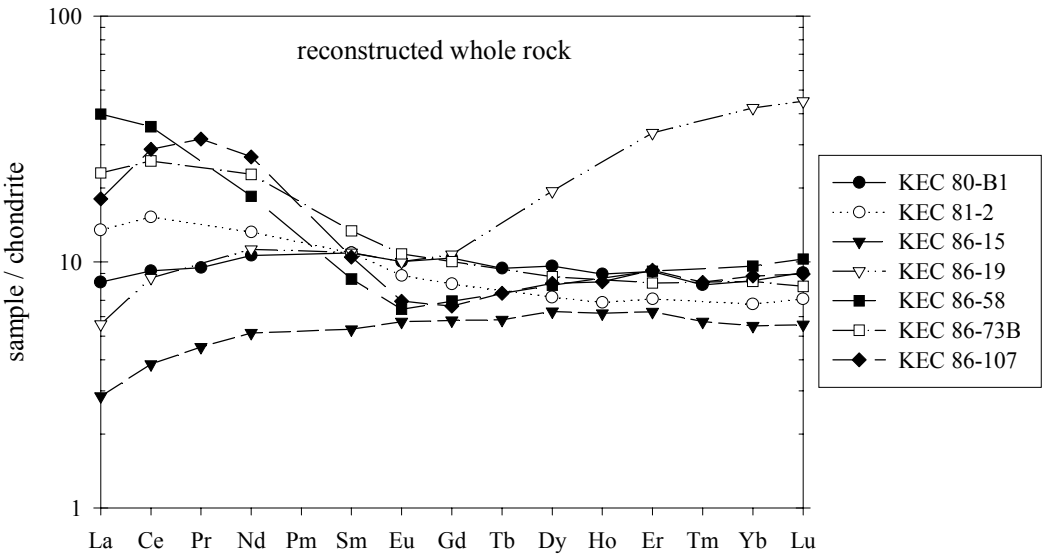

Figure 3.8. Chondrite-normalized reconstructed whole rock REE diagram for the Koidu high MgO eclogite xenoliths. Normalized as in Figure 3.2.

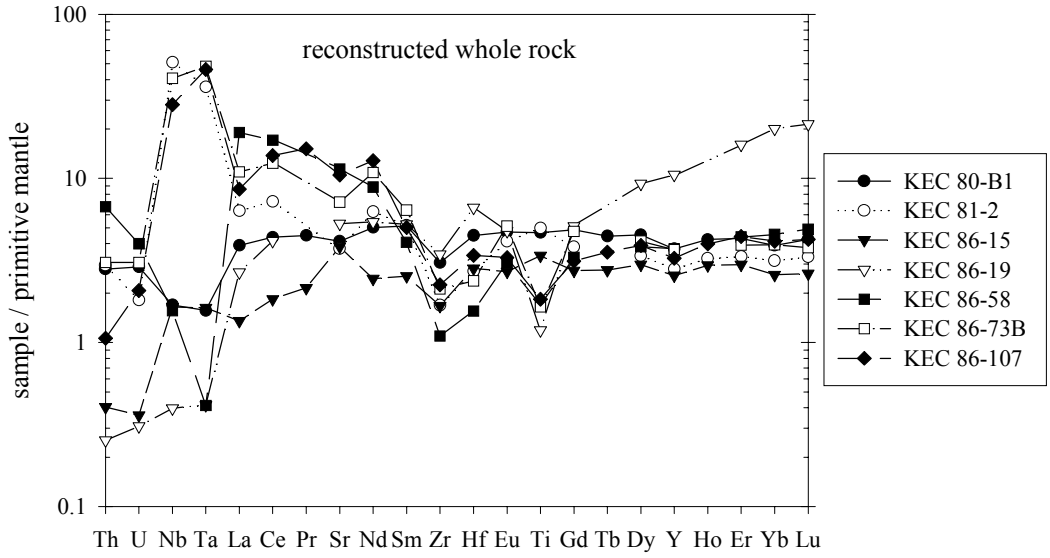

Figure 3.9. Mantle-normalized reconstructed whole rock trace element diagram for Koidu high MgO eclogite xenoliths. Normalized as in Figure 3.3.

Table 3.6. Reconstructed whole rock compositions of the Koidu high MgO eclogites. Concentrations are given in ppm (μg/g). wr = modal amount of ilmenite calculated by mass balance using whole rock Ti contents. c = modal amount of rutile calculated assuming no Ti anomaly. See text for details. n. d. = not determined. Mineral modes and reconstructed major element compositions are published in Hills and Haggerty (1989) and Fung and Haggerty (1995).

	KEC 80-B1 1.6% ilm	KEC 81-2 1.7% ilm	KEC 86-15 0.92% ilm	KEC 86-19 no ilmenite	KEC 85-58 0.28% ilm	KEC 86-73B 0.46% ilm	KEC 86-107 0.36% ilm
	c	wr	wr	wr	wr	wr	wr
Sc	44	43	39	53	64	59	57
Ti	5633	5989	4072	1432	2035	1985	2212
V	300	332	239	216	356	294	330
Cr	1037	239	478	673	972	2683	1676
Ni	161	219	144	160	77	131	85
Sr	82	74	76	105	227	143	209
Y	16	12	11	45	16	16	14
Zr	32	18	18	36	11	22	24
Nb	1.1	34	1.1	0.3	1.0	27	19
La	2.5	4.1	0.9	1.7	12	7.1	5.6
Ce	7.3	12	3.1	7.0	29	21	23
Pr	1.1	n. d.	0.5	n. d.	n. d.	n. d.	3.8
Nd	6.3	7.8	3.1	6.8	11	14	16
Sm	2.1	2.1	1.0	2.1	1.7	2.6	2.0
Eu	0.7	0.6	0.4	0.7	0.5	0.8	0.5
Gd	2.6	2.1	1.5	2.8	1.8	2.6	1.7
Tb	0.4	n. d.	0.3	n. d.	n. d.	n. d.	0.4
Dy	3.1	2.3	2.0	6.2	2.6	2.8	2.6
Ho	0.6	0.5	0.4	n. d.	n. d.	n. d.	0.6
Er	1.9	1.5	1.3	7.0	1.9	1.7	1.9
Yb	1.7	1.4	1.1	8.8	2.0	1.7	1.8
Lu	0.29	0.22	0.18	1.4	0.33	0.26	0.29
Hf	1.3	0.77	0.80	1.9	0.44	0.67	0.96
Ta	0.058	1.3	0.060	0.015	0.015	1.8	1.7
Th	0.22	0.23	0.032	0.020	0.53	0.24	0.084
U	0.059	0.037	0.007	0.006	0.081	0.062	0.042

3.5. Metasomatic Overprinting

Enrichment of incompatible trace elements caused by infiltration and alteration by the host kimberlite is manifested by the presence of secondary phlogopite and amphibole in veins, which may be up to 20 modal % in some xenoliths (Hills and Haggerty, 1989). For example, combined petrographic observations and trace element analyses show that primary cpx in KEC 86-73B, which is depleted in Rb, Ba, Nb, and Ta, is partially replaced by secondary amphibole (amph) that has much higher concentrations of these elements (Fig. 3.10). For other trace elements secondary amph has similar concentrations to primary cpx, suggesting that amph inherited these elements from cpx. This observation further demonstrates that amph is not in high-temperature trace element equilibrium with cpx, indicating that the growth of secondary amph occurred shortly before the eruption of the host kimberlite (see below). See Barth et al. (2001) for an evaluation of the effect of this modal (patent) metasomatism on the whole rock chemistry.

While cryptic metasomatism has not been observed in the Koidu low MgO eclogites, the Koidu high MgO eclogites show evidence of cryptic metasomatism in addition to modal metasomatism. Cryptic metasomatism is defined as enrichment in incompatible elements such as Rb, Sr, Ba, and REE without visible evidence of metasomatism (Dawson, 1984). In some Koidu high MgO eclogites (KEC 86-15, KEC 86-19, and KEC 86-107), analyses of optically unaltered, crack-free minerals show trace element concentrations that are significantly higher than in other grains of the same mineral and are therefore not in high-temperature equilibrium with the other mineral

phases. In sample KEC 86-15, primary garnet is depleted in LREE and other highly incompatible elements while altered garnet contains noticeable concentrations of these elements (Fig. 3.11). Primary garnet is in trace element equilibrium with cpx and ilmenite; Sr and LREE partition into cpx (Harte and Kirkley, 1997) and Nb and Ta into ilmenite. The high concentrations of Sr and LREE in the altered garnet illustrate that the altered parts of garnet are in disequilibrium with the other phases in the eclogite. Electron microprobe analyses show that the major element compositions of primary and metasomatized garnet are indistinguishable (Table 3.7). This type of metasomatism, where major element and incompatible trace element concentrations are decoupled and concentrations of trace elements such as Sr apparently disobey normal partitioning relationships, has been named isolated trace element enrichment by Harte (1987).

Table 3.7. Major element composition of altered and primary garnet in high MgO eclogite KEC 86-15. H + H = data from Hills and Haggerty (1989).

KEC 86-15	altered garnet		primary garnet		H + H
	n = 4	1 σ	n = 8	1 σ	(1989)
SiO_2	41.77	0.04	41.65	0.19	42.09
TiO_2	0.07	0.01	0.10	0.03	0.24
Al_2O_3	23.43	0.06	23.31	0.15	21.58
Cr_2O_3	0.12	0.02	0.09	0.02	0.25
FeO	13.37	0.17	13.38	0.12	14.30
MnO	0.30	0.01	0.30	0.01	0.36
MgO	18.17	0.10	17.77	0.22	17.49
CaO	3.86	0.09	4.19	0.25	4.16
Na_2O	0.05	0.01	0.06	0.01	0.09
K_2O	0.00	0.00	0.00	0.00	0.00
Total	101.15		100.84		100.56

Both modal and cryptic metasomatism are most likely related to infiltration or exchange with a kimberlitic magma or a fluid derived from a kimberlitic magma because

Ba, Sr, Nb, Ta, and LREE are highly enriched in kimberlites compared to the primary eclogite minerals (Figs. 3.10 and 3.11). Trace element data suggest that the liquids giving rise to the metasomatism, while not necessarily being identical to the kimberlite carrying the xenoliths to the surface, have probably formed part of the same set of magmatic events (cf. Harte, 1987). Thus, the trace element pattern of the altered garnet in KEC 86-15 is approximately parallel to that of the host kimberlite for the most incompatible elements (Fig. 3.11). The metasomatic enrichment must have occurred shortly before the eruption of the host kimberlite because at the high temperatures of the high MgO eclogites (1080 – 1130 °C) diffusion would rapidly erase trace element disequilibrium. The experimentally determined diffusion coefficient of Sr in garnet at the equilibration temperature of KEC 86-15 (1100 °C) is 1.6×10^{-16} cm²/s (Coghlan, 1990). Thus, taking $t = \frac{d^2}{4D}$ as the homogenization time (t) for a sphere (diameter d) with diffusion coefficient D, we calculate that a grain with a diameter of 4 mm would be homogenized in about 8 Ma.

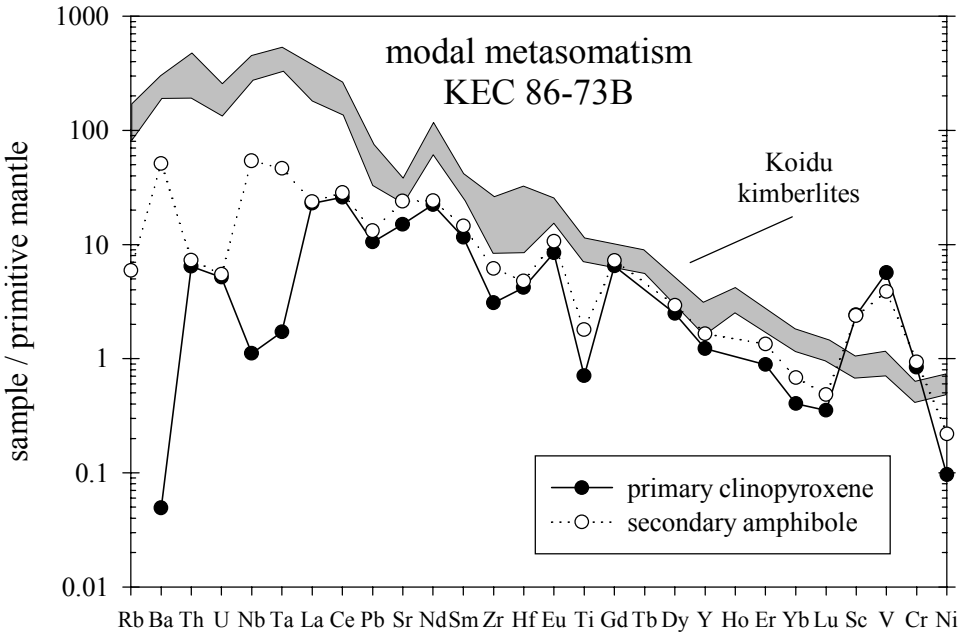

Figure 3.10. Mantle-normalized trace element diagram illustrating kimberlite-related modal metasomatism of clinopyroxene in high MgO eclogite KEC 86-73B. Gray field shows the range of kimberlite compositions at Koidu, Sierra Leone (Taylor et al., 1994). Solid circles denote the primary clinopyroxene composition; open circles denote secondary amphibole replacing clinopyroxene. Normalized as in Figure 3.3.

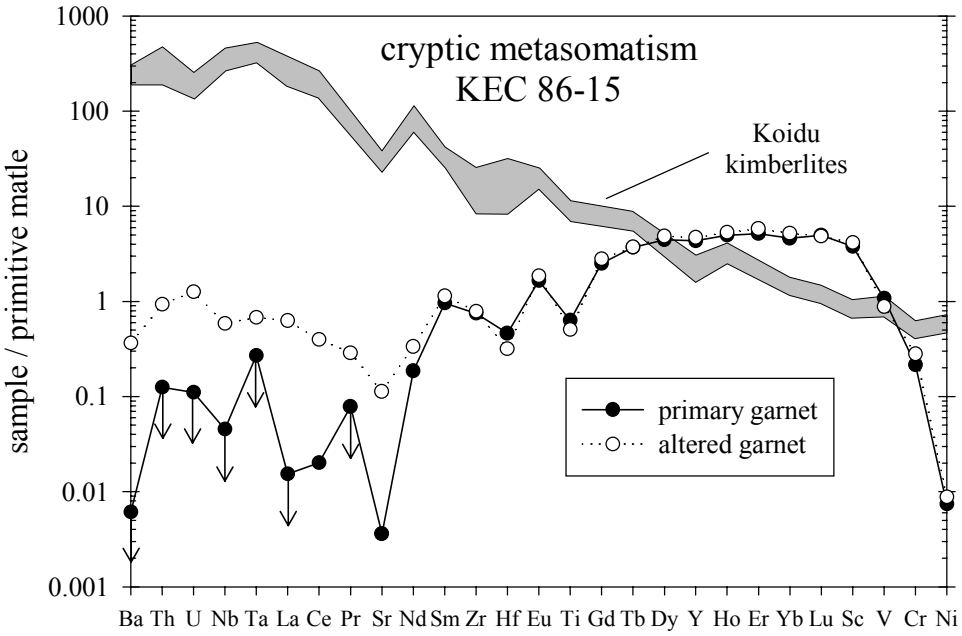

Figure 3.11. Mantle-normalized trace element diagram illustrating kimberlite-related cryptic metasomatism of garnet in high MgO eclogite KEC 86-15. Gray field shows the range of kimberlite compositions at Koidu, Sierra Leone (Taylor et al., 1994). Solid circles denote the primary garnet composition; open circles denote garnet that has been affected by cryptic metasomatism. Arrows indicate elemental concentrations below the detection limit. Normalized as in Figure 3.3.

Ancient metasomatic enrichment, prior to the kimberlite-related alteration, is an important mantle process that can significantly change the chemical composition of mantle-derived samples. Metasomatism by passing melts can increase Mg# (molar Mg/(Mg+Fe)), Ba, Nb, Zr, and LREE contents of the original eclogite (Dawson, 1984; Harte, 1987; Zindler and Jagoutz, 1988; Ireland et al., 1994). Evidence of metasomatic

enrichment of a LREE depleted rock are sigmoidal and 'double hump' cpx and/or whole rock REE patterns (Johnson et al., 1990; Ireland et al., 1994). Such REE patterns are predicted for early stages of metasomatism by melt percolation models (Navon and Stolper, 1987), whereas the final results of porous flow are smooth, LREE-enriched patterns (Navon and Stolper, 1987; Takazawa et al., 1992). These latter patterns cannot easily be distinguished from undepleted, enriched rocks.

Some Koidu high MgO eclogites are LREE-enriched and have 'humps' in their REE pattern (e.g., KEC 86-107, Fig. 3.8). Furthermore, the high MgO eclogites have Mg#'s (74-88) that overlap or exceed Ireland et al.'s (1994) metasomatized eclogites (Mg# = 74) and primitive, peridotite-derived melts (Mg# 74-80, Fig. 3.13). Primary (texturally equilibrated) amphibole in sample KEC 81-AB-11 has been cited as evidence for mantle metasomatism that predated the kimberlite-related metasomatism (Hills and Haggerty, 1989). Thus, in addition to the recent kimberlite-associated metasomatism documented above, we conclude that at least some of the high MgO eclogites have experienced ancient metasomatism that resulted in an enrichment of incompatible elements. However, less incompatible elements such as HREE and transition elements appear to have been affected to a much lesser extent (cf. Figs. 3.10 and 3.11). These more conservative elements might still reflect the original trace element composition of the protoliths of the high MgO eclogites and, thus, can be used to constrain the origin(s) of these rocks.

3.6. The Origins of the Koidu high MgO Eclogites

The mafic compositions and lithospheric equilibration conditions of the Koidu high MgO eclogites could be the result of (1) mantle melting and crystallization of these magmas and their cumulates at high pressures ("mantle" hypothesis), (2) metamorphism and foundering of underplated basaltic magmas at the base of the continental crust, and (3) metamorphism ± partial melting of subducted oceanic crust.

The Koidu low MgO eclogites have been interpreted to represent ancient altered oceanic crust that underwent an episode of partial melting during subduction (Barth et al., 2001). Weak correlations of Mg vs. Ni suggest that the high MgO eclogites are not simply picritic equivalents of the low MgO eclogites (Hills and Haggerty, 1989) and that the high MgO and low MgO eclogites are not related to each other by simple partial melting or crystal fractionation trends. Additionally, the high MgO eclogites have both higher $(La/Yb)_N$ and higher Cr concentrations than the low MgO eclogites (Fig. 3.12). However, the high LREE contents of some high MgO eclogites might be the result of metasomatism (see above) and, therefore, do not necessarily prove that the low MgO and high MgO eclogites are genetically unrelated.

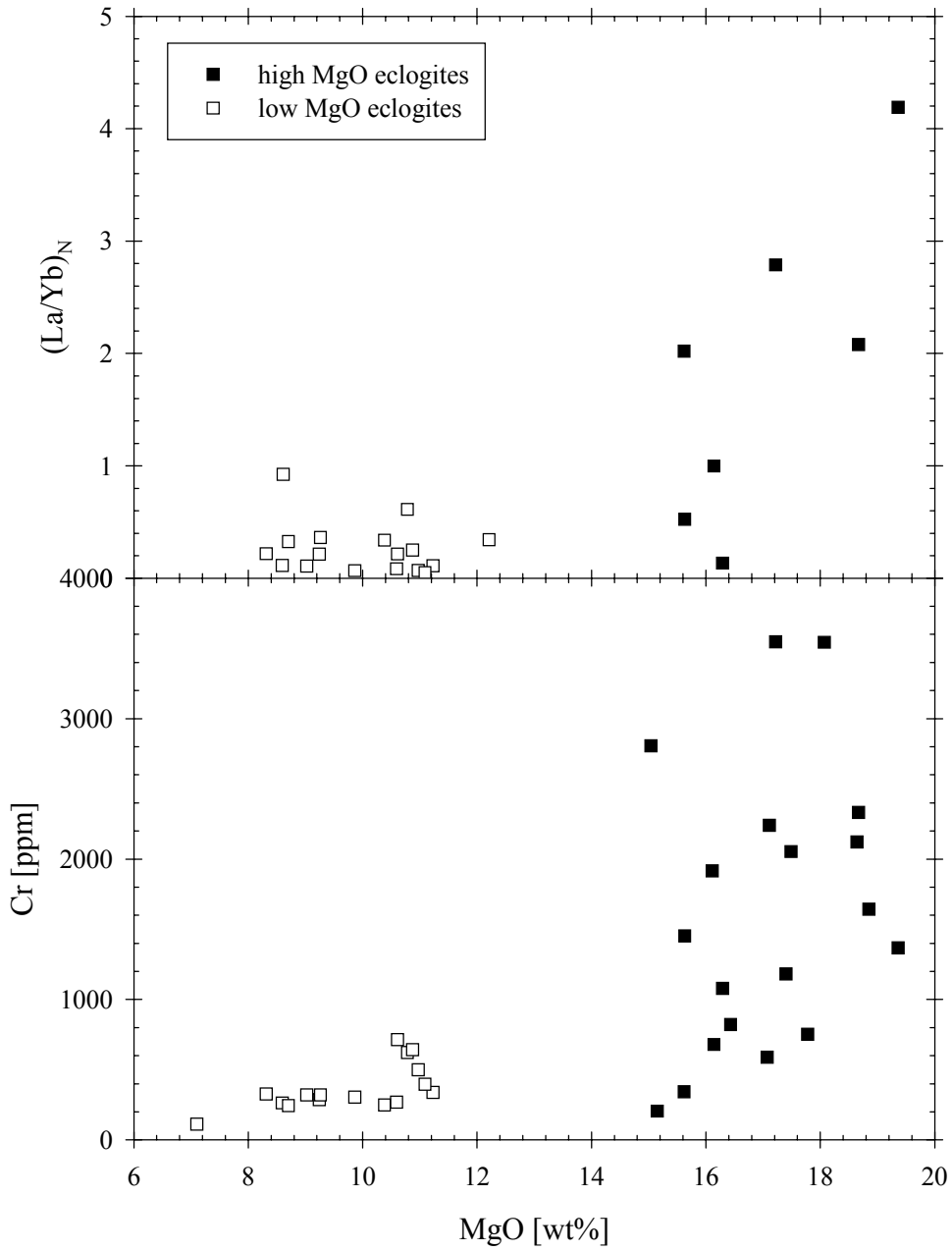

Figure 3.12. Plot of reconstructed whole rock MgO vs. $(La/Yb)_N$ (top) and Cr (bottom). Solid squares: Koidu high MgO eclogite xenoliths (this study). Open squares: Koidu low MgO eclogites (Barth et al., 2001).

3.6.1 High Pressure Mantle Melts and Cumulates

3.6.1.1. Origin as picritic high-pressure liquids

In the "mantle" hypothesis, peridotite melting must have occurred at pressures exceeding 4 GPa, since pressure estimates of the high MgO eclogites cluster between 4.0 and 4.5 GPa (see above). However, only few Koidu high MgO eclogites have major element compositions similar to primary, high-pressure mantle melts (Figs. 3.13 and 3.14). On average, the high MgO eclogites have higher Al_2O_3, slightly higher Na_2O, lower FeO, and slightly lower MgO contents than picritic mantle melts generated at high pressure (4 GPa). High-pressure mantle melts have low Al_2O_3 contents due to increased stability of garnet with increasing pressure (Falloon and Green, 1988; Kinzler and Grove, 1992; Kushiro, 1996; Walter, 1998).

3.6.1.2. Origin as cumulates of primary high-pressure melts

If the Koidu high MgO eclogites do not represent primary high-pressure melts, could they be cumulates derived from such melts? The high MgO eclogites have major element compositions similar to pyroxenite xenoliths and pyroxenite veins in ophiolites (Figs. 3.13 and 3.14), which have been interpreted as cumulates of mafic magmas (e.g., Frey, 1980; Bodinier et al., 1987; Pearson et al., 1993). In support of this hypothesis, the high MgO eclogites have high Mg#'s (74-88); some of them higher than primary high-pressure melts (Mg# = 76-80 at 4 GPa; Walter, 1998), moderate to high Cr and Ni (Fig. 3.15) combined with low V contents, LREE-enriched cpx, and mantle-like $\delta^{18}O$ values. These features are broadly similar to the Group A eclogites from South Africa (Taylor and Neal, 1989), which have been interpreted as high-pressure cumulates of a basaltic

Figure 3.13. Whole rock MgO content plotted against Al_2O_3 (top) and total FeO (bottom) concentration. Solid squares: Koidu high MgO eclogites (reconstructed using data of Hills and Haggerty, 1989, and Fung and Haggerty, 1995). Crosses: Pyroxenite veins in ophiolites (Loubet and Allègre, 1982; Pearson et al., 1993) and pyroxenite xenoliths (Irving and Green, 1970; Wilkinson, 1975; Frey, 1980; Griffin et al., 1988; Kumar et al., 1996). Dotted triangles and reverse triangles: experimental pyrolite melts at 1 and 4 GPa, respectively (Baker and Stolper, 1994; Walter, 1998). Open circles: oceanic gabbros (Gunn and Roobol, 1977; Dick et al., 1999; Hart et al., 1999). Light and dark gray fields show Archean basalts and Archean picrites and komatiites, respectively (compiled from the literature).

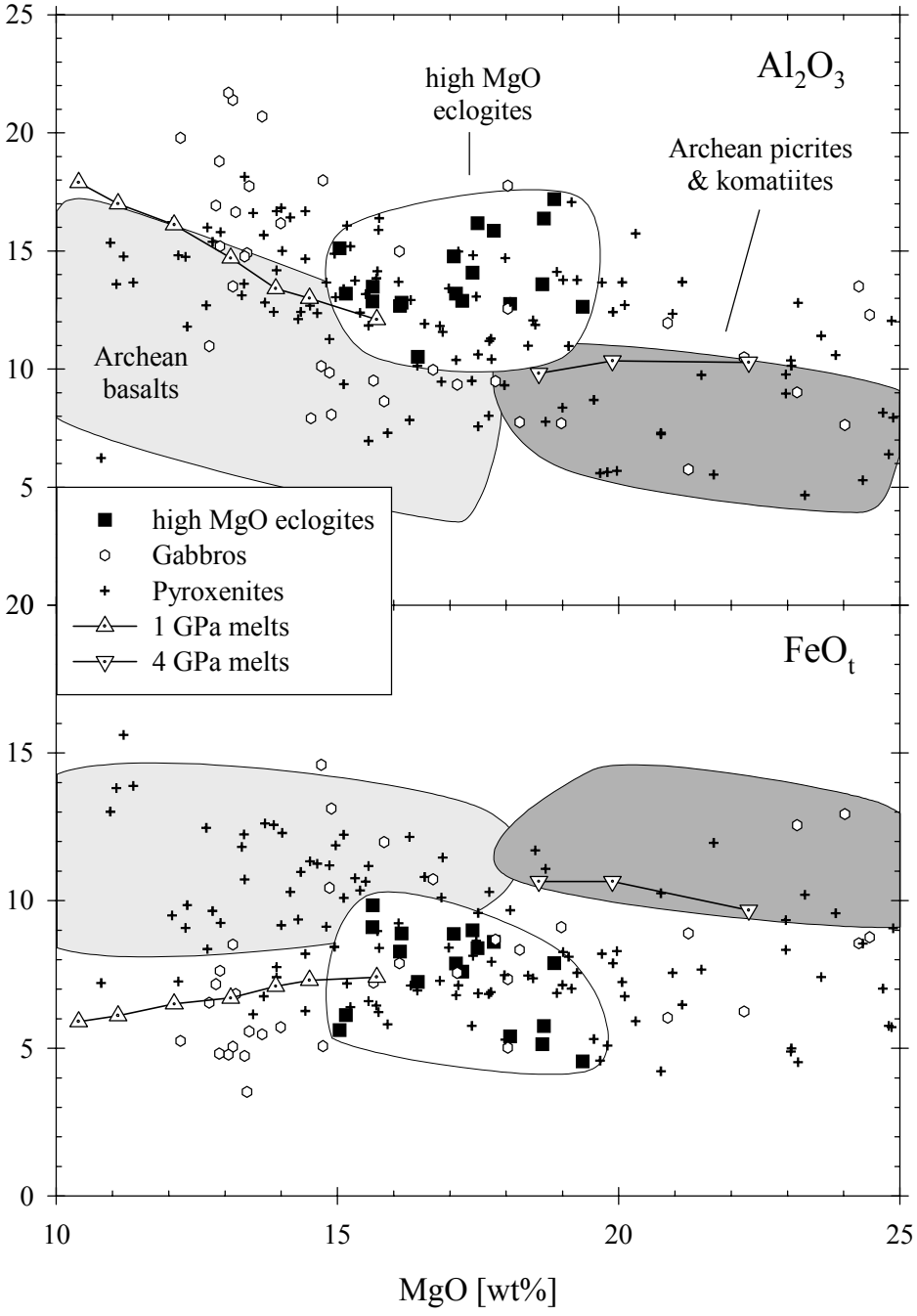
Al_2O_3
high MgO eclogites
Archean picrites & komatiites
Archean basalts
high MgO eclogites
Gabbros
Pyroxenites
1 GPa melts
4 GPa melts
FeO_t
MgO [wt%]

melt. In this model the LREE enriched whole rock compositions are attributed to trapped liquid (Shervais et al., 1988; Taylor and Neal, 1989).

An observation that is difficult to reconcile with an origin of the Koidu high MgO eclogites as cumulates derived from primary mantle melts is the absence of modal olivine. As first pointed out by Hatton and Gurney (1987), partial melting of peridotite at pressures exceeding ~3.5 GPa is not a feasible process for the generation of bi-mineralic eclogites, because the partial melts generated would crystallize to an assemblage containing olivine. Assuming a garnet lherzolite source, the solidus melting reaction is eutectic (ol + cpx + grt = melt) at pressures >3.3 GPa, with the degree of melting at which the melting reaction changes from eutectic to the peritectic type (ol + cpx + grt = melt + opx) increasing with pressure (Walter, 1998). For example, at 4 GPa the peritectic reaction begins at ~12% melting. At low degrees of partial melting, i.e., eutectic reaction, fractional crystallization does not yield any evolved liquids and the melt crystallizes completely to a rock of its own composition (ol + cpx + grt). At higher degrees of partial melting, i.e., peritectic reaction, fractional crystallization drives the melt towards a more evolved composition by crystallization of ol + cpx + grt (Milholland and Presnall, 1998). On further cooling, the liquid probably crystallizes cpx and spinel (Milholland and Presnall, 1998). Thus, while some garnet pyroxenites and eclogites may be magmatic cumulates crystallized from alkalic or moderately fractionated tholeiitic magmas in the uppermost mantle (cf. Liu and Presnall, 2000), experimental data suggest that bi-mineralic (olivine-free) eclogites cannot be generated by fractional crystallization of garnet lherzolite melts at pressures exceeding ~3.3 GPa.

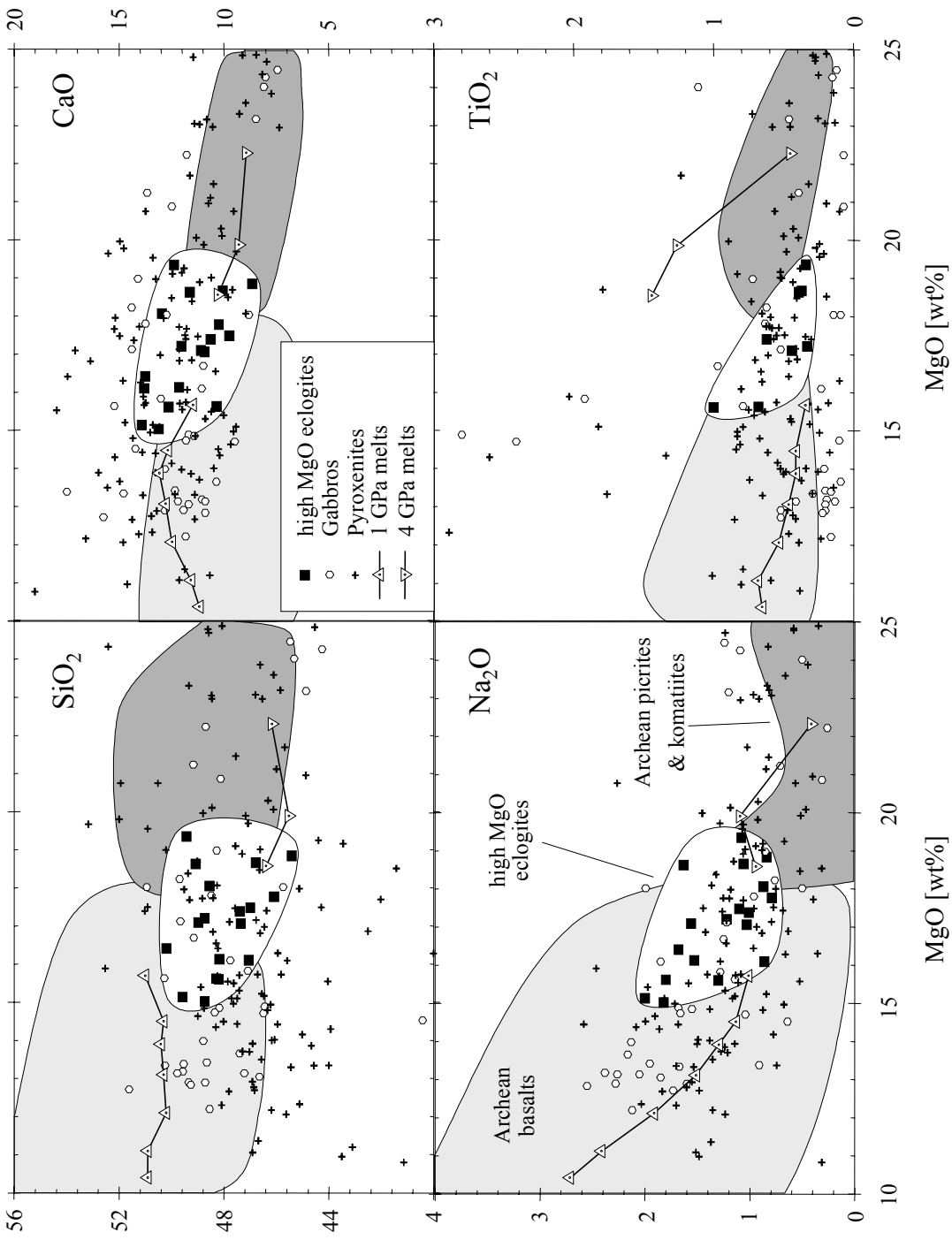

Figure 3.14. Plot of SiO_2, CaO, Na_2O, and TiO_2 vs. MgO whole rock content. Symbols and data sources as in Figure 3.13.

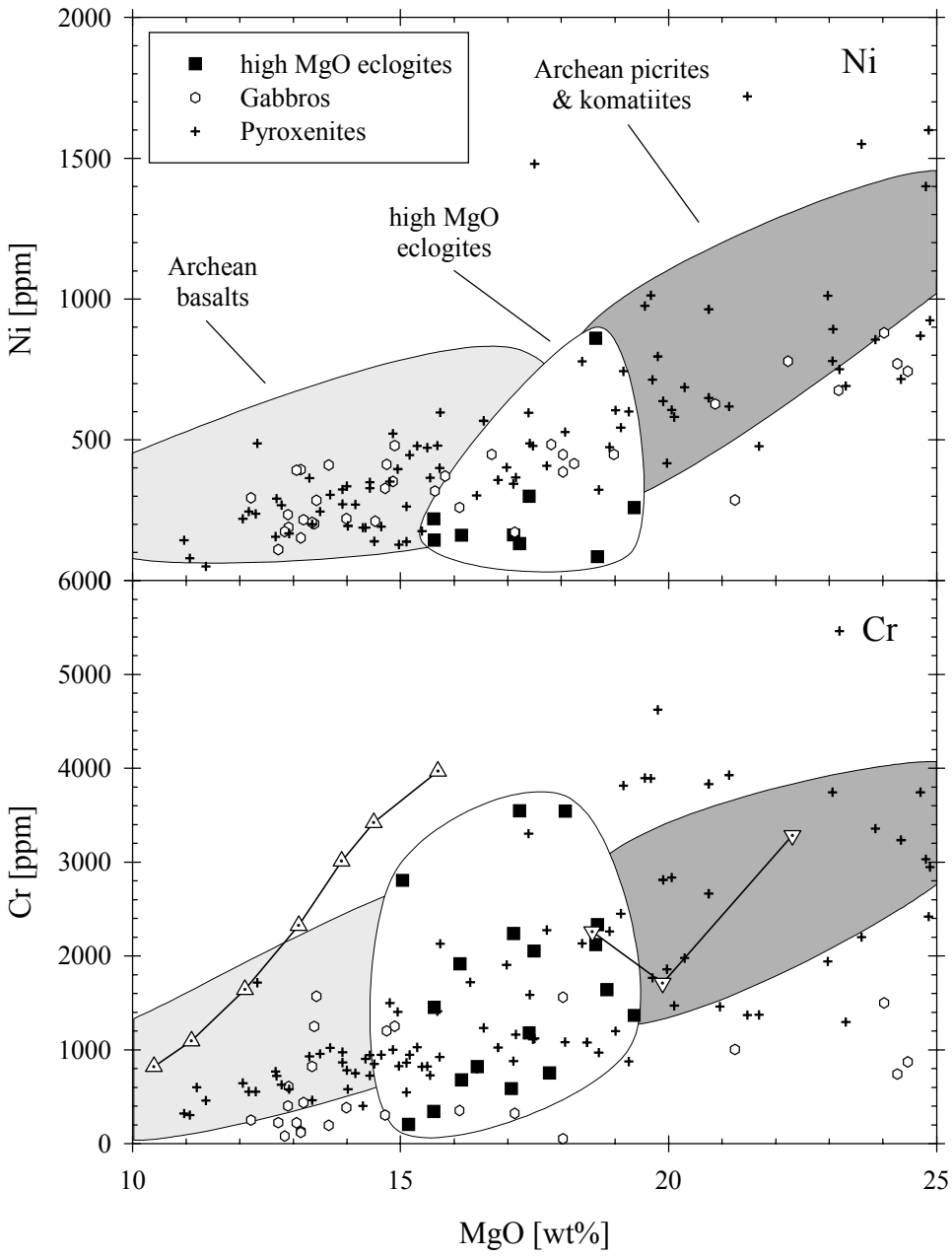

Figure 3.15. Plot of Ni (top) and Cr (bottom) vs. whole rock MgO content. Symbols and data sources as in Figure 3.13.

The above observations do not rule out a mantle cumulate origin for the Koidu high MgO eclogites. However, if they did originate in this manner one must invoke a) a

source rock for the melt that was itself olivine-free or b) eclogite formation by fractional crystallization from a mantle melt at pressures <3.3 GPa. In support of the first possibility, some garnet pyroxenites and eclogites have been interpreted to represent high-pressure cumulates from silicic melts of subducted oceanic crust (Hatton and Gurney, 1987; Pearson et al., 1991). However, the Koidu high MgO eclogites do not require an origin involving high-pressure crystal fractionation. For example, the trace element compositions of the high MgO eclogites do not show a clear correlation with their modal mineralogy: sample KEC 86-107 has the highest modal garnet abundance (67%) but a flat HREE pattern. Since no unambiguous contact relationships between high MgO eclogite and ambient peridotitic mantle have been observed, i.e., no composite xenoliths have been reported at Koidu, it remains unresolved if the Koidu high MgO eclogites are cumulates from a melt derived from an olivine-free source rock and crystallized at high pressures or if the high MgO eclogites were formed at lower pressures and re-equilibrated in the diamond stability field. This second possibility is explored in section 3.6.2.

3.6.1.3. Origin as pyroxene cumulates derived from differentiated liquids

Some garnet pyroxenites have been interpreted to derive from nearly monomineralic pyroxenites by garnet exsolution from pyroxene (e.g., Frey, 1980; Bodinier et al., 1987). These pyroxenites precipitated from evolved alkalic or tholeiitic basalts. While none of the high MgO eclogites studied have exsolution textures, some granoblastic garnet pyroxenites were interpreted to have formed by exsolution and complete recrystallization of garnet-free assemblages (Griffin et al., 1984). This model

could account for the lack of a garnet signature in the trace element patterns of the Koidu high MgO eclogites. However, several observations are inconsistent with this model.

(1) Typical pyroxenite suites include orthopyroxene-bearing samples. Additionally, unmixing of clinopyroxene results in exsolution of orthopyroxene ± spinel in addition to garnet (Frey, 1980; Griffin et al., 1984; Bodinier et al., 1987). Orthopyroxene is absent in the Koidu high MgO eclogites.

(2) Pyroxenites without primary (magmatic) garnet have lower Al_2O_3 contents than the Koidu high MgO eclogites (10.4-16.5 wt% Al_2O_3). For example, type I and II pyroxenites from Salt Lake Crater, Oahu, Hawaii, have only 7.6-9.5 wt% Al_2O_3 (Frey, 1980).

(3) The pyroxenites equilibrated at much lower pressures (1.1 – 2.4 GPa) than the Koidu high MgO eclogites (4.0 – 4.5 GPa). As argued above, it is not feasible to crystallize olivine-free assemblages at pressures exceeding ~3.3 GPa.

Given these inconsistencies, we consider garnet-free pyroxene cumulates unlikely protoliths for the high MgO eclogites.

3.6.2. Low Pressure Origin

3.6.2.1. Subducted Oceanic Crust

While the Koidu high MgO eclogites have MgO, CaO, Na_2O, and TiO_2 contents similar to picrites (Fig. 3.14), the high MgO eclogites fall outside the compositional range of Archean basalts and komatiites (Fig. 3.13). The high MgO eclogites have higher Al_2O_3 and lower FeO contents than picrites (and higher Mg#'s than Archean basalts). Thus, we

conclude that the protoliths of the high MgO eclogites do not represent extrusive mafic or ultramafic magmas.

3.6.2.2. Gabbros and Layered Intrusions

Major element compositions of the high MgO eclogites point towards an origin as cumulates or intrusive mafic to ultramafic magmas. The MgO content and Mg#'s (74-88) are high, and eclogites that are both high in MgO and Al_2O_3 (e.g., KEC 86-107, Table 3.8) do not represent reasonable liquid compositions. Several samples are more MgO-rich than experimental peridotite melts at 1 GPa, suggesting olivine accumulation (Figs. 3.13 and 3.14). CIPW norms (Hills and Haggerty, 1989) are consistent with olivine gabbros as precursors of the high MgO eclogites (Table 3.8). On average, the high MgO eclogites contain 40% normative plagioclase, 14% cpx, 12% opx, and 29% olivine. Note that olivine breaks down during eclogite-facies metamorphism by reactions of the type

$$\text{plag} + \text{cpx} \pm \text{opx} \pm \text{ol} = \text{grt} + \text{omp} \pm \text{qtz}$$

(e.g., Green and Ringwood, 1967; Mottana et al., 1990).

Typical gabbros have relatively evolved compositions, close to those of basaltic melts, because the cotectic proportions of olivine, plagioclase, and pyroxene have a basaltic bulk composition (cf. Dick et al., 2000). Such gabbros are more similar to the Koidu low MgO eclogites than to the high MgO eclogites. For example, Hart et al.'s (1999) average oceanic gabbro has 8.8 wt% MgO and Mg# = 62.9. However, olivine gabbros and troctolites, which can be found in the deeper, more mafic parts of gabbroic cumulates in oceanic crust, ophiolites, and layered intrusion, have whole rock compositions with high MgO and Al_2O_3 contents similar to the high MgO eclogites. For example, gabbros and troctolites recovered from DSDP Site 334 (Aumento et al., 1977)

Table 3.8. Whole rock chemistry determined by XRF and 1 bar normative CIPW mineralogies of the Koidu high MgO eclogites. Data from Hills and Haggerty (1989).

	KEC-81-2	KEC 81-AB-11	KEC 86-15	KEC 86-19	KEC 86-58	KEC 86-73A	KEC 86-73B	KEC 86-90	KEC 86-107
SiO_2	47.39	47.84	46.17	47.73	48.59	47.83	48.32	43.99	44.52
TiO_2	1.00	0.39	0.68	0.32	0.34	0.44	0.33	0.62	0.37
Al_2O_3	12.72	12.96	15.83	13.67	14.12	14.53	13.38	18.95	20.15
FeO_t	9.42	4.97	10.49	8.17	4.56	7.77	6.48	10.61	6.45
MnO	0.23	0.19	0.21	0.32	0.19	0.24	0.22	0.26	0.27
MgO	16.68	19.51	15.90	16.29	19.62	17.65	18.38	18.13	20.15
CaO	11.07	10.8	9.49	12.49	11.57	9.90	10.87	7.06	7.37
Na_2O	1.18	2.55	0.91	0.88	1.04	1.33	1.30	0.42	0.36
K_2O	0.57	0.42	0.47	0.48	0.17	0.33	0.68	0.28	0.44
P_2O_5	0.18	0.06	0.07	0.05	0.03	0.04	0.04	0.04	0.07
total	100.44	99.69	100.22	100.40	100.23	100.06	100.00	100.36	100.15
Mg #	75.9	87.5	73.0	78.0	88.5	80.2	83.5	75.3	84.8
or	3.37	2.48	2.78	2.84	1.00	1.95	4.02	1.65	2.60
ab	9.98	11.04	7.70	7.45	8.80	11.25	11.00	3.55	3.05
an	27.73	22.68	37.72	31.93	33.36	32.70	28.67	34.76	36.11
plag	37.71	33.72	45.42	39.38	42.16	43.95	39.67	38.31	39.16
di	20.92	24.17	7.19	23.86	18.87	12.93	19.92	0.00	0.00
hy	6.62	0.00	13.86	6.38	11.33	11.12	4.56	27.46	26.11
ne	0.00	5.71	0.00	0.00	0.00	0.00	0.00	0.00	0.00
ol	29.50	32.74	29.51	27.22	26.15	29.18	31.11	26.45	25.58
il	1.90	0.74	1.29	0.61	0.65	0.84	0.63	1.18	0.70
ap	0.42	0.14	0.16	0.12	0.07	0.09	0.09	0.09	0.16
c	0.00	0.00	0.00	0.00	0.00	0.00	0.00	5.22	5.85
total	100.44	99.70	100.21	100.41	100.23	100.06	100.00	100.36	100.16

show increasing MgO content (from 10 wt% to 22 wt%) with depth (Gunn and Roobol, 1977). The inferred crystallization sequence of the Site 334 gabbro suite is olivine followed by plagioclase, clinopyroxene, and finally orthopyroxene or pigeonite (Hodges and Papike, 1976), similar to the 1 bar normative mineralogy of the high MgO eclogites.

The transition element systematics of the high MgO eclogites are consistent with an origin as olivine-pyroxene-plagioclase cumulates. Both the gabbros from DSDP Site 334 and the high MgO eclogites have comparatively low contents of Cr and Ni (Fig. 3.15). The relatively flat middle to heavy REE patterns combined with the observation that one eclogite (KEC 86-15) with low HREE content has a positive Sr anomaly and eclogites with high HREE contents have negative Sr anomalies (Fig. 3.11) is suggestive of plagioclase fractionation. Plagioclase accumulation at crustal pressures could also explain the high Al_2O_3 contents of the high MgO eclogites without Cr enrichment that would be caused by garnet or spinel addition at higher pressures.

An observation that is inconsistent with an origin of the Koidu high MgO eclogites as plagioclase-rich cumulates is the absence of positive Eu anomalies (Fig. 3.8). It is unlikely that metasomatic overprinting has erased the Eu anomalies. While some of the high MgO eclogites show evidence for ancient metasomatic overprinting (see above), only the REE La to Sm are enriched. Furthermore, eclogites without clear signs of metasomatic enrichment (e.g., KEC 86-15) also do not show Eu anomalies.

3.6.2.3. Origin in the Uppermost Mantle

Major element compositions of the high MgO eclogites fall between the 1 GPa and 4 GPa partial melting curves (Figs. 3.13 and 3.14), i.e., the high MgO eclogites could represent liquids generated at pressures intermediate between crustal pressures and their estimated equilibration pressures. High Mg#'s and moderate Ni contents (Fig. 3.15) imply that these liquids experienced only small degrees of olivine fractionation, whereas flat HREE patterns (Fig. 3.8) and moderate Cr (Fig. 3.15) contents suggest only minor amounts of garnet and/or spinel accumulation.

On the other hand, some high MgO eclogites have higher Mg#, higher Al_2O_3 and lower FeO contents than expected from primary pyrolite melts (Fig. 3.13), pointing towards accumulation of a MgO- and Al_2O_3-rich and FeO-poor phase such as pyropic garnet or spinel. However, it remains unresolved why the high MgO eclogites do not show other signs of garnet or spinel accumulation such as HREE and Cr enrichment.

3.6.3. Tectonic Setting of the Protoliths of the High MgO Eclogites

Three different low-pressure origins of the Koidu high MgO eclogites are possible. First, the high MgO eclogites could represent deep cumulus portions of subducted oceanic crust. It remains unresolved if the high MgO eclogites experienced an episode of partial melting during subduction. While the LREE-enriched patterns of some high MgO eclogites do not support partial melting, these incompatible elements might have been re-enriched by metasomatism (see above). Similarly, it is unclear whether the

precursors of the high MgO eclogites have been hydrothermally altered. The restricted range of oxygen isotope values suggests that the precursors either have not interacted with seawater or have coincidentally approximately normal igneous values. In the lowermost oceanic crust hydrothermal alteration is localized along fractures and veins (Gregory and Taylor, 1981; Dick et al., 2000). Thus, it is conceivable that the precursors of the high MgO eclogites did not (or at least not extensively) interact with hydrothermal fluids. On the other hand, the 'coincidence' phenomenon is a characteristic feature of seawater-hydrothermal systems. Because of the ^{18}O shifts and the relatively high initial $\delta^{18}O$ value of seawater, there is a significant range of temperatures over which the whole rock $\delta^{18}O$ value of a gabbro that has been thoroughly hydrothermally altered in the presence of large amounts of water will, simply by coincidence, be very close to the primary magmatic value of +5.7 (Gregory and Taylor, 1981).

Second, the protoliths of the high MgO eclogites could have formed by magmatic underplating of continental crust, which involves intrusion of basaltic magmas near the crust-mantle boundary. During thermal relaxation (cooling), these gabbroic rocks may be converted to mafic granulites and eclogites (Griffin et al., 1990; El Fadili and Demaiffe, 1999). Although the estimated equilibration pressures of the Koidu high MgO eclogites, in excess of 2.8 GPa, imply that these eclogites are derived from the lithospheric mantle (>100 km depth), it is conceivable that the high MgO eclogites represent former crustal material that has foundered or delaminated from the lower continental crust. The xenoliths studied by Griffin et al. (1990) and El Fadili and Demaiffe (1990) have lower MgO contents (5-15 wt% MgO) than the Koidu high MgO suite (16-20 wt% MgO). While the depth of the transformation of gabbro to eclogite depends on bulk composition

and temperature, at the estimated P-T conditions of the high MgO eclogites all mafic to ultramafic rocks will be converted to eclogite (Green and Ringwood, 1967; Harley and Carswell, 1990).

Third, the high MgO eclogites could have originated as pyroxenite veins emplaced in the uppermost mantle (P < 3 GPa). Later, these mafic veins were transported to greater depth, possibly tectonically during terrain accretion in the Archean. High-pressure recrystallization could account for the lack of correlation of modal mineralogy and trace element composition.

3.7. Conclusions

Due to the absence of modal olivine and orthopyroxene in the Koidu high MgO eclogites, high-pressure crystal fractionation systematics suggest that the high MgO eclogites most likely formed at pressures lower than those inferred from applying their estimated equilibration temperatures to a cratonic geotherm. The high MgO eclogites have whole rock major element compositions suggestive of a cumulate origin, generated either as garnet-pyroxene cumulates emplaced in the uppermost mantle (P < 3 GPa) or as low-pressure (crustal) plagioclase-pyroxene-olivine cumulates. Trace element concentrations of the high MgO eclogites are affected by both recent and ancient metasomatism and do not allow a clear distinction between high-P and low-P origin. For a low-P origin two different tectonic settings are possible: The high MgO eclogites could represent either the basal section of oceanic crust that has been subducted or foundered mafic lower continental crust.

3.8. References

Aumento F., Melson W. G. et al. (1977) Site 334. In *Initial reports of the Deep Sea Drilling Project*, Vol. 37 (ed. F. Aumento, W. G. Melson et al.), pp. 239-287. U.S. Government Printing Office.

Baker M. B. and Stolper E. M. (1994) Determining the composition of high-pressure mantle melts using diamond aggregates. *Geochim. Cosmochim. Acta* **58**, 2811-2827.

Barth M. G., Rudnick R. L., Horn I., McDonough W. F., Spicuzza M. J., Valley J. W., and Haggerty S. E. (2001) Geochemistry of xenolithic eclogites from West Africa, Part I: A link between low MgO eclogites and Archean crust formation. *Geochim. Cosmochim. Acta* **65**, 1499-1527.

Bodinier J. L., Guiraud M., Fabriès J., Dostal J., and Dupuy C. (1987) Petrogenesis of layered pyroxenites from Lherz, Freychinède and Prades ultramafic bodies (Ariège, French Pyrénées). *Geochim. Cosmochim. Acta* **51**, 279-290.

Boynton W. V. (1984) Cosmochemistry of the REE: Meteorite studies. In *REE geochemistry* (ed. P. Henderson). Elsevier.

Caporuscio F. A. and Smyth J. R. (1990) Trace element crystal chemistry of mantle eclogites. *Contrib. Mineral. Petrol.* **105**, 550-561.

Coghlan R. A. N. (1990) Studies in diffusional transport: grain boundary transport of oxygen in feldspars, diffusion of oxygen, strontium, and REEs in garnet, and thermal histories of granitic intrusions in South-Central Maine using oxygen isotopes. Ph.D. Thesis, Brown Univ., Providence, R.I.

Coplen T. B. (1996) New guidelines for reporting stable hydrogen, carbon, and oxygen isotope-ratio data. *Geochim. Cosmochim. Acta* **60**, 3359-3360.

Dawson J. B. (1984) Contrasting types of upper-mantle metasomatism. In *Kimberlites II: The mantle and crust-mantle relationships* (ed. J. Kornprobst), pp. 289-294. Elsevier.

Deines P. and Haggerty S. E. (2000) Small-scale oxygen isotope variations and petrochemistry of ultradeep (>300 km) and transition zone xenoliths. *Geochim. Cosmochim. Acta* **64**, 117-131.

Dick H. J. B., Natland J. H., Miller D. J., et al. (1999) *Proc. ODP, Initial Reports* **176** [CD-ROM]. Ocean Drilling Program, College Station, TX.

Dick H. J. B., Natland J. H., Alt J. C., Bach W., Bideau D., Gee J. S., Haggas S., Hertogen J. G. H., Hirth G., Holm P. M., Ildefonse B., Iturrino G. J., John B. E.,

Kelley D. S., Kikawa E., Kingdon A., LeRoux P. J., Maeda J., Meyer P. S., Miller D. J., Naslund H. R., Niu Y.-L., Robinson P. T., Snow J., Stephen R. A., Trimby P. W., Worm H.-U., and Yoshinobu A. (2000) A long in situ section of the lower ocean crust: results of ODP Leg 176 drilling at the Southwest Indian Ridge. *Earth Planet. Sci. Lett.* **179**, 31-51.

El Fadili S. and Demaiffe D. (1999) Petrology of eclogite and granulite nodules from the Mbuji Mayi kimberlites (Kasai, Congo): Significance of kyanite-omphacite intergrowths. In *Proceedings of the 7th International Kimberlite Conference*, Vol. 1 (ed. J. J. Gurney, J. L. Gurney, M. D. Pascoe, and S. H. Richardson), pp. 205-213. Red Roof Design.

Ellis D. J. and Green D. H. (1979) An experimental study of the effect of Ca upon garnet-clinopyroxene Fe-Mg exchange equilibria. *Contrib. Mineral. Petrol.* **71**, 13-22.

Falloon T. J. and Green D. H. (1988) Anhydrous partial melting of peridotite from 8 to 35 kbar and the petrogenesis of MORB. In *Oceanic and continental lithosphere: Similarities and differences* (ed. M. A. Menzies and K. G. Cox), pp. 379-414. Clarendon Press.

Frey F. A. (1980) The origin of pyroxenites and garnet pyroxenites from Salt Lake Crater, Oahu, Hawaii: Trace element evidence. *Am. J. Sci.* **280-A**, 427-449.

Fung A. T. and Haggerty S. E. (1995) Petrography and mineral compositions of eclogites from the Koidu Kimberlite Complex, Sierra Leone. *J. Geophys. Res.* **100**, 20,451-20,473.

Green D. H. and Ringwood A. E. (1967) An experimental investigation of the gabbro to eclogite transformation and its petrological applications. *Geochim. Cosmochim. Acta* **31**, 767-833.

Gregory R. T. and Taylor H. P. (1981) An oxygen isotope profile in a section of Cretaceous oceanic crust, Samail ophiolite, Oman: Evidence for $\delta^{18}O$ buffering of the oceans by deep (>5 km) seawater-hydrothermal circulation at mid-ocean ridges. *J. Geophys. Res.* **86**, 2737-2755.

Griffin W. L., O'Reilly S. Y., and Stabel A. (1988) Mantle metasomatism beneath western Victoria, Australia: II. Isotopic geochemistry of Cr-diopside lherzolites and Al-augite pyroxenites. *Geochim. Cosmochim. Acta* **52**, 449-459.

Griffin W. L., O'Reilly S. Y., and Pearson N. J. (1990) Eclogite stability near the crust-mantle boundary. In *Eclogite facies rocks* (ed. D. A. Carswell), pp. 291-314. Blackie.

Gunn B. and Roobol M. J. (1977) Geochemistry of the igneous rocks. In *Initial reports of the Deep Sea Drilling Project*, Vol. 37 (ed. F. Aumento, W. G. Melson et al.), pp. 735-755. U.S. Government Printing Office.

Harley S. L. and Carswell D. A. (1990) Experimental studies on the stability of eclogite facies mineral parageneses. In *Eclogite facies rocks* (ed. D. A. Carswell), pp. 53-82. Blackie.

Hart S. R., Blusztajn J., Dick H. J. B., Meyer P. S., and Muehlenbachs K. (1999) The fingerprint of seawater circulation in a 500-meter section of ocean crust gabbros. *Geochim. Cosmochim. Acta* **63**, 4059-4080.

Harte B. (1987) Metasomatic events recorded in mantle xenoliths: an overview. In *Mantle Xenoliths* (ed. P. H. Nixon), pp. 625-640. John Wiley & Sons.

Harte B. and Kirkley M. B. (1997) Partitioning of trace elements between clinopyroxene and garnet: data from mantle eclogites. *Chem. Geol.* **136**, 1-24.

Hatton C. J. and Gurney J. J. (1987) Roberts Victor eclogites and their relation to the mantle. In *Mantle Xenoliths* (ed. P. H. Nixon), pp. 453-463. John Wiley & Sons.

Helmstaedt H. and Doig R. (1975) Eclogite nodules from kimberlite pipes of the Colorado Plateau - samples of subducted Franciscan-type oceanic lithosphere. *Phys. Chem. Earth* **9**, 95-111.

Hills D. V. and Haggerty S. E. (1989) Petrochemistry of eclogites from the Koidu Kimberlite Complex, Sierra Leone. *Contrib. Mineral. Petrol.* **103**, 397-422.

Hodges F. N. and Papike J. J. (1976) DSDP Site 334: Magmatic cumulates from oceanic layer 3. *J. Geophys. Res.* **81**, 4135-4151.

Ireland T. R., Rudnick R. L., and Spetsius Z. (1994) Trace elements in diamond inclusions from eclogites reveal link to Archean granites. *Earth Planet. Sci. Lett.* **128**, 199-213.

Irving A. J. and Green D. H. (1970) Experimental duplication on mineral assemblages in basic inclusions of the Delegate breccia pipes. *Phys. Earth Planet. Interior* **3**, 385-389.

Jacob D., Jagoutz E., Lowry D., Mattey D., and Kudrjavtseva G. (1994) Diamondiferous eclogites from Siberia: Remnants of Archean oceanic crust. *Geochim. Cosmochim. Acta* **58**, 5195-5207.

Johnson K. T., Dick H. J. B., and Shimizu N. (1990) Melting in the oceanic upper mantle: an ion microprobe study of diopsides in abyssal peridotites. *J. Geophys. Res.* **95**, 2661-2678.

Kinzler R. J. and Grove T. L. (1992) Primary magmas of mid-ocean ridge basalts 1. Experiments and methods. *J. Geophys. Res.* **97**, 6885-6906.

Kohn M. J. and Valley J. W. (1998) Effects of cation substitutions in garnet and pyroxene on equilibrium oxygen isotope fractionations. *J. metamorphic Geol.* **16**, 625-639.

Kumar N., Reisberg L., and Zindler A. (1996) A major and trace element and strontium, neodymium, and osmium isotopic study of a thick pyroxenite layer from the Beni Bousera ultramafic complex of northern Morocco. *Geochim. Cosmochim. Acta* **60**, 1429-1444.

Kushiro I. (1996) Partial melting of a fertile mantle peridotite at high pressures: an experimental study using aggregates of diamond. In *Earth processes: reading the isotopic code*, Vol. 95 (ed. A. Basu and S. Hart), pp. 109-122. American Geophysical Union.

Liu T.-C. and Presnall D. C. (2000) Liquidus phase relations in the system CaO-MgO-Al_2O_3-SiO_2 at 2.0 GPa: Applications to basalt fractionation, eclogites, and igneous sapphirine. *J. Petrol.* **41**, 3-20.

Loubet M. and Allègre C. J. (1982) Trace elements in orogenic lherzolites reveal the complex history of the upper mantle. *Nature* **298**, 809-814.

Mattey D., Lowry D., and Macpherson C. (1994) Oxygen isotope composition of mantle peridotite. *Earth Planet. Sci. Lett.* **128**, 231-241.

McCandless T. E. and Gurney J. J. (1989) Sodium in garnet and potassium in clinopyroxene: criteria for classifying mantle eclogites. In *Kimberlites and related rocks*, Vol. 2 (ed. J. Ross), pp. 827-832. Blackwell Scientific.

McDonough W. F. and Sun S.-S. (1995) Composition of the Earth. *Chem. Geol.* **120**, 223-253.

Milholland C. S. and Presnall D. C. (1998) Liquidus phase relations in the CaO-MgO-Al_2O_3-SiO_2 system at 3.0 GPa: the aluminous pyroxene thermal divide and high-pressure fractionation of picritic and komatiitic magmas. *J. Petrol.* **39**, 3-27.

Mottana A., Carswell D. A., Chopin C., and Oberhänsli R. (1990) Eclogite facies mineral parageneses. In *Eclogite Facies Rocks* (ed. D. A. Carswell), pp. 16-52. Blackie.

Navon O. and Stolper E. (1987) Geochemical consequences of melt percolation: The upper mantle as a chromatographic column. *J. Geol.* **95**, 285-308.

Pearson D. G., Davies G. R., Nixon P. H., Greenwood P. B., and Mattey D. P. (1991) Oxygen isotope evidence for the origin of pyroxenites in the Beni Bousera peridotite massif, North Morocco: derivation from subducted oceanic lithosphere. *Earth Planet. Sci. Lett.* **102**, 289-301.

Pearson D. G., Davies G. R., and Nixon P. H. (1993) Geochemical constraints on the petrogenesis of diamond facies pyroxenites from the Beni Bousera peridotite massif, North Morocco. *J. Petrol.* **34**, 125-172.

Rosenbaum J. M. and Mattey D. (1995) Equilibrium garnet-calcite oxygen isotope fractionation. *Geochim. Cosmochim. Acta* **59**, 2839-2842.

Rudnick R. L. and Nyblade A. A. (1999) The thickness and heat production of Archean lithosphere: constraints from xenolith thermobarometry and surface heat flow. In *Mantle petrology: field observations and high pressure experimentation: a tribute to Francis R. (Joe) Boyd* (ed. Y. Fei, C. M. Bertka, and B. O. Mysen), pp. 3-12. The Geochemical Society.

Rudnick R. L., Barth M., Horn I., and McDonough W. F. (2000) Rutile-bearing refractory eclogites: the missing link between continents and depleted mantle. *Science* **287**, 278-281.

Shervais J. W., Taylor L. A., Lugmair G. W., Clayton R. N., Mayeda T. K., and Korotev R. L. (1988) Early Proterozoic oceanic crust and the evolution of subcontinental mantle: Eclogites and related rocks from southern Africa. *Geol. Soc. Am. Bull.* **100**, 411-423.

Smyth J. R., Caporuscio F. A., and McCormick T. C. (1989) Mantle eclogites: evidence of igneous fractionation in the mantle. *Earth Planet. Sci. Lett.* **93**, 133-141.

Snyder G. A., Taylor L. A., Beard B. L., Crozaz G., Halliday A. N., Sobolev V. N., and Sobolev N. V. (1998) Reply to a comment by D. Jacob *et al.* on 'The origins of Yakutian eclogite xenoliths'. *J. Petrol.* **39**, 1535-1543.

Takazawa E., Frey F. A., Shimizu N., Obata M., and Bodinier J. L. (1992) Geochemical evidence for melt migration and reaction in the upper mantle. *Nature* **359**, 55-58.

Taylor L. A. and Neal C. R. (1989) Eclogites with oceanic crustal and mantle signatures from the Bellsbank kimberlite, South Africa, Part I: Mineralogy, petrography, and whole rock chemistry. *J. Geol.* **97**, 551-567.

Taylor W. R., Tompkins L. A., and Haggerty S. E. (1994) Comparative geochemistry of West African kimberlites: Evidence for a micaceous kimberlite endmember of sublithospheric origin. *Geochim. Cosmochim. Acta* **58**, 4017-4037.

Valley J. W., Kitchen N., Kohn M. J., Niendorf C. R., and Spicuzza M. J. (1995) UWG-2, a garnet standard for oxygen isotope ratios: Strategies for high precision and accuracy with laser heating. *Geochim. Cosmochim. Acta* **59**, 5223-5231.

Walter M. J. (1998) Melting of garnet peridotite and the origin of komatiite and depleted lithosphere. *J. Petrol.* **39**, 29-60.

Wilkinson J. F. G. (1975) An Al-spinel ultramafic-mafic inclusion suite and high pressure megacrysts in an analcimite and their bearing on basaltic magma fractionation at elevated pressures. *Contrib. Mineral. Petrol.* **53**, 71-104.

Zindler A. and Jagoutz E. (1988) Mantle cryptology. *Geochim. Cosmochim. Acta* **52**, 319-333.

Chapter 4

Geochronological Re-Os and U-Pb Constraints on the Eclogite–Tonalite Connection in the Archean Man Shield, West Africa

4.1. Abstract

Both mantle-derived eclogite xenoliths and Archean TTGs occur in the Man Shield, West Africa. Major element, trace element, and oxygen isotope systematics indicate that the low MgO eclogites from the Koidu kimberlite are remnants of subducted oceanic crust and residues from Archean crust formation. Re-Os whole rock isotopic data for these eclogites yield an Archean age (3.32 +0.58/-0.77 Ga), with Re-Os model ages ranging from 1.4 to 3.9 Ga. This age overlaps the age range for crust formation and metamorphism on the Man Shield. In situ U-Pb ages of zircons from crustal rocks have been measured by laser ablation ICP-MS. A tonalitic gneiss has discordant zircons with rare old cores (~3.6 Ga) and an upper Concordia intercept at 2889 ± 12 Ma. Zircons from a mafic lower crustal granulite xenolith are concordant at 2686 ± 32 Ma. Our results, together with previously published ages for the Man Shield, indicate an Early Archean crust formation event followed by major crustal growth at 2.9-3.0 Ga and a last major metamorphic event at 2.7 Ga. These data show that the eclogites and the continental crust of the West African Craton overlap in time of formation. They also imply that Archean crustal growth was accomplished, in part, by direct addition of evolved magmas from the mantle.

4.2. Introduction

Granitoids of tonalitic, trondhjemitic, and granodioritic (TTG) composition and grey gneisses, their high-grade metamorphic equivalent, are a major constituent of the Earth's early continental crust. Based on their major element compositions and strongly fractionated REE patterns, these rocks appear to be derived from a mafic, garnet-bearing (i.e., deep seated) source, such as subducted oceanic crust. Mantle-derived eclogite xenoliths carried in kimberlites have been interpreted as former oceanic crust and may represent residues generated by TTG production. This hypothesis has been proposed based on circumstantial evidence of general complementary geochemical characteristics in the two groups of rocks. Better constraints on the age and origin of eclogite xenoliths are thus important for understanding Archean crustal growth processes.

Both mantle-derived eclogite xenoliths and Archean TTGs occur in the Man Shield, West Africa. Major element, trace element, and oxygen isotope systematics indicate that the low MgO eclogites from the Koidu kimberlite complex are remnants of subducted oceanic crust and residues from Archean crust formation (Rollinson, 1997; Barth et al., 2001).

The objective is firstly to constrain the age of the Archean basement in the Man Shield of Sierra Leone and of the Koidu eclogite suite and then to establish age relationships between the TTG and eclogite suites, using U-Pb and Re-Os methods.

4.3. Geological Setting and Previous Geochronological Work

The West African Craton consists of two major basement domains of Archean and Paleoproterozoic age, the Reguibat Rise in the north and the Man Shield in the south. They are separated by the Proterozoic to Paleozoic sedimentary basin of Taoudéni and are entirely surrounded by Panafrican and Hercynian belts. The Proterozoic parts of these two domains have been well studied and it was demonstrated that this Proterozoic crust arose from a major crustal growth event at ca. 2.1 Ga (e.g., Abouchami et al., 1990; Boher et al., 1992). In contrast, Archean terrains from the West African Craton have not been extensively studied. Recent geochronological studies of the Amsaga area, in the southwestern Reguibat Rise, confirm the Archean age of this area and demonstrate the presence of Early Archean relicts (ca. 3.5 Ga) in the basement of the Reguibat Rise (Potrel et al., 1996, 1998).

The Man Shield has been divided into three age provinces (MacFarlane et al., 1981): Leonean (~3.0 Ga), Liberian (~2.7 Ga), and Eburnian (~2.0 Ga). However, due to the limited radiometric dating (Rb-Sr and Pb-Pb whole rock) there is a debate as to whether the Leonean and Liberian are two separate events or a single, long-lived event (Williams, 1978). Poorly constrained Rb-Sr studies (Hedge et al., 1975; Hurley et al., 1975) and Nd model ages (Kouamelan et al., 1997) point towards a pre-Leonian crustal growth event (>3.2 Ga). A younger Pan-African age province defines a tectonic event at ~550 Ma in the coastal belt of Sierra Leone and Liberia (Fig. 1.2).

The Archean basement (Leonean and Liberian provinces) of Sierra Leone is typical of granite-greenstone terrains found in ancient continental nuclei. The older TTG

gneisses (~3 Ga, Beckinsale et al., 1980) form between 60-70% of the outcrop area and are the major rock type of the Man Shield. Younger granites (2.7-2.8 Ga) intrude the margins of the greenstone belts or occur as thick sheets cross-cutting the greenstones at high structural levels.

4.4. Sample Description

Zircon separates of sample "old gneiss 278" representing the older basement were provided by Dr. Hugh Rollinson. Granulite xenolith KGR 86-75 from the Koidu kimberlite complex, Sierra Leone, consists of garnet, pyroxene, and plagioclase with accessory rutile. Petrography, whole rock and mineral major element data are given in Hills and Haggerty (1989). Zircons in KGR 86-75 were probed in thin section.

Hills and Haggerty (1989) and Barth et al. (2001a, 2001b) have described the Koidu eclogite samples analyzed for Re-Os. Whole rock powders were prepared by crushing in alumina ceramics in some cases and tungsten carbide for the remaining samples (see Table 4.3).

4.5. Analytical Methods

4.5.1. Zircon U/Pb Isotopic Measurement

U/Pb zircon isotopic data were determined by simultaneous solution nebulization and laser ablation (LA-) ICP-MS, utilizing a home-built excimer system (Horn et al, 2000). Ablation is achieved by a 193 nm Ar-F excimer laser system using a pulse

repetition rate of 10 Hz and pulse energy of ≤0.5 mJ (Horn et al., 2000). Typically, a ~50 μm spot diameter was used. Analyses were performed on a Fisons (VG Elemental) PQ II+ in pulse counting mode (one point per peak); dwell time and quadrupole settling time were set to 10 ms and 5 ms, respectively. Data reduction follows the procedures outlined in Longerich et al. (1996) and Horn et al. (2000). The time-resolved spectra were processed off-line using a spreadsheet program to apply the background subtraction and mass discrimination, fractionation, interference, and common lead corrections (modified version of LAMTRACE© by Simon Jackson). Zircon 91500 and Phalaborwa baddeleyite were measured to monitor accuracy. Measurement of zircon 91500 yielded a weighted mean $^{207}Pb/^{206}Pb$ age of 1093±30 Ma (n=12; TIMS age 1062.4±0.8 Ma, Wiedenbeck et al., 1995). Phalaborwa baddeleyite yielded an upper intercept age of 2057±28 Ma and a weighted mean $^{207}Pb/^{206}Pb$ age of 2068±21 Ma (n=4; TIMS ages 2060.5±1.9 Ma and 2060.2±2.1, respectively, Reischmann, 1995). Concordia intercepts and weighted mean ages reported in this study were calculated in the program Isoplot/Ex of Ludwig (1998).

4.5.2. Re/Os Chemistry and Measurement

Rhenium and osmium isotopes were determined on whole rock eclogites following the procedures of Pearson et al. (1995a), Shirey and Walker (1995), and Shirey (1997). Dissolutions were performed in Carius tubes to overcome problems of spike-sample equilibration (Shirey and Walker, 1995). A mixed spike with ^{190}Os and ^{185}Re was added prior to digestion with reverse aqua regia. Os was extracted with HBr-CCl_4. Samples were distilled from H_2SO_4 using CrO_3 as an oxidant, and trapped into HBr. The

Re-containing pot solution was taken up in 1N HCl and centrifuged to remove solids. Re was separated by anion exchange using 1 ml of AG-1 X8 resin, Re being eluted with 4N HNO_3. Re was further purified using a second, smaller column.

Rhenium and Osmium were run as ReO_4^- and OsO_3^- ions by negative thermal ionization mass spectrometry (N-TIMS) at the Department of Terrestrial Magnetism, generally following procedures outlined by Creaser et al. (1991). Both Re and Os were loaded onto single Pt filaments using $Ba(NO_3)_2$ as an electron donor. Os isotope compositions are corrected for mass dependent isotope fractionation and are normalized to $^{192}Os/^{188}Os = 3.082614$. Isotopic data are reported as $^{187}Os/^{188}Os$.

4.6. Results

4.6.1. U-Pb Dating of "Old Gneiss 278"

Zircons in sample "Old Gneiss 278" are dominated by prismatic grains with slightly etched rims. Grains show internal structures ranging from primary, oscillatory zoning to rims with only faint traces of original oscillatory zoning and cores with secondary phases discordant with the original oscillatory zoning (Fig. 4.1). Fine-scale oscillatory zoned grains are interpreted as typical of having crystallized from a felsic magma (e.g., Poldervaart, 1956; Pidgeon et al., 1998). Following the recrystallization model of Pidgeon et al. (1998), grains with weakly zoned rims and cores with discordant secondary phases are the result of decomposition of zircon during cooling of felsic magma or during metamorphism. Decomposition of zircon results in the formation of a stable low trace element zircon phase around the rim of the zircon and the relocation of

expelled trace elements to concentrate in one or two bands, located initially along primary zones, towards the center of the grain (Pidgeon et al., 1998).

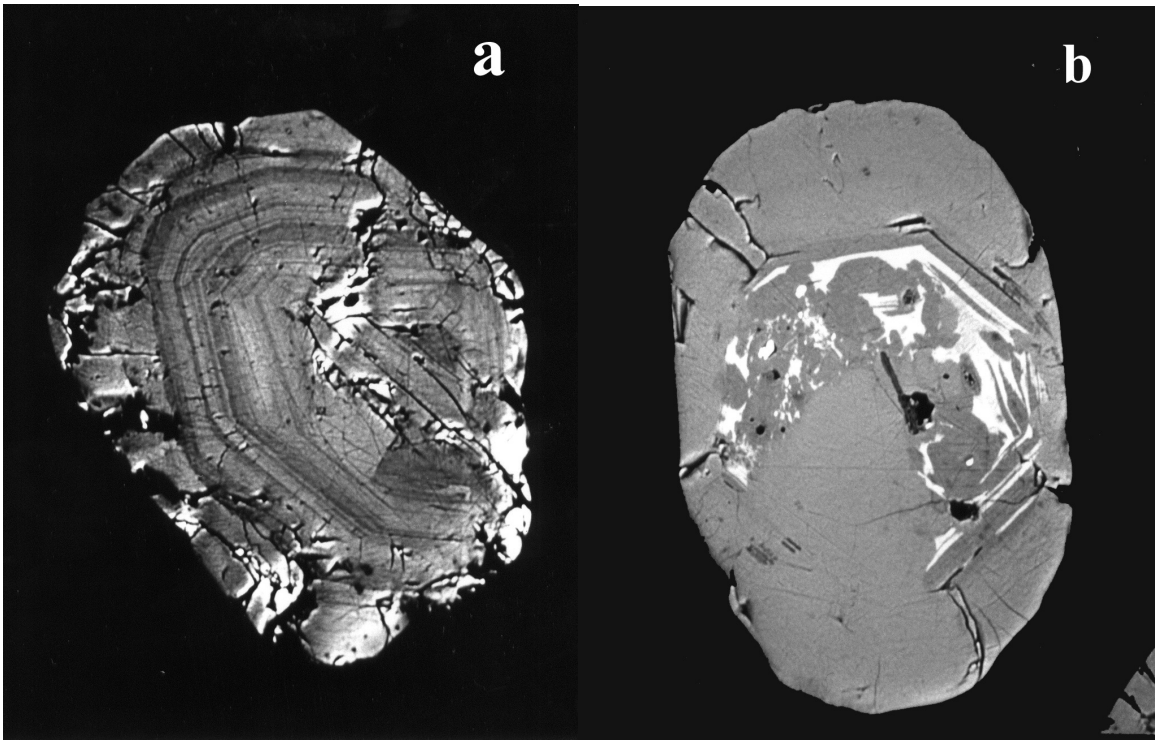

Figure 4.1. Back scattered electrons (BSE) images of two zircon grains in tonalitic gneiss sample "old gneiss 278". a) Grain with etched rim and preserved primary, fine-scale oscillatory zoning parallel to grain faces. b) Grain with pale, recrystallized rim with only faint traces of oscillatory zoning and with secondary phases (baddeleyite) discordant to original oscillatory zoning in the core. Grain sizes ~100 μm.

Ages determined from prismatic zircons with oscillatory zoning parallel to grain exteriors, devoid of inherited cores and without younger shells of oscillatory zoned zircon give the igneous age of quartzo-feldspathic meta-igneous rocks (e.g., Nutman et al.,

2000). The recrystallized outer rims of zircons with only faint traces of oscillatory zoning might record the time interval between primary crystallization and the onset of zircon decomposition during cooling of the igneous body, the age of metamorphism, or an unresolvable mixed age (Pidgeon et al., 1998).

Single spot LA-ICP-MS zircon analyses are presented in Table 4.1. Zircons are discordant to slightly reverse discordant (excess radiogenic Pb). The analyses do not define a single discordance line within analytical uncertainties (MSWD = 14). The concordia intercepts calculated are 2889 ± 12 Ma and 201 ± 59 Ma (Fig. 4.2). The $^{207}Pb/^{206}Pb$ ratios give ages up to, and even slightly above, the concordia intersection age. The weighted mean $^{207}Pb/^{206}Pb$ age yields 2877 ± 11 Ma (n=53).

The range of internal structures combined with the discordance pattern of the zircons is consistent with all zircons having the same age, but having responded very differently to later isotopic disturbance. The internal structure of the pale rims, i.e., the survival of ghost euhedral zoning, leaves little doubt that the rims are the result of recrystallization during metamorphism rather than being new zircon growth. Analyses that fall off the discordance line towards younger ages probably reflect mixed ages between the time of crystallization of the igneous protolith and the time of metamorphism. Therefore, the youngest $^{207}Pb/^{206}Pb$ age of 2759 ± 24 Ma is a maximum age for metamorphism.

Xenocrystic cores were found in four zircon grains. Three of the four analyses fall on a discordance line with concordia intercepts at 3555 ± 57 Ma and 337 ± 240 Ma (Fig. 4.3).

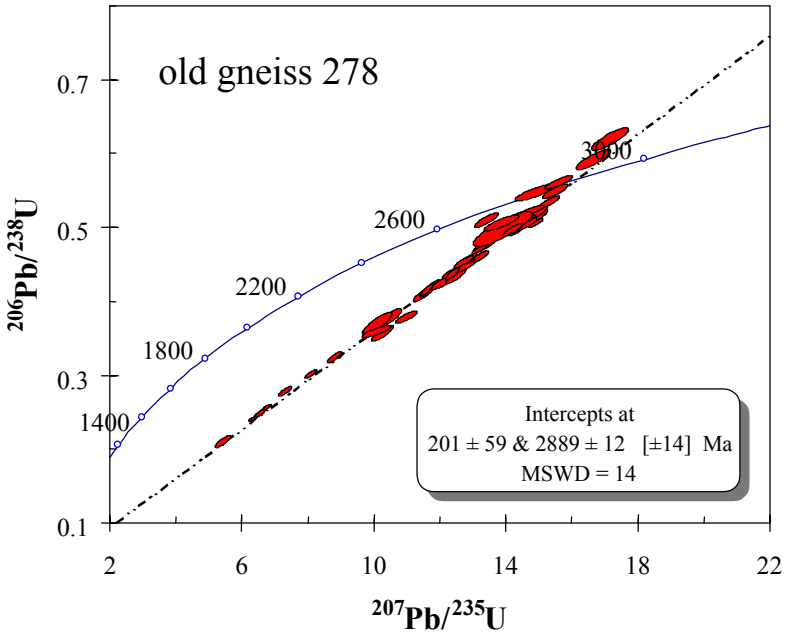

Figure 4.2. Concordia diagram showing results for sample "old gneiss 278", with spots ranging from discordant to reverse discordant. Error ellipses are 2σ.

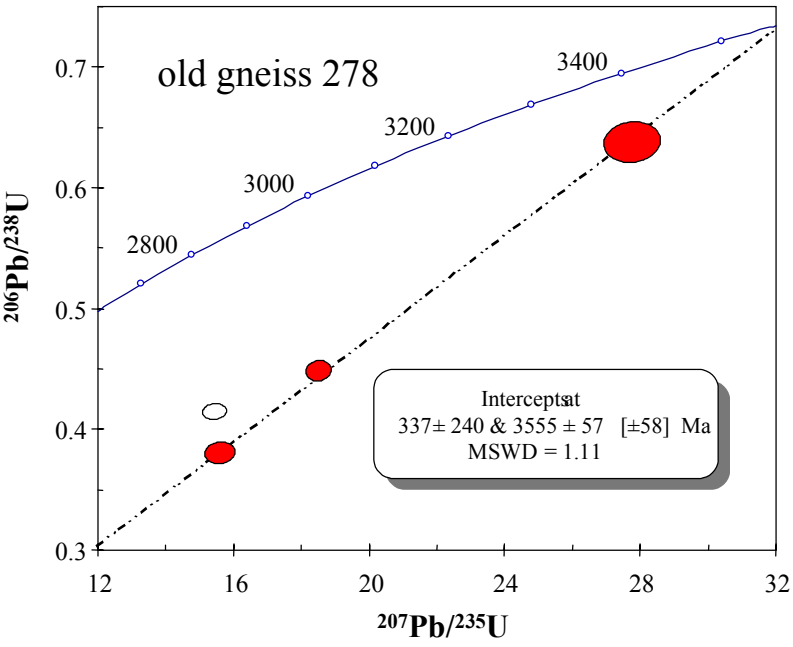

Figure 4.3. Concordia diagram showing results for xenocrystic cores of sample "old gneiss 278". Error ellipses are 2σ.

Table 4.1. Single spot LA-ICP-MS isotope ratio and age determinations of sample "old gneiss 278".

Spot No.	$^{238}U/^{206}Pb$	2 σ	$^{207}Pb/^{206}Pb$	2 σ	$^{207}Pb/^{206}Pb$ age
1	1.961	0.033	0.1919	0.0028	2759 ± 24
2	2.179	0.029	0.2100	0.0026	2905 ± 20
3	2.449	0.046	0.2065	0.0020	2878 ± 16
4	2.818	0.065	0.2116	0.0026	2918 ± 20
5	3.949	0.056	0.1963	0.0019	2795 ± 16
6	2.188	0.028	0.2066	0.0026	2879 ± 20
7	2.769	0.048	0.2003	0.0019	2829 ± 15
8	3.102	0.055	0.2009	0.0020	2833 ± 16
9	1.946	0.031	0.2136	0.0028	2933 ± 21
10	2.422	0.038	0.2062	0.0026	2876 ± 20
11	3.351	0.052	0.1992	0.0024	2820 ± 20
12	3.630	0.073	0.1956	0.0020	2790 ± 16
13	1.922	0.030	0.2106	0.0028	2910 ± 21
14	2.177	0.029	0.2109	0.0018	2912 ± 14
15	1.990	0.060	0.2050	0.0028	2867 ± 22
16	2.002	0.032	0.2066	0.0031	2879 ± 24
17	1.872	0.022	0.2096	0.0024	2902 ± 18
18	2.101	0.040	0.2058	0.0029	2872 ± 23
19	1.993	0.025	0.2087	0.0030	2896 ± 23
20	4.843	0.162	0.1951	0.0015	2786 ± 13
21	2.367	0.028	0.2047	0.0015	2864 ± 12
22	2.228	0.040	0.2079	0.0019	2889 ± 15
23	1.961	0.031	0.2056	0.0021	2871 ± 17
24	2.352	0.045	0.2082	0.0034	2892 ± 26
25	2.024	0.020	0.2121	0.0014	2922 ± 11
26	2.670	0.078	0.2036	0.0046	2855 ± 36
27	2.417	0.032	0.2056	0.0016	2871 ± 12
28	2.287	0.035	0.2072	0.0029	2884 ± 23
29	2.004	0.033	0.2086	0.0028	2895 ± 21
30	2.210	0.031	0.2061	0.0026	2875 ± 20
31	2.706	0.088	0.2011	0.0021	2835 ± 17
32	1.690	0.033	0.2055	0.0040	2870 ± 32
33	1.977	0.019	0.2151	0.0018	2944 ± 13
34	2.018	0.026	0.2080	0.0023	2890 ± 18
35	1.917	0.024	0.2069	0.0040	2881 ± 32
36	1.997	0.038	0.2107	0.0046	2911 ± 36
37	1.828	0.033	0.1983	0.0058	2812 ± 48
38	2.310	0.046	0.2112	0.0024	2915 ± 18
39	1.780	0.023	0.2034	0.0037	2854 ± 29
40	4.080	0.072	0.1971	0.0047	2803 ± 39
41	4.202	0.050	0.1970	0.0017	2802 ± 14
42	2.246	0.032	0.2091	0.0030	2899 ± 23
43	2.294	0.033	0.2087	0.0017	2895 ± 13
44	2.796	0.052	0.2065	0.0060	2878 ± 47
45	1.962	0.022	0.2092	0.0033	2899 ± 26
46	2.131	0.020	0.2062	0.0019	2876 ± 15
47	2.006	0.030	0.2080	0.0036	2890 ± 28
48	2.009	0.078	0.2044	0.0057	2862 ± 46
49	1.613	0.033	0.2021	0.0029	2843 ± 23

Table 4.1. continued.

Spot No.	$^{238}U/^{206}Pb$	2 σ	$^{207}Pb/^{206}Pb$	2 σ	$^{207}Pb/^{206}Pb$ age
50	2.651	0.046	0.2134	0.0034	2932 ± 26
51	1.977	0.034	0.2012	0.0048	2836 ± 39
52	1.823	0.025	0.2065	0.0033	2878 ± 26
53	2.015	0.028	0.2097	0.0023	2903 ± 18
Xenocrystic Cores					
1	1.566	0.034	0.3184	0.0040	3562 ± 19
2	2.246	0.036	0.3037	0.0020	3489 ± 10
3	2.435	0.034	0.2740	0.0030	3481 ± 14
4	2.658	0.053	0.3021	0.0027	3329 ± 17

4.6.2. U-Pb Dating of Granulite Xenolith KGR 86-75

Zircons in granulite xenolith KGR 86-75 from the Koidu kimberlite complex occur as prismatic to rounded inclusions in garnet and plagioclase. Internal structures show only faint traces of oscillatory zoning. Due to the small grain size of most of the zircons, only two grains could be measured by LA-ICP-MS (Table 4.2). The zircons are concordant and overlap in ages (Fig. 4.4). The zircon included in garnet has a $^{206}Pb/^{238}U$ age of 2674 ± 35 Ma and a $^{207}Pb/^{206}Pb$ age of 2707 ± 29 Ma. The zircon included in plagioclase has a less precise $^{206}Pb/^{238}U$ age of 2759 ± 86 Ma and a $^{207}Pb/^{206}Pb$ age of 2843 ± 124 Ma.

Table 4.2. Single spot LA-ICP-MS isotope ratio and age determinations of granulite xenolith KGR 86-75.

Spot No.	$^{238}U/^{206}Pb$	2 σ	$^{207}Pb/^{206}Pb$	2 σ	$^{207}Pb/^{206}Pb$ age
1	1.946	0.032	0.1859	0.0033	2707 ± 29
2	1.872	0.072	0.2021	0.0154	2843 ± 124

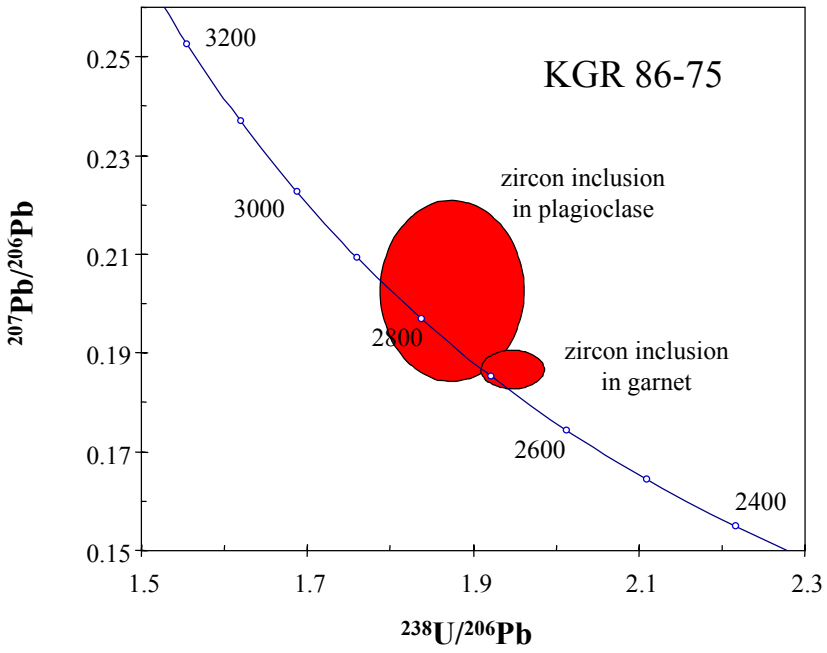

Figure 4.4. Tera-Wasserburg concordia diagram showing individual spot analyses of zircons in granulite xenoliths KGR 86-75. Error ellipses are 2σ.

4.6.3. Re-Os Dating of the Koidu Eclogite Suite

Re and Os abundances and $^{187}Re/^{188}Os$ and $^{187}Os/^{188}Os$ isotopic compositions of the Koidu eclogites are given in Table 4.3 and in Fig. 4.5 – 4.7. Both low MgO and high MgO eclogites have a wide range of Re and Os contents (0.02-3.4 ppb Re and 0.026-2.2 ppb Os), with the low MgO eclogites having, on average, higher Re and lower Os concentrations (Fig. 4.5). All samples have superchondritic $^{187}Re/^{188}Os$ (2.2-93) and radiogenic $^{187}Os/^{188}Os$ (0.22-8.8).

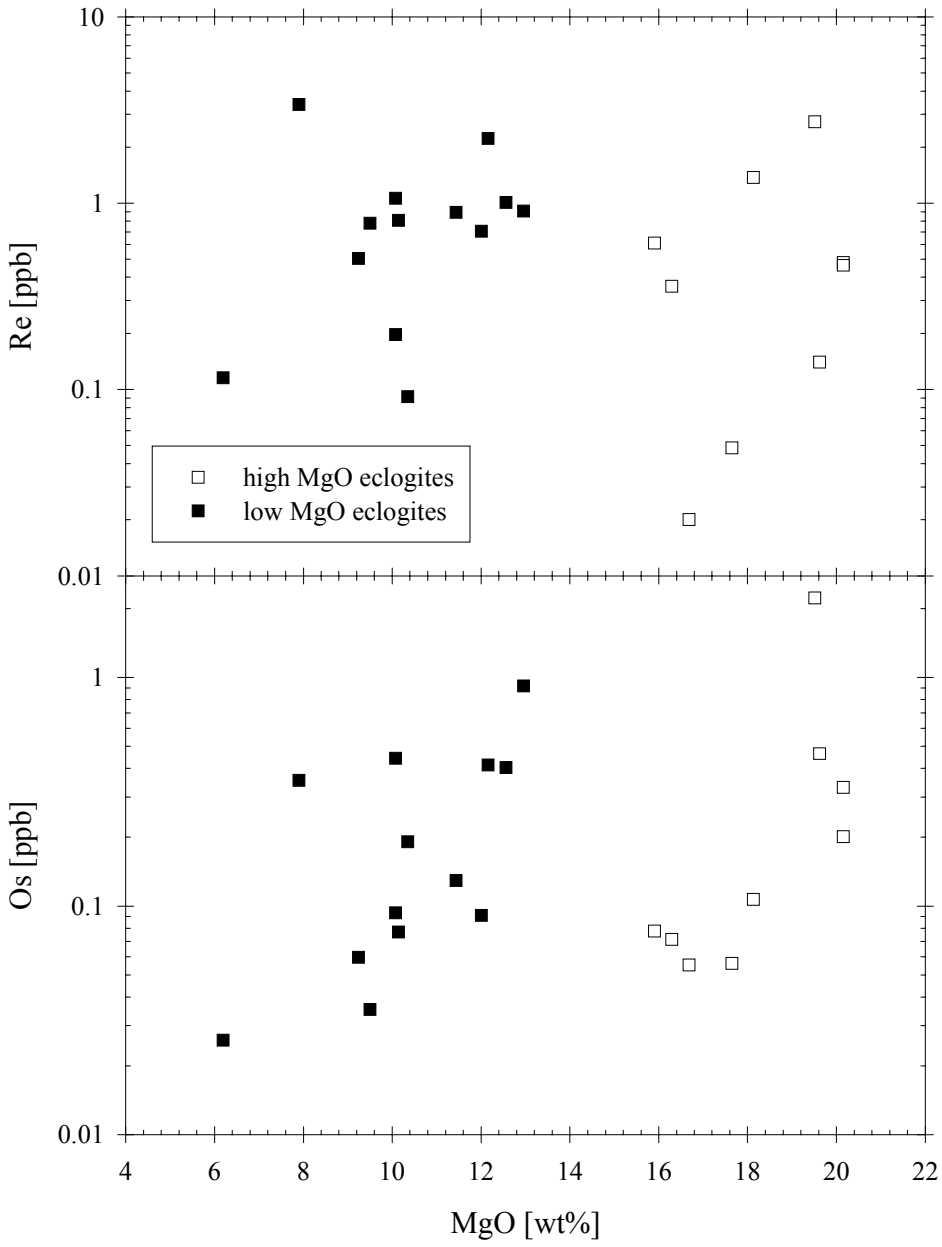

Figure 4.5. Plot of whole rock MgO content vs. Re (top) and Os (bottom) concentration of Koidu eclogites Open squares: High MgO eclogites. Solid squares: Low MgO eclogites.

The Koidu eclogites have a similar range of Re-Os abundances and Re-Os isotopic compositions to eclogite xenoliths from Udachnaya, Siberia (Pearson et al.,

1995b) and a wider range than eclogite xenoliths from the Newlands kimberlite, South Africa (Menzies et al., 1998).

The isochron plot (Fig. 4.6) defines a correlation with a slope equivalent to an age of 3.32 +0.58/-0.77 Ga (at the 95% confidence level).

Table 4.3. MgO content, Re-Os abundances, and Re-Os isotopic compositions of Koidu eclogite xenoliths (all samples have KEC prefix). MgO contents from Hills and Haggerty (1989). Errors are calculated at the 2 σ level either from blank correction or mass spectrometry (whichever is greater). Blank corrections were made for all data in the table. Samples 86-107 and 86-107 w are two powders prepared from different parts of the same xenolith. Samples were crushed in alumina ceramics except samples with the suffix w (crushed in tungsten carbide).

Sample	MgO [wt%]	Re [ppb]	Os [ppb]	$^{187}Re/^{188}Os$	$^{187}Os/^{188}Os$
low MgO eclogites					
81-3	9.24	0.506 ± 0.001	0.0597 ± 0.0010	51.43 ± 0.88	2.106 ± 0.042
81-4	12.56	1.01 ± 0.01	0.404 ± 0.004	13.29 ± 0.03	0.934 ± 0.002
81-5 w	10.35	0.0914 ± 0.0005	0.191 ± 0.001	2.368 ± 0.019	0.326 ± 0.001
81-7	12.96	0.909 ± 0.004	0.919 ± 0.014	5.163 ± 0.007	0.767 ± 0.001
81-8	10.08	1.06 ± 0.01	0.0934 ± 0.0010	93.37 ± 0.96	5.493 ± 0.094
81-10A	11.44	0.893 ± 0.001	0.129 ± 0.002	50.70 ± 0.40	4.140 ± 0.048
81-18	12.01	0.707 ± 0.001	0.0911 ± 0.0011	80.14 ± 0.93	8.833 ± 0.218
81-21	12.16	2.23 ± 0.02	0.415 ± 0.002	31.95 ± 0.08	1.917 ± 0.005
86-13 w	10.14	0.808 ± 0.001	0.0769 ± 0.0010	92.14 ± 1.21	6.362 ± 0.150
86-71A w	10.08	0.197 ± 0.001	0.443 ± 0.005	2.174 ± 0.007	0.220 ± 0.000
86-72A w	7.90	3.39 ± 0.001	0.354 ± 0.001	67.84 ± 0.20	3.717 ± 0.015
86-72B w	9.50	0.781 ± 0.001	0.0353 ± 0.0010	158.5 ± 4.5	3.829 ± 0.162
86-74B w	6.19	0.116 ± 0.0005	0.0259 ± 0.0010	28.65 ± 1.06	2.662 ± 0.127
high MgO eclogites					
81-2	16.68	0.0200 ± 0.0005	0.0553 ± 0.0010	3.716 ± 0.115	8.742 ± 0.344
81-11	19.51	2.73 ± 0.029	2.23 ± 0.03	6.362 ± 0.003	0.713 ± 0.000
86-15 w	15.90	0.611 ± 0.001	0.0778 ± 0.0010	56.18 ± 0.7418	3.808 ± 0.072
86-19 w	16.29	0.358 ± 0.0005	0.0715 ± 0.0010	46.17 ± 0.63	7.108 ± 0.184
86-58 w	19.62	0.140 ± 0.001	0.464 ± 0.004	1.476 ± 0.006	0.221 ± 0.000
86-73A w	17.65	0.0486 ± 0.0005	0.0561 ± 0.0010	4.899 ± 0.101	1.448 ± 0.027
86-90 w	18.13	1.374 ± 0.001	0.107 ± 0.001	90.46 ± 0.85	3.655 ± 0.048
86-107	20.15	0.480 ± 0.002	0.330 ± 0.001	7.406 ± 0.022	0.572 ± 0.001
86-107 w	20.15	0.464 ± 0.001	0.201 ± 0.001	11.91 ± 0.06	0.674 ± 0.002

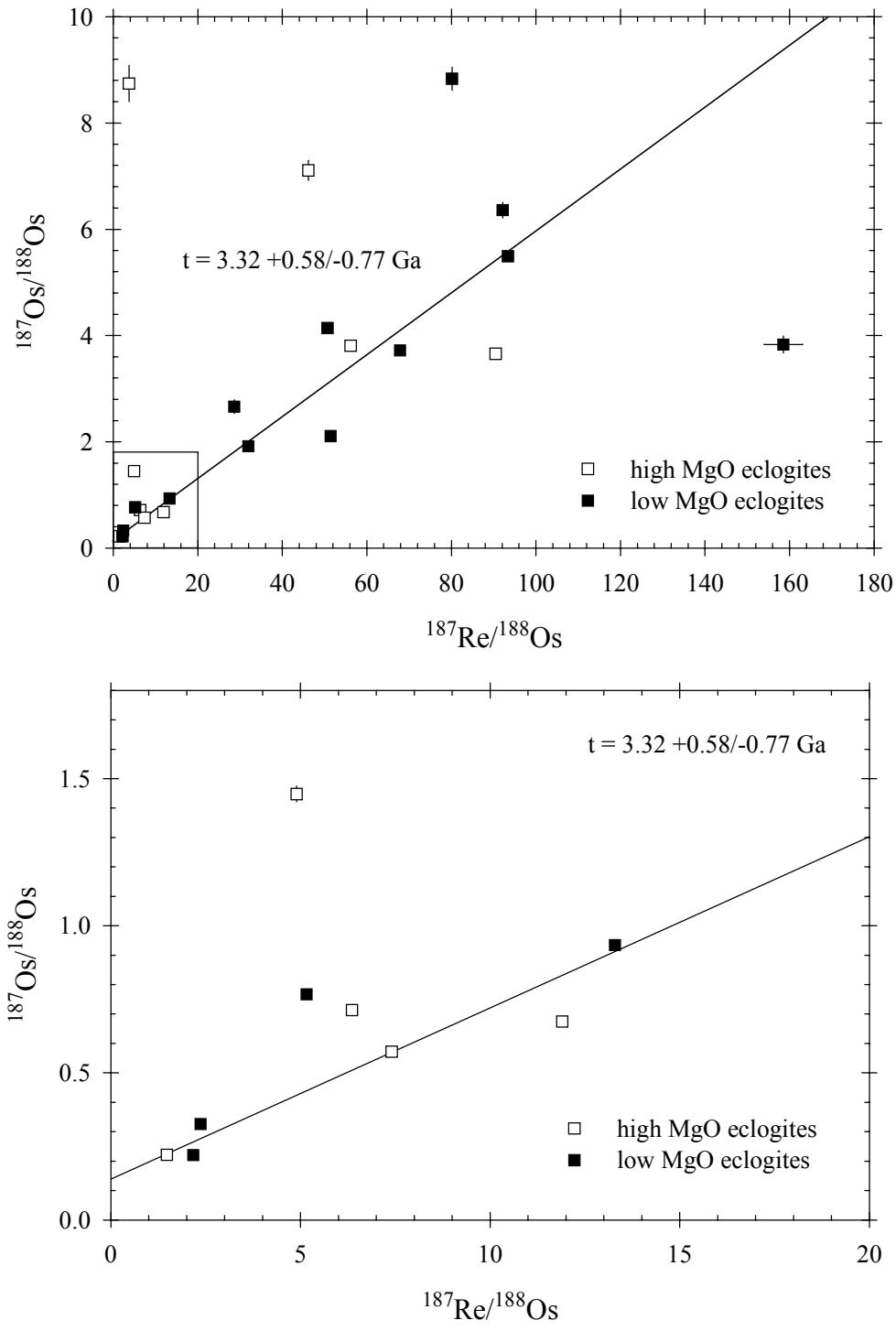

Figure 4.6. Re-Os isochron plot of Koidu eclogites (top). Inset is shown in the bottom graph. Error bars are 2σ.

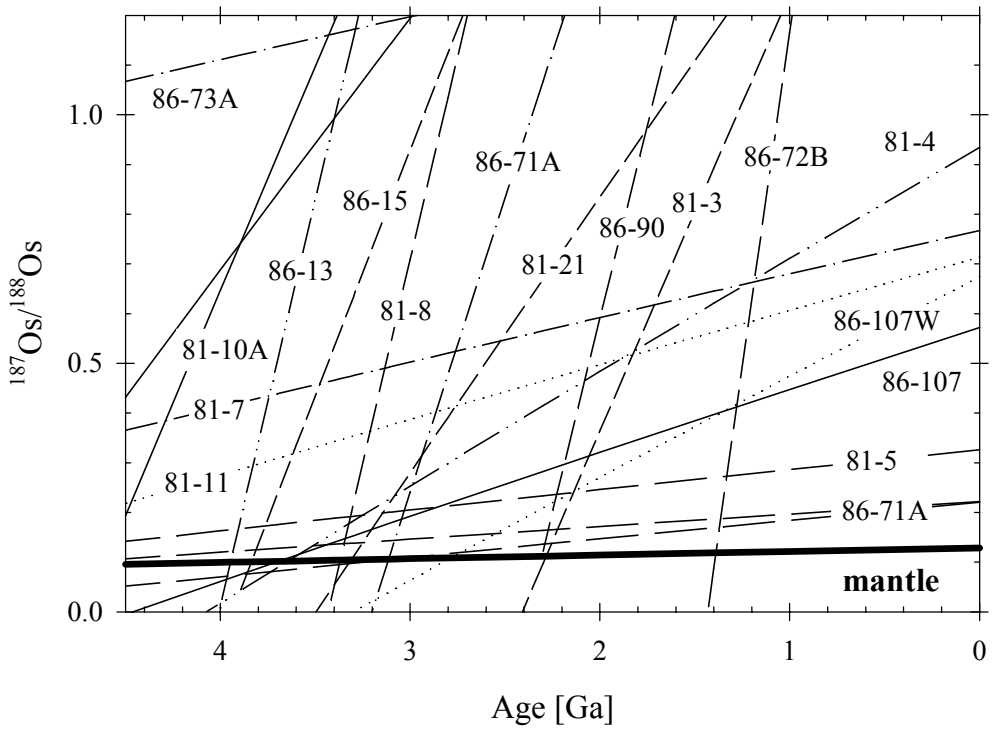

Figure 4.7. Osmium isotope evolution diagram for Koidu eclogites (all samples have KEC prefix). Lines define the isotopic evolution of a sample (given by adjacent labels) through time. A model age is given by the intersection of the sample isotopic evolution line with that of the Earth's mantle (thick solid line) and indicates the possible age of a sample, if it originated from a mantle source by a single stage event.

Osmium isotope evolution trajectories (Fig. 4.7) show general convergence between 2.0 and 3.9 Ga and have Re-Os model ages, based on extraction from a chondritic mantle, of between 1.4 and 3.9 Ga. Thus, if the system has remained closed since initial eclogite formation from an assumed chondritic mantle, twelve of the 22 samples could be between 1.4 and 3.9 Ga old. Ten of the samples are clearly divergent on the Os isotope evolution plot and give Os model ages exceeding the age of the Earth (4.6-

77 Ga), suggesting a multistage evolution for the Re-Os system in these samples and/or post-formation metasomatic overprinting.

4.7. Geological Implications of the Isotopic Data

4.7.1. Evolution of the Archean Basement in Sierra Leone

The oldest zircons in sample "old gneiss 278" are the xenocrystic cores, which point towards to presence of Early Archean (3.5-3.6 Ga) zircon-bearing rocks in the basement of Sierra Leone. This age overlaps the oldest zircon ages reported from Guinea (3.5 Ga; Thieblemont et al., 2000), the Amsaga area, Reguibat Rise (3.5 Ga; Potrel et al., 1996), and from northern Nigeria (3.57 Ga; Kröner et al., 2000), suggesting the presence of Early Archean crust in parts of West Africa.

The zircons in sample "old gneiss 278" that are devoid of inherited cores, although scattered and showing in some cases a small amount of excess radiogenic Pb, form a coherent group with concordia intercepts at 2889 ± 12 Ma and 201 ± 59 Ma. The fact that the analyses do not fit to a discordia line within analytical uncertainty suggests that their discordance was produced by at least two events, both older and younger than 201 Ma. Thus, the lower intercept probably has no direct age significance. The younger event is most likely zero-age Pb loss due to weathering and erosion of the grey gneiss. The older event is probably the Liberian event at 2.7 Ga, consistent with the youngest $^{207}Pb/^{206}Pb$ age of 2759 ± 24 Ma in the zircon population, which is interpreted to be a maximum age for metamorphism.

Two of the analyses show reverse discordance, i.e., excess radiogenic Pb. The fact that the disturbance of the Pb isotopic system generated local excesses of radiogenic Pb complicates the interpretation of the data by removing the constraint on crystallization age normally imposed by $^{207}Pb/^{206}Pb$ apparent ages. The abnormal enrichment of ^{207}Pb in the excess Pb due to its early separation from its parent elements (possibly at 2.7 Ga) means that areas where excess Pb is present give $^{207}Pb/^{206}Pb$ apparent ages that geologically are too old (cf. Black et al., 1986). To determine the minimum age for the zircon population it is therefore incorrect to use the maximum $^{207}Pb/^{206}Pb$ age measured (2944 ± 13 Ma). The most accurate age for the zircon population is probably given by the upper concordia intersection of 2889 ± 12 Ma, which is identical within uncertainty with the weighted mean $^{207}Pb/^{206}Pb$ age of 2877 ± 11 Ma.

The emplacement age of the igneous protolith of 2889 ± 12 Ma is slightly younger than the Leonean Pb-Pb whole rock age of 2959 ± 50 Ma of a gneiss in the Fadugu district, Sierra Leone, determined by Beckinsale et al. (1980) and significantly younger than the Leonean crustal growth event identified in the Amsaga area, Reguibat Rise, of 2986 ± 8 Ma (Potrel et al., 1998). The emplacement age is also younger than pre-Leonean to Leonean events recognized in western Côte d'Ivoire (3.0 – 3.2 Ga; Kouamelan et al., 1997). Thus, the Leonean crustal growth event either occurred later in Sierra Leone than in other parts of the West African Craton or the sample analyzed represents a separate, younger event.

The zircons in the granulite xenolith KGR 86-75 are concordant and their age is probably most accurately given by their mean weighted $^{206}Pb/^{238}U$ age of 2686 ± 32 Ma, which also coincides with the $^{207}Pb/^{206}Pb$ age of 2707 ± 29 Ma of the zircon inclusion in

garnet. Based on the absence of igneous oscillatory zoning in the zircon grains, this age is interpreted as the age of granulite-facies metamorphism. This metamorphic age represents the Liberian event and is consistent with the maximum age of metamorphism of 2759 ± 24 Ma derived from the grey gneiss.

The age of the Liberian event derived from the granulite xenolith is identical within uncertainty with the Rb-Sr whole rock age of 2753 ± 61 Ma of a gneiss in the Fadugu district, Sierra Leone, (Beckinsale et al., 1980) and within the age range of younger granites in Sierra Leone (2.7 – 2.8 Ga; Hurley et al., 1971; Rollinson and Cliff, 1982). The metamorphic age, however, is slightly younger than the Liberian age recognized in the Amsaga area, Reguibat Rise (2.73 Ga; Potrel et al., 1998) and significantly younger than the Liberian age in western Côte d'Ivoire (2.8 Ga; Kouamelan et al., 1997).

In summary, U-Pb isotopes in zircons from a grey gneiss and a granulite xenolith record the times of four principal events in the history of the basement in Sierra Leone:

(1) A first crustal growth event in the Early Archean (3.5 – 3.6 Ga) is recorded in rare xenocrystic cores.

(2) Emplacement of the igneous precursor of the grey gneiss occurred at ca. 2.9 Ga, when most of the zircons crystallized.

(3) High-grade metamorphism during the Liberian event at 2.7 Ga, when the zircons in the granulite xenolith and the rims of some zircons in the grey gneiss recrystallized.

(4) Zero-age Pb loss in the grey gneiss.

The older isotopic systems in the zircons in the grey gneiss were relatively little affected by the high-grade metamorphism at 2.7 Ga. They were, however, strongly affected by zero-age Pb loss most likely caused by weathering and erosion. In contrast, the zircons analyzed in the granulite xenolith were strongly affected by the 2.7 Ga Liberian event but do not record zero-age Pb loss.

4.7.2. Constraints on Archean tectonics

Reliable formation ages for basement in the Man Shield range from 2.9 to 3.2 Ga, with possibly an Early Archean (3.5 – 3.6 Ga) crustal growth episode (see above), within error of the lithospheric mantle age documented by the eclogites (3.32 +0.58/-0.77 Ga). Eclogite formation thus appears to have occurred during the periods of crustal formation, suggestive of a genetic link between these two groups of rocks. Major element, trace element, and oxygen isotope systematics indicate that the low MgO eclogites from the Koidu kimberlite complex are remnants of subducted oceanic crust that was partially melted during subduction (Rollinson, 1997; Barth et al., 2001a). I therefore suggest that Archean crustal growth in the Man Shield was accomplished, in part, by direct addition of evolved magmas from the mantle.

4.8. References

Abouchami W., Boher M., Michard A., and Albarède F. (1990) A major 2.1 Ga event of mafic magmatism in West Africa: An early stage of crustal accretion. *J. Geophys. Res.* **95**, 17,605-17,629.

Barth M. G., Rudnick R. L., Horn I., McDonough W. F., Spicuzza M. J., Valley J. W., and Haggerty S. E. (2001a) Geochemistry of Xenolithic Eclogites from West Africa, Part I: A Link between low MgO Eclogites and Archean Crust Formation. *Geochim. Cosmochim. Acta* **65**, 1499-1527.

Barth M. G., Rudnick R. L., Horn I., McDonough W. F., Spicuzza M. J., Valley J. W., and Haggerty S. E. (2001b) Geochemistry of Xenolithic Eclogites from West Africa, Part II: Origins of the high MgO eclogites, in prep.

Beckinsale R. D., Gale N. H., Pankhurst R. J., Macfarlane A., Crow M. J., Arthurs J. W., and Wilkinson A. F. (1980) Discordant Rb-Sr and Pb-Pb whole rock isochron ages for the Archaean basement of Sierra Leone. *Precambrian Res.* **13**, 63-76.

Black L. P., Williams I. S., and Compston W. (1986) Four zircon ages from one rock: the history of a 3930 Ma-old granulite from Mount Sones, Enderby Land, Antarctica. *Contrib. Mineral. Petrol.* **94**, 427-437.

Boher M., Abouchami W., Michard A., Albarède F., and Arndt N. T. (1992) Crustal growth in West Africa at 2.1 Ga. *J. Geophys. Res.* **97**, 345-369.

Creaser R., Papanastassiou D., and Wasserburg G. (1991) Negative thermal ionization mass spectrometry of osmium, rhenium, and iridium. *Geochim. Cosmochim. Acta* **55**, 397-401.

Hedge C. E., Marvin R. F., and Naeser C. W. (1975) Age provinces in the basement rocks of Liberia. *Jour. Research U.S. Geol. Survey* **3**, 425-429.

Hills D. V. and Haggerty S. E. (1989) Petrochemistry of eclogites from the Koidu Kimberlite Complex, Sierra Leone. *Contrib. Mineral. Petrol.* **103**, 397-422.

Horn I., Rudnick R. L., and McDonough W. F. (2000) Precise elemental and isotopic ratio determination by combined solution nebulization and laser ablation ICP-MS: application to U/Pb geochronology. *Chem. Geol.* **164**, 281-301.

Hurley P. M., Leo G. W., White R. W., and Fairbairn H. W. (1971) Liberian age province (about 2,700 m.y.) and adjacent provinces in Liberia and Sierra Leone. *Geol. Soc. Am. Bull.* **82**, 3483-3490.

Hurley P. M., Fairbairn H. W., and Gaudette H. E. (1975) Progress report on early Archean Rocks in Liberia, Sierra Leone and Guayana, and their general stratigraphic setting. In *The early history of the Earth* (ed. B. F. Windley), pp. 511-521. Wiley.

Kouamelan A. N., Delor C., and Peucat J.-J. (1997) Geochronological evidence for reworking of Archean terrains during the early Proterozoic (2.1 Ga) in the western Cote d'Ivoire (Man Rise-West African Craton). *Precambrian Res.* **86**, 177-199.

Kröner A., Ekwueme B. N., and Pidgeon R. T. (2000) The oldest rocks in West Africa: SHRIMP zircon age for early Archean migmatitic orthogneiss at Kaduna, northern Nigeria. *J. Geol.*, in press.

Longerich H. P., Jackson S. E., and Günther D. (1996) Laser ablation inductively coupled plasma mass spectrometric transient signal data acquisition and analyte concentration calculation. *J. Anal. At. Spectrom.* **11**, 899-904.

Ludwig K. R. (1998) Isoplot/Ex. Berkeley Geochronological Center Special Publication 1.

Macfarlane A., Crow M. J., Arthurs J. W., Wilkinson A. F., and Aucott J. W. (1981) The geology and mineral resources of northern Sierra Leone. *Overseas Mem. Inst. Geol. Sci.* **7**, 103 p.

Menzies A. H., Shirey S. B., Carlson R. W., and Gurney J. J. (1998) Re-Os systematics of diamond-bearing eclogites and peridotites from Newlands Kimberlite. *7th Internat. Kimberlite Conf., extended abstracts*, 579-581.

Nutman A. P., Bennett V. C., Friend C. R. L., and Mcgregor V. R. (2000) The early Archaean Itsaq Gneiss Complex of southern West Greenland: the importance of field observations in interpreting age and isotopic constraints for early terrestrial evolution. *Geochim. Cosmochim. Acta* **64**, 3035-3060.

Pearson D. G., Shirey S. B., Carlson R. W., Boyd F. R., Pokhilenko N. P., and Shimizu N. (1995a) Re-Os, Sm-Nd, and Rb-Sr isotope evidence for thick Archaean lithospheric mantle beneath the Silurian craton modified by multistage metasomatism. *Geochim. Cosmochim. Acta* **59**, 959-977.

Pearson D. G., Snyder G. A., Shirley S. B., Taylor L. A., Carlson R. W., and Sobolev N. V. (1995b) Archaean Re-Os age for Siberian eclogites and constraints on Archaean tectonics. *Nature* **374**, 711-713.

Pidgeon R. T., Nemchin A. A., and Hitchen G. J. (1998) Internal structures of zircons from Archaean granites from the Darling Range batholith: implications for zircon stability and the interpretation of zircon U-Pb ages. *Contrib. Mineral. Petrol.* **132**, 288-299.

Poldervaart A. (1956) Zircons in rocks. 2. Igneous rocks. *Am. J. Sci.* **254**, 521-554.

Potrel A., Peucat J., Fanning C. M., Auvray B., Burg J. P., and Caruba C. (1996) 3.5 Ga old terranes in the West African Craton, Mauritania. *J. Geol. Soc. London* **153**, 507-510.

Potrel A., Peucat J. J., and Fanning C. M. (1998) Archean crustal evolution of the West African Craton; example of the Amsaga area (Reguibat Rise); U-Pb and Sm-Nd evidence for crustal growth and recycling. *Precambrian Res.* **90**, 107-117.

Reischmann T. (1995) Precise U/Pb age determination with baddeleyite (ZrO_2), a case study from the Phalaborwa igneous complex, South Africa. *S. Afr. J. Geol.* **98**, 1-4.

Rollinson H. (1997) Eclogite xenoliths in west African kimberlites as residues from Archaean granitoid crust formation. *Nature* **389**, 173-176.

Rollinson H. R. and Cliff R. A. (1982) New Rb-Sr age determinations on the Archaean basement of eastern Sierra Leone. *Precambrian Res.* **17**, 63-72.

Shirey S. B. (1997) Re-Os isotopic compositions of Midcontinent Rift System picrites: implications for plume-lithosphere interaction and enriched mantle sources. *Can. J. Earth Sci.* **34**, 489-503.

Shirey S. B. and Walker R. J. (1995) Carius tube digestion for low-blank rhenium-osmium analysis. *Anal. Chem.* **67**, 2136-2141.

Wiedenbeck M., Alle P., Corfu F., Griffin W. L., Meier M., Ober F., von Quandt A., Roddick J. C., and Spiegel J. (1995) Three natural zircon standards for U-Th-Pb, Lu-Hf, trace element and REE analyses. *Geostand. Newslett.* **19**, 1-23.

Williams H. R. (1978) The Archaean geology of Sierra Leone. *Precambrian Res.* **6**, 251-268.

Chapter 5

Conclusions

The low MgO eclogites from Koidu, Sierra Leone, have variable oxygen isotopic compositions that exceed the mantle range and reconstructed trace element patterns that are depleted in Ba, Th, U, and light REE but have a positive Nb anomaly. The Koidu low MgO eclogites may represent fragments of processed oceanic crust that are residues from Archean continental crust formation. The subducted oceanic crust was partially melted in order to produce tonalite-trondhjemite-granodiorite suites (TTG), and thus created these residual eclogites, which were subsequently emplaced into the subjacent lithospheric environment.

The complementary silicic melt to the median low MgO eclogite is enriched in incompatible trace elements and has Nb and HREE depletions, as observed in TTG suites, which make up large portions of the crust in Archean cratons. TTGs also show high Zr/Sm and Th/U, complementary to the eclogites. Therefore, the low MgO eclogites have the trace element characteristics expected for residues from TTG generation. This notion is supported by the restitic major element composition of these xenoliths. Thus, the Koidu low MgO eclogites may represent parts of the missing mafic reservoir needed to explain the silicic composition of the crust in Archean cratons. The volume of mafic residue produced during the production of TTGs exceeds by far the volume of mafic lower crust and eclogite in the lithospheric mantle currently present in Archean cratons. During partial melting of subducted oceanic crust, portions of the residue (the oceanic crust of the slab) are likely to be transported deeper into the mantle, possibly all the way

to the core-mantle boundary. The silicic melts rise (driven by the density contrast between melt and solids) and variably interact with the peridotitic mantle wedge on their way to the surface, forming the Archean TTG suites. It is also likely that portions of the slab may be left behind in the lithosphere and later sampled by passing kimberlites.

Due to the absence of modal olivine and orthopyroxene in the Koidu high MgO eclogites, high-pressure crystal fractionation systematics suggest that the high MgO eclogites most likely formed at pressures lower than those inferred from applying their estimated equilibration temperatures to a cratonic geotherm. The high MgO eclogites have whole rock major element compositions suggestive of a cumulate origin, generated either as garnet-pyroxene cumulates emplaced in the uppermost mantle ($P < 3$ GPa) or as low-pressure (crustal) plagioclase-pyroxene-olivine cumulates. Reconstructed trace element concentrations of the high MgO eclogites may be affected by ancient metasomatism and do not allow a clear distinction between high-P and low-P origin. For a low-P origin two different tectonic settings are possible: The high MgO eclogites could represent either the basal section of oceanic crust that has been subducted or foundered mafic lower continental crust.

U-Pb zircon ages and Nd model ages for basement in the Man Shield range from 2.9 to 3.2 Ga, with possibly an Early Archean (3.5 – 3.6 Ga) crustal growth episode, within error of the lithospheric mantle age documented by the eclogites from a whole rock Re-Os isochron (3.32 +0.58/-0.77 Ga). Eclogite formation thus appears to have occurred during the periods of crustal formation, suggestive (but not conclusive evidence) of a genetic link between these two groups of rocks. Major element, trace element, and oxygen isotope systematics indicate that the low MgO eclogites from the Koidu

kimberlite complex are remnants of subducted oceanic crust that was partially melted during subduction. I therefore suggest that Archean crustal growth in the Man Shield was accomplished, in part, by direct addition of evolved magmas from the mantle.

Although the Koidu low MgO eclogites probably represent ancient altered oceanic crust that has been recycled in the mantle and partially melted at high pressures, this does not mean that the tectonic environment was exactly analogous to modern subduction zones (i.e., similar to slab melting and generation of adakites in the Aleutians, southern Andes, and Kamtchatka). An alternative scenario to slab melting is tectonic emplacement of oceanic crust directly below the continental crust and partial melting in the garnet stability field. Such overthickening of continental crust may be caused by terrain collision or could be associated with oceanic plateaux. Higher mantle temperatures in the Archean may have resulted in more buoyant slabs due to higher melt production at mid-ocean ridges, thicker oceanic crust, and more depleted lithospheric mantle. If slabs were positively buoyant and difficult to subduct, a different tectonic style would have been necessary to remove heat from the Archean mantle. Rather than being subducted, oceanic crust might have accumulated over downwellings and, after cooling, "dripped" back into the mantle. Irrespective of the exact tectonic setting, the Koidu low MgO eclogites demonstrate recycling of oceanic crust and formation of Archean continental crust at convergent plate boundaries.

Appendix A

Tracking the budget of Nb and Ta in the continental crust

Matthias G. Barth *, William F. McDonough, and Roberta L. Rudnick
Department of Earth and Planetary Sciences, Harvard University, 20 Oxford Street, Cambridge, MA 02138, U.S.A

Chemical Geology (2000) **165**, 197-213

* Corresponding author. Tel.: +1 617 496-4356; Fax: +1 617 496-0434; E-mail: barth@eps.harvard.edu

A.1. Abstract

High precision trace element data are reported for representative samples of the upper continental crust: 11 loess samples and 22 shale samples (PAAS) previously used by Taylor and McLennan to define the rare earth element (REE) content of the upper crust. Our results confirm the rare earth element concentrations of Taylor and McLennan's (1985) estimate of the upper continental crust but suggest substantial revisions for Nb and Ta, in agreement with recent work of Plank and Langmuir (1998). From our data, the upper continental crust has average Nb = 11.5±2.6 ppm (instead of 25 ppm) and Ta = 0.92±0.12 ppm (instead of 2.2 ppm), which translates into a bulk crust Nb = 8 ppm, Ta = 0.7 ppm, La/Nb = 2.2, and Nb/Ta = 12-13. These revisions confirm the crustal subchondritic Nb/Ta and superchondritic La/Nb ratios and reinforce the observation that the continental crust and the Depleted Mantle are not strictly complementary: an additional Nb- and Ta-rich reservoir having superchondritic Nb/Ta is required to balance the Silicate Earth. Using the continental crust's La/Nb ratio to estimate the proportions of crustal growth in convergent margin and intraplate settings, we suggest a plume contribution of only between 5 to 20 % to the continents, even lower than previous estimates.

keywords: composition of continental crust; loess; shale; Niobium; Tantalum

A.2. Introduction

The refractory lithophile elements Nb, Ta, and rare earth elements (REE) are assumed to be in chondritic proportions in the Silicate Earth. Nb and Ta are identical in charge and nearly identical in size and hence show strongly coherent geochemical behavior. For these reasons, fractionation of Nb and Ta from REE has provided crucial constraints on crust-mantle differentiation and crustal growth processes (Hofmann et al., 1986; Rudnick, 1995).

Although the continental crust comprises only a small fraction of the mass of the earth, a significant portion of the Earth's incompatible trace elements resides in the continents. Therefore, defining the crust's composition is crucial for understanding mass balance of these elements in the Earth. Specifically, it is well established that the continental crust is depleted in Nb and Ta relative to other highly incompatible elements such as La. Likewise, average MORB is depleted in Nb and Ta relative to La and one can therefore assume that the Depleted Mantle (i.e., MORB source) shows a similar depletion, given that Nb and Ta are more incompatible than La during MORB genesis (Hofmann, 1988; Sun and McDonough, 1989). The superchondritic La/Nb values for the continental crust (1.3-2.2, Rudnick and Fountain, 1995; and references therein) and for average MORB (1.1-1.3, Hofmann, 1988; Sun and McDonough, 1989) demonstrate that these are not complementary silicate reservoirs (Sun and McDonough, 1989; McDonough, 1991). Although the continental lithospheric mantle has subchondritic La/Nb, its low La and Nb concentrations imply that the continental lithospheric mantle is not an important Nb-bearing reservoir within the Earth (McDonough, 1991). Thus, other Nb- and Ta- rich reservoirs are needed to balance the Silicate Earth.

It is also debated whether Nb and Ta are fractionated from each other during crust-mantle differentiation. The primitive mantle has a chondritic Nb/Ta ratio of 17.4±0.5, and the Depleted Mantle a subchondritic ratio of 15.5±1 (Jochum et al., 1997). The crustal Nb/Ta values of about 11-12 (Taylor and McLennan, 1985; Rudnick and Fountain, 1995) are less well established due to the lack of high-quality data for Nb and Ta on representative crustal samples.

Finally, determining the concentrations of high field strength elements (HFSE) in the continental crust can be important for establishing the style of crustal growth. The depletion of Nb relative to light REE, as seen in the crust, is indicative of crustal growth at convergent margins rather than intraplate settings, but determining the proportions of these two end members is critically dependent on defining the La/Nb ratio of the crust.

Because Nb, Ta and REE are concentrated in the upper continental crust (UCC) relative to the lower crust, determining its composition is critical for understanding the bulk crust composition. Fortunately, the upper crust is accessible to large-scale sampling through the processes of sedimentation. Previous studies have demonstrated that the average composition of UCC can be obtained for elements that are insoluble in water from aeolian deposits as well as from fine-grained clastic sediments (Nance and Taylor, 1976; Taylor et al., 1983; Gallet et al., 1998).

A.3. Samples of the Upper Continental Crust

To address the question of Nb and Ta abundances in the continental crust we have undertaken precise trace element measurements on a fundamental suite of representative samples that were previously analyzed by Taylor and colleagues to estimate the REE content of the UCC. The suite consists of 11 loess samples from Banks Peninsula, New Zealand, Kansas and Iowa, U.S.A., and Kaiserstuhl, Germany (Taylor et al., 1983) and 22 shales (post-Archean average Australian shale (PAAS), Nance and Taylor, 1976; McLennan, 1981).

Because loess is an aeolian deposit, derived from glacial outwash and from desert environments (e.g., Smalley and Vita-Finzi, 1968; Flint, 1971), weathering has a relatively small effect on its chemistry. However, major element systematics imply that loess deposits have experienced at least one cycle of aquatic sedimentary differentiation processes (Gallet et al., 1998). The very nature of the aeolian transport mechanism also ensures that a geographically widespread area will be sampled.

In contrast, shales are formed by more complex processes compared with the simple abrasion process experienced during glacial erosion, and they generally show higher degrees of weathering than loess. However, elements with low solubility in natural waters (e.g., Nb, Ta and REE) are considered immobile. Consequently, it is likely that these elements are transferred nearly quantitatively from the site of weathering into clastic sediments. Although REE patterns in loess and shales are parallel to upper crustal patterns, they overestimate the absolute abundances by about 20% due to the presence of sediments with much lower REE concentrations, such as sandstones, carbonates, and evaporites (Taylor and McLennan, 1985).

A.4. Analytical Methods

Nb, Ta, REE, and other trace elements were determined by inductively coupled plasma-mass spectrometry (ICP-MS). The principal difficulties of measuring high-field strength elements (HFSE) in dissolved rocks are incomplete acid digestion, solution instability, and memory effects. These obstacles can cause poor precision (e.g., Jenner et al., 1990; Xie et al., 1994) and lower concentrations compared with other techniques that do not require sample dissolution, such as spark source mass spectrometry (SSMS), X-ray fluorescence (XRF), and INAA (e.g., Hall and Plant, 1992; Totland et al., 1992). The procedure described below was developed to overcome these analytical problems.

Samples were dissolved in a mixture of ultrapure, concentrated HF–HNO_3 and then spiked with a mixed multi-element/enriched isotope internal standard solution prior to analysis, following the technique of Eggins et al. (1997). Complete dissolution of the samples was ensured by the use of conventional oven bombs. The HFSE, especially Ta, have a strong tendency for precipitation or adsorption on container walls. Therefore, analyte stability was enhanced by addition of dilute HF to the solutions (see discussion in Münker, 1998). Dilution of the samples in 2% HNO_3 and 0.1% HF gave satisfactory results for HFSE in the reference materials AGV-1 and GSP-1 (Table A.1). The latter standard was chosen to demonstrate the efficiency of bomb dissolutions. Our Zr value is high compared to that in Govindaraju (1994) (628 vs. 530 ppm), but overlaps the rather large range of Zr concentrations determined by Owen and Faure (1974) by isotope dilution. This range, coupled with visible particles in our USGS powder aliquots (split 27, position 20), suggests sample heterogeneity with respect to zircons. Note that the Nb and Ta abundances are the same as reported by Govindaraju (1994).

Table A.1. Blank levels and USGS reference standards AGV-1 and GSP-1 analyzed by ICP-MS.

	AGV-1 reference value	AGV-1 ppm n = 11	RSD %	GSP-1 reference value	GSP-1 ppm n = 11	RSD %	blank ppb n = 8	detection limits ppb (3 σ)
Ga	21.2	20.1	6.0	23	22.4	3.9	0.017	0.017
Sr	660	666	11.5	234	194	5.4	0.240	0.373
Y	19.5	19.9	8.6	27	26.8	3.8	0.005	0.006
Zr	230	241	7.3	595	628	2.8	0.082	0.107
Nb	14.5	14.5	4.5	27.9	26.8	3.5	0.005	0.020
Cs	1.25	1.2	9.8	1.02	1.0	7.0	0.001	0.002
Ba	1210	1203	9.3	1310	1317	2.8	0.854	5.349
La	39	38.7	13.6	184	189	2.6	0.006	0.008
Ce	69	68.4	3.9	399	448	4.6	0.010	0.017
Pr	8	8.27	7.3	52	57.9	3.4	0.002	0.003
Nd	32	31.2	7.1	196	201	3.3	0.008	0.018
Sm	5.9	5.62	4.8	26.3	26.3	5.5	0.011	0.009
Eu	1.55	1.64	4.9	2.33	2.31	3.9	0.001	0.001
Gd	4.7	4.50	5.2	12.1	12.6	4.7	0.001	0.003
Tb	0.7	0.68	7.5	1.34	1.46	4.1	0.000	0.001
Dy	3.8	3.59	6.0	5.5	6.59	4.4	0.001	0.003
Ho	0.7	0.68	3.8	1.01	0.98	2.8	0.000	0.001
Er	1.9	1.92	4.2	2.7	2.57	3.0	0.001	0.002
Yb	1.75	1.62	3.7	1.7	1.74	3.4	0.001	0.002
Lu	0.27	0.257	5.6	0.214	0.234	5.4	0.001	0.001
Hf	5.17	5.32	6.3	15.5	16.3	3.5	0.003	0.005
Ta	0.90	0.90	3.2	0.97	0.93	4.4	0.004	0.007
Th	6.5	6.25	3.2	106	109	5.6	0.002	0.004
U	1.90	1.92	3.5	2.54	2.51	4.5	0.001	0.001

Notes to Table 1:
The values for both AGV-1 and GSP-1 are averages of 11 repeat analyses of 4 digestions. The RSD is the relative standard deviation in percent. The blank values are the average of 8 repeated analyses of 4 different procedural blanks. Recommended values from Govindaraju (1994) except Zr in GSP-1 (595±21 ppm) from Owen and Faure (1974).

Analyses were performed on a Fisons (VG Elemental) PQ II+ in pulse counting mode (three points per peak). Dwell time and quadrupole settling time were set to 10 ms and 5 ms, respectively. Sensitivity of the instrument was on average ~50 MHz (counts per second per ppm) for ^{115}In. Rinsing time and sample uptake time were set at 2 min and 5 min, respectively, in order to avoid the considerable memory effects observed for Ta. Free HF in the solutions required the use of a corrosion-resistant nebulizer (V-groove).

The concentrations of Nb and Ta were further verified by standard addition experiments in selected samples. For the analytical setup described here, blank levels of 0.005 ppb Nb and 0.004 ppb Ta were determined by 8 measurements of blank solution. Detection limits of 0.020 ppb Nb and 0.007 ppb Ta were calculated at 3σ of signal variation of blank solution. At a dilution factor of 1/2500 for analysis, this results in detection limits of 0.050 ppm Nb and 0.018 ppm Ta for the samples, two orders of magnitude below the lowest observed abundances of 6.9 ppm Nb and 0.61 ppm Ta (shale sample MI 2). Long term external reproducibility is ±3.5% for Nb and ±4.4% for Ta (1σ) as determined by 11 measurements of the reference material GSP-1. Internal (within run) reproducibilities for these solutions are 2-3% (1σ).

A.5. Results

Trace element data for the loess and shale samples are given in Table A.2. The loess samples show remarkably similar trace element patterns between different regions (Fig. A.1) and within a specific region (Fig. A.2, see also Fig. 3 in Taylor et al., 1983). Loess is highly enriched in large ion lithophile elements (LILE; e.g., Cs, Ba) and light REE relative to primitive mantle, with relatively flat heavy REE profiles and consistent negative Nb, Ta, and Ti anomalies relative to REE of similar incompatibilities. The Kaiserstuhl samples have lower absolute trace element abundances (but higher Sr) due to the diluting effect of their higher carbonate contents. In general, the trace element patterns resemble estimates of upper crustal composition. UCC-normalized trace element

Table A.2. Trace element concentrations (in ppm) of loess determined by ICP-MS

	Banks Peninsula					Kansas			Iowa	Kaiserstuhl	
	BP-1	BP-2	BP-3	BP-4	BP-5	CY-4a-A	CY-4a-B	CY-4a-C		1	2
Ga	16.6	16.7	17.3	16.7	15.6	11.3	12.0	12.4	12.3	6.9	6.8
Sr	271	304	300	276	300	170	192	216	139	389	300
Y	29.1	26.5	33.1	26.3	26.3	26.4	32.0	31.4	29.9	26.5	28.8
Zr	437	410	576	401	425	645	645	664	445	303	293
Nb	11.6	11.2	17.6	11.8	11.4	14.0	15.7	15.1	15.1	10.0	9.5
Cs	4.4	4.5	4.0	4.7	4.3	2.5	3.0	2.7	3.1	2.7	2.6
Ba	564	614	590	583	564	515	664	684	713	210	192
La	34.4	33.7	41.1	34.3	35.8	33.6	39.1	43.1	32.7	26.0	25.9
Ce	68.5	75.2	75.0	72.0	74.2	70.7	75.1	82.6	65.5	53.1	52.4
Pr	8.78	8.48	10.2	8.37	8.60	8.69	9.23	10.5	7.84	5.00	6.44
Nd	32.5	30.8	37.8	30.2	31.0	31.5	33.5	37.1	29.1	24.0	23.8
Sm	6.58	5.98	7.46	5.78	5.89	5.94	6.05	6.66	5.43	4.96	5.00
Eu	1.45	1.41	1.71	1.36	1.31	1.19	1.16	1.31	1.23	0.86	0.91
Gd	6.12	5.64	6.57	5.54	5.55	5.39	5.46	5.52	4.95	4.40	4.76
Tb	0.847	0.787	0.982	0.769	0.760	0.760	0.770	0.857	0.769	0.685	0.733
Dy	4.70	4.28	5.39	4.29	4.24	4.37	4.50	4.90	4.67	3.86	4.35
Ho	0.98	0.88	1.09	0.86	0.85	0.87	0.93	1.02	0.98	0.80	0.89
Er	2.82	2.47	3.04	2.47	2.47	2.66	2.87	3.04	2.93	2.26	2.59
Yb	2.83	2.42	2.82	2.41	2.42	2.80	2.98	3.15	3.07	2.12	2.51
Lu	0.452	0.376	0.442	0.380	0.380	0.453	0.485	0.509	0.480	0.334	0.373
Hf	10.6	9.9	13.7	9.8	10.2	15.6	15.0	16.8	10.9	7.07	7.15
Ta	0.95	1.05	1.73	0.95	0.90	1.12	0.98	1.00	1.02	0.76	0.75
Th	11.0	13.0	11.0	11.8	12.2	11.4	11.8	13.2	10.8	7.95	8.45
U	2.75	3.03	3.11	2.74	2.82	2.91	3.13	3.12	2.85	2.59	2.93
La/Nb	3.0	3.0	2.3	2.9	3.2	2.4	2.5	2.9	2.2	2.6	2.7
Nb/Ta	12.2	10.7	10.2	12.9	12.6	12.5	16.1	15.1	14.8	13.1	12.7

Table A.2 (continued). Trace element concentrations (in ppm) of shales determined by ICP-MS

	Mt. Isa Group				State Circle Shale						
	MI 1	MI 2	MI 4	MI 5	SC 1	SC 2	SC 3	SC 4	SC 5	SC 7	SC 8
Ga	16.6	8.2	16.0	18.4	21.1	20.5	19.4	22.0	21.6	20.7	20.7
Sr	10.6	41.8	52.8	36.4	16.4	12.9	18.1	14.4	16.2	20.7	25.1
Y	8.82	20.4	20.8	18.8	22.8	31.9	25.4	24.3	20.3	27.9	22.1
Zr	93.6	91.2	129	198	144	146	161	146	133	133	137
Nb	10.1	6.89	12.0	14.2	14.4	14.8	14.3	14.5	14.6	14.0	14.1
Cs	4.6	3.6	7.9	13.6	7.8	9.4	6.6	8.4	9.6	9.1	7.8
Ba	274	25	276	240	369	258	293	495	408	349	332
La	20.3	38.6	33.4	33.2	28.1	41.1	29.7	43.5	24.5	44.2	32.8
Ce	34.0	77.1	71.3	78.6	62.8	84.2	63.4	89.8	63.5	88.7	75.5
Pr	4.61	8.44	7.67	7.72	7.29	10.0	7.08	10.2	6.70	10.3	8.41
Nd	16.2	29.8	26.4	27.5	30.0	36.2	27.9	37.2	24.5	37.0	32.2
Sm	2.85	5.25	4.89	4.89	6.07	7.30	5.61	7.67	4.84	4.97	6.59
Eu	0.51	0.76	0.82	0.87	1.31	1.45	1.12	1.48	0.92	0.90	1.07
Gd	2.32	4.40	4.20	4.13	5.93	7.54	5.95	5.95	4.31	4.27	5.19
Tb	0.32	0.60	0.63	0.61	0.75	0.99	0.79	1.00	0.65	0.64	0.81
Dy	1.81	3.25	3.55	3.50	4.48	5.42	4.32	5.35	3.74	3.68	4.71
Ho	0.37	0.69	0.73	0.72	0.93	1.12	0.95	1.05	0.76	0.77	0.98
Er	1.13	2.08	2.10	2.11	2.68	2.96	2.57	2.84	2.13	2.16	2.63
Yb	1.07	2.15	1.98	1.97	2.37	2.55	2.27	2.51	2.08	2.03	2.70
Lu	0.168	0.352	0.291	0.307	0.379	0.465	0.373	0.444	0.302	0.305	0.417
Hf	2.85	2.64	3.60	5.47	4.09	4.43	4.90	4.21	4.01	3.90	4.09
Ta	0.78	0.61	0.99	1.19	1.43	1.42	1.39	1.41	1.22	1.11	1.19
Th	5.71	9.66	13.1	11.0	10.6	9.03	9.50	16.7	12.2	10.3	9.54
U	2.03	2.55	9.03	2.90	2.41	2.19	2.24	2.50	2.56	2.46	2.61
La/Nb	2.0	5.6	2.8	2.3	1.9	2.8	2.1	3.0	1.7	3.2	2.3
Nb/Ta	12.7	11.1	12.2	11.6	10.1	10.4	10.7	10.2	11.6	12.5	11.8

Table A.2 (continued). Trace element concentrations (in ppm) of shales determined by ICP-MS

	Perth Basin			Canning Basin		Amadeus Basin					
	PW-4	PW-5	PW-7	PL-1	PL-6	AO 6	AO 7	AO 8	AO 9	AO 10	AO 12
Ga	28.4	27.1	22.9	22.2	19.7	19.2	19.7	17.5	19.3	21.3	23.9
Sr	96.0	86.4	63.4	43.9	218.4	60.1	74.6	66.7	37.6	64.7	60.8
Y	32.0	32.5	22.6	27.1	33.7	23.1	23.0	22.7	15.4	22.2	30.4
Zr	245	179	235	199	221	176	202	207	176	187	163
Nb	26.7	25.2	22.5	18.0	16.1	14.3	15.3	14.6	14.9	15.8	15.5
Cs	8.2	9.2	3.8	10.1	9.8	12.5	13.3	10.0	11.1	11.8	16.2
Ba	626	595	404	580	319	245	245	170	189	274	372
La	55.0	54.1	26.4	41.6	47.1	27.3	36.2	35.6	20.5	33.0	46.3
Ce	120	111	67.8	88.6	94.9	63.8	76.3	68.5	38.4	67.8	84.1
Pr	12.4	14.0	7.24	10.71	11.13	6.77	8.15	8.14	5.06	5.26	10.3
Nd	43.8	52.3	26.4	29.9	39.5	24.5	28.2	28.7	18.7	20.3	36.5
Sm	8.29	10.3	5.76	6.01	7.37	4.85	5.15	5.41	3.60	4.19	6.04
Eu	1.59	1.90	1.19	1.01	1.23	0.91	0.94	0.94	0.67	0.81	1.12
Gd	7.15	8.31	5.47	4.92	5.95	4.18	4.38	4.57	2.99	4.81	5.46
Tb	1.08	1.25	0.913	0.852	0.983	0.694	0.710	0.727	0.513	0.597	0.867
Dy	6.09	7.34	5.43	5.10	5.58	4.10	4.08	4.16	3.04	3.40	5.11
Ho	1.26	1.44	1.11	1.21	1.15	0.846	0.845	0.841	0.626	0.991	1.06
Er	3.65	4.02	3.22	3.56	3.36	2.45	2.52	2.43	1.88	2.79	3.04
Yb	3.54	3.66	2.99	3.49	3.19	2.42	2.50	2.31	1.87	2.50	3.01
Lu	0.531	0.557	0.443	0.499	0.478	0.366	0.382	0.355	0.287	0.407	0.444
Hf	6.81	5.08	6.95	5.71	5.72	4.90	5.55	5.73	4.98	5.46	4.51
Ta	1.88	1.90	1.69	1.44	1.37	1.14	1.24	1.16	1.22	1.27	1.19
Th	20.3	23.4	12.5	18.0	21.5	17.0	16.8	14.3	9.10	15.6	19.0
U	3.93	3.24	3.25	2.98	3.71	2.62	2.82	2.70	2.05	2.70	2.22
La/Nb	2.1	2.1	1.2	2.3	2.9	1.9	2.4	2.4	1.4	2.1	3.0
Nb/Ta	13.4	12.8	13.4	12.5	11.8	12.3	12.1	12.1	12.1	12.3	12.9

diagrams are shown in Fig. A.2. The Sr depletion seen in these samples is due to its solubility during continental weathering (e.g., Nesbitt et al., 1980), demonstrating that loess is derived from areas of moderate weathering (Gallet et al., 1998). Zr and Hf are enriched relative to upper crustal abundances, indicating that zircon is concentrated by the loess-forming process (Taylor et al., 1983). Nb and Ta are depleted relative to UCC (see below). The shales, although more heterogeneous than the loess samples, have similar trace element patterns to loess and UCC (Figs. A.3 and A.4). The shales show stronger Sr depletions, reflecting their higher degree of weathering compared to loess. Nb and Ta are depleted relative to UCC in the shales (except in the shales from the Perth Basin).

Our new trace element data show excellent agreement between ICP-MS and SSMS analyses for La and reasonable agreement for Nb. The average La concentration of loess and PAAS and the average Nb concentration of PAAS agree between the two techniques to within 10% (Table A.3). The average Nb concentration of loess determined by ICP-MS is ~20% lower than the SSMS value (Table A.3). For the individual samples, our La concentrations of the loess samples and all but one of Taylor et al.'s (1983) values agree within 10%. The La concentration of sample CY-4a-B determined by ICP-MS is ~25% higher than the SSMS value (39.1 ppm instead of 31 ppm). For half of the shale samples, our La concentrations and Nance and Taylor's (1976) values agree within 10%. Four shale samples show up to ~30% higher concentrations in comparison with the SSMS data; 7 samples have up to ~40% lower concentrations. For six loess samples and eight shale samples, our Nb concentrations are up to ~35% lower than the SSMS values, e.g., the Nb concentration of sample BP-3 determined by ICP-MS is 17.6 ppm instead of

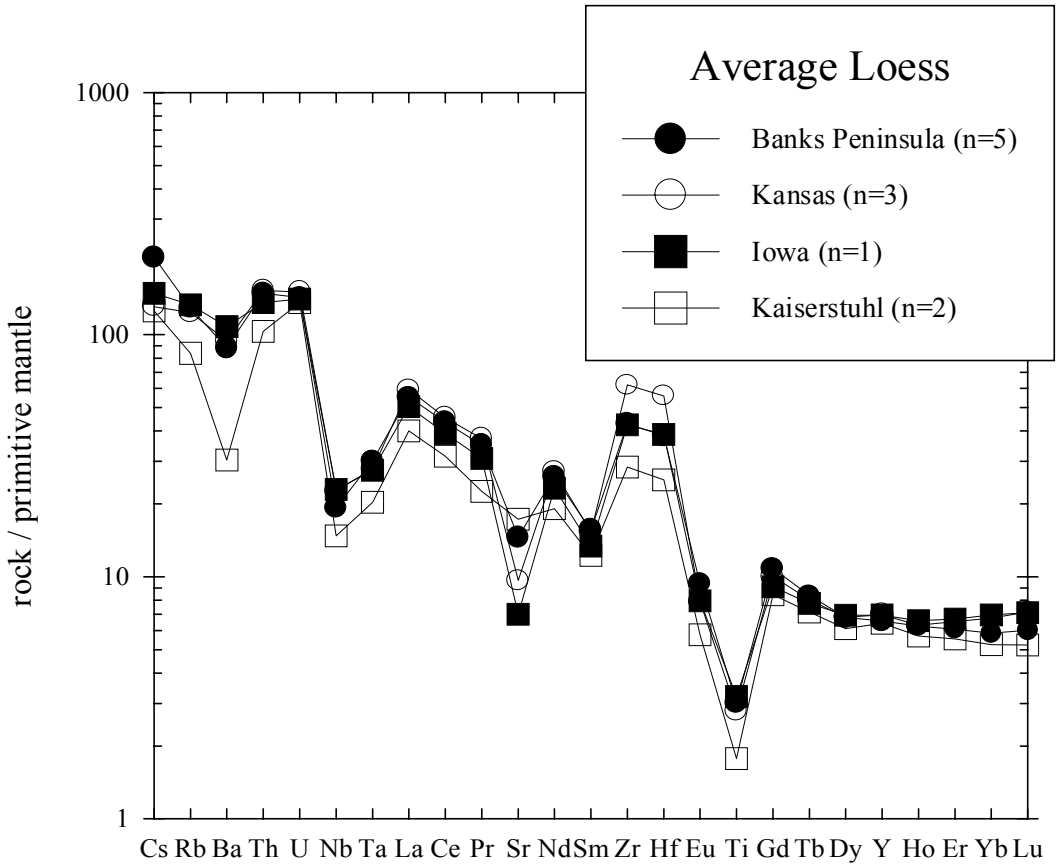

Figure A.1. Mantle-normalized diagram for incompatible elements in loess. Shown are the average values of loess samples from Banks Peninsula, New Zealand, Kansas and Iowa, U.S.A., and Kaiserstuhl, Germany. The average values from different regions have very similar trace element patterns characterized by LILE and LREE enrichment, negative Nb-, Ta-, and Ti-anomalies, Zr and Hf enrichment and flat HREE. The trace element patterns of the Kaiserstuhl samples are nearly parallel to the other loess samples (except for Ba and Sr) but tend to have slightly lower abundances. This is best explained by dilution effects of carbonate minerals, which are abundant in these two samples but absent in the others. Element abundances are normalized to the primitive mantle values of McDonough and Sun (1995).

Figure A.2. Upper continental crust- normalized diagram for incompatible elements in loess. A: Banks Peninsula, New Zealand. B: Kansas, U.S.A. C: Iowa, U.S.A. and Kaiserstuhl, Germany. Element abundances are normalized to the upper crustal values of Taylor and McLennan (1985), except for Cs value from McDonough et al. (1992).

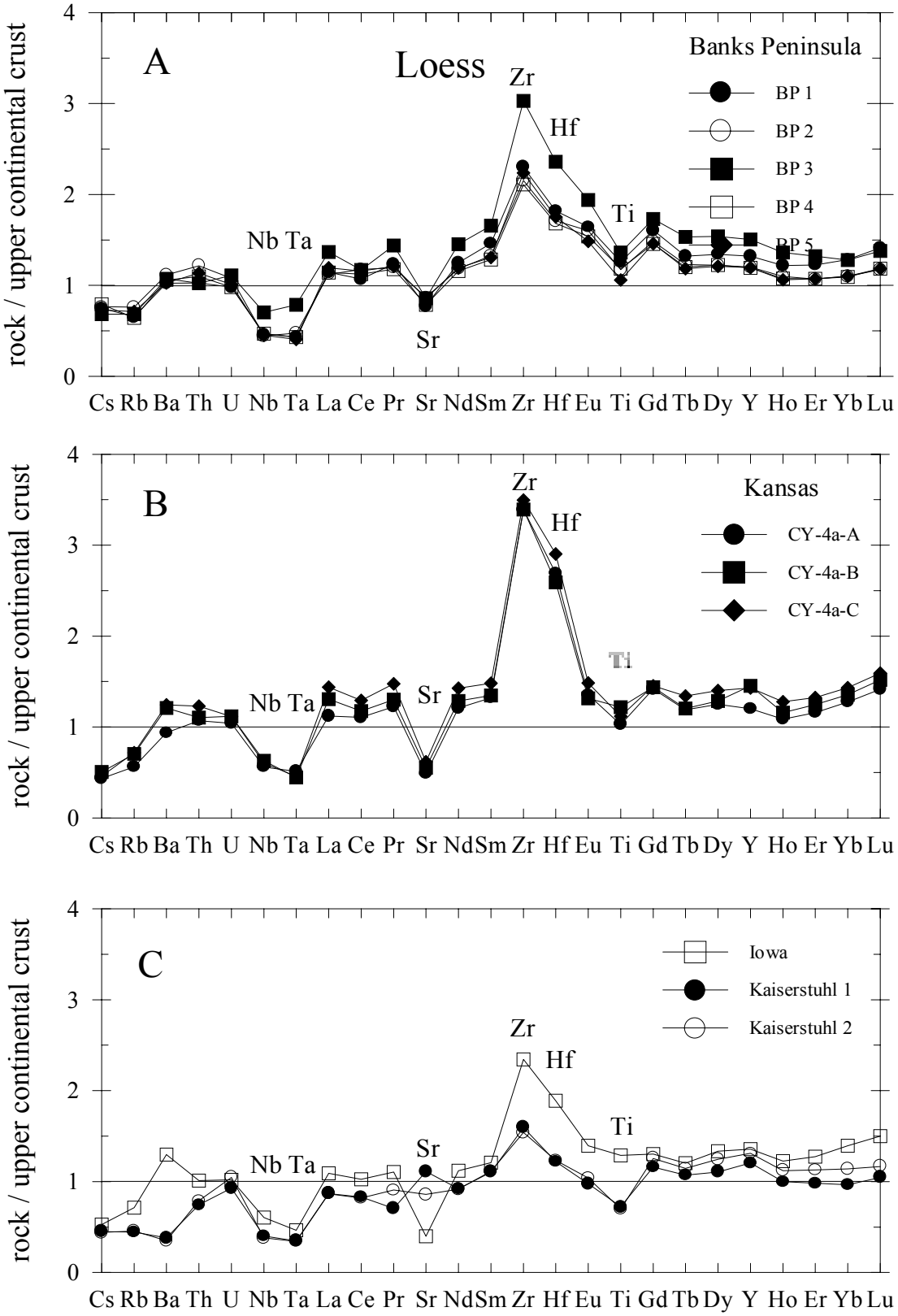
A
Loess
Banks Peninsula
BP 1
BP 2
BP 3
BP 4
BP 5
Zr
Hf
Ti
Nb Ta
Sr
rock / upper continental crust
Cs Rb Ba Th U Nb Ta La Ce Pr Sr Nd Sm Zr Hf Eu Ti Gd Tb Dy Y Ho Er Yb Lu
B
Kansas
CY-4a-A
CY-4a-B
CY-4a-C
C
Iowa
Kaiserstuhl 1
Kaiserstuhl 2

27 ppm determined by SSMS. Only one sample (shale SC 2) shows a significantly higher Nb concentration determined by ICP-MS (14.8 ppm instead of 12 ppm determined by SSMS).

Possible explanations for the discrepancies in La concentrations may be powder heterogeneity, i.e., fractionation of accessory REE-rich heavy minerals. Powder heterogeneity is supported by the observation that, for some samples, different digestions of the same sample resulted in different REE and Th contents, while other trace elements (e.g., Ga, Zr, Nb) showed the same concentrations. Enrichment or depletion of REE and Th suggests that small amounts of allanite or monazite are causing the sample heterogeneity (McLennan, 1989, and references therein). However, we do not consider sample heterogeneity to be an obstacle to the interpretation of our data since our average La concentration for PAAS is in excellent agreement with Nance and Taylor's (1976) average (Table A.3).

It is unlikely that the lower Nb values determined by ICP-MS are due to incomplete sample dissolution. Our own time series experiments have shown that zircon is more resistant to acid dissolution than Nb-bearing minerals (e.g., rutile and ilmenite) and only one sample (shale PL 1) shows lower Zr concentrations in comparison with the SSMS data. The higher SSMS values may be due to molecular interferences on ^{93}Nb ($^{29}Si^{16}O_4$ and $^{27}Al_3{}^{12}C$; Jochum et al., 1990) caused by the high concentrations of silica, aluminum, and carbon in the sample–graphite mixtures used during SSMS measurements. The sample preparation for ICP-MS (see above) effectively removes silica from the samples and, thus, greatly reduces consequent molecular interferences. Furthermore, the plasma ion source of the ICP-MS, unlike SSMS, also eliminates such complex polyatomic species in this mass region.

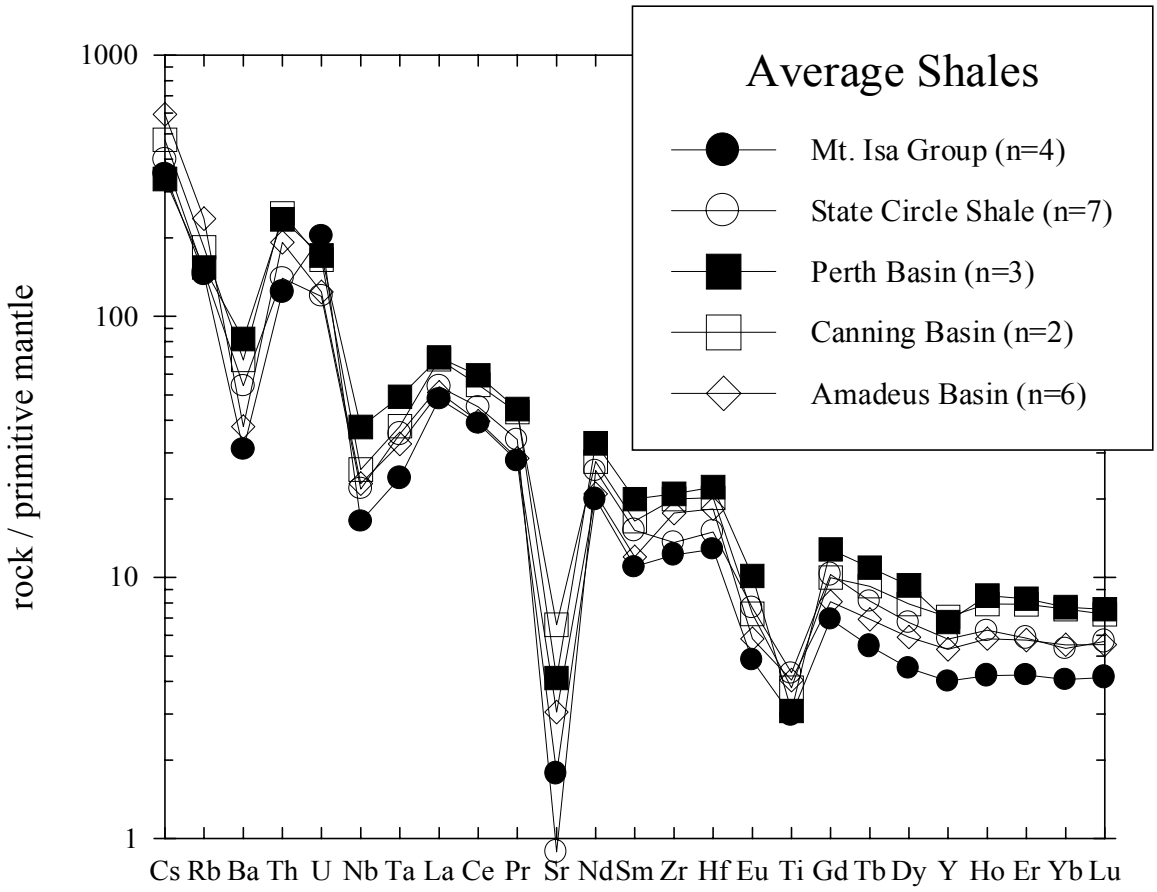

Figure A.3. Post-Archean Australian shales (normalized as in Fig.A.1). Shown are the average values of four Middle Proterozoic shales from the Mt. Isa Group, seven Silurian State Circle shales, three Paleozoic to Mesozoic shales from the Perth Basin, two Paleozoic shales from the Canning Basin, and six Upper Proterozoic to Cambrian shales from the Amadeus Basin. Note the parallel nature of the patterns and the decreasing REE abundances with increasing age (see discussion in Nance and Taylor, 1976).

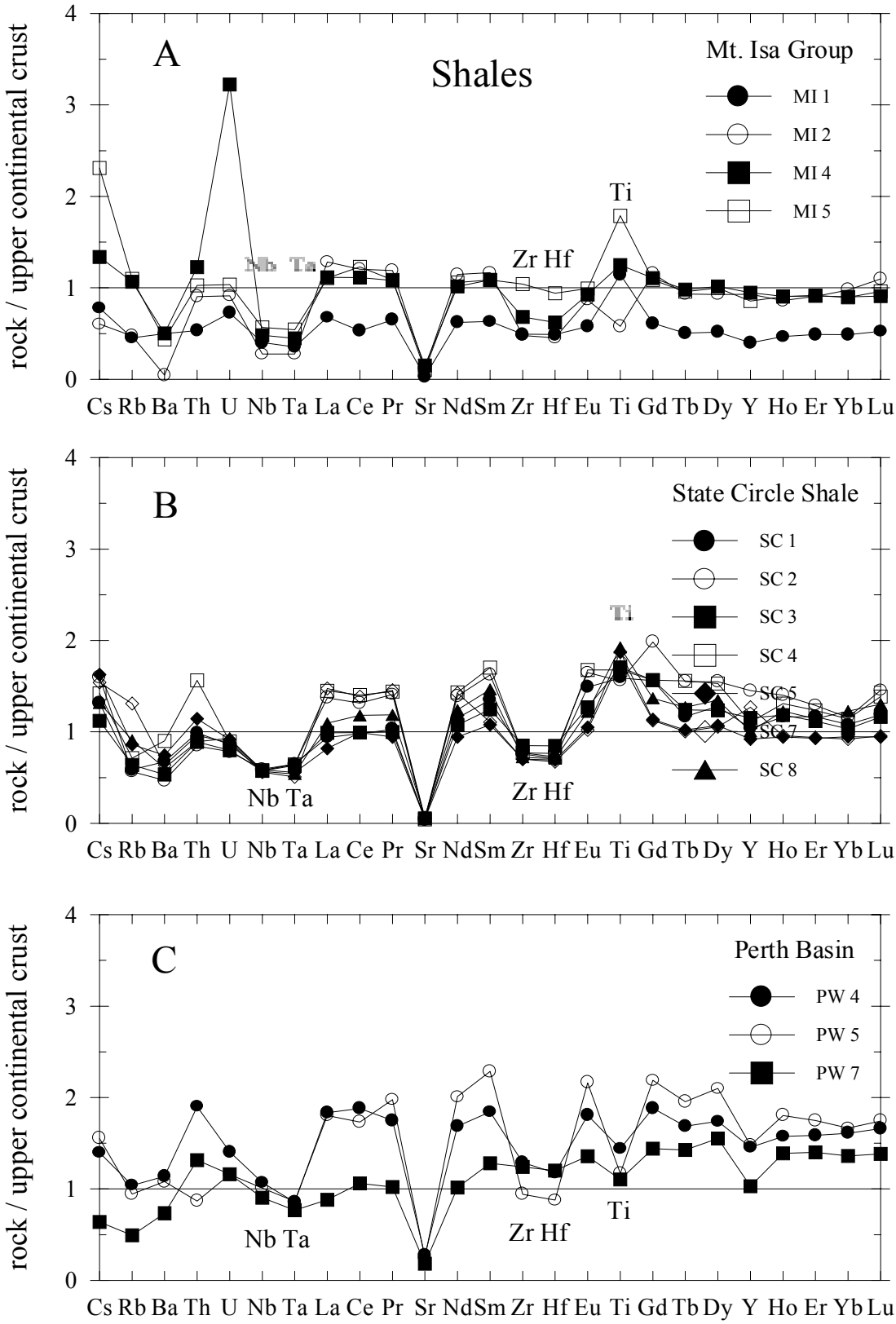
A
Shales
Mt. Isa Group
MI 1
MI 2
MI 4
MI 5
Ti
Zr Hf
Nb Ta
rock / upper continental crust
4
3
2
1
0
Cs Rb Ba Th U Nb Ta La Ce Pr Sr Nd Sm Zr Hf Eu Ti Gd Tb Dy Y Ho Er Yb Lu
B
State Circle Shale
SC 1
SC 2
SC 3
SC 4
SC 5
SC 7
SC 8
Ti
Nb Ta
Zr Hf
rock / upper continental crust
4
3
2
1
0
Cs Rb Ba Th U Nb Ta La Ce Pr Sr Nd Sm Zr Hf Eu Ti Gd Tb Dy Y Ho Er Yb Lu
C
Perth Basin
PW 4
PW 5
PW 7
Nb Ta
Zr Hf
Ti
rock / upper continental crust
4
3
2
1
0
Cs Rb Ba Th U Nb Ta La Ce Pr Sr Nd Sm Zr Hf Eu Ti Gd Tb Dy Y Ho Er Yb Lu

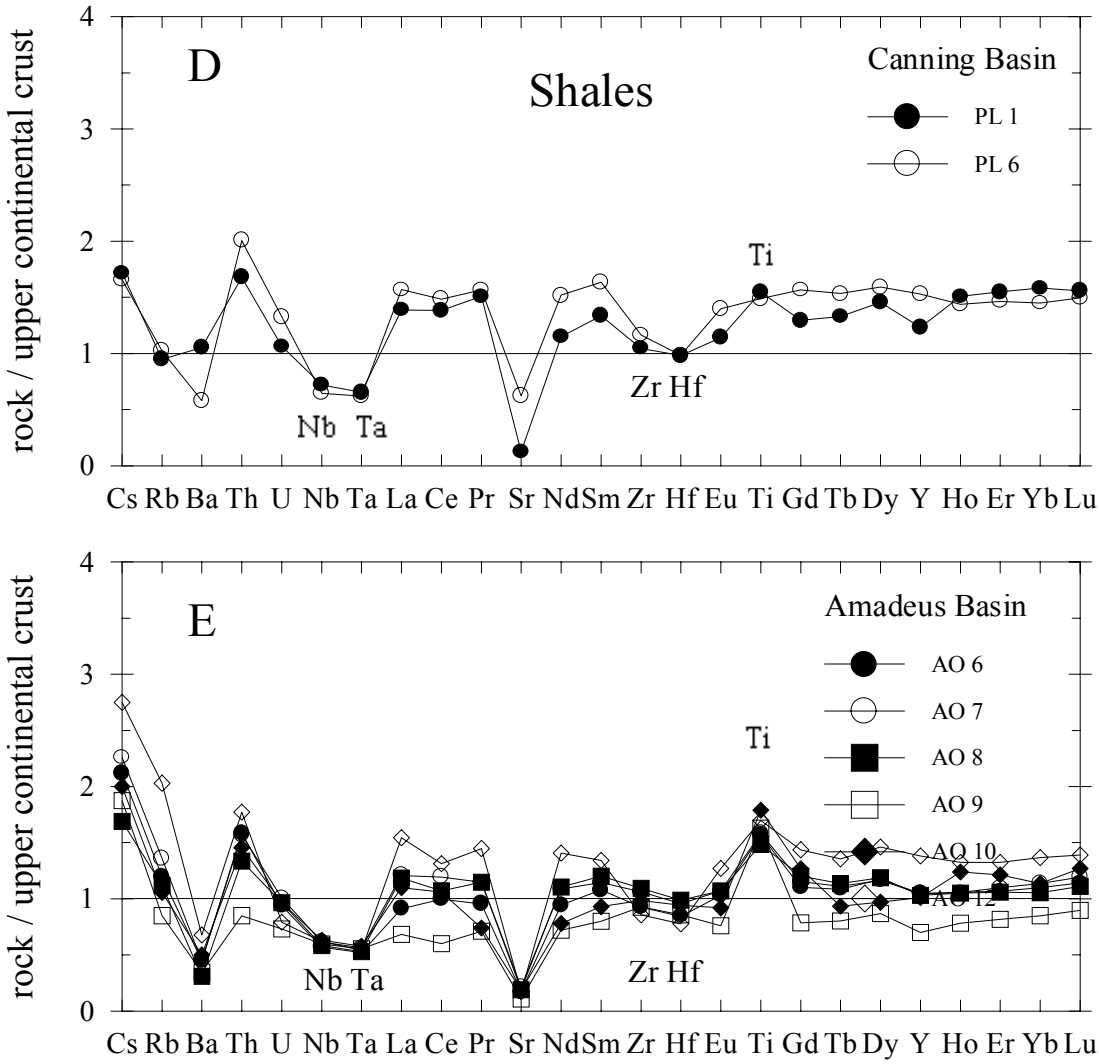

Figure A.4. Post-Archean Australian shales (normalized as in Fig.A.2). A: Middle Proterozoic shales from the Mt. Isa Group. B: Silurian State Circle shale. C: Paleozoic to Mesozoic shales from the Perth Basin. D: Paleozoic shales from the Canning Basin. E: Upper Proterozoic to Cambrian shales from the Amadeus Basin.

Our sediment samples have Nb, Ta, and La concentrations similar to other clastic sediments. The Nb, Ta, and La contents of our loess samples are nearly indistinguishable from loess from other regions (Gallet et al., 1996, 1998; Pye and Johnson, 1988; Liu et al., 1993). Oceanic sediments (Fig. A.5) tend to have lower trace element concentrations due to the dilution of terrigenous material with biogenic, hydrothermal and hydrogenous components (Plank and Langmuir, 1998). The La concentrations of the loess and shale samples are about 20% higher than Taylor and McLennan's (1985) estimate for the upper continental crust (TMUC, Table A.2). If we decrease our numbers by 20%, as per Taylor and McLennan's arguments (see above), we find good agreement between Taylor and McLennan's upper crust and ours.

The loess samples and most of the shales have lower Nb concentrations than TMUC (Fig. A.5) and show apparent negative Nb and Ta anomalies relative to TMUC (Figs. A.2 and A.4). It is unlikely that these anomalies are due to fractionation of heavy minerals (e.g., rutile) during transport of the sediments because we would expect Ti to show a similar depletion. However, the loess samples (except the Kaiserstuhl samples) and most of the shales have similar or higher Ti concentrations than TMUC. These observations suggest that the estimates of Nb and Ta for the UCC by Taylor and McLennan (1985) are too high. The estimate of the Nb concentration in TMUC (25 ppm; Taylor, 1977) is based on composite samples from the Canadian Shield (Shaw et al., 1976). (TMUC's Ta content is derived from an assumed Nb/Ta ratio of 11-12.) Shaw et al.'s average value is not well established; the composite samples show large regional variation in concentration (4 to 50 ppm Nb) and several samples were below or very close to the detection limit of their XRF technique at that time. Our Nb concentrations are comparable to those reported for clastic sediments worldwide (e.g., Condie, 1993; Gallet

et al., 1998) and agree with Plank and Langmuir's (1998) estimate of the upper continental crust (PLUC, Table A.3) based on global subducting oceanic sediment (GLOSS). The same trend holds true for Ta (Table A.3). Our data support the revision in upper crust composition suggested by Plank and Langmuir (1998). Moreover, Gao et al.'s (1998) estimate of the upper crust in central East China, based on wide-scale sampling with analysis of composite samples, has a similarly high La/Nb (Table A.3).

Table A.3. Trace element concentrations of average loess, shales and the continental crust Sources: Taylor et al. (1983), N + T = Nance and Taylor (1976) and McLennan (1981), G = Gao et al. (1998), T + M = Taylor and McLennan (1985), P + L = Plank and Langmuir (1998), R + F = Rudnick and Fountain (1995).

	Loess	Loess	PAAS	PAAS	East China
	This study	Taylor et al.	This study	N + T	G
Nb (ppm)	13.0±2.6	16.2±5.8	15.6±4.4	17.8±5.4	12
Ta (ppm)	1.02±0.26	–	1.28±0.30	–	0.74
La (ppm)	35.0±6.1	33.1±4.9	38.4±7.8	38.2±8.3	34.8
Nb/Ta	12.9±1.8	–	12.1±1.1	–	16
La/Nb	2.7±0.3	2.2±0.6	2.6±0.8	2.2±0.4	2.9

	Upper crust	Upper crust	Upper crust	Bulk crust	Bulk crust
	This study	T + M	P + L	This study	R + F
Nb (ppm)	11.5±2.6	25	13.7±0.9	8	12
Ta (ppm)	0.92±0.12	2.2	0.96±0.12	0.7	1.1
La (ppm)	30	30	30	18	18
Nb/Ta	12.5±1.8	11.4	14.2±1.8	12-13	11
La/Nb	2.6±0.8	1.2	2.2	2.2	1.5

The Nb discrepancies also lead to differences in La/Nb of the upper crust. Our new data show that La/Nb increases to 2.7±0.3 and 2.6±0.8 for the loess and shale

samples, respectively, leading to an even greater contrast between UCC and primitive mantle (1.0, McDonough and Sun, 1995). In order to obtain the upper crustal Nb concentration, we can either use our La/Nb ratio combined with Taylor and McLennan's (1985) La value or decrease our Nb value by 20%, by analogy to the crustal La concentration. In both cases, we get 11.5±2.6 ppm Nb, less than half of the Nb reported in TMUC.

Our average Nb/Ta ratios (12.9±1.8 for loess and 12.1±1.1 for shales) agree within uncertainty with both TMUC (11-12) and GLOSS (14.2±1.8). All of our Nb/Ta values are significantly lower (10.1-16.1) than the chondritic value (17.4±0.5; Jochum et al., 1997). The crustal Ta concentration of 0.92±0.12 ppm is calculated from our average Nb/Ta = 12.5±1.8. Both Nb and Ta are lower than Plank and Langmuir's (1998) estimate of the upper continental crust but they agree within error, which is remarkable because Plank and Langmuir's (1998) and our crustal estimates are derived from different and independent sample sets. Plank and Langmuir's (1998) estimate is based on marine sediments that (1) have a complex history of weathering, transport, and marine deposition in comparison with terrigeneous sediments and (2) do not include samples from the Atlantic Ocean, i.e., its sample set excludes detrital material derived from eastern North America and Europe, where many of the loess samples originate.

Figure A.5. Plot of Nb concentration vs. Nb/Ta ratio (upper panel) and La/Nb ratio (lower panel) for the loess (small stars) and shale (open circles) samples. Also shown are oceanic sediments (small dots; Plank and Langmuir, 1998), the chondritic ratios (gray bars; Jochum et al., 1997; McDonough and Sun, 1995), and the upper crustal values of this study (large star) and Taylor and McLennan (1985; open triangle). Note that the majority of the sediments have lower Nb concentrations and higher La/Nb than Taylor and McLennan's upper crustal estimate. All sediments show subchondritic Nb/Ta and superchondritic La/Nb.

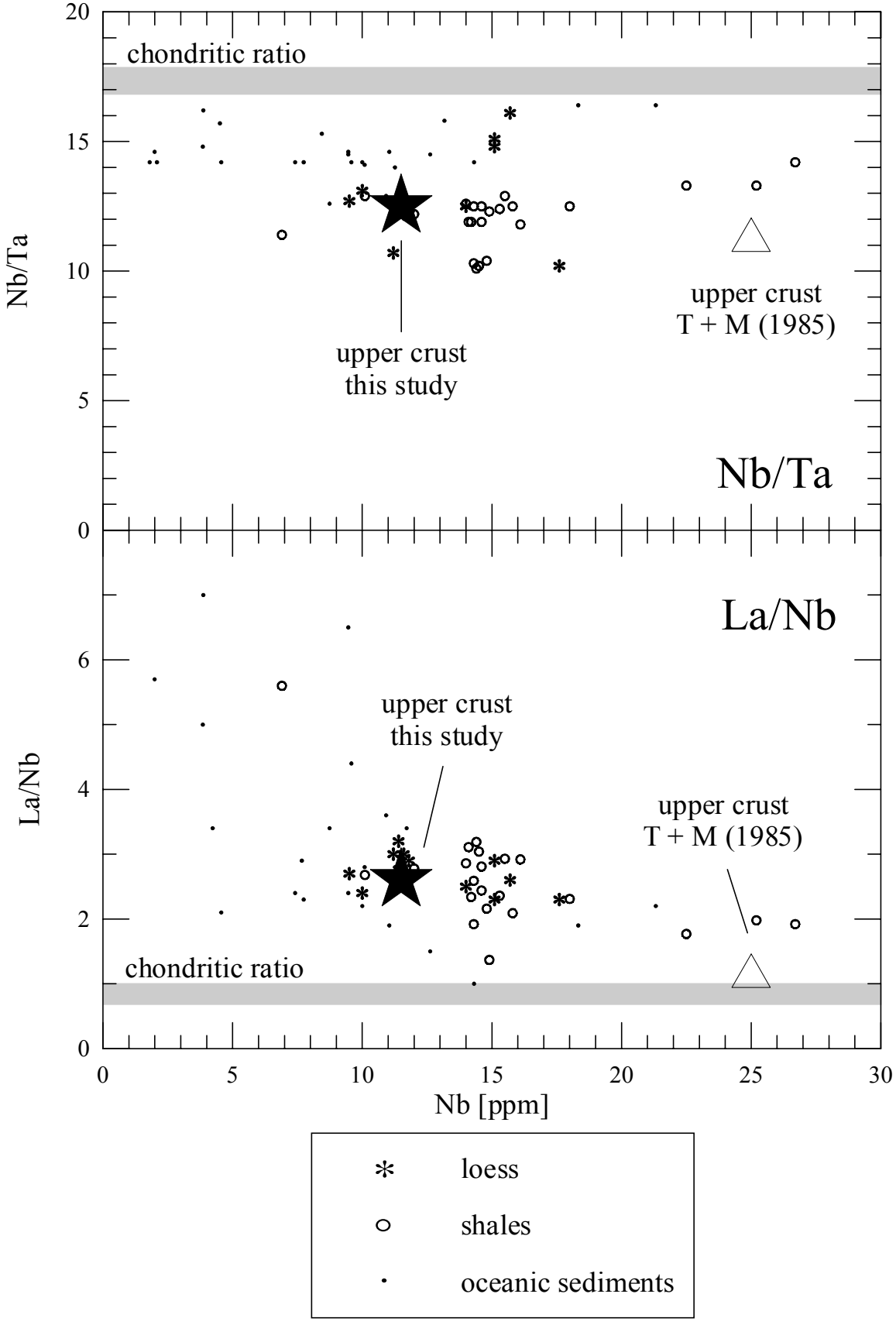
chondritic ratio
upper crust
this study
upper crust
T + M (1985)
Nb/Ta
La/Nb
upper crust
this study
upper crust
T + M (1985)
chondritic ratio
Nb/Ta
La/Nb
Nb [ppm]
0
5
10
15
20
25
30
0
2
4
6
0
5
10
15
20
loess
shales
oceanic sediments

A.6. Discussion

When we apply our Nb and Ta values for the upper crust to the recent estimate of the bulk continental crust of Rudnick and Fountain (1995), both Nb and Ta concentrations decrease by ~30%, leading to Nb = 8 ppm (instead of 12) and Ta = 0.7 ppm (instead of 1.1). La/Nb of the bulk crust increases from 1.5 to 2.2, only slightly higher than Plank and Langmuir's (1998) estimate. These revisions lead to Nb/U = 5.6 (instead of 8.5) and, thus, to an even greater contrast between the continental crust and the oceanic mantle (47±10; Hofmann et al., 1986) for this element ratio.

Both the crustal Nb/Ta ratio and the increased crustal La/Nb ratio support the observation that the continental crust and the Depleted Mantle are not complementary silicate reservoirs with respect to La, Nb, and Ta (Fig. A.6; Sun and McDonough, 1989; McDonough, 1991). Both the continental crust (Plank and Langmuir, 1998; this study) and the Depleted Mantle (Jochum et al., 1997; Niu and Batiza, 1997) have subchondritic Nb/Ta and superchondritic La/Nb. These trace element ratios support the suggestion of a Nb- and Ta-rich reservoir within the Earth having high Nb/Ta and low La/Nb. There are several implications of these observations. Firstly, the Nb/U ratio cannot be used to model crust-mantle differentiation with simple two-reservoir models which assume that the continental crust and the Depleted Mantle are complementary to one another (cf. Hofmann et al., 1986; Sylvester et al., 1997). Secondly, in order to balance the Silicate Earth, McDonough (1991) proposed a refractory rutile-bearing eclogite reservoir exists (~2% by mass of the Silicate Earth) that is sequestered deep in the mantle. Our recent analysis of eclogite xenoliths supports the contention that refractory rutile-bearing

eclogite, presumably formed through subduction of mafic oceanic crust, does indeed solve the Nb-Ta-La mass balance problem (Rudnick et al., 1998).

It has been proposed that the continental crust's La/Nb can be used to place constraints on the proportion of crust formed in intraplate vs. convergent margin settings (Rudnick, 1995). This is because intraplate magmas have La/Nb generally <1.0 (Sun and McDonough, 1989) whereas convergent margin magmas typically have high La/Nb ratios (e.g., McCulloch and Gamble, 1991, and references therein). Mixing between average arc basalts and possible intraplate basalts is illustrated in Fig. A.7. This mixing scenario assumes that the crust grows by basalt addition. The higher La/Nb ratio of the crust suggested here and by Plank and Langmuir (1998) implies a lower contribution of intraplate magmas to the growth of the continental crust. The calculation is not very sensitive to the composition of the convergent margin component: we found our own average arc basalt taken from our literature compilation is indistinguishable from McCulloch and Gamble's (1991). However, the proportion of intraplate component needed to explain the crustal La/Nb ratio depends strongly on its composition. If the intraplate component has high trace element concentrations (average ocean island basalt, Sun and McDonough, 1989), less than 5% is sufficient. Alternatively, the continental crust could accommodate about 20% of an intraplate component with low trace element concentrations, e.g. the Ontong Java Plateau basalts (Neal et al., 1997).

While this mixing calculation is able to reproduce the La/Nb ratio, it fails to account for the evolved bulk composition of the continents. Three different processes may explain the intermediate composition of the continents, as reviewed in Rudnick (1995): 1) Direct addition of silicic melts of tonalitic-trondhjemitic-granodioritic (TTG) composition with subduction of the complementary rutile-bearing mafic oceanic crust

Figure A.6. Plot of Nb concentration vs. Nb/Ta ratio (upper panel) and La/Nb ratio (lower panel) for the chondritic ratios (gray bars; Jochum et al., 1997; McDonough and Sun, 1995), primitive mantle (open circle), depleted mantle (solid square; Jochum et al., 1998), and the upper crustal value of this study (solid star). Also shown is an estimate of a possible Nb-rich reservoir required to balance Nb and Ta in the Silicate Earth (McDonough, 1991; Jochum and Hofmann, 1998; Rudnick et al., 1998). Note the logarithmic scale of the Nb concentration. Both the depleted mantle and the continental crust have subchondritic Nb/Ta and superchondritic La/Nb, indicating that depleted mantle and continental crust are not complementary reservoirs with respect to Nb and Ta. Thus, an additional Nb- and Ta-rich reservoir having superchondritic Nb/Ta is required to balance the Silicate Earth, supporting the suggestion of sequestered eclogite in the deep earth.

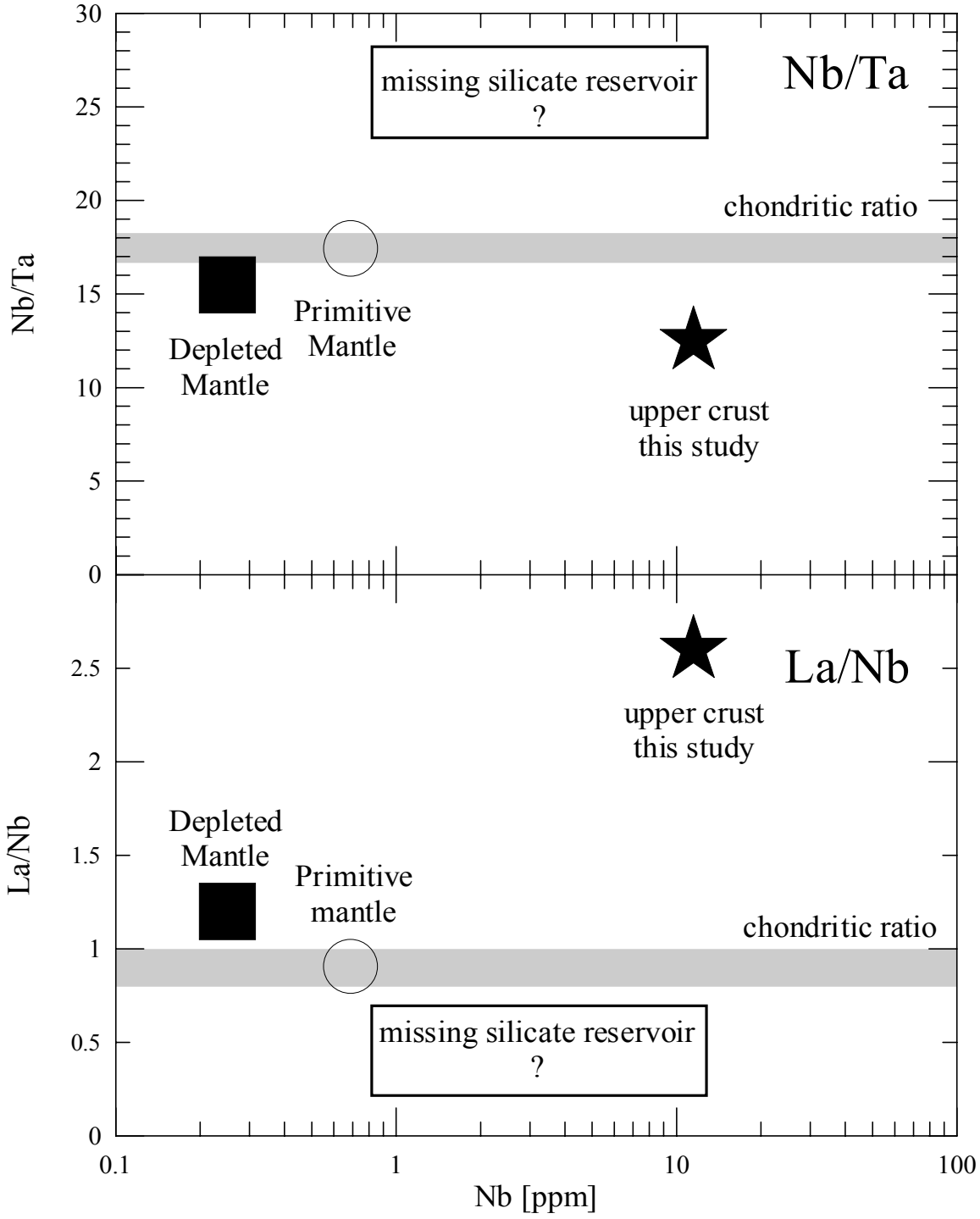
Nb/Ta
La/Nb
missing silicate reservoir
?
chondritic ratio
Primitive
Mantle
Depleted
Mantle
upper crust
this study
upper crust
this study
Depleted
Mantle
Primitive
mantle
chondritic ratio
missing silicate reservoir
?
Nb/Ta
La/Nb
Nb [ppm]
0.1
1
10
100
0
5
10
15
20
25
30
0
0.5
1
1.5
2
2.5

(e.g., Martin, 1986). 2) Intracrustal differentiation of basaltic crust to form evolved melts and the subsequent delamination of parts of the mafic to ultramafic residues (e.g., Arndt and Goldstein, 1989; Kay and Kay, 1991). 3) Chemical weathering of surface rocks drives the crust to more evolved compositions by preferential recycling of Mg to mantle (e.g., Anderson, 1982; Albarède, 1998).

How might these processes affect the La/Nb ratio of the bulk crust? The first process would increase La/Nb and be inherently a convergent margin process. Process 2 could drive the crust to higher La/Nb if the delaminated residue has subchondritic La/Nb. La/Nb decreases with depth in the continental crust, but it never reaches the chondritic value (Rudnick and Fountain, 1995). So, although delamination is expected to increase the bulk crust La/Nb, it is unlikely to have produced the superchondritic La/Nb in the first place. Finally, chemical weathering (process 3) does not change La/Nb because both La and Nb are immobile (see above).

Thus, although the mixing calculation shown in Fig. A.7 is clearly an oversimplification of how the crust forms, the main conclusion, that the crust is primarily a product of convergent margin magmatism, is robust.

Figure A.7. Mixing relationships between average arc basalt (McCulloch and Gamble, 1991) and intraplate magmas (Sun and McDonough, 1989; Neal et al., 1997). The upper panel shows a plot of the La concentration vs. the La/Nb ratio. Diamonds and circles represent 10% increments. Continental crust bars represent range of ratios from estimates of previous studies (Gao et al., 1992; Rudnick and Fountain, 1995; Wedepohl, 1995; Taylor and McLennan, 1985) and this study. The lower panel shows a plot of the proportion of the convergent margin component vs. the La/Nb ratio. Horizontal bar represents an estimated average value for the continental crust. Where it intersects the mixing lines, the percentage of intraplate component can be read from the x-axis (marked by arrows). Note that the La/Nb ratio of this study (solid arrows) results in a smaller percentage of intraplate component than previous estimates. Modified from Rudnick (1995).

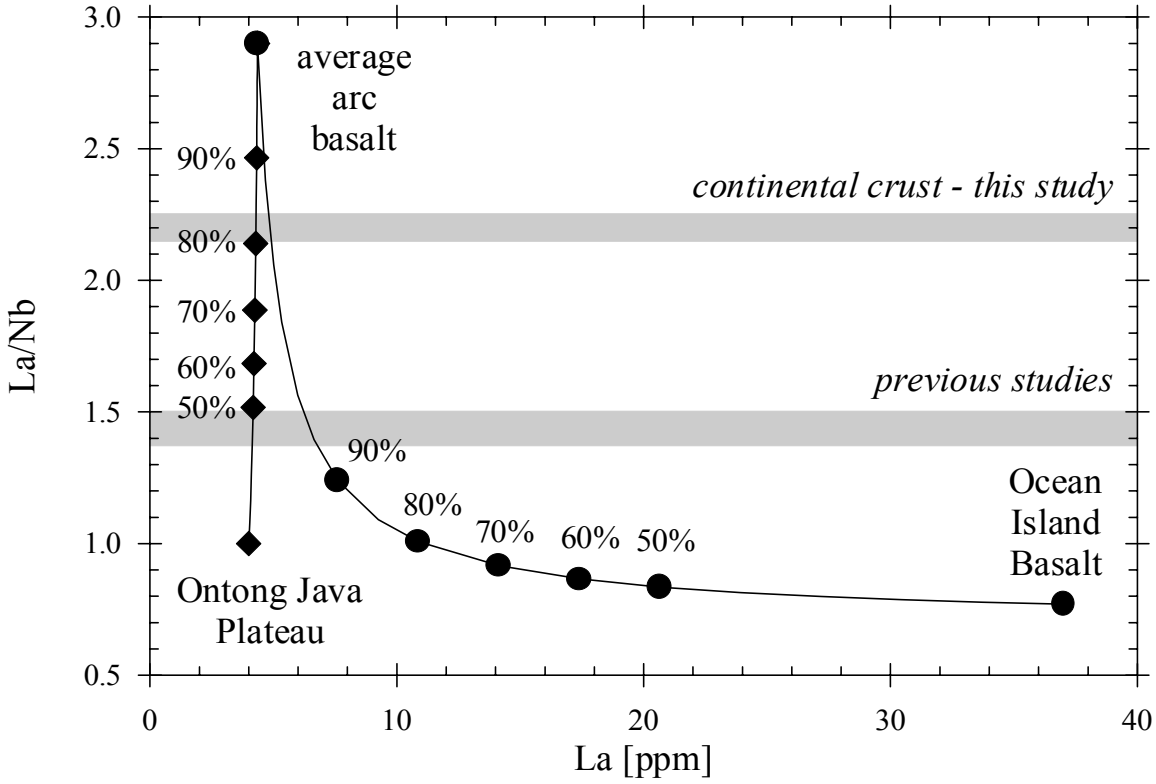
3.0
2.5
2.0
1.5
1.0
0.5
La/Nb
0
10
20
30
40
La [ppm]
average
arc
basalt
90%
80%
70%
60%
50%
continental crust - this study
previous studies
90%
80%
70%
60%
50%
Ocean
Island
Basalt
Ontong Java
Plateau

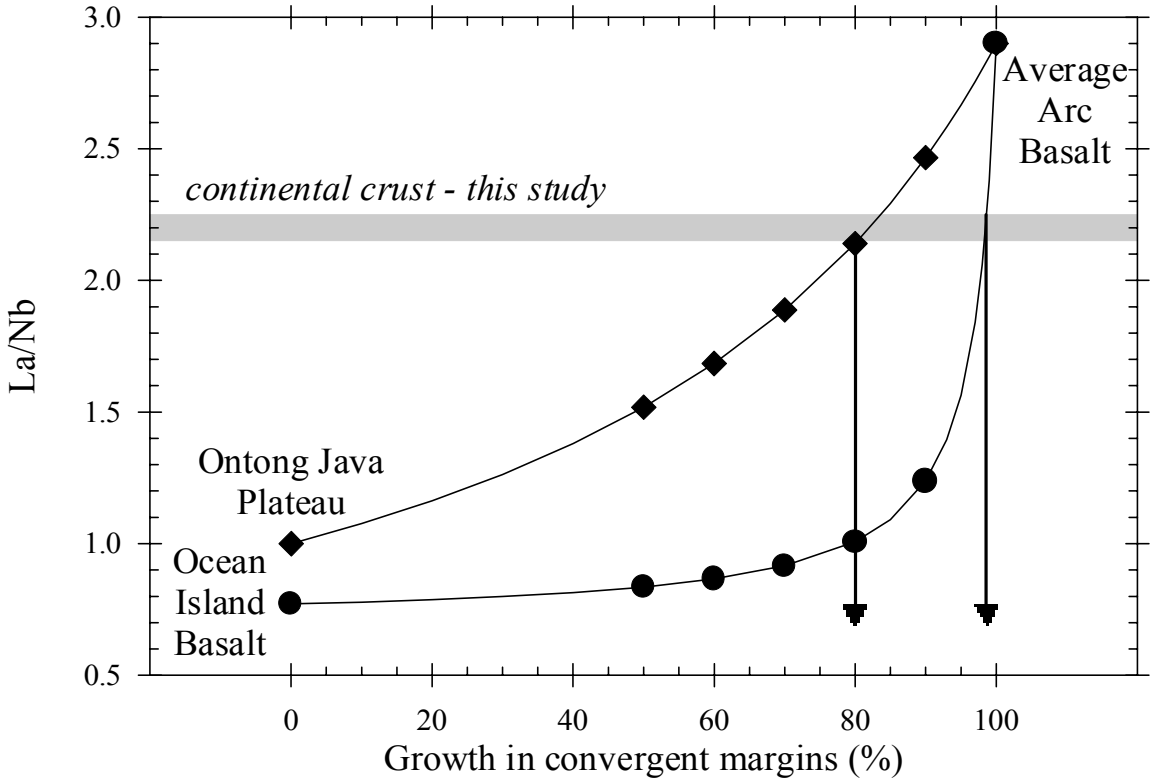
3.0
2.5
2.0
1.5
1.0
0.5
La/Nb
0
20
40
60
80
100
Growth in convergent margins (%)
continental crust - this study
Average
Arc
Basalt
Ontong Java
Plateau
Ocean
Island
Basalt

A.7. Conclusions

Our new data for the classic loess and shale (PAAS) samples of Taylor and McLennan lead to the following conclusions:

The upper continental crust has average Nb = 11.5 ppm and Ta = 0.92 ppm, which translates into a bulk crust Nb = 8 ppm, Ta = 0.7 ppm, La/Nb = 2.2, and Nb/Ta = 12-13.

The subchondritic Nb/Ta and Nb/La in both continental crust and Depleted Mantle demonstrate that these reservoirs are not strictly complementary with respect to La, Nb, and Ta and supports the suggestion of a Nb-rich eclogitic reservoir sequestered in the deep earth (McDonough, 1991).

The higher La/Nb suggests an even lower plume contribution to the continents — 5–20 % — than estimated by Rudnick (1995).

A.8. Acknowledgements

Both the loess and the PAAS sample sets are kindly supplied by Prof. S.R. Taylor and S.M. McLennan. I. Horn is thanked for guidance through the pitfalls of ICP-MS analysis. We are grateful to B.-m. Jahn, K.P. Jochum, and S.M. McLennan for comments which improved the original manuscript.

A.9. References

Albarède F. (1998) The growth of continental crust. *Tectonophysics* **296**, 1-14.

Anderson A. T., Jr. (1982) Parental basalts in subduction zones: implications for continental evolution. *J. Geophys. Res.* **87**, 7047-7060.

Arndt N. T. and Goldstein S. L. (1989) An open boundary between lower continental crust and mantle: its role in crust formation and crustal recycling. *Tectonophysics* **161**, 201-212.

Condie K. C. (1993) Chemical composition and evolution of the upper continental crust: Contrasting results from surface samples and shales. *Chem. Geol.* **104**, 1-37.

Eggins S. M., Woodhead J. D., Kinsley L. P. J., Mortimer G. E., Sylvester P., McCulloch M. T., Hergt J. M., and Handler M. R. (1997) A simple method for the precise determination of > 40 trace elements in geological samples by ICPMS using enriched isotope internal standardisation. *Chem. Geol.* **134**, 311-326.

Flint R. F. (1971) *Glacial and Quaternary Geology*. Wiley.

Gallet S., Jahn B.-M., and Torii M. (1996) Geochemical characterization of the Luochuan loess-paleosol sequence, China, and paleoclimatic implications. *Chem. Geol.* **133**, 67-88.

Gallet S., Jahn B.-m., van Vliet Lanoë B., Dia A., and Rossello E. (1998) Loess geochemistry and its implications for particle origin and composition of the upper continental crust. *Earth Planet. Sci. Lett.* **156**, 157-172.

Gao S., Luo T.-C., Zhang B.-R., Zhang H.-F., Han Y.-W., Zhao Z.-D., and Hu Y.-K. (1998) Chemical composition of the continental crust as revealed by studies in East China. *Geochim. Cosmochim. Acta* **62**, 1959-1975.

Gao S., Zhang B. R., Luo T. C., Li Z. J., Xie Q. L., Gu X. M., Zhang H. F., Ouyang J. P., Wang D. P., and Gao C. L. (1992) Chemical composition of the continental crust in the Qinling orogenic belt and its adjacent North China and Yangtze cratons. *Geochim. Cosmochim. Acta* **56**, 3933-3950.

Govindaraju K. (1994) 1994 compilation of working values and sample description for 383 geostandards. *Geostand. Newslett.* **18**, 1-158.

Hall G. E. M. and Plant J. A. (1992) Analytical errors in the determination of high field strength elements and their implications in tectonic interpretation studies. *Chem. Geol.* **95**, 141-156.

Hofmann A. W. (1988) Chemical differentiation of the Earth: the relationship between mantle, continental crust, and oceanic crust. *Earth Planet. Sci. Lett.* **90**, 297-314.

Hofmann A. W., Jochum K. P., Seufert M., and White W. M. (1986) Nb and Pb in oceanic basalts: new constraints on mantle evolution. *Earth Planet. Sci. Lett.* **79**, 33-45.

Jenner G. A., Longerich H. P., Jackson S. E., and Fryer B. J. (1990) ICP-MS - A powerful tool for high-precision trace-element analysis in Earth sciences: Evidence from analysis of selected U.S.G.S. reference samples. *Chem. Geol.* **83**, 133-148.

Jochum K. P., Seufert H. M., and Thirlwall M. F. (1990) High-sensitivity Nb analysis by spark-source mass spectrometry (SSMS) and calibration of XRF Nb and Zr. *Chem. Geol.* **81**, 1-16.

Jochum K.P., Pfänder J., Snow J.E., and Hofmann A.W. (1997) Nb/Ta in mantle and crust. *EOS (Trans. Am. Geophys. Union)* **78**, 804.

Jochum K.P. and Hofmann A.W. (1998) Nb/Ta in MORB and continental crust: Implications for a superchondritic Nb/Ta reservoir in the mantle. *EOS (Trans. Am. Geophys. Union)* **79**, S354.

Jochum K.P., Hofmann A.W., and Pfänder J. (1998) Constraints on the abundances and abundance ratios of Nb, Ta, Th and U in the Earth's mantle and crust using high precision MIC-SSMS data. *GERM Workshop La Jolla*, 45-47.

Kay R. W. and Kay S. M. (1991) Creation and destruction of lower continental crust. *Geol. Rundschau* **80**, 259-278.

Liu C.-Q., Masuda A., Okada A., Yabuki S., Zhang J., and Fan Z.-L. (1993) A geochemical study of loess and desert sand in northern China: Implications for continental crust weathering and composition. *Chem. Geol.* **106**, 359-374.

Martin H. (1986) Effect of steeper Archean geothermal gradient on geochemistry of subduction-zone magmas. *Geology* **14**, 753-756.

McCulloch M. T. and Gamble A. J. (1991) Geochemical and geodynamical constraints on subduction zone magmatism. *Earth Planet. Sci. Lett.* **102**, 358-374.

McDonough W. F. (1991) Partial melting of subducted oceanic crust and isolation of its residual eclogitic lithology. *Phil. Trans. R. Soc. Lond.* **A 335**, 407-418.

McDonough W. F. and Sun S.-S. (1995) Composition of the Earth. *Chem. Geol.* **120**, 223-253.

McDonough W. F., Sun S.-S., Ringwood A. E., Jagoutz E., and Hofmann A. W. (1992) Potassium, rubidium, and cesium in the Earth and Moon and the evolution of the mantle of the Earth. *Geochim. Cosmochim. Acta* **56**, 1001-1012.

McLennan S. M. (1981) Trace element geochemistry of sedimentary rocks: implications for the composition and evolution of the continental crust. PhD thesis, Australian National University.

McLennan S. M. (1989) Rare earth elements in sedimentary rocks: influence of provenance and sedimentary processes. In *Geochemistry and Mineralogy of rare earth elements* (ed. B. R. Lipin and G. A. McKay), pp. 169-200. Mineral. Soc. Am.

Münker C. (1998) Nb/Ta fractionation in a Cambrian arc/back arc system, New Zealand: source constraints and application of refined ICPMS techniques. *Chem. Geol.* **144**, 23-45.

Nance W. B. and Taylor S. R. (1976) Rare earth element pattern and crustal evolution - I. Australian post-Archean sedimentary rocks. *Geochim. Cosmochim. Acta* **40**, 1539-1551.

Neal C. R., Mahoney J. J., Kroenke L. W., Duncan R. A., and Petterson M. G. (1997) The Ontong Java Plateau. In *Large Igneous Provinces: Continental, Oceanic, and Planetary Flood Volcanism* (ed. J. J. Mahoney and M. F. Coffin), pp. 183-216. AGU.

Nesbitt H. W., Markovics G., and Price R. C. (1980) Chemical processes affecting alkalis and alkaline earths during continental weathering. *Geochim. Cosmochim. Acta* **44**, 1659-1666.

Niu Y. and Batiza R. (1997) Trace element evidence from seamounts for recycled oceanic crust in the eastern Pacific mantle. *Earth Planet. Sci. Lett.* **148**, 471-483.

Owen L. B. and Faure G. (1974) Simultaneous determination of Hafnium and Zirconium in silicate rocks by isotope dilution. *Anal. Chem.* **46**, 1323-1326.

Plank T. and Langmuir C. H. (1998) The chemical composition of subducting sediment and its consequences for the crust and mantle. *Chem. Geol.* **145**, 325-394.

Pye K. and Johnson R. (1988) Stratigraphy, geochemistry, and thermoluminescence ages of Lower Mississippi Valley loess. *Earth Surf. Process. Landforms* **13**, 103-124.

Rudnick R. L. (1995) Making continental crust. *Nature* **378**, 571-578.

Rudnick R. L. and Fountain D. M. (1995) Nature and composition of the continental crust: A lower crustal perspective. *Rev. Geophys.* **33**, 267-309.

Rudnick R.L., Barth M.G., McDonough W.F., and Horn I. (1998) Rutiles in eclogites: a missing Earth reservoir found? *GSA abstr.* **30**(7), Toronto, A-207.

Shaw D. M., Dostal J., and Keays R. R. (1976) Additional estimates of continental surface Precambrian shield composition in Canada. *Geochim. Cosmochim. Acta* **40**, 73-83.

Smalley I. J. and Vita-Finzi C. (1968) The formation of fine particles in sandy deserts and the nature of "desert" loess. *J. Sediment Petrol.* **38**, 766-775.

Sun S.-S. and McDonough W.F. (1989) Chemical and isotopic systematics of oceanic basalts; implications for mantle composition and processes. In *Magmatism in the Ocean Basins* (ed. A. D. Saunders and M. J. Norry) Geol. Soc. Lond. Spec. Pub. **42**, pp. 313-345.

Sylvester P. J., Campbell I. H., and Bowyer D. A. (1997) Niobium/Uranium evidence for early formation of the continental crust. *Science* **275**, 521-523.

Taylor S. R. (1977) Island arc models and the composition of the continental crust. In *Island Arcs, Deep Sea Trenches and Back-Arc Basins* (ed. M. Talwani and W. C. Pitman III), pp. 325-335. AGU.

Taylor S. R. and McLennan S. M. (1985) *The Continental Crust: its Composition and Evolution*. Blackwell Scientific.

Taylor S. R., McLennan S. M., and McCulloch M. T. (1983) Geochemistry of loess, continental crustal composition and crustal model ages. *Geochim. Cosmochim. Acta* **47**, 1897-1905.

Totland M., Jarvis I., and Jarvis K. E. (1992) An assessment of dissolution techniques for the analysis of geological samples by plasma spectrometry. *Chem. Geol.* **95**, 35-62.

Wedepohl K. H. (1995) The composition of the continental crust. *Geochim. Cosmochim. Acta* **59**, 1217-1232.

Xie Q., Jain J., Sun M., Kerrich R., and Fan J. (1994) ICP-MS analysis of basalt BIR-1 for trace elements. *Geostand. Newslett.* **18**, 53-63.

Appendix B

Rutile-Bearing Refractory Eclogites: Missing Link between Continents and Depleted Mantle

Roberta L. Rudnick, Matthias Barth, Ingo Horn, William F. McDonough

Department of Earth and Planetary Sciences, Harvard University, 20 Oxford Street, Cambridge, MA 02138, USA.

Science (2000) **287**, 278-281

A mass imbalance exists in Earth for Nb, Ta, and possibly Ti: continental crust and depleted mantle both have subchondritic Nb/Ta, Nb/La, and Ti/Zr, which requires the existence of an additional reservoir with superchondritic ratios, such as refractory eclogite produced by slab melting. Trace element compositions of minerals in xenolithic eclogites derived from cratonic lithospheric mantle show that rutile dominates the budget of Nb and Ta in the eclogites and imparts a superchondritic Nb/Ta, Nb/La, and Ti/Zr to the whole rocks. About 1 to 6 percent by weight of eclogite is required to solve the mass imbalance in the silicate Earth, and this reservoir must have an Nb concentration ≥2 parts per million, Nb/La ≥ 1.2, and Nb/Ta between 19 and 37 — values that overlap those of the xenolithic eclogites. As the mass of eclogite in the continental lithosphere is significantly lower than this, much of this material may reside in the lower mantle, perhaps as deep as the core-mantle boundary.

The elements Ti, Zr, Nb, Ta, and rare earth elements (REE) are refractory and lithophile and therefore should exist in chondritic relative abundances in the silicate Earth. Continental crust and depleted mantle (DM) [mid-ocean ridge basalt (MORB) source] generally are assumed to be geochemically complementary reservoirs within the Earth. However, both reservoirs have subchondritic Nb/La (*1–4*). A similar observation is made about Nb/Ta ratios. These elements share the same valence state (+5) and have matching atomic radii (*5*), and they are thought to be geochemically inseparable. However, recent analyses (*6*) have demonstrated that Nb/Ta ratios are subchondritic in MORB and near-ridge seamounts (*7–9*), ocean island basalts (OIB) (*7*, *10*), and the upper continental crust (*11*, *12*). Because Nb is more incompatible than Ta in clinopyroxene

during mantle melting (*13*), the DM and the source of OIB should have even lower Nb/Ta ratios. A third element ratio that also may not mass balance in Earth is Ti/Zr. The continental crust, MORB, and OIB have Ti/Zr ratios below 115, the chondritic ratio (*1*). However, because Zr is more incompatible than Ti (*13*), partial melts should have lower Ti/Zr than their source regions and the mass imbalance in this case is not clear. The DM and OIB sources could have chondritic or even superchondritic Ti/Zr [as massif peridotites do (*14*)]. Nevertheless, the subchondritic Ti/Zr in MORB and continental crust suggests that another reservoir exists that is Ti enriched relative to Zr.

The above observations require the existence of an additional reservoir that contains appreciable Nb, Ta, and Ti with superchondritic Nb/La, Nb/Ta, and Ti/Zr — features that, until now, have not been observed in common igneous and metamorphic rocks (*15*). McDonough (*1*) suggested that refractory, rutile-bearing eclogite may satisfy the mass balance requirements for Ti, Nb, and Ta in the silicate Earth. Here we show that eclogites, sampled in xenoliths from cratonic kimberlites, do indeed have the requisite trace element compositions to satisfy this mass imbalance.

Rutile (TiO_2) is a common accessory phase in metamorphic rocks and it can have high concentrations of high field strength elements, particularly Nb and Ta. For this reason, rutile has been considered by some to be the phase that is responsible for the marked Nb and Ta depletions seen in arc magmas (*16*). Rutiles from continental crustal rocks (*17*, *18*) have Nb contents greater than 100 parts per million (ppm) with Nb/Ta ratios that generally cluster about the chondritic ratio of 17.4 ± 0.5 (*19*) or lower (*20*) (Fig. B.1A). Metasomatic rutiles from cratonic peridotites (*21*, *22*) are characterized by

Figure B.1. (A) Nb versus Nb/Ta for a variety of rock types and model compositions: xenolithic eclogites (black dots), crustal igneous and metamorphic rocks (open squares), and metasomatic peridotite xenoliths from Tanzania (pluses). Stars represent geometric mean (*26*) for the eclogitic and crustal populations. Field of MORB from (*9*). Diamonds, various estimates of bulk crust composition (*2*); UC, field of upper crust derived from GLOSS (*12*), loess, and PAAS (*11*). Only three crustal rutile samples have Nb/Ta significantly above the chondritic ratio and two of these are from a carbonatite complex (Magnet Cove, Arkansas) (*20*); the third is from a South Carolina beach sand deposit of unknown provenance. Eclogite whole rock compositions are calculated from modal mineralogy (*32*); crustal and metasomatic mantle whole rock compositions are calculated assuming that rutile makes up 0.5% of the rock and is the sole contributor of Nb and Ta to the whole rock budget. (B) Nb versus Nb/La for reconstructed whole rock eclogites (solid circles), field of MORB, average continental crust (black squares on gray field), and OIB (triangles). Data sources are as listed for (A) and from the literature. Star, geometric mean of the eclogite population. (C) Ti versus Ti/Zr for reconstructed eclogites (solid circles), field of MORB, continental crust, OIB, and Massif peridotites (open squares). Data sources are as listed for (A) and from the literature. Star, geometric mean of the eclogite population.

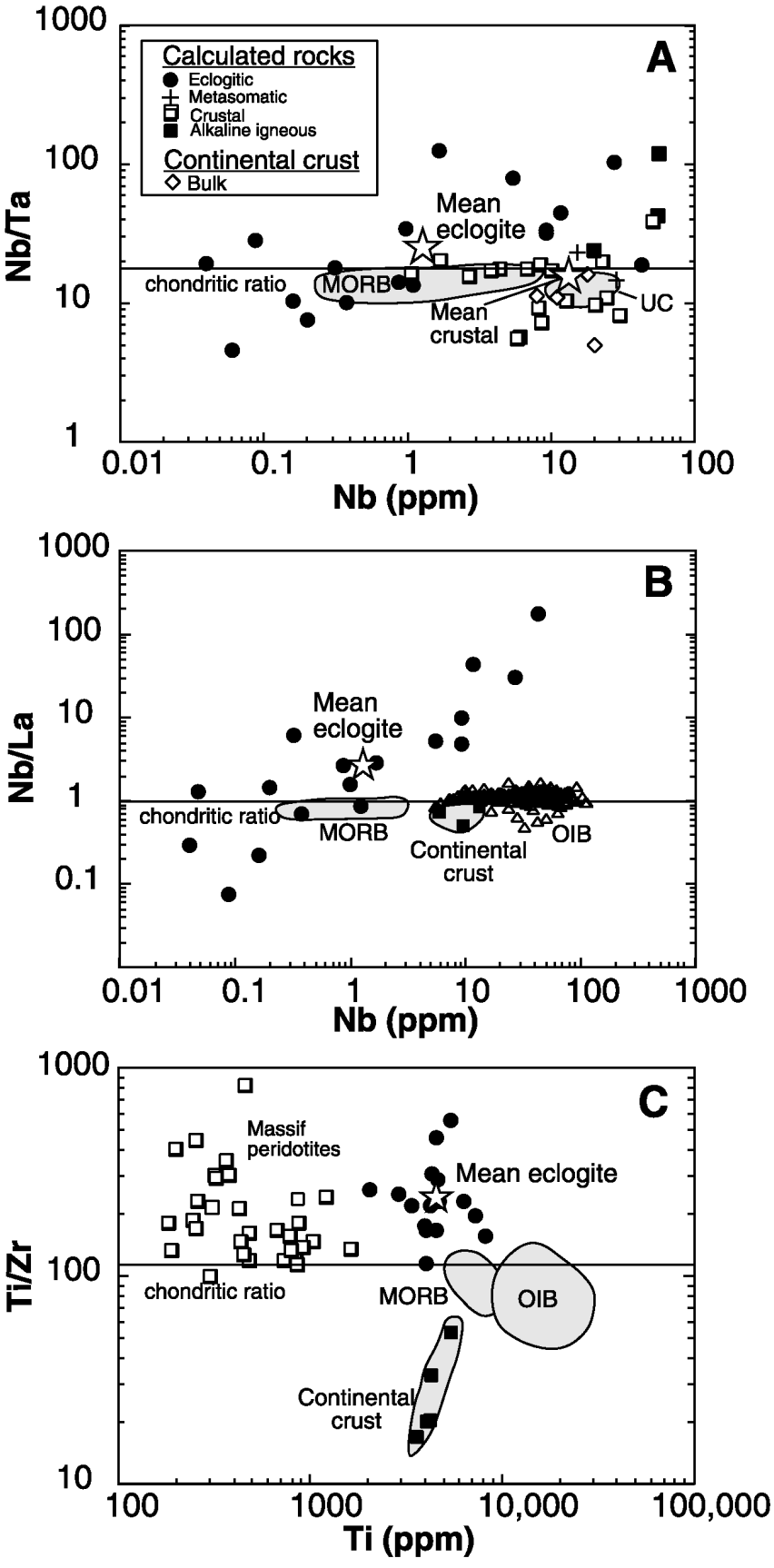
A
Calculated rocks
Eclogitic
Metasomatic
Crustal
Alkaline igneous
Continental crust
Bulk
Mean eclogite
chondritic ratio
MORB
Mean crustal
UC
Nb/Ta
Nb (ppm)
1000
100
10
1
0.01
0.1
1
10
100
B
Mean eclogite
chondritic ratio
MORB
Continental crust
OIB
Nb/La
Nb (ppm)
1000
100
10
1
0.1
0.01
0.1
1
10
100
1000
C
Massif peridotites
Mean eclogite
chondritic ratio
MORB
OIB
Continental crust
Ti/Zr
Ti (ppm)
1000
100
10
100
1000
10,000
100,000

high Nb contents (0.3 to 0.5 weight %) and chondritic Nb/Ta ratios. In contrast, rutiles from eclogite xenoliths carried in kimberlite pipes from Siberia (*23*) and western Africa (*24, 25*) have more variable Nb contents and Nb/Ta ratios and many have Nb/Ta ratios that are chondritic to strongly superchondritic; the population forms a log-normal distribution and has a geometric mean value of 24 (n = 19) (*26*).

Although rutile is an accessory phase in the eclogites (*27*), it dominates the budget of Nb and Ta (*28*). Thus, the Nb/Ta ratio of the whole rock eclogite equals that of the rutile, and we can conclude that, on average, the xenolithic eclogites have superchondritic Nb/Ta ratios.

Determining the Nb/La ratio of the eclogites is more difficult. Whole rock data are unreliable because of variable degrees of large-ion lithophile element (*29*) enrichment produced by interaction with the host kimberlite (*30*). Thus, the preentrainment eclogite compositions must be calculated from primary mineral compositions and modes (*31*). This requires relatively precise knowledge of the modal abundance of rutiles, which cannot be determined from point-counting these coarse-grained rocks. We therefore calculated modal rutile from Ti mass balance (*32*), which yields proportions of 0.1 to 0.9% by weight, with a relative error of ≤10%. The resulting Nb/La of all but five of the reconstructed eclogites are superchondritic, with a geometric mean Nb/La of 2.7 (n = 17) (*26*) (Fig. B.1B).

In a similar fashion we calculated the Ti/Zr ratio of the bulk eclogites. All but one of our samples have superchondritic ratios (Fig. B.1C). These eclogites are thus distinct from MORB, continental crust, and OIB, which have subchondritic Ti/Zr ratios. Interestingly, this feature is a result of Zr (and Hf) depletion in the eclogites rather than

Ti enrichment; that is, on mantle-normalized plots, Ti is not anomalous relative to REE of similar incompatibility such as Eu and Gd, but Zr and Hf are distinctly depleted (relative to Sm and Eu).

The above data demonstrate that xenolithic eclogites have, on average, superchondritic Nb/Ta, Nb/La, and Ti/Zr ratios and thus support the contention that refractory, rutile-bearing eclogites may be important in the mass balance of Nb, Ta, and Ti in Earth. The mass of this reservoir is not easily constrained from the trace-element compositions of the eclogites, given the rather large standard deviations of Nb/Ta, Nb/La, and Ti/Zr observed for these samples. We have therefore calculated its mass as a function of the mass fraction of DM by using the Al_2O_3 contents of continental crust (*2*), primitive mantle (*33*), median worldwide eclogite (*34*), and DM, assuming that the DM contains between 80 and 95% of the Al_2O_3 present in the primitive mantle. Al_2O_3 was chosen for this calculation because it is the only major element that meets all of the following criteria: (i) its concentration is well defined in the continental crust, (ii) its concentration is markedly different between DM and eclogites, and (iii) it exhibits a relatively narrow range of variability in eclogites (*34*). An Al_2O_3 deficit exists in Earth if the DM is 40% or more of the mantle (Fig. B.2A), a likely minimum proportion based on the concentrations of incompatible elements present in the continental crust (*2*). The mass fraction of eclogite needed to compensate for this deficit ranges between 0.5 and 6% of the silicate Earth, equal to or greater than the mass of the continental crust and approximately equivalent to the mass of oceanic crust subducted through time (*1*, *35*) (Fig. B.2B). This mass overlaps that of the continental lithospheric mantle (1.5 to 2.5% of silicate Earth)

Figure B.2. (A) Gray field shows the deficit in Al_2O_3 that exists in the silicate Earth as a function of the proportion of DM. Calculated Al_2O_3 composition of the silicate Earth is derived from the sum of Al_2O_3 contributed from the DM, continental crust (CC), and primitive mantle (PM) (mantle that has not differentiated = $1 - M_{CC} - M_{DM}$, where M is mass fraction). Continental crust is assumed to contain 2% of the Al_2O_3 in the silicate Earth ($0.0057 \times 15.8/4.45$); there is little variation in this value for different published estimates (*2*). The DM composition, which is more poorly constrained, is allowed to vary from a moderately depleted composition with 95% of the Al_2O_3 of the primitive mantle to a strongly depleted composition, containing 80% of the Al_2O_3 of the primitive mantle. Primitive mantle composition is from (*33*). (B) Gray field shows range of Al_2O_3 contents in the silicate Earth needed to eliminate the Al_2O_3 deficit shown in (A), calculated from mass balance as a function of the mass of a refractory eclogite reservoir. In this calculation, the mass of the DM is allowed to vary between 50 and 80% of the silicate Earth. Moderately depleted and strongly depleted mantle compositions are as defined above. Intersection of the gray field with the Al_2O_3 content of the primitive mantle defines the upper and lower bounds on the mass of eclogite that might exist in the Earth — that is, between 0.5 and ~6% by mass, if it accounts for the missing Al_2O_3.

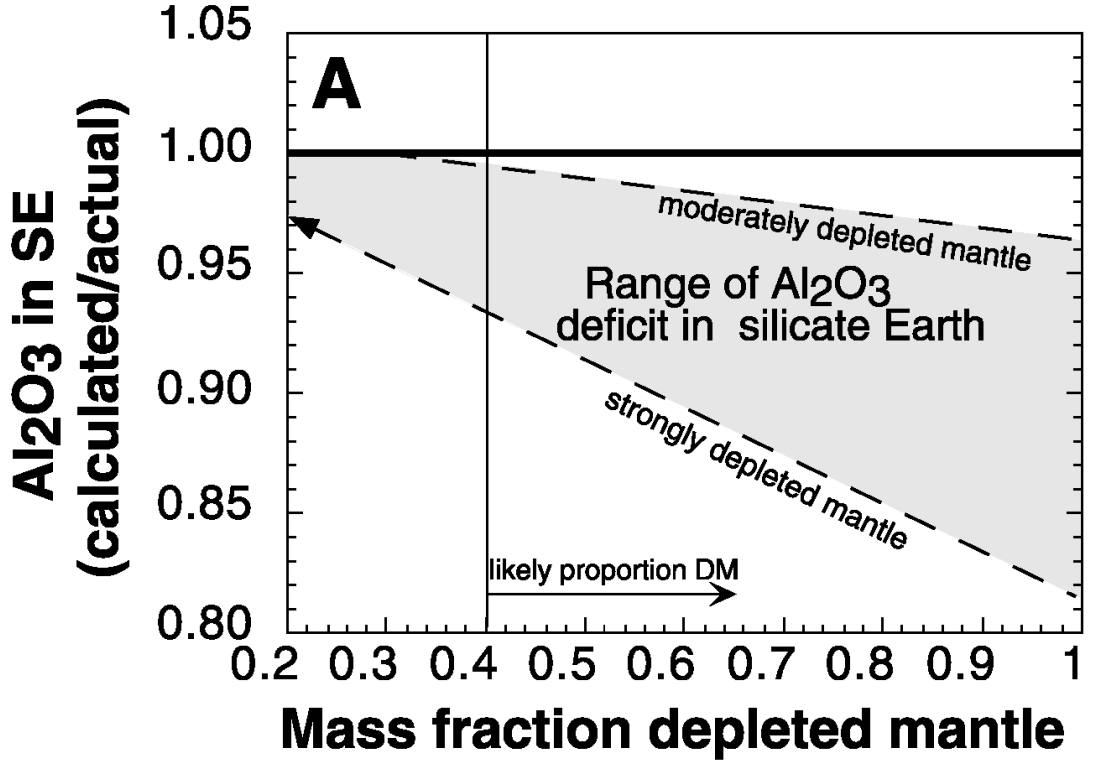
A
1.05
1.00
0.95
0.90
0.85
0.80
Al2O3 in SE
(calculated/actual)
moderately depleted mantle
Range of Al2O3
deficit in silicate Earth
strongly depleted mantle
likely proportion DM
0.2 0.3 0.4 0.5 0.6 0.7 0.8 0.9 1
Mass fraction depleted mantle

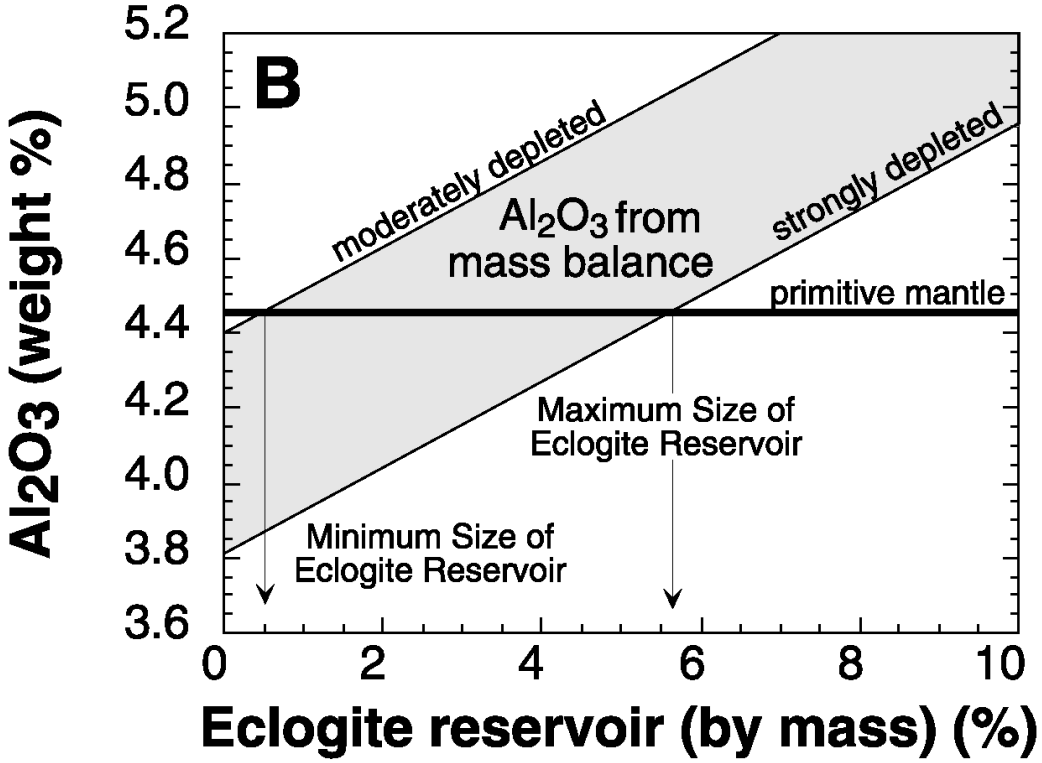
B
5.2
5.0
4.8
4.6
4.4
4.2
4.0
3.8
3.6
Al2O3 (weight %)
moderately depleted
Al2O3 from
mass balance
strongly depleted
primitive mantle
Maximum Size of
Eclogite Reservoir
Minimum Size of
Eclogite Reservoir
0 2 4 6 8 10
Eclogite reservoir (by mass) (%)

(*1*, *36*) and, although these and other eclogite samples originate from the lithospheric mantle, population studies of xenocrysts and xenoliths in kimberlites demonstrate that eclogite is a minor component of the continental lithosphere, probably below 1 to 2% by volume (*37*). Thus, our estimates suggest that much of this eclogitic reservoir exists at deeper levels of the mantle, possibly in the lower mantle (*38*).

Given the mass of refractory eclogite calculated above, some constraints on its trace element composition can also be obtained from mass balance calculations (*39*) (Fig. B.3A). The mean eclogite lies near the low end of the Nb concentration range of the calculated eclogitic reservoir and within its range of Nb/La. In view of the large spread in concentrations and ratios observed in the eclogites, this agreement is good. Likewise, the range in Nb/Ta ratios for the eclogites is large, but the mean eclogite falls within the range of Nb/Ta calculated for the missing reservoir (Fig. B.3B).

We propose that the eclogite reservoir forms a missing link between continental crust and DM. We envisage that fractionation of Nb from La and Ta (and possibly Ti from Zr) is produced as altered oceanic crust transforms to eclogite, giving up a melt or fluid phase during subduction. During the Archean [when the eclogites we examined here are likely to have formed (*40*)] higher mantle temperatures resulted in a thicker and more mafic oceanic crust that underwent dehydration melting upon subduction (*41*). The major and trace element compositions of xenolithic eclogites are consistent with them being residues of tonalite-trondhjemite-granodorite production from a higher MgO oceanic crust (*42*). As Earth cooled, dehydration melting of slab basalts in subduction zones may have given way to dehydration only. Because the partitioning of Nb and Ta between fluid and rutile is extremely low (*43*), dehydration should not fractionate Nb from Ta. Thus the

Figure B.3. Composition of refractory eclogite reservoir, calculated from mass balance (*39*), compared with the range of eclogite compositions reported here. Solid circles, individual eclogites; stars, geometric mean of xenolithic eclogite population (*26*); curves, end member outcomes of the mass balance calculations; circles and pluses, results assuming the eclogite reservoir represents 6% by mass of the silicate Earth; triangles and diamonds, results assuming the eclogite reservoir represents only 0.5% by mass of the silicate Earth. A range of DM compositions were assumed (Nb in DM = 0.12 to 0.35 ppm), corresponding to the range of Nb contents calculated for the DM from representative MORB compositions, assuming 5 to 10% batch melting and bulk D values of 0.0005 and 0.00028 (*13*). Other elements in the DM were calculated assuming Nb/La = 0.9 (*3*) and Nb/Ta = 15.5 (*7*). Pluses and diamonds, moderately depleted mantle with 0.35 ppm of Nb (about half the concentration of the PM); circles and triangles, more strongly depleted mantle with 0.12 ppm of Nb (about 20% of the PM). Because the continental crust has a Nb/La ratio significantly smaller than either DM or PM, the mass balance calculation for Nb/La (A) is very sensitive to the mass of the crust. Increasing the crust's mass from 0.57 to 0.60% of the silicate Earth, results in a factor of 2 increase in the Nb/La calculated for the refractory eclogite reservoir. For this reason, minimum bounds are shown for this reservoir by the gray box, which is considered the only robust constraint that can be placed on its Nb/La composition [that is, the Nb/La could be significantly higher than that depicted by the curves in (A) but not lower]. Because the Nb/Ta ratio of the crust is not significantly different from the DM, the Nb/Ta calculations shown in (B) do not depend on crustal mass.

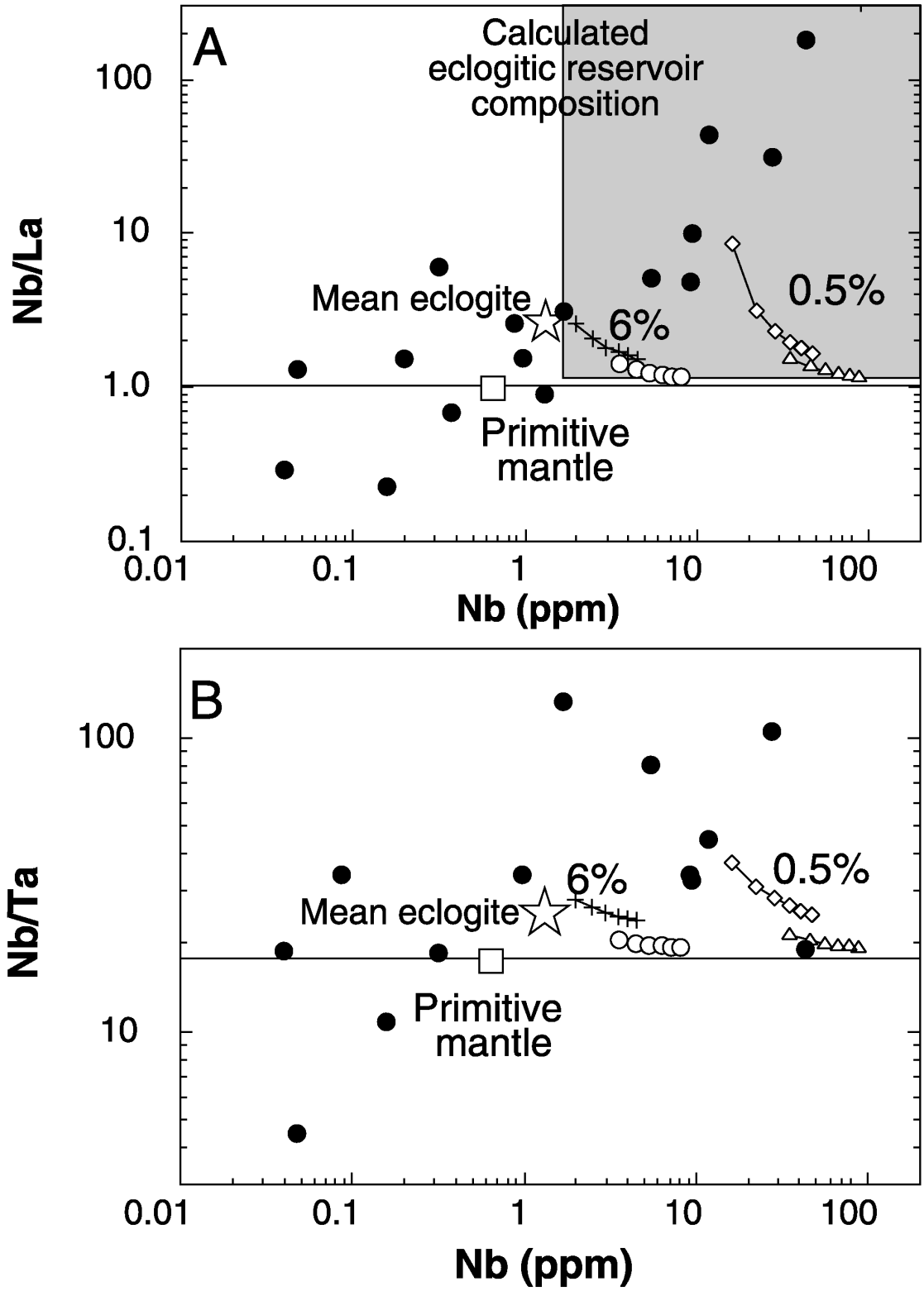
A
Calculated
eclogitic reservoir
composition
100
10
1.0
0.1
Nb/La
Mean eclogite
6%
0.5%
Primitive
mantle
0.01
0.1
1
10
100
Nb (ppm)
B
100
10
Nb/Ta
6%
0.5%
Mean eclogite
Primitive
mantle
0.01
0.1
1
10
100
Nb (ppm)

Nb/Ta ratio of rutiles in Phanerozoic eclogites reflects that of their protolith. For example, if the rutiles are in metamorphosed MORB, their Nb/Ta should be low (*7*–*9*).

Table B.1. Parameters used to calculate refractory eclogite composition from mass balance. Numbers in plain type are input parameters for mass balance calculations; numbers in italics are derived from mass balance calculations.

	Mass fraction of silicate Earth	Al_2O_3 (weight %)	Nb (ppm)	La (ppm)	Ta (ppm)	Nb/ La	Nb/ Ta
DM	0.4 - 0.9	3.6 - 4.2	0.12 - 0.35	0.13 - 0.38	0.007 - 0.022	0.91	15.5
Continental crust (*2*)	0.0057	15.8	8.6	18	0.7	0.48	12.3
Primitive mantle (*33*)	0.03 - 0.59	4.45	0.658	0.648	0.037	1.01	17.5
Refractory eclogite reservoir*	0.005 - 0.06	15.8	>1.6*	>0.75*	>0.04*	>1.18*	19 - 37

*Concentrations of Nb and the Nb/La ratio in the eclogite reservoir are highly sensitive to the mass of the continental crust because of its relatively high concentrations and large fractionation of Nb/La relative to other reservoirs. For example, increasing the crustal mass by 5% causes a factor of 2 increase in the Nb/La ratio in the eclogite reservoir in some cases.

Finally, a relevant question is whether the refractory eclogite reservoir, once transported into the deep mantle, is ever seen again. A number of persuasive arguments

have been made for incorporation of recycled oceanic crust into the source regions of OIB (*44*). Although some OIB [particularly the HIMU family (*45*)] exhibit high Nb/La, they apparently do not have elevated Nb/Ta (*10*). This observation suggests that the amount of refractory eclogite in the OIB source is small. For example, if OIB are derived from sources that are mixtures of refractory eclogite and peridotite (DM or primitive mantle), ≤10% eclogite is able to dominate the Nb and Ta contents of the mixture, giving rise to superchondritic Nb/Ta in the source. However, because recycled oceanic lithosphere is likely to contain both oceanic crust (now eclogite) and sediment, which will have high concentrations of Nb and Ta and low Nb/Ta (*11*, *12*), one expects to see a range of Nb/Ta in OIB, depending on the amount and nature of the recycled component in their source (one would predict HIMU to have high Nb/Ta and EM I (*45*) to have low Nb/Ta). Therefore, a search for systematics in Nb and Ta contents of well-characterized OIB offers an additional test of the importance of recycled oceanic lithosphere in the source regions of OIB *(46)*.

References and Notes

1. W. F. McDonough, *Philos. Trans. R. Soc. London* **335**, 407 (1991).

2. B. L. Weaver and J. Tarney, *Nature* **310**, 575 (1984); S. R. Taylor and S. M. McLennan, *The Continental Crust: Its Composition and Evolution* (Blackwell Scientific Publications, Oxford, 1985), p. 67; R. L. Rudnick and D. M. Fountain, *Rev. Geophys.* **33**, 3 (1995); K. H. Wedepohl, *Geochim. Cosmochim. Acta* **59**, 1217 (1995).

3. A. W. Hofmann, *Earth Planet. Sci. Lett.* **90**, 297 (1988); S.-S. Sun and W. F. McDonough, in *Magmatism in the Ocean Basins*, A. Saunders and M. Norry, Eds. (Geological Society, London, special edition, 1989), vol. 42, pp. 313–345.

4. MORB are depleted in Nb relative to La, and because Nb is more incompatible than La during mantle melting (*13*) it follows that the source region of MORB, the so-called DM, must have even lower Nb/La.

5. Both are 0.064 nm for octahedral coordination [R. D. Shannon, *Acta Crystallog*r. **32**, 751 (1976)].

6. We consider here only data from high-precision techniques where both elements are analyzed simultaneously, such as inductively coupled plasma mass spectrometry (ICP-MS) [S. M. Eggins *et al.*, *Chem.Geol.* **134**, 311 (1997)] and multichannel spark source mass spectrometry [K.-P. Jochum *et al*., *J. Anal. Chem*. **359**, 385 (1997)].

7. K.-P. Jochum, J. Pfänder, J. E. Snow, A. W. Hofmann, *Eos* **78**, F805 (1997).

8. T. Plank and W. M. White, *Eos* **76**, F655 (1995).

9. Y. Niu and R. Batiza, *Earth Planet. Sci. Lett*. **143**, 471 (1997).

10. A. W. Hofmann and K.-P. Jochum, *J. Geophys. Re*s. **101**, 11831 (1996); K.-P. Jochum, A. W. Hofmann, A. J. Stolz, *Eos* **77**, F785 (1996).

11. M. G. Barth, W. F. McDonough, R. L. Rudnick, *Chem. Geol*., in press.

12. T. Plank and C. H. Langmuir, *Chem. Geol.* **145**, 325 (1998).

13. C. C. Lundstrom, H. F. Shaw, F. J. Ryerson, Q. Williams, J. Gill, *Geochim Cosmochim. Acta* **62**, 2849 (1998), and references therein.

14. F. A. Frey, C. J. Suen, H. W. Stockman *Geochim. Cosmochim. Acta* **49**, 2469 (1985); E. Takazawa, thesis, Massachusetts Institute of Technology, Cambridge, MA (1996); O. Muetner, thesis, Swiss Federal Institute of Technology (1997).

15. To date, superchondritic Nb/Ta has been observed only in some high K island arc lavas [A. J. Stolz, K.-P. Jochum, B. Spettel, A. W. Hofmann, *Geology* **24**, 587 (1996); T. Elliott, T. Plank, Z. Zindler, W. White, B. Bourdon, *J. Geophys. Res.* **102**, 14991 (1997); C. Münker, *Chem. Geol.* **144**, 23 (1998)], which can have Nb/Ta up to 33. However, these lavas are volumetrically minor and share the low Nb/La typical of other convergent margin magmas. Therefore, they do not appear to derive from a source with the necessary chemical composition to achieve the mass balance. Similarly, some OIB have superchondritic Nb/La but not Nb/Ta (*10*) or Ti/Zr ratios (*1*). Superchondritic Ti/Zr is observed in massif peridotites, but these have strongly subchondritic Nb/Ta and Nb/La (*14*).

16. F. J. Ryerson and E. B. Watson, *Earth Planet. Sci. Lett.* **86**, 225 (1987), and references therein.

17. Supplementary material is available at www.sciencemag.org/feature/data/1044137.shl (Web table 1).

18. Major and minor elements, including Al_2O_3 , Cr_2O_3, MgO, ZrO_2 , and Nb_2O_5 were determined with a Camebax MBX electron microprobe operated at 15 kV and a 30-nA beam current, using a rastered spot of 100 mm. Trace elements were determined by laser ablation ICP-MS with a home-built excimer laser that operates in the deep ultraviolet at 193 nm. This laser is coupled to a VG Plasmaquad II+ ICP-MS, which has sensitivity in solution mode of ~1×10^8 cps/ppm at mass 115. Details of the laser system are in (I. Horn, R. L. Rudnick, W. F. McDonough, *Chem. Geol.*, in press) and can also be viewed at http://www-eps.harvard.edu/people/faculty/rudnick/la-icp-ms.html. Data reduction follows the procedure outlined in [H. Longerich, S. E. Jackson, D. Günther*, J. Anal. Atom. Spectrom*. **11**, 899 (1996)]. For the rutile analyses, ^{49}Ti was used as the internal standard and NIST 610 glass was used for the calibration standard. Excellent agreement exists between electron microprobe and LA-ICP-MS data for elements analyzed by both techniques (Al, Fe, Cr, Zr, and Nb).

19. K.-P. Jochum and A. J. Stolz, *Meteoritics Planet. Sci.* **32**, Suppl. 67 (1997).

20. The only exception to this generalization are rutiles from the Magnet Cove carbonatite complex and a rutile from a South Carolina beach sand of unknown provenance.

21. Supplementary material is available at www.sciencemag.org/feature/data/1044137.shl (Web table 2).

22. The two rutiles occur in veins in harzburgite xenoliths carried in volcanoes of the eastern African Rift: Labait and Pello Hill. In the Labait sample (LB-17) the rutile is associated with secondary zircon, sulfide, orthopyroxene, chromite, and minor phlogopite [R. L. Rudnick *et al.,* in *Proc. Seventh International Kimberlite Conference*, Cape Town, South Africa, J. J. Gurney and S. R. Richardson, Eds. (Red Barn, Cape Town, South Africa, 1999)]. In the sample from Pello Hill (PEL-40), rutile occurs in a phlogopite vein that also contains abundant sulfide.

23. Siberian eclogites come from the Udachnaya pipe courtesy of Z. Spetsius and N. Sobolev.

24. D. V. Hills and S. E. Haggerty, *Contrib. Mineral Petrol.* **103**, 397 (1989).

25. The western African eclogites come from the Koidu kimberlite pipe, Sierra Leone, and constitute the low MgO suite of (*24*). They are essentially bimineralic rocks with accessory sulfides and rutile. Kyanite, coesite, graphite, and diamond also occur as accessory phases. See (*24*) for a complete description.

26. The Nb/Ta, Nb/La, and Ti/Zr ratios of the eclogites follow log-normal distributions. We have therefore chosen the geometric mean as the value most representative of the population.

27. Rutile occurs in the eclogites as equant grains, from 100 mm to several millimeters in diameter. The rutiles generally occur interstitial to altered garnet and omphacite, but occasionally they occur fully included in omphacite. They typically show exsolution of ilmenite 6 spinel at 90° angles. Some rutiles show thin (several micrometers) rims of ilmenite with variable MgO and MnO contents. Rims were not measured in laser ablation analyses. Metasomatic rutile is distinguished by highly heterogeneous Nb and Ta contents and occasionally by a skeletal texture. Based on textures, trace element homogeneity, and evidence for equilibrium between rutile and primary silicates, all rutiles reported in Web table 2 (*21*) are considered primary phases.

28. Unpublished data show that garnets and omphacites in rutile-bearing samples have Nb and Ta concentrations generally below detection limits, which vary as a function of spot size. For the spot sizes used in this study (50 to 100 mm), detection limits of 10 to 400 ppb are typical for both Nb and Ta. In contrast, garnet and omphacite contain significant Nb and Ta concentrations in rutile-free eclogites. About 70% of the low MgO eclogites from Koidu are rutile bearing.

29. Large ion lithophile elements include light weight REE, K, Rb, Cs, Sr, and Ba.

30. E. Jagoutz, J. B. Dawson, S. Hoernes, B. Spettel, H. Wänke, *Proc. 15th Lunar Planet. Sci. Conf*., 395 (1984); Neal *et al*., *Earth Planet Sci. Lett.* **99**, 362 (1990); T. R. Ireland, R. L. Rudnick, Z. Spetsius, *Earth Planet Sci. Lett.* **128**, 199 (1994). In addition, the western African whole rock powders were ground in a tungsten carbide mill, which has led to significant Ta contamination. This is reflected by the good correlation between W and Ta values and very low Nb/Ta ratios (down to 1) in the whole rocks.

31. E. A. Jerde, L. A. Taylor, G. Crozaz, N. V. Sobolev, V. N. Sobolev, *Contrib. Mineral. Petrol*. **114**, 189 (1993); B. L. Beard *et al*., *Contrib. Mineral. Petrol.* **125**, 293 (1996).

32. The weight percent of rutile in the eclogites was determined from Ti mass balance by using the measured Ti contents of garnet and omphacite and their modal abundances [both given in (*24*)] to calculate their contribution to the whole rock Ti budget. Because both garnet and omphacite have lower TiO_2 than the bulk rock, this invariably led to a Ti deficit, which was made up by assuming that the remaining Ti was present in rutile. For the two samples lacking bulk rock TiO_2 concentrations, the TiO_2 content of the whole rock was calculated by assuming it has no Ti anomaly (that is, Ti is not depleted or enriched relative to elements of similar incompatibility such as Eu). The methodology described above yields the maximum amount of rutile in the sample, because it does not account for any Ti that is in secondary phases such as amphibole (0.5 to 2.5 weight % TiO_2) and phlogopite (1.6 to 4 weight % TiO_2). However, the overestimation is small and within the errors of the estimate. For example, sample KEC 81-18 has the highest measured bulk K_2O content of 1 weight %. If all this K_2O is contained within phlogopite, it corresponds to 11% phlogopite in the whole rock by weight, which in turn corresponds to only 0.03 weight % of the bulk rock's TiO_2 content. Decreasing the whole rock TiO_2 content by this amount

leads to an estimated rutile abundance of 0.61% compared with 0.64% if the phlogopite is ignored. We thus conclude that our estimates of rutile proportions are accurate to within ±0.05% absolute or 10% relative uncertainty.

33. W. F. McDonough and S.-S. Sun, *Chem. Geol.* **120**, 223 (1995); C. J. Allegre, J.-P. Poirier, E. Humler, A. W. Hofmann, *Earth Planet. Sci. Lett.* **134**, 515 (1995).

34. The Al_2O_3 contents of xenolithic eclogites are derived from a literature compilation of major element compositions for 77 samples normalized to 100%, anhydrous. The population follows neither a log-normal nor a normal distribution but is skewed to high values. We therefore adopt the median Al_2O_3 content of xenolithic eclogites (15.8 weight %) as best representative of the population. Further statistics: average = 17.6% ± 5.9% (1σ), minimum = 7.4%, maximum = 31%.

35. A minimum estimate of the amount of oceanic crust subducted though Earth history is 1.3×10^{26} g, or 3.3% of the silicate Earth by mass. This is derived by assuming the present mass of oceanic crust (5.3×10^{24} g) is subducted every 100 million years for the last 2.5 billion years (Ga). This estimate is nearly identical to that commonly assumed in recycling models for OIB generation (*44*). We consider this estimate a minimum bound because subduction may well have operated before 2.5 Ga, the ocean basins may have been larger than at present (if the mass of the continents has increased with time), and the mantle was hotter in the Archean, which would produce a greater thickness of oceanic crust at a faster rate.

36. W. F. McDonough, *Earth Planet. Sci. Lett*. **101**, 1 (1990).

37. D. J. Schulze, *J. Geophys. Res*. **94**, 4205 (1989); P. H. Nixon, Ed. *Mantle Xenoliths* (Wiley, New York, 1989). However, in rare occurrences, eclogite may dominate some areas of the lithospheric mantle, see [N. V. Sobolev, E. S. Yefimova, D. M. DeR. Channer, P. F. N. Anderson, K. M. Barron, *Geology* **26**, 971 (1998)] and references therein.

38. S. Kaneshima and G. Helffrich, *Science* **283**, 1888 (1999); R. D. van der Hilst, S. Widiyantoro, E. R. Engdahl, *Nature* **386**, 578 (1997).

39. La, Nb, and Ta contents of the eclogitic reservoir were calculated from mass balance assuming that the silicate Earth (SE) is made up of four components: DM, continental crust (CC), primitive mantle (PM), and a refractory eclogite reservoir (EC). The concentration of an element in the eclogite reservoir is $X_{EC}^i = (X_{SE}^i - M_{CC}X_{CC}^i - M_{DM}X_{DM}^i - M_{PM}X_{PM}^i)$, where X_{zz}^i is the concentration of element i in reservoir zz and M_{zz} is the mass fraction of the reservoir relative to the total silicate Earth. The mass fraction of the reservoirs and the range in concentrations used in the calculations are given in Table B.1.

40. D. G. Pearson *et al*., *Nature* **374**, 711 (1995); M. G. Barth, R. L. Rudnick, R. W. Carlson, I. Horn, W. F. McDonough, *Eos* **80**, F1192 (1999).

41. H. Martin, *Geology* **14**, 753 (1986).

42. T. R. Ireland, R. L. Rudnick, Z. Spetsius, *Earth Planet. Sci. Lett*. **128**, 199 (1994); R. L. Rudnick, in *Extended Abstracts 6th International Kimberlite Conference* (1995), p. 473; H. Rollinson, *Nature* **389**, 173 (1997).

43. J. M. Brenan, H. F. Shaw, D. L. Phinney, F. J. Ryerson, *Earth Planet. Sci. Lett*. **128**, 327 (1994); R. Stalder, S. F. Foley, G. P. Brey, I. Horn, *Geochim. Cosmochim. Acta* **62**, 1781 (1998).

44. A. W. Hofmann, *Nature* **385**, 219 (1997) and references therein.

45. See [A. Zindler and S. R. Hart, *Annu. Rev. Earth Planet. Sci*. **14**, 493 (1986)] for a lexicon of OIB end members.

46. A. N. Halliday, *Nature* **399**, 733 (1999).

47. We thank S. Haggerty, Z. Spetsius, and N. Sobolev for eclogite samples; D. Lange for electron microprobe analyses and back-scattered electron images; and C. Francis for rutiles from the Harvard Mineralogical Museum collection. K. Lehnert and C. Langmuir provided access to their nascent MORB database, which we greatly appreciate. S. Haggerty, A. Hofmann, T. Plank, and an anonymous reviewer provided thoughtful comments on the manuscript. This work was supported by NSF grants EAR 9804677 to R.L.R., EAR 9506517 to W.F.M., and EAR 9711008 to R.L.R. and W.F.M.

2 August 1999; accepted 19 November 1999

Supplemental Table 1. Rutiles from rocks of the continental crust. Major elements (wt. %) by EMP except those designated "LA", which are by laser ablation ICP-MS. Trace elements (ppm) by LA-ICP-MS except those designated "EMP", which are by electron microprobe. n = number of spots averaged in analyses. No standard deviations are reported for the majority of crustal rutiles because data represent single spot analyses.

Sample	81-12	1 σ	22201	1 σ	83741	1 σ	83742	1 σ	110328	1 σ	96293	1 σ	96279	1 σ	131178	1 σ
Location	Koidu		Georgia		Switz.		Switz.		Virginia		Maryland		Norway		N.C.	
Rock type	Granulite		Ky schist		Alp. Vein		Alp. Vein		vein		Alp. Vein		qtz vein		Alp. Vein	
n	4		3		3		4		3		3		3		6	
SiO_2	0.04	0.009	0.013	0.005	0.008	0.003	0.134	0.13	0.015	0.007	0.022	0.011	0.035	0.013	0.013	0.007
TiO_2	97.51	1.04	98.29	0.26	99.13	0.12	99.31	0.6	98.79	0.05	99.21	0.23	98.26	0.33	98.97	0.62
Al_2O_3	0.11	0.05	0.02	0.004	0.015	0.005	0.04	0.036	0.055	0.018	0.018	0.005	0.038	0.001	0.02	0.004
Al_2O_3 LA	0.33	0.02	0.1		0.05		0.24		0.16				0.24			
Cr_2O_3	0.14	0.05	0.09	0.001	0.36	0.05	0.05	0.01	0.05	0.01	0.33	0.08	0.038	0.007	0.58	0.4
FeO	0.99	0.28	0.83	0.14	0.11	0.02	0.11	0.03	0.82	0.04	0.28	0.02	0.8	0.03	0.12	0.09
FeO LA	1.2	0.25	1.39		0.16		0.18		1.53		0.52		2.05		0.29	
MnO	0.01	0.01	0.002	0.003	0.002	0.003	0.005	0.007	0.011	0.01			0.012	0.017	0.0008	0.0012
MnO LA							0.007									
MgO	0.01	0.01	0.004	0.005	0.0001	0.0002	0.002	0.005			0.003	0.005	0.002	0.003	0.001	0.002
Sc							148								93	
V	3688	1049	4504		3248		1537		1567		3028		1222		1816	
Cr	833	201	729		3514		318		474		2702		498		8625	
Cr EMP	979	329	613	7	2483	376	338	79	349	51	2268	541	259	45	3938	2717
Zn													34		57	
Zr	975	706	64		167		33		1093		41		168		51	
Zr EMP	704	301														
Nb	599	18	865		4889		538		1360		1634		3992		3601	
Nb EMP	1255	923	815	230	2351	38	311	109	1021	212	1248	13	2947	70	2011	1824
Mo	45	16	15						66							
Sn	37	1														
Sb			615		5		2				6				30	
Ce									0.49		0.09					
Hf	27	16	4.63		7.93		3.45		41.6		3.39		8.32		2.14	
Ta	30	2	49		440		34.2		77		175		407		467	
W	262	66	334		363		0.39		14.4		398		467		1370	
U	1.3	0.2	1.15		3.85		0.04		0.34		4.56		24.28		8.01	
Nb/Ta	20		17.8		11.1		15.7		17.7		9.3		9.8		8.3	
Zr/Hf	36		14		21		10		26		12		20		25	

Supplemental Table 1 (continued).

Sample	92647	1 σ	96300	1 σ	96841	1 σ	97238	1 σ	96276	1 σ	115515	1 σ	97707	1 σ	103742	1 σ
Location	Brazil		Italy		Mt. Cove, AK		Mt. Cove, AK		Mt. Cove, AK		Germany		Madag.		Bolivia	
Rock type	Topaz dep.				Ne syenite		Ne syenite		Ne syenite		Diorite				pegmatite	
n	2		2		3		4		5		3		2		3	
SiO_2	0.004	0.006	0.01	0.002	0.05	0.069	0.073	0.116	0.011		0.034	0.004	0.009	0.01	0.013	0.003
TiO_2	95.92	0.04	99.66	0.71	98.43	0.88	98.51	0.86	5.29		99.87	0.35	97.62	0.34	97.77	0.54
Al_2O_3	0.046	0.005	0.015	0.0002	0.01	0.01	0.015	0.015	0.012	0	0.026	0.007	0.01	0.006	0.018	0.006
Al_2O_3 LA	0		0.09								0.09					
Cr_2O_3	0.09		0.03	0.01	0.03	0.004	0.05	0.04	0.05	0.04	0.027	0.005	0.87	0.01	0.86	0.14
FeO	1.51	0.07	0.38	0.003	0.53	0.15	0.41	0.11	1.94	1.39	0.3	0.01	0.21	0.02	0.11	0.01
FeO LA	0.11		0.62		0.72		1.04		0.4		0.48		0.44		0.19	
MnO					0.016	0.023	0.006	0.01			0.001	0.002			0.002	0.002
MnO LA					0.01		0.006	0.01	0.01						0.003	
MgO					0.002		0.004	0.003	0.004	0.006	0.056	0.005			0.001	0.003
Sc											141		760			
V	20		1315		1174		1709		1323		1611		9696		5778	
Cr	40		309		193		254		88		263		8578		10052	
Cr EMP	614	0	197	37	210	27	347	299	349	242	245	37	5962	46	5885	987
Ni																
Zn			212						53		59		34			
Zr	3		1510		148		297		76		82		836		1434	
Zr EMP																
Nb	211		2548		11145		11012		4549		757		1669		3970	
Nb EMP	3803	233	2136	251	8757	559	8065	1719	38336	30109	546	81	1454	488	3646	888
Mo	5.69		5.83		1.32								26		2.51	
Sn																
Sb	711		5		0.72						36		22		3.53	
Ce	0.01				0.21		12.79		0.31				0.14			
Hf	0.21		46.69		5.38		8.33		3.91		3.63		38		66	
Ta	13		240		91		253		226		44		87		165	
W	71		20		37		106		1.57		93		402		1169	
U	1.75		75		0.07		1.62				0.62		41.1		12.8	
Nb/Ta	16.5		10.6		122.6		43.5		20.2		17.3		19.3		24.1	
Zr/Hf	14		32		27.4		35.7		19.4		22.5		21.8		21.6	

Supplemental Table 1 (continued).

Sample	104737	1 σ	108374	1 σ
Location	France		S.C.	
Rock type	Glauc. Schist		Beach sand	
n	2		2	
SiO_2	0.021	0.002	0.024	0.009
TiO_2	99.68	0.1	98.33	0.15
Al_2O_3	0.014	0.0001	0.023	0.013
Al_2O_3 LA			0.1	
Cr_2O_3	0.19	0.04	0.36	0.07
FeO	0.42	0.02	0.2	0.06
FeO LA	1.8		0.95	
MnO				
MnO LA				
MgO	0.0007	0.001	0.006	0.009
Sc	103			
V	1146		2351	
Cr	2380		1059	
Cr EMP	1279	265	2433	447
Ni				
Zn				
Zr	57		859	
Zr EMP				
Nb	335		10219	
Nb EMP	259	238	5156	1871
Mo		10.6		
Sn				
Sb	5.16			
Ce				
Hf	2.94		41.55	
Ta	16		260	
W	35		1157	
U			61.1	
Nb/Ta	20.7		39.4	
Zr/Hf	19.2		20.7	

Supplemental Table 2. Major and trace element compositions of mantle rutiles. Major elements (wt. %) by EMP except those designated "LA", which are by laser ablation ICP-MS. Trace elements (ppm) by LA-ICP-MS except those designated "EMP", which are by electron microprobe. Rock types: Diam-Ec = diamond-bearing eclogite, Coes-Ec = coesite-bearing eclogite, Ec = bimineralic eclogite, Ky-Ec = kyanite-bearing eclogite, Harz = harzburgite. n = number of spots averaged in LA analyses, *Metasomatic rutiles excluded from LA analyses, but included in EMP analyses.

Sample	90-389	1 σ	90-390	1 σ	2301	1 σ	2290	1 σ	81-3	1 σ	81-4	1 σ	81-5	1 σ	81-7	1 σ
Location	Siberia		Siberia		Siberia		Siberia		Koidu		Koidu		Koidu		Koidu	
Rock type	Diam-Ec		Diam-Ec				Coes-Ky-Ec		Ec		Ec		Ec		Ec	
n	5		8		5		5		11		9		5		5	
SiO_2	0.04	0.01	0.02	0.01	0.02	0.01	0.02	0.01	0.03	0.01	0.02	0.01	0.07	0.01	0.02	
TiO_2	96.25		97.77	1.6	99.36	0.4	99.02	1.25	94.8	0.89	97.14	0.51	95.18	0.8	94.88	0.72
Al_2O_3	0.53	0.01	0.4	0.17	0.24	0.06	0.72	0.67	0.52	0.27	0.32	0.05	0.41	0.07	0.65	0.34
Al_2O_3 LA	0.94	0.59	0.45	0.15	0.31	0.06	0.74	0.63								
Cr_2O_3	0.16		0.06	0.01	0.05	0.01	0.06	0.01	0.13	0	0.18	0.02	0.25	0.02	0.24	0.02
FeO	0.78	0.03	1.97	0.64	0.58	0.17	0.98	0.48	3.33	0.46	1.85	0.25	3.39	0.64	3.15	0.6
FeO LA	0.63	0.11	1.51	0.65	0.3	0.04	0.38	0.21								
MnO	0.01		0.01	0.01	0.004		0.004		0.01	0.01	0.01	0.01	0.03	0.01	0.01	0.01
MnO LA			0.01	0.01					0.018	0.016	0.003	0.002	0.003		0.015	0.01
MgO	0.21		0.18	0.09	0.03	0.02	0.09	0.07	0.33	0.09	0.15	0.07	0.28	0.1	0.31	0.16
MgO LA									0.38	0.2	0.21	0.1	0.12	0.06	0.28	0.18
Sc			5.29	0.33							4.1	0.5				
V	1217	48	941	46	863	71	1163	59	2135	198	1568	106	1794	81	1080	30
Cr	1060	119	256	3	286	19	372	49	956	181	1296	62	1314	57	1256	25
Cr EMP	1063	91	432	46	327	68	405	68	889	0	1232	137	1711	137	1642	137
Ni											11	3.9	11	6	17	6
Zn	24	9	19	5	15	4	13	4	82	35	27	10	21	3	26	9
Zr	1005	34	1086	35	1972	172	574	28	658	94	1140	155	789	33	1743	78
Zr EMP	1242	177	827	223	2236	309	550	159	962	222	962	222	814	222	2221	148
Nb	1020	57	20	2	148	122	78	7	1337	135	14	5	21	0.5	1375	78
Nb EMP	1028	193	27	62	143	94	63	95	1398	280					1517	140
Mo	6.5	2.4			6.1	1	0.6	0.1	14	2					5	0.23
Sn	28	4	16	1	51	7	23	3	26	4					28	0.9
Sb	0.53	0.2			0.05	0.02	0.19	0.17	2.7	0.6					0.85	0.15
Ce	0.09	0.14			0.01		0.07	0.07	0.039	0.042						
Hf	29	2	40	4	52	4	24	2	18	3	38	3.2	34	2	56	1.9
Ta	31	2	1	0.3	14.9	17.3	4.2	0.5	19	21	0.4	0	1.8	0.1	39.7	4.7
W	13.7	1.6	0.3	0.1	1.5	0.9	0.4	0.2	18	10			0.28	0.01	12.4	1.4
Th							0.018	0.01								
U	0.6	0.1	0.04	0.01	1.4	0.3	0.4	0.1	10.5	0.5	5	0.4	2.4	0.1	4.1	0.3
Nb/Ta	33		19		10		18		70		34		12		35	
Zr/Hf	35		27		38		24		37		30		23		31	

Supplemental Table 2 (continued).

Sample	81-8	1 σ	80-A2	1 σ	81-18*	1 σ	81-21	1 σ	86-KB-31	σ	86-KB-4	1 σ	86-56	1 σ	86-6	1 σ
Location	Koidu		Koidu		Koidu				Koidu		Koidu		Koidu		Koidu	
Rock type	Ec		Ec		Ec		Ec		Ky-Ec		Ky-Ec		Ec		Ec	
n	4		4		2		11		8		15		9		3	
SiO_2	0.02	0.01	0.02	0.01	0.03	0.02	0.07	0.08	0.02	0.01	0.03	0.01	0.02634	0.01388	0.0186	0.00698
TiO_2	96	0.59	95.42	0.78	95.09	1.08	93.04	1.06	97.22	0.81	97.21	0.16	94.5	0.84	97.59748	0.72283
Al_2O_3	0.52	0.3	0.43	0.12	0.14	0.09	0.69	0.4	0.73	0.24	0.57	0.08	0.55	0.16	0.1726	0.04745
Al_2O_3 LA					0.17	0.08	0.98	0.54	0.82	0.44	0.91	0.44	0.62	0.21	0.18	0.01
Cr_2O_3	0.11	0.02	0.13	0.01	0.09	0.01	0.16	0.02	0.12	0.01	0.38	0.02	0.09	0.11	0.13244	0.00633
FeO	2.19	0.35	3.19	0.68	3.66	0.12	4.07	0.51	1.24	0.14	0.32	0.13	4.42	0.45	1.56966	0.18619
FeO LA					3.86	0.67	4.09	0.54			0.48	0.37	4.55	0.34	2.1	0.01
MnO			0.04	0.06	0.02	0.02	0.02	0.02	0.01	0.02			0.01	0.02		
MnO LA	0.001	0.001	0.011	0.011	0.018	0.017	0.02	0.02	0.002	0.001			0.02	0.02		
MgO	0.16	0.09	0.15	0.04	0.57	0.32	0.49	0.25	0.09	0.05	0.03	0.03	0.32	0.28	0.01	0.01
MgO LA	0.1	0.07	0.13	0.06	0.62	0.21			0.09	0.11	0.07	0.06				
Sc					4.6	0.4	7.2	0.8					4.3	0.66	7.2	1.6
V	1434	489	1843	29	1650	44	1201	27	1128	50	5408	299	2143	65	2426	5
Cr	484	60			558	22	969	21	879	76	2460	47	653	32	841	76
Cr EMP	753	137	889	68	616	68	1113	108	821	68	2600	137	795	99		
Ni	25	4	7.4	1.9	20	15			21	18						
Zn	32	5			57	10	35	8.4	45	35	21	8	6	2	5.7	2.7
Zr	514	132	463	22	1030	132	1061	25	589	96	477	19	1218	58	1219	1.6
Zr EMP	444	370	447	148	888	148	849	158	592	74	296	222	1042	143	1043	228
Nb	200	152	1641	45	147	53	16301	515	23.5	2.5	96	16	87	16	34	0.5
Nb EMP	276	207	1655	210	896	1034	16034	648			69	69	107	110	118	144
Mo	16	5			9	1.7	49	3.8	4	0.5	10	1	4.1	0.7	5.6	0.6
Sn	11	1			24	1	12	1	13	1.6	10.4	1.1	13	1	37	1.6
Sb					0.7	0.15							0.37	0.06		
Ce			0.007	0.005												
Hf	30	5.6	25	3	35	5.5	30	1.4	25.2	5.5	18.5	2.1	36	1.8	48	0.4
Ta	1.4	0.1	36	14	3.72	0.21	847	150	5.3	0.5	0.28	0.1	6	1.5	4.3	0.04
W	4.1	5.9			10	5	18	1.4	5.5	4	23.2	31	1.4	0.5		
Th																
U	8.1	1.1	1.2	0.07	5.1	0.65	0.62	0.07			2.3	0.47	1.9	0.2	0.32	0.02
Nb/Ta	139		46		40		19		4		343		15		8	
Zr/Hf	17		19		29		35		23		26		34		25	

Supplemental Table 2 (continued).

Sample	86-12	1 σ	86-70	1 σ	86-72B	1 σ	LB-17	1 σ	PEL 40	1 σ
Location	Koidu		Koidu		Koidu		Labait, TZ		Pello, TZ	
Rock type	Ec		Ec		Ec		Harz		Harz	
n	8		6		9		8		7	
SiO_2	0.03	0.01	0.02	0.01	0.03	0.01	0.08		0.04	0.02
TiO_2	99.07	0.47	98.87	0.73	94.28	0.58	92.14		96.96	1.2
Al_2O_3	0.39	0.11	0.25	0.07	0.25	0.08	0.09		0.09	0.02
Al_2O_3 LA	0.48	0.08	0.22	0.08	0.42	0.12	0.08	0.09	0.12	0.03
Cr_2O_3	0.06	0.02	0.15	0.01	0.1	0.01	3.55		0.95	0.23
FeO	0.99	0.48	1.16	0.29	5.13	0.77	1.12		0.35	0.2
FeO LA	1.56	0.57	1.02	0.33			0.52	0.25	0.52	0.23
MnO					0.03	0.03	0.01		0.01	0.01
MnO LA	0.004	0.002	0.002	0.0018					0.003	0.002
MgO	0.08	0.06	0.06	0.051	0.39	0.18	0.27		0.09	0.07
MgO LA	0.17	0.08			0.5	0.35			0.15	0.13
Sc	5.5	0.9	2	0.2	4.5	0.6			10.5	0.8
V	919	356	574	11	1672	126	1165	244	1132	39
Cr	442	131	1018	35	637	49	27691	3735	6687	2139
Cr EMP	422	125	1055	84	651	73	24289	741	6513	1549
Ni					14	4				
Zn	21	7.8	16.7	4.2	40	15	33	12	12	4
Zr	2227	408	1481	49	1309	74	10774	1481	5131	568
Zr EMP	2170	245	1809	95	1417	194	12623	625	4963	641
Nb	31	4.8	240	15	4092	633	5313	615	3061	1049
Nb EMP	69	89	276	117	3936	521	6824	1504	3030	1151
Mo	4.1	1	2.89	0.73	14	1.5	2.8	0.8	15.2	1.6
Sn	45	10	12	0.98	28	5	35	5	43	4
Sb					1.1	0.04	0.09	0.07		
Ce										
Hf	59	13	44	1.8	31.8	2.1	269	41	133	16
Ta	2.98	0.37	17.3	2.2	30.3	11.4	393	60	133	37
W	16.7	2.8	10.9	1.6	21	7.8	1.9	0.2	19	6
Th										
U			2.4	0.28	7.2	0.23	1.9	0.2	23	6
Nb/Ta	10.4		13.9		135		13.5		23	
Zr/Hf	38		33		41		40		39	